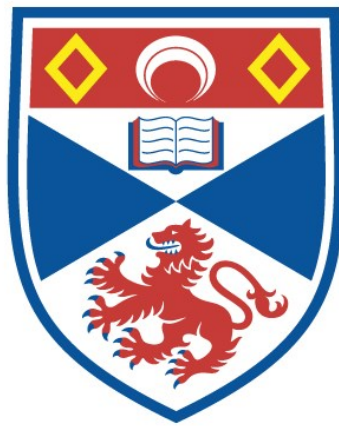


ELEMENTS OF A 200 WATT PULSED EXCIMER
LASER

Glen McDuff

A Thesis Submitted for the Degree of PhD
at the
University of St Andrews



1998

Full metadata for this item is available in
St Andrews Research Repository
at:

<http://research-repository.st-andrews.ac.uk/>

Please use this identifier to cite or link to this item:

<http://hdl.handle.net/10023/13926>

This item is protected by original copyright

ELEMENTS OF A 200 WATT
PULSED EXCIMER LASER

by

GLEN MCDUFF

for

ST. ANDREWS UNIVERSITY
ST. ANDREWS, FIFE, SCOTLAND
AUGUST 1987



ProQuest Number: 10166919

All rights reserved

INFORMATION TO ALL USERS

The quality of this reproduction is dependent upon the quality of the copy submitted.

In the unlikely event that the author did not send a complete manuscript and there are missing pages, these will be noted. Also, if material had to be removed, a note will indicate the deletion.



ProQuest 10166919

Published by ProQuest LLC (2017). Copyright of the Dissertation is held by the Author.

All rights reserved.

This work is protected against unauthorized copying under Title 17, United States Code
Microform Edition © ProQuest LLC.

ProQuest LLC.
789 East Eisenhower Parkway
P.O. Box 1346
Ann Arbor, MI 48106 – 1346

ELEMENTS OF A 200 WATT PULSED EXCIMER LASER

A thesis presented by George Glen McDuff, B.S.E.E., to the University of St. Andrews in application for the degree of Doctor of Philosophy.

August, 1987

AUTHOR'S CAREER

George Glen McDuff was born in Lubbock, Texas in 1956. After attending the local public schools he received a Bachelor of Science degree in Electrical Engineering from Texas Tech University in 1979. After graduation he was employed at the Los Alamos National Laboratory to establish and operate a laboratory specifically for the assessment and development of high repetition rate components for pulsed excimer lasers of high average power and various other systems. Mr. McDuff remained at Los Alamos until March of 1987 except for a one year excursion into the commercial sector to design a modulator for a repetitively pulsed x-ray source. Mr. McDuff has worked as a consultant for seven commercial laser companies and numerous other facilities. In 1985, Mr. McDuff was appointed as the Program Manager for the Strategic Defence Initiative Organization's High Power Thyatron Development Program. He also sits on the technical committee of the IEEE Power Modulator Symposia, the U.S. Department of Defence High Voltage Workshops, and is a member of the Power Advisory Group for the Strategic Defence Initiative Organization.

DECLARATION

I hereby certify that this thesis has been composed by me, and is a record of my original work, and has not previously been presented for any degree.

George Glen McDuff

CERTIFICATE

I certify that George Glen McDuff has spent nine terms of research work, under my supervision, that he has fulfilled the conditions of Ordinance No. 16 (St. Andrews) and that he is qualified to submit the following thesis in application for the degree of Doctor of Philosophy.

Dr. A. Maitland
Department of Physical Sciences
University of St. Andrews

ACKNOWLEDGMENT

It is not practical in this short space to acknowledge everyone that contributed to this work with comments, suggestions, and discussions. However, I would like to express my appreciation to Phillip N. Mace, who for over a decade, has supported high repetition rate circuit development on a wide range of topics. Without this continued support none of the developments reported herein in the area of repetitive circuits and lasers would have been made on such a timely scale.

ELEMENTS OF A 200 WATT PULSED EXCIMER LASER

Abstract

This thesis describes the theoretical and experimental investigation into many aspects of circuit and component design for high average power short pulse systems. The primary objective of this work is to develop both circuit design criteria and pulsed components for long life rare gas halide lasers.

A pulsed system consists of three major components, energy storage, switches, and load. This investigation considers the type of circuit which uses capacitive energy storage in combination with a closing switch to transfer electrical power to a load. Specific loads are not addressed but the implications of load characteristics that affect circuit/component design and life are considered.

The investigation reported, describes the physical and electrical characteristics and analysis of phenomena that adversely affect the performance and life of pulse duty components. In the area of capacitive storage, lifetimes of one particular design was improved by 3 orders of magnitude and a means of detecting the imminent failure of oil filled capacitors was devised and patented. In the area of switching, methods are described by which hydrogen thyratrons can be operated in parallel with equal current sharing without the need for inductive or resistive ballasting. Finally, the design and testing of a 200 watt XeCl laser modulator is presented.

ELEMENTS OF A 200 WATT PULSED EXCIMER LASER

INDEX

	Page	
Chapter 1	Introduction	1
	1.1 Objectives	3
	1.2 Motivation	4
	1.3 Approach	5
	References	9
Chapter 2	Component Descriptions	
	2.1 Capacitors	10
	2.2 Switches	16
	References	23
Chapter 3	Experimental Apparatus	
	3.1 Laboratory Design and Layout	24
	3.2 Charging Systems	25
	3.3 Diagnostics	28
	3.4 Grounding and Shielding	37
	References	47
Chapter 4	Capacitors	
	4.1 Capacitance	48
	4.2 Inductance	56
	4.3 ESR	69
	4.4 Mechanical Forces	85
	4.5 Lifetimes and Failure Mechanisms	101
	References	131
Chapter 4A	Device for Detecting the Imminent Failure of High Dielectric Stress Capacitors	139
Chapter 5	Switches	
	5.1 General	147
	5.2 Spark Gaps	148
	5.3 Thyratrons	153
	References	174
Chapter 6	High Repetition Rate Modulator Design for a Pulsed Excimer Laser	177
	References	226
Appendix 1	Voltage Probe Construction Details	
Appendix 2	Forces on a Capacitor	
Appendix 3	Charging System Analysis	

LIST OF FIGURES

- Figure 2.1.1 Basic spirally wound capacitor construction.
- Figure 2.1.2 Basic ceramic dielectric capacitor construction.
- Figure 2.1.3 Reconstituted mica paper capacitor construction.
- Figure 2.1.4 High repetition rate pulse discharge test capacitors.
- Figure 2.1.5 Pulse capacitor equivalent circuit.
- Figure 2.2.1 Basic ceramic hydrogen thyratron design.
- Figure 2.2.2 Cross sectional diagram of a ceramic thyratron with a "hollow anode".
- Figure 2.2.3 Cross sectional diagram of a typical dispenser cathode metal-envelope thyratron.
- Figure 2.2.4 The race track style core constructed of ferrite tiles.
- Figure 3.1.1 Laboratory grounding and shielding layout.
- Figure 3.2.1 Schematic of discharge circuit with resonant charge.
- Figure 3.2.2 Electrical waveforms for resonant charge circuit.
- Figure 3.2.3 Pulse transformer charging and discharge circuit schematic diagram.
- Figure 3.4.1 Spurious signals from power distribution wiring techniques.
- Figure 3.4.2 Power distribution diagram for laboratory.
- Figure 3.4.3 High Repetition Rate Component Development Laboratory.
- Figure 4.2.1 Lumped equivalent of discharge circuit.
- Figure 4.2.2 Model of outer winding and current return of a spirally wound capacitor pack.
- Figure 4.2.3 Cross section of winding layer of a spirally wound capacitor pack.
- Figure 4.2.4 Three generations of spirally wound dielectric film capacitors.

- Figure 4.3.1 Low frequency equivalent AC circuit and resultant vector diagram.
- Figure 4.3.2 Effect of lead inductance on measured value of capacitance.
- Figure 4.3.3 Temperature dependence of dissipation factor in capacitor grade Teflon.
- Figure 4.3.4 Dissipation factor as a function of frequency for Teflon and Teflon compounds.
- Figure 4.3.5 Modulator/calorimeter schematic diagram.
- Figure 4.4.1 Diagram for force analysis in ceramic capacitors.
- Figure 4.4.2 Time varying capacitance of a normal dielectric film oil impregnated capacitor during the discharge.
- Figure 4.5.1 Electrical waveforms for short pulse capacitor test circuit.
- Figure 4.5.2 Damage caused by arcing between compression bonded capacitor packs.
- Figure 4.5.3 Pictorial of 1 nF 30 kV spirally wound capacitor.
- Figure 4.5.4 CAT scanned capacitor pack.
- Figure 4.5.5 Dielectric damage in a spirally wound silicone oil polypropylene capacitor.
- Figure 4.5.6 Life versus repetition rate for polypropylene capacitors.
- Figure 4.5.7 Case temperature for a mylar/paper and a Teflon dielectric test capacitor.
- Figure 4.5.8 Weibull statistical plot for G2.7 capacitors.
- Figure 5.2.1 High Repetition rate trigatron spark gap.
- Figure 5.2.2 High repetition rate, gas blown, coaxial spark gap [Veradyne, 1976].
- Figure 5.3.1 Anode fall as a function of trigger impedance for a 7.62 cm (3") diameter thyatron.
- Figure 5.3.2 Switching jitter as a function of trigger impedance for a 7.62 cm (3") diameter thyatron.
- Figure 5.3.3 Thyatron life as a function of peak current for a 7.62 cm (3") diameter thyatron.

- Figure 5.3.4 Life as a function of di/dt in 11.4 cm (4.5") diameter thyratrons.
- Figure 5.3.5 Energy dissipated in a thyatron switched, 120 nS pulsewidth, 1000 pps modulator.
- Figure 5.3.6 Conventional circuit for parallel operation of thyratrons [Glasoe and Lebacqz, 1946].
- Figure 5.3.7 Trigger control system block diagram.
- Figure 5.3.8 Three thyatron 10 ohm "hard" parallel thyatron test circuit.
- Figure 6.1.1 The capacitor pulse charge laser circuit.
- Figure 6.1.2 Illustration of laser head cross section.
- Figure 6.1.3 Layout for minimum inductance and equivalent circuit of the discharge loop.
- Figure 6.1.4 Diagram for defining terms in Equation 6.1.8.
- Figure 6.1.5 Final equivalent circuit of the laser discharge loop.
- Figure 6.1.6 Proposed equivalent circuit of the primary loop.
- Figure 6.1.7 General layout of the laser head and modulator.
- Figure 6.1.8 Layout and equivalent circuit of one fifteenth of the C_1 capacitor bank.
- Figure 6.1.9 High repetition rate laser prototype modulator cross sectional diagram.
- Figure 6.1.10 Capacitor bank C_1 buss plate showing thyatron connections.
- Figure 6.1.11 The primary and discharge loop equivalent circuits for the repetitive laser modulator.
- Figure 6.1.12 Primary loop current waveform.
- Figure 6.1.13 Laser gap voltage waveform.
- Figure 6.1.14 Discharge loop current waveform.
- Figure 6.2.1 Cross sectional diagram of upgraded laser modulator.
- Figure 6.2.2 Modulator schematic with magnetic pulse compressor circuitry.
- Figure 6.2.3 BH curve for lithium zinc material used in the magnetic core.

- Figure 6.2.4 Final lumped equivalent circuit for the upgraded laser modulator.
- Figure 6.2.5 Primary loop current waveform.
- Figure 6.2.6 Voltage waveform across C_2 , the primary side of the magnetic switch.
- Figure 6.2.7 Voltage waveform across C_3 , or laser gap voltage.
- Figure 6.2.8 Discharge loop current waveform (one-half amplitude).

CHAPTER 1

INTRODUCTION

During World War II, a tremendous research and development effort was undertaken into the development of radar. Under the direction of the Office of Scientific Research and Development, the Massachusetts Institute of Technology Radiation Laboratory was formed to document and coordinate the research effort. Thousands of researchers in the United States, the United Kingdom, Australia, Canada, and many commercial laboratories were involved. The sum of the results were documented in 28 volumes.

One part of this massive research program was the development of pulsed circuitry to drive the microwave oscillators. The original goal of the pulse generator effort was to develop a long life reliable unit to produce a 100 kilowatt pulse of 1 microsecond duration at 1000 pps into a 50 ohm load. The development program extended far beyond the original goal in all aspects. It became clear to the researchers that their work was not only applicable to radar but to many aspects of physics and engineering. Many of the original researchers went on to lucrative careers in the radar, accelerator, and weapons industry.

Out of the research, one particular circuit became dominant over all others. It used a capacitor as an energy store and a hydrogen thyratron as a closing switch to discharge the store into the load. To this day, these are still the most used components in the generation of high power pulses. Hydrogen thyratrons are used more than all

other switches combined in the generation of repetitive high power pulses and the pulse capacitor requirement is large enough to support more than 30 companies worldwide that specialize in this type of device.

Over the past 45 years the need for repetitive circuits has expanded and changed to the point where today, there are hundreds of different uses. The radar market is still quite large but accelerators, lasers, and pulsed RF generation are growing uses of repetitive pulse power technology. Repetitive accelerators have greatly expanded the need for new high power components. Beam deflectors requiring 200 kHz kilovolt pulses at low impedances are under development in the Soviet Union [Breslavtsev, 1972]. Short pulses on the order of 5 ns at 1000 pps are needed for electron drives in LINACs [Kitchen, 1982]. The Advanced Test Accelerator [Reginato, 1980], an induction LINAC, has need of pulse components capable of operation at over a hundred amperes average and 5000 amperes RMS at repetition rates of 5000 pps. This application pushes the repetitive pulse technology well into the Megawatt average power range. With the invention of the discharge laser, a whole new realm of pulse requirements emerged. In the late 1970's and early 1980's many of the laser and accelerator "laboratory devices" moved into industrial and military environments where the available technology is stressed to the breaking point in terms of life and reliability. The investigations reported herein are just some of those which were initiated in the United States to extend the effective range of high power pulse circuitry.

1.1 OBJECTIVES

This thesis describes a theoretical and experimental investigation into many aspects of circuit and component design for pulsed systems which operate at average powers up to the Megawatt level. The primary objective is to develop both circuit design criteria and components for reliable generation of short pulses at high repetition rates with long life. Closing switches and capacitors are the main area of investigation and several types of switches are reviewed as well as many types of capacitors. Pulsed systems deliver energies in times from picoseconds to seconds at rates from a few pulses per day to hundreds of thousands of pulses per second, at voltages from thousands to millions, at currents up to a Megampere. It is impossible to investigate all the characteristics of components over such a wide dynamic range of parameters so a specific range was chosen for this investigation. The main goal of this endeavour is the development of a pulse generation system with lifetimes of 10^{10} pulses operating into low impedance loads. Specific electrical parameters set forth at the beginning of the programme are:

Switch Voltages = 50 kV

Switch Currents = 50 kA

Switch di/dt = 10^{12} A/s

Repetition Rates = 1000 pps

Reliability > 0.99

Load Impedance < 0.5 ohms.

1.2 MOTIVATION

The major driving factor behind this investigation is the requirement for reliable discharge pumped laser with long life. As "laboratory devices" moved into the "real world" where life, reliability, and availability are major concerns, switches and capacitors were quickly shown to have major limitations. The ensuing industrial and military applications demanded higher repetition rates and average power which simply could not be achieved with the available components. Accurate data on the performance and life of pulsed components in these circuits was sketchy at best and practically no guidelines for the design engineer existed. This led to a jumble of short-term development efforts aimed at solving only the immediate system problems without understanding the physical mechanisms that limited the performance of the components. For years device development by empirical methods was the only means in which the needs of many systems could possibly be met. This resulted in sporadically placed data points of life and discharge parameters as the only reference a designer had available when a new set of parameters was encountered. With no component data base on which to base new designs, many multi-million dollar systems failed completely or fell well short of their goals due to the lack of reliable high repetition rate components. The prime example of this short-fall is the discharge pumped excimer laser. Excimer lasers designed to deliver powers of a kilowatt appeared only four years after the discovery of this type of laser. Commercial companies (many of which are no longer with us)

based their products on the premise that scaling to higher powers was a trivial matter. They believed that to increase the duty cycle it was merely necessary to increase the repetition rate of the one pulse-per-second laser to 1000 pps by simply getting a larger switch, a gas flow system, and a bigger power supply. The U.S. government based a hundred million dollar program on this premise. Unfortunately this premise proved to be ill-founded. Both the switches and the energy storage capacitors proved to be inadequate and short lived under the new duty. If a large dollar investment goes sour because the primary switch only lasts a few hours and the energy storage just a few more, it is a hard lesson to learn. In retrospect, it was learned that perhaps if the "homework" had been more thorough, failure would not have followed. From these experiences, it was evident that a careful investigation of the effects of duty cycle on switches and capacitors was essential to provide the data required for scaling to higher average powers.

1.3 APPROACH

The research programme which forms the basis of this thesis aims to provide data relevant to the scaling of pulse systems to higher powers. The main aspects of the research plan are outlined in Table 1.1.1.

Probably the most important part of the plan is the actual testing of the devices. Since developing highly reliable lasers is the principle motivation behind the investigation it would be ideal to test these components in

1. Develop an accurate electro-mechanical model of the test components.
2. Test components in simulated discharge circuits.
3. Collect statistical data.
4. Autopsy of failures to determine failure mechanisms.
5. Model the failure mechanisms.
6. Develop diagnostics to detect imminent failure.
7. Develop criteria for accelerated testing.

Table 1.1.1 High Repetition Rate Component Development
Programme Plan

an actual discharge laser. However, operating a laser for the extended periods of time required to accumulate sufficient data for analysis is prohibitively expensive so the testing is done with a circuit designed to simulate a discharge laser. This consequence of economics will always cast doubt as to the effectiveness of the results in predicting performance in a real laser system.

Along with the electrical data taken during testing, statistical data are acquired. This will give future engineers a basis for justifying designs of high repetition rate circuits. Data are evaluated in terms of the Weibull distribution of fatigue life of components.

Autopsies are necessary to determine the cause of component failure. Detailed electrical, mechanical, and chemical parameters are taken of each specimen. Once the

causes of failure are identified, the sequence in which the phenomena occurred can be derived and appropriate changes in design can be recommended.

In circuits operated at high average powers, failure is often catastrophic. When hundreds of kilowatts of average power are involved this often leads to a dangerous situation. With this in mind, it was planned to investigate means of detecting when a component would fail and ways of averting a catastrophic failure. For fluid impregnated film capacitors this effort was successful and the resulting device was patented.

The last major topic of Table 1.1.1 is addressed on the assumption that the investigation would lead to device improvements. As pulse components achieve longer lives, evaluation takes longer. To reduce the amount of time and money spent in testing components and to reduce the time which laboratory equipment is occupied, accelerated testing procedures were established.

In the following thesis a brief description of the capacitors and switches investigated is given in Chapter Two in order that the reader may become acquainted with the terminology used throughout this report. Figures and description presented in this chapter will be used and referred to throughout the thesis. Because previous work is scattered and disjointed, most of this information will be presented in the body of the text as needed for explanation. Chapter Three will review the experimental apparatus including the basic test circuit (variations to the test circuits will be discussed as appropriate). Models of the

components discussed in Chapter Two will be explained and the diagnostics used in the investigation are reviewed. The remainder of the report presents the body of the research investigation into capacitors and switching. Chapter Six relates a complete detailed design and test results of a 200 watt average power excimer laser with one stage of magnetic pulse compression.

References for Chapter 1

- Breslavtsev, I.D., Venikov, V.D., Dvornikov, N.I., Kuleshov, I.L., Latushkin, S.T., Resov, V.A., Chumakov, N.I., and Yudin, L.I., "Use of Deflection Bunching to Obtain Intense Short Neutron Pulses in the Cyclotron," *Pribery i tekhnika eksperimenta*, No.4, July-August 1972.
- Kitchen, H.D. and Salome, J.M., "Thyratron Switch Generation of Multi-Kilovolt Pulses in the Nanosecond Region for LINAC Electron Gun Drive," *Sixteenth Power Modulator Symposium*, June 1982.
- McDuff, G., "Advanced Pulsed Power Techniques in High Average Power Excimer Lasers," *High Voltage Workshop*, Sponsored by the Dept. of Defense, Adelphi, MD, October 3-4, 1983 [CLASSIFIED].
- Reginato, L.L., and Hester, R.E., "Overview of the ETA/ATA Pulse Power," *Fourteenth Power Modulator Symposium*, June 1980

CHAPTER 2
COMPONENT DESCRIPTIONS

2.1 CAPACITORS

High repetition rate discharge capacitors come in essentially two styles. The first to be described is the dielectric fluid impregnated spirally wound film type. The basic spirally wound impregnated capacitor section with descriptive nomenclature is seen in Figure 2.1.1. This type of capacitor section is wound on a removable bobbin in a conductive foil/dielectric sandwich.

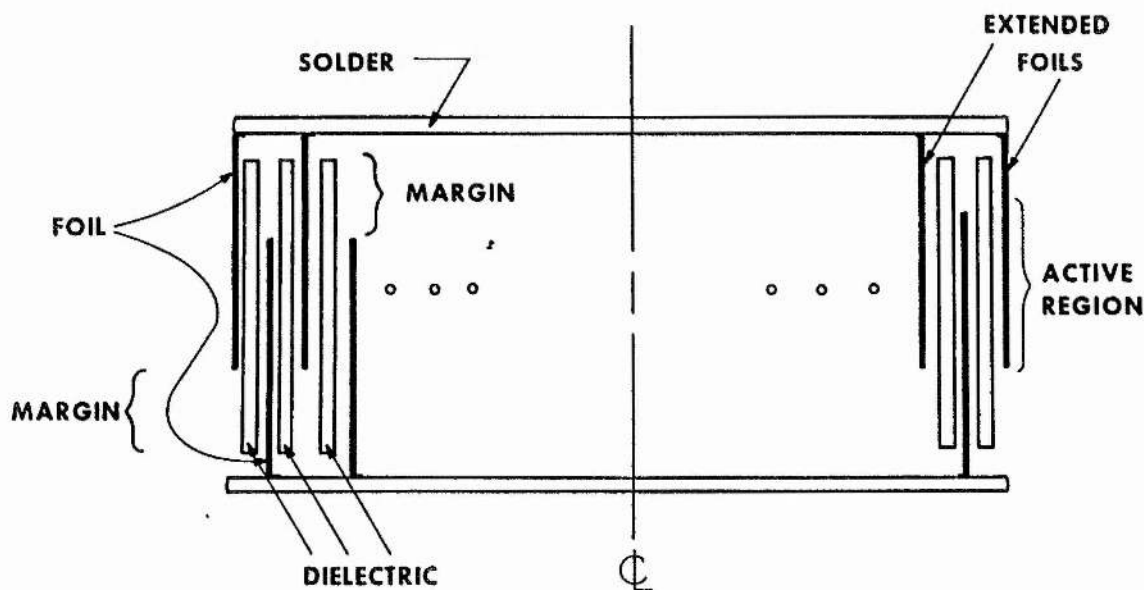


Figure 2.1.1 Basic spirally wound capacitor construction.

It can be seen in Figure 2.1.1 that the actual capacitance is in the active region (overlap). The dielectric is extended out past the active region in an area called the margin to prevent high voltage breakdown between the charge conductors or plates. A breakdown in the margin is referred

to as a flashover. The section depicted illustrates the extended foil type of construction. This is where the foils of the winding are extended past the dielectric film, folded radially inward and soldered together. In cross section, the unit appears as a set of nested coaxial cylinders. The dielectric always consists of several (minimum of three) thinner film layers. Using multiple layers of thin dielectrics increases the overall dielectric strength by reducing the chances of a bulk failure caused by an imperfection in one of the layers. Further details on construction considerations and techniques along with electrical characteristics are discussed in following sections. The capacitor sections (Figure 2.1.1) are designed to operate in the range of 5 to 10 kV. Depending upon the exact material, there is a minimum in the energy density - margin length curve between 5 and 10 kV. These sections are connected in series/parallel arrangements via wide foil conductors to arrive at the desired capacitance and voltage rating.

Another common type of pulsed capacitor incorporates a solid ceramic dielectric. Figure 2.1.2 depicts the construction of the industry standard for ceramic titanate capacitor. The dielectric slug is ground to exacting tolerances to determine the capacitance. Both ends of the slug are metallized and stress relief plates are brazed onto the slug. The function of the stress relief plates is to grade the electric field stress on the edge of the metallization and to provide a large area of contact. A threaded terminal is welded or brazed onto the stress relief

plate. A strong bond between the terminal and the dielectric slug is essential due to electrostrictive nature of the ceramic. Mechanical forces produced in a ceramic capacitor can attain multiple kilo-Newton magnitudes resulting in damage to the capacitor connections. This topic is addressed in detail in Section 4.4. Strontium and barium titanate compounds are the most common materials used in ceramic type capacitors. Dielectric voltage stress for ceramic capacitors is in the range of 10 to 30 kV/cm depending on the dielectric material and unit design.

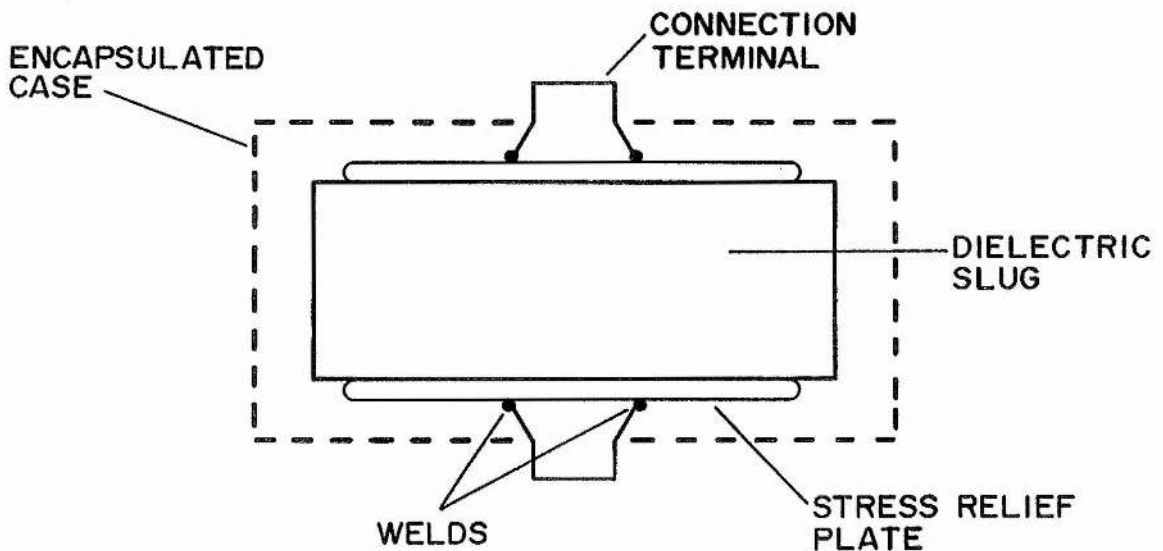


Figure 2.1.2 Basic ceramic dielectric capacitor construction.

The second common type of solid dielectric capacitors uses reconstituted mica paper as a dielectric. Natural mica is ground into a crystal powder, mixed with a binder, and processed into a paper. This type of capacitor can be designed to have an extremely long life. Aluminum and

reconstituted paper are over-lapped in a multilayer sandwich configuration as depicted in Figure 2.1.3. The foil ends

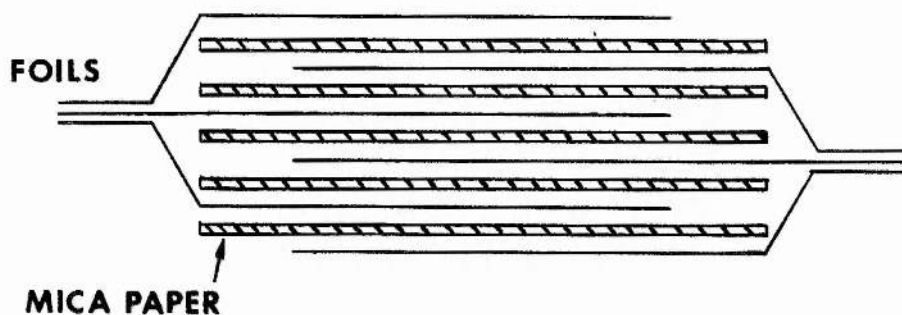


Figure 2.1.3 Reconstituted mica paper capacitor construction.

are extended, folded over, and soldered to make a basic capacitor pack. A typical capacitive pack will operate at a maximum voltage of 5 to 10 kV (cf. spiral packs). These voltages are rarely exceeded because the "margin" areas begin to reduce the volume energy density. A number of these packs are then connected in series/parallel in much the same way as with the spirally wound units to create the desired capacitance value.

Capacitors of the types described are the subjects of this investigation. A photograph of six of the test capacitors are shown in Figure 2.1.4. Working from left to right, the rectangular black capacitor is of the mica paper construction. Note the large surface area leads that help to reduce the inductance of the connections. In front is a brown phenolic cylinder containing an example of the third

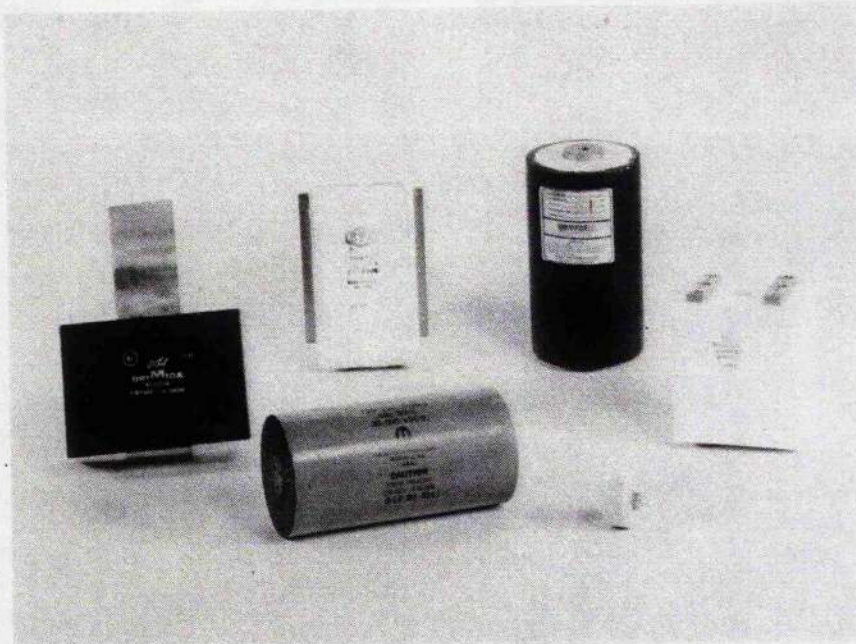


Figure 2.1.4 Six high repetition rate pulse capacitors.

generation of silicon oil/Teflon-film spirally wound capacitor. Behind this is a rectangular style silicon oil/polysulfone spiral unit and to the right is a silicon oil/polypropylene capacitor of the spiral type. The small disk shape capacitor in the foreground is a SrTiO_3 ceramic unit and the last capacitor on the far right is another spirally wound silicon oil/polypropylene unit. It is interesting to note that all the capacitors in Figure 2.1.4 have identical electrical specifications. The size variations are due to the difference in relative dielectric constants of the storage material. Polypropylene has a constant of 2.5 and can operate at a D.C. voltage gradient up to 197,000 V/mm (5000 volts/mil) in low repetition rate service. Polysulfone is slightly higher in dielectric constant at 3.1 and operates at about the same voltage gradient. Reconstituted mica paper has a relative

dielectric constant of 7-8 but can operate only at gradients up to 39,400 V/mm (1000 volts/mil). Strontium titanate used in capacitors has a dielectric constant greater than 1500 so these units are much smaller and store energy at much greater densities than the spirally wound type. However, SrTiO_3 can tolerate no more than 7870 V/mm (<200 volts/mil) in low repetition rate operation. The dielectric stresses quoted above are from the existing data base [Boicort, 1970] and manufacturer data for single shot to one pulse per second duty.

EQUIVALENT CIRCUIT

To investigate the electrical properties of a pulsed capacitor it is convenient to describe the device in terms of a lumped model. A basic equivalent circuit for a capacitor is seen in Figure 2.1.5. Series losses, also known as equivalent series resistance, ESR, are defined by

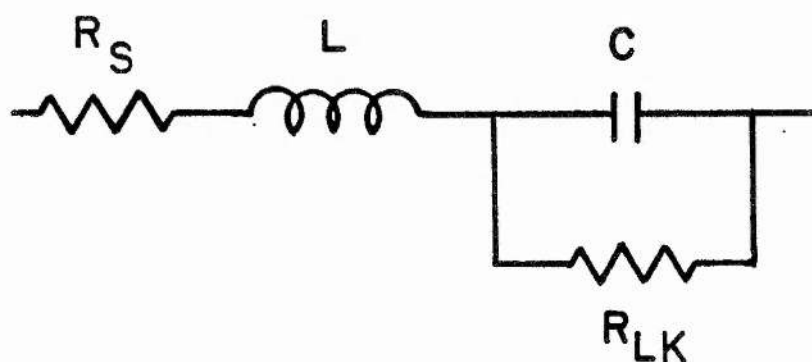


Figure 2.1.5 Pulse capacitor equivalent circuit.

R_S , these include connections, skin effect resistance, and dielectric losses. Resistor R_{LK} , represents the dielectric

loss associated with leakage currents and case dissipation. Since a quantitative theory of dipolar materials relevant to capacitors is poorly developed, total dielectric losses are lumped into both R_S and R_{LK} . The dielectrics available today have such extremely small losses that the leakage resistance can approach many tens of Megohms. For the purpose of service at high repetition rates where the times between charging and discharging are short, this element has no significant effect on the electrical characteristics. Thus, the equivalent circuit becomes a simple RLC series network. In contrast to the leakage resistance, with the advent of low loss dielectrics, the series resistance has become extremely small and is commonly less than a milliohm. This presents a real challenge for detection and measurement as will be seen in Section 4.3. The inductor L , is the lumped series inductance which the capacitor exhibits in circuit. Values of L typical for high repetition rate capacitors are from 5 nH to 500 nH. Factors determining the series inductance are discussed in Section 4.2. Element C , is simply the real capacitance of the unit as defined in Equation 4.3.6 of Section 4.3.

2.2 SWITCHES

Several types of switches are commonly used in high repetition rate service. Of the six most common, only two have life and switching characteristics suitable for use in high reliability short pulse modulators. General switch characteristics for commonly used repetitive switches are detailed in Chapter 5. In this section, the physical

descriptions of the two switches, thyratrons and magnetics, that are the main subject of this investigation will be presented.

The most commonly used switch in all high power pulse applications is the hydrogen thyatron. Life, power gain, and switching characteristics of thyratrons make them the ideal switch for short pulse modulators operating at very high repetition rates and very high average powers. Because of the great versatility of hydrogen thyratrons, variations of the basic types are as numerous as there are applications [Burkes and McDuff, 1987]. During this investigation, 26 different thyratrons were evaluated. Obviously, it is not appropriate to describe the construction of all the switches tested. Likewise, to protect manufacturers' proprietary information, it is not ethical to describe, in detail, the most successful thyatron designs which were made available for development purposes during the programme. Rather, a general description of thyratrons for laser circuits is presented to acquaint the reader with the devices.

High power thyratrons come in two basic types, the oxide cathode/ceramic envelope and the dispenser cathode/metal envelope. At last count, there were over 150 different ceramic and a dozen or so metal envelope thyratrons available commercially. However, since the main motivation for this investigation is high power pulsed lasers, this narrows the number of thyatron candidates to just a few.

A typical oxide cathode/ceramic envelope thyatron for use in a short pulse circuit is shown in Figure 2.2.1. The

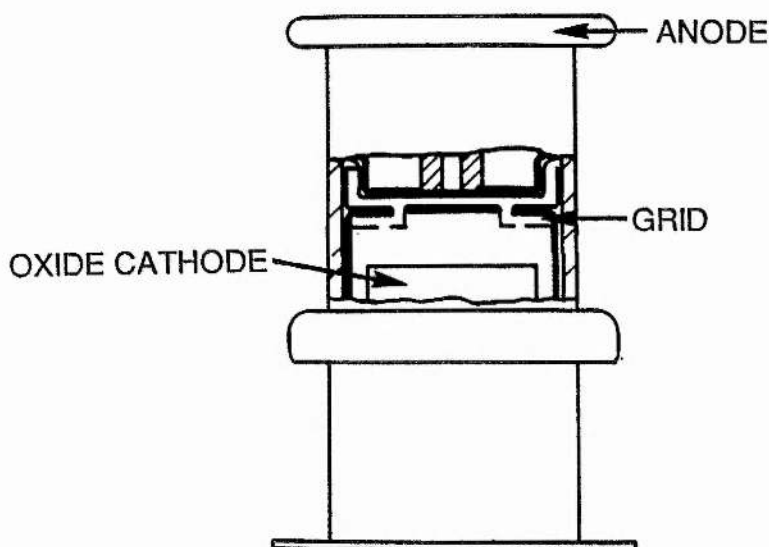


Figure 2.2.1 Basic ceramic hydrogen thyatron design.

tube consists of a cathode coated with a mix of calcium, strontium, and barium oxides, a grid(s), and an anode. The basic thyatron is essentially a gridded diode that can conduct in only one direction. In 1978, a new type of thyatron was introduced designed specifically for pulsed lasers [Menown and Neale, 1978]. This new thyatron incorporated a "hollow anode" which allows the tube to conduct in the reverse direction without arcing. A cross sectional diagram of a ceramic envelope hollow anode thyatron is shown in Figure 2.2.2. The cavity anode provides a source of electrons to support conduction in the reverse direction. Because of the time varying and extremely low impedance of a laser discharge, efficient matching of the impedance of the energy store to the load

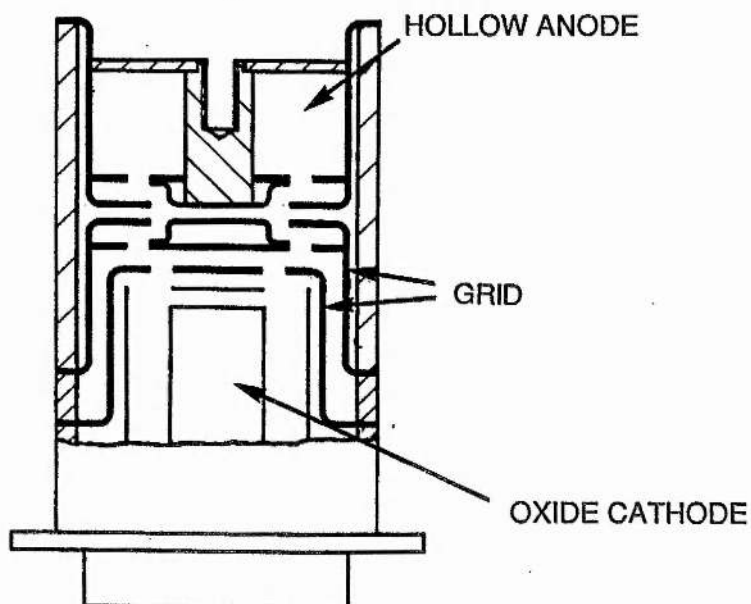


Figure 2.2.2 Cross sectional diagram of a ceramic thyatron with a "hollow anode".

is practically impossible. It was concluded in the early stages of this investigation that it would be far easier and more economical to develop a switch that would operate in a mismatched circuit, than to attempt to develop nonlinear circuitry to match the load. For this reason, a large development effort was undertaken to advance the hollow anode thyatron [McDuff et.al.,1983,1984]. Successes with oxide cathode designs were excellent but the power handling capability of a single tube is inadequate for use with excimer lasers of mean power greater than about 100 watts. An 11.4 cm diameter, 30 cm long ceramic hollow anode thyatron can switch about 10 kw of average power in a laser circuit. A dispenser cathode/metal envelope thyatron of the same physical size, can switch approximately three times as much power. Thus the development proceeded with the investigation of the hollow anode dispenser cathode tubes. Higher average power can be switched in a metal envelope

thyatron because of the greater emission properties of the dispenser cathode and the construction methods. A detailed examination of this type of thyatron is given by Cook [1961]. While the ceramic thyatron is constructed of cup shaped electrodes supported by ceramic tubes, the metal-envelope tube is somewhat more complex. A cross section of a typical dispenser cathode/metal envelope thyatron is seen in Figure 2.2.3. An important feature of this design

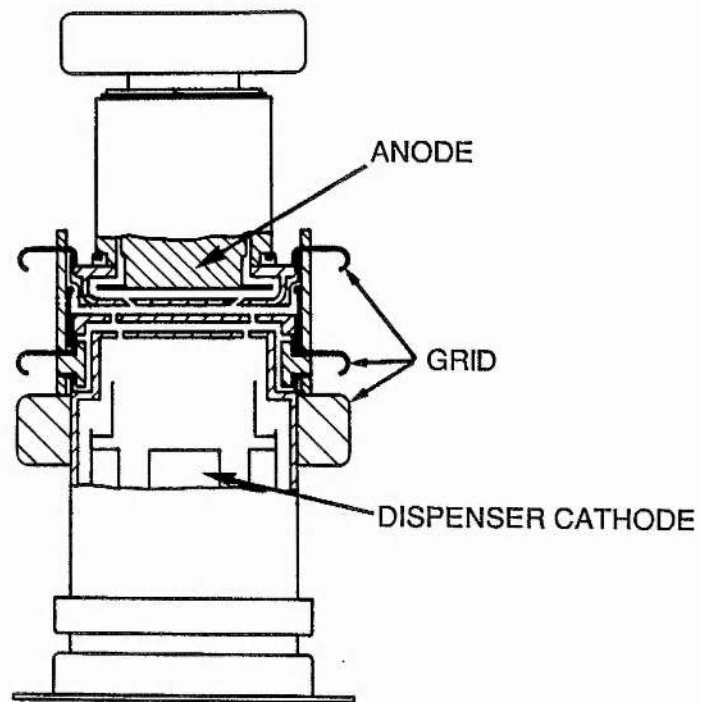


Figure 2.2.3 Cross sectional diagram of a typical dispenser cathode metal-envelope thyatron.

is the manner in which the massive anode is completely enclosed by the grid structure. This enhances the cooling of the anode and the high voltage recovery of the tube [Cook 1960, 1962]. Fast recovery is an all-important requirement

in a high repetition rate circuit, so the metal envelope thyratron is a natural choice for these applications.

The other type of switch which is well suited for high repetition rate applications is the magnetic switch. Magnetic switching, as the name implies, uses the nonlinear properties of magnetic material to perform a closing switch function. A magnetic switch is designed for a particular set of electrical and physical properties so there are no "typical" devices. Because of the physical properties of ferrite, this type of material is better suited for short pulse applications than metallic tapes or powders. The particular design chosen in this investigation is constructed of 60 ferrite tiles cemented together to form the "race track" core pictured in Figure 2.2.4. A complete

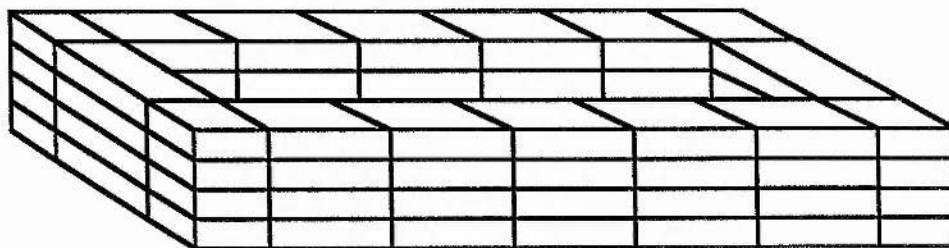


Figure 2.2.4 The race track style core constructed of 60 ferrite tiles.

design of the magnetic switch in Figure 2.2.4 is given in Chapter 6.

Several types of spark gaps were examined for use in laser circuits. Spark gaps surpass every requirement of a laser switch except lifetimes. In a high repetition rate modulator of a 200 watt excimer laser, the best spark gap will only give several hours [Butcher, et.al.,1982] of reliable operation. Rail gaps can extend this life somewhat, but life is still millions of shots less than that of a thyratron. A more detailed look at all of the high repetition rate switches is found in Chapter 5.

References for Chapter 2

- Burkes, T.R., ed., "A Critical Assessment of High Power Switches--1987 Edition," Naval Surface Weapons Center, Dahlgren, VA, 1987, G. McDuff Chapter author.
- Butcher, R.R., Tennant, R.A., Erickson, G.F., Swisher, S.L., Willis, W.L., "A High Average Power Excimer Laser," Proceedings of CLEO, 1981.
- Boicourt, G., "Problems in the Design and Manufacture of Energy Storage Capacitors," Los Alamos Scientific Laboratory report LA-4142-MS, 1970.
- Cook, K.G., "A High Power Metal Envelope Deuterium Thyatron," Sixth Symposium on Hydrogen Thyratrons, 1960.
- Cook, K.G., "A Compact Metal-Ceramic Deuterium Thyatron," Seventh Symposium on Hydrogen Thyratrons and Modulators, 1962.
- McDuff, G., "Test and Evaluation of the CX-1574 Thyatron," EEV Technical Reprint, EEV Co. Ltd. Chelmsford, Essex, England, CMI 2QU, 1983.
- McDuff, G. and Rust, K., "Evaluation of Bidirectionally Conducting Thyratrons for Pulsed Excimer Lasers," IEEE Sixteenth Power Modulator Symposium, June 1984.
- McDuff, G. and Rust, K., "A Short Note on Hollow Anode Metal Envelope Thyratrons for High-Power High Repetition-Rate Lasers," EEV Technical Reprint 159, EEV Co. Ltd. Chelmsford, Essex, England, CMI 2QU, 1985.
- Menown, H. and Neale, C., "Thyratrons for Short Pulse Laser Circuits," IEEE Thirteenth Pulse Power Modulator Symposium, June, 1978.

CHAPTER 3
APPARATUS AND DIAGNOSTICS

3.1 LABORATORY DESIGN AND LAYOUT

The laboratory houses four major sub-systems; these are: {1} charging circuits; {2} diagnostics; {3} grounding and shielding; and {4} the component development circuits. The block diagram in Figure 3.1.1 illustrates the general layout of the laboratory. An important feature is that any sub-system can be operated separately or in conjunction with the other sub-systems or with outside components.

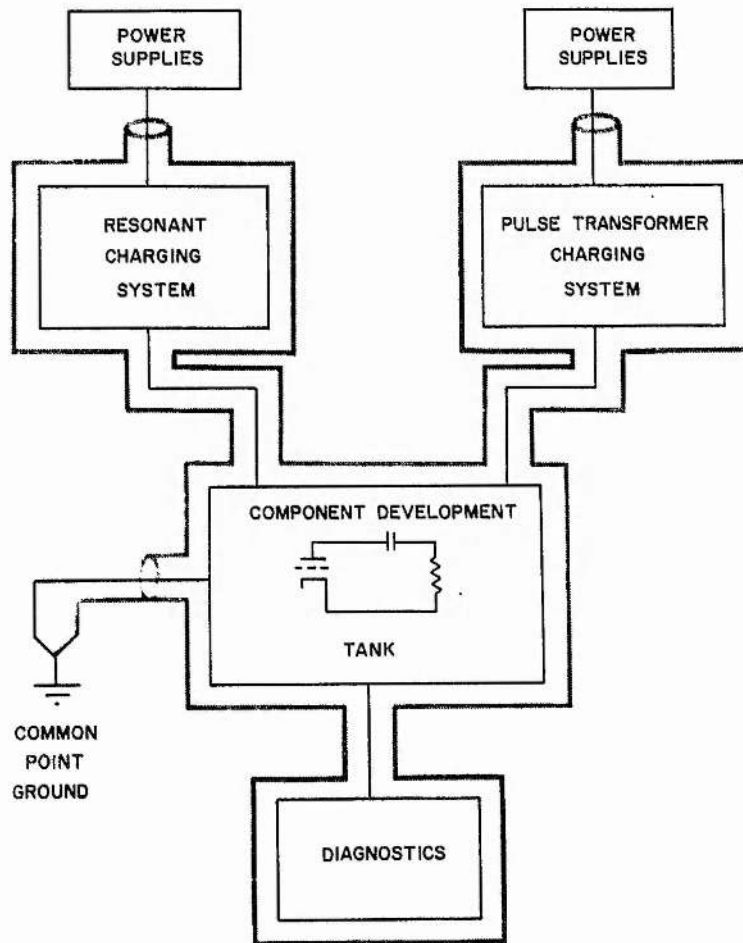


Figure 3.1.1 Laboratory grounding and shielding.

3.2 CHARGING SYSTEMS

Two charging systems were constructed as part of the research programme. One charging system is a conventional series resonant circuit [Glasoe and Lebacqz, 1948]. This is the most common type of charging in repetitive circuit because it uses only passive components. The second system utilizes a transformer with a thyatron switch in its primary circuit to control the time which charging occurs. This system is often called transformer command charging. Both forms of charging are needed to gain a better understanding of the time-dependent effects of electric fields on component life.

A schematic diagram of the discharge and resonant charge circuit is presented in Figure 3.2.1. A mathematical analysis of the resonant charge circuit is given in Appendix 3. The resonant circuit charges the storage capacitor with relatively low values of dV/dt . At low repetition rates, the time which voltage is applied to the capacitor is nearly equal to the interpulse period. The laboratory circuit can operate at voltages up to 80 kV, at average powers up to 20 kW, at repetition rates up to 2000 pps, and a maximum charging dV/dt of 160×10^6 volts/second. Figure 3.2.2 shows an oscilloscope photo of a typical pair of charge voltage and current waveforms. The "1 - cos" waveform is the charge voltage and the sinusoidal waveform is the charge current. The time-scale in Figure 3.2.2 is 200 μ S/division and the amplitude is arbitrary. Pulse currents are measured with current viewing resistors, CVRs,

and are described later in the section on current diagnostics.

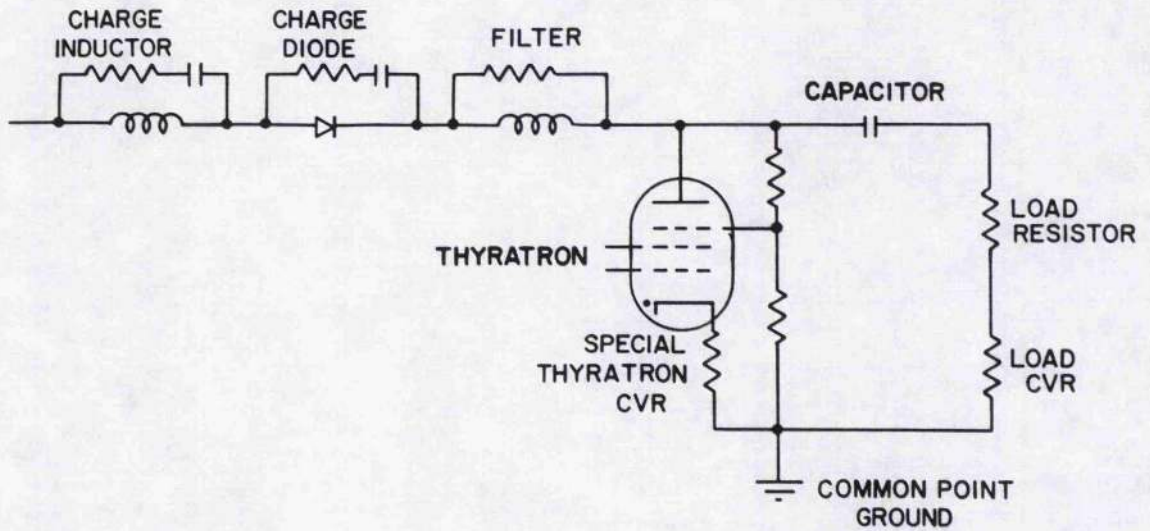


Figure 3.2.1 Schematic of discharge circuit with resonant charging.

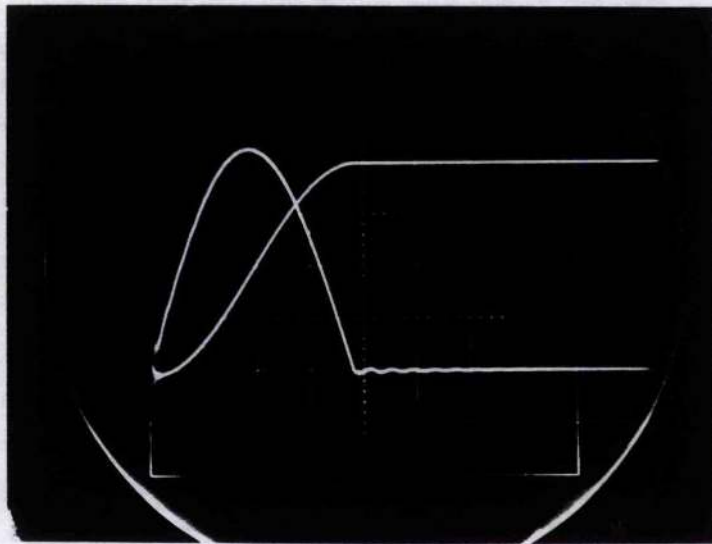


Figure 3.2.2 Electrical waveforms for resonant charge circuit.

The second charging method employed is a pulse transformer technique. This circuit is schematically represented in Figure 3.2.3. Pulse transformer charging is, in principle, similar to resonant charging as described above with the addition of a charge thyatron and step up transformer. With the addition of the charge thyatron, the time at which the charging cycle commences is accurately controlled. The circuit consist of two resonant loops. The resonant frequency of the primary circuit of the transformer defines the charge time of the fast pulse discharge capacitor in the secondary. The value of the primary capacitor, or charge capacitor in Figure 3.2.3, is determined by the square of the turns ratio of the transformer. In the laboratory, a 4:1 step up transformer

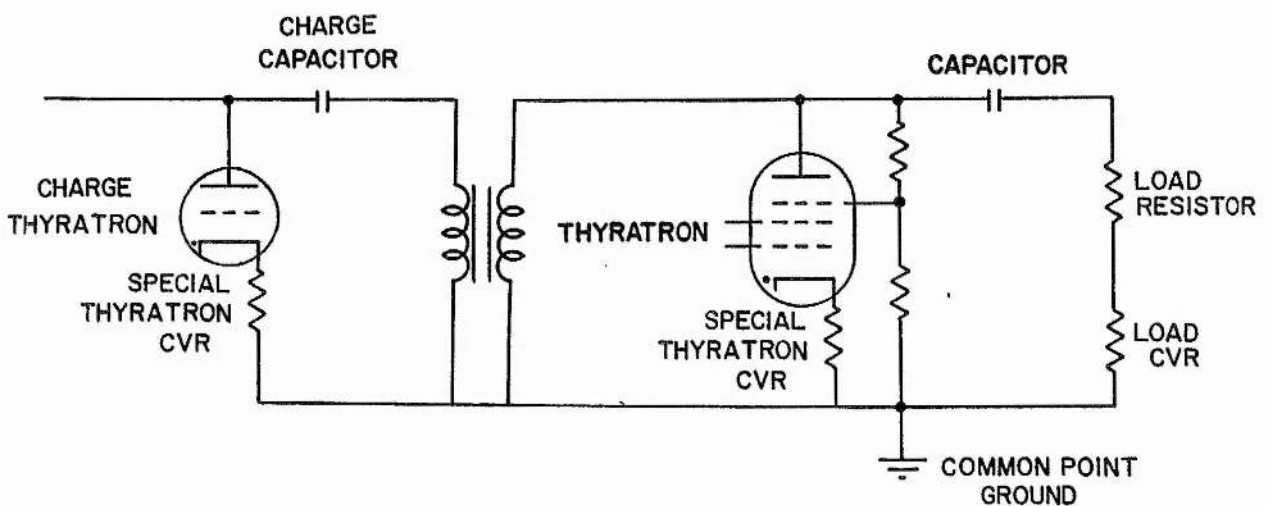


Figure 3.2.3 Pulse transformer charging and discharge circuit schematic diagram.

is used making the primary capacitor 16 times the value of the secondary capacitor. The primary resonant frequency

could be adjusted, depending on the total value of secondary capacitance, between 50 and 100 kHz to give a charge time of between 5 and 10 μ s. By decreasing the charge time several points can be addressed. Many breakdown mechanisms have statistical times in the tens to hundreds of microsecond range, so fast charging allows higher dielectric stresses to be achieved by eliminating those breakdown processes such as margin flashover which take longer to develop. In the case of BaTiO_3 ceramic capacitors, a voltage level three times that which can be achieved by resistive charging has been demonstrated [Sarjeant, 1979]. This in turn will increase the energy density factor of a given capacitor design greatly because of the v^2 dependence. It is postulated that reducing the time which a dielectric is stressed will increase the useful life of the dielectric. Fast charging will also reduce the effects of mechanical stresses in fluid impregnated film capacitors because of the very slow response times of material motion.

3.3 DIAGNOSTICS

Data acquisition and control of high power repetition rate circuits is a formidable undertaking. Life tests for some components require several months of 24 hour a day operation. Since the test circuit is attended only a few hours a day, to minimize damage of circuits and components at the high average powers attained during the test, a "stand-alone" fault sensor is incorporated into the charge systems to detect major disruptions in key experimental parameters and take appropriate corrective action. The

fault detection circuits are completely separate from the data acquisition system.

The long life test can result in a huge quantity of data which can only be processed efficiently using a computer. Along with the wide variety of data collected during this investigation, a data reduction system designed for research and development is needed to minimize the time involved in programme writing. Such a system is available from Tektronix, Inc. The heart of the diagnostic and data acquisition system is a six channel Tektronix WP2222 transient digitizer with integral DEC computer. Using Tektronix SPS Graphics Basic language reduces the time spent on programming to an insignificant amount thus allowing full effort to be concentrated on the component development. Over sixty data reduction programmes were written to perform specific tasks with the data recorded during the course of the investigations.

CURRENT DIAGNOSTICS

The most important electrical parameter measured in a pulse circuit is the current, $i(t)$. Pulse currents in this investigation vary from a few amperes in millisecond time frames (charge currents) to multiple kiloamperes in a few nanoseconds (discharge currents). Often both of these quantities are present in the same circuit. Referring to Figure 3.2.1, it is seen that both the charge current and pulse discharge current flow through the load. Using a single device to measure both of these currents in the test circuit increases the accuracy of the measurements as well

as reducing the number of signal cables. Such a current monitor must have a wide bandwidth to accurately reproduce both the long and short pulses without distortion. Low inductance is a prerequisite for short pulse circuits with large values of di/dt . This requires that the current monitor has negligible insertion impedance, i.e. inductance, so as not to influence the electrical characteristics of the discharge circuit. The current viewing resistor, CVR, is designed and constructed with all of the desired characteristics. Pulse currents throughout the investigation are measured with current viewing resistors. The CVR is constructed of a calibrated resistive thin foil laminated onto a ceramic substrate in a low inductance geometry. All CVRs used in this investigation are manufactured by T&M Research Products, Inc. of Albuquerque, New Mexico. T&M Research produces CVRs for a wide variety of applications. One style, the type W, is specifically designed with extremely low inductance for stripline geometries. The load CVR in Figures 3.2.1 and 3.2.3 are of the type W style. A data sheet for the type W CVRs is attached at the end of Appendix 1.

A high di/dt circuit can take basically two geometries, stripline and coaxial. The type W CVR fills the needs of stripline type geometries, but at the outset of this investigation there was no wideband current monitor suited to our needs for use in a coaxial geometry. Because the capacitor test circuits use thyratrons exclusively, a current monitor in a cylindrical geometry which mates with a thyatron was essential. A CVR designed for use in a

thyatron circuit should have D.C. response for measurement of heater power, and a bandwidth of several hundred megahertz for accurate reproduction of the discharge current pulse. To meet this requirement, a coaxial CVR, designated type DLI, was developed [Muehlenweg and McDuff, 1980; Muehlenweg, 1981]. Insertion inductance for the DLI type CVRs ranges from 0.5 to 3 nH depending on the diameter of the thyatron for which it was designed.

Frequency response and calibration of all CVRs was checked with a high voltage fast risetime hydrogen relay pulser. Resistance calibration was found to be $\pm 2\%$ of marked value and all units had bandwidths greater than 350 MHz (< 1 nS risetime).

VOLTAGE DIAGNOSTICS

Voltages measured in this investigation ranged from those of the D.C. power supply to rapidly changing thyatron anode voltages. Slowly changing pulse voltages with risetimes of greater than 1 μ S can accurately be measured with commercially available probes. Likewise, with low frequency pulse voltages, physical coupling between the probe and the test circuit with regard to inductance is not critical. To measure rapidly changing voltages, connections between the probe and the points of measurement must be designed to minimize inductance. Designing the fast voltage diagnostics into a circuit in the initial design phase is the best solution to this problem. The one voltage diagnostic difficulty which cannot be overcome is the measurement of voltage across a component passing current

with a high rate of rise. Often the $L \cdot di/dt$ voltage drop will dominate the voltage measured across a component in a fast discharge circuit.

In this investigation two voltage probes were used. For general purpose voltage measurement, the choice was the commercially available Tektronix P6015 High Voltage X1000 probe. The Tektronix P6015 has a specified response from D.C. to 4 nS risetime. The 40 kV peak voltage rating of the probe was extended to 80 kV by making the modifications described in Appendix 1. Risetime of the P6015 when terminated into a Megohm impedance is specified at 4 nS. The major drawback of the P6015 is the 3 meter long probe cable. The short cable requires that the voltage recording instrument be located physically close to the experiment. With the 80 kV modification the output of 80 volts exceeded the maximum input voltage of the digitizer input amplifiers. To overcome this limitation, a fast risetime line driver/amplifier with a gain of 0.1 was designed to convert the high impedance output of the P6015 probe to 50 ohms. Using the 50 ohm line driver allows the voltage recording instrument to be located up to 100 meters from the compensation box of the P6015 probe connected via a 50 ohm cable. The risetime of the Tektronix P6015/line driver combination is typically 9 nS. Further details about the line driver for the Tektronix 6015 voltage probe are given in Appendix 1.

Short voltage pulses from very low impedance sources, such as the load voltage, are measured with a homemade low resistance probe. The construction detail of this probe can

also be found in Appendix 1. Because of the energy input limitations and power dissipation capability of the low resistance probe, it is used exclusively for short pulse measurements. A risetime of less than 1 nS is measured for this probe when coupled to the point of measurement using impedance matching and low inductance techniques. Accuracy of the low resistance probe is determined by the tolerance of the the resistors used in its construction.

MISCELLANEOUS DIAGNOSTICS

Throughout the investigation many diverse diagnostic tools are employed to address specific issues. One of the most useful instruments that no lab should be without is the C-Meter capacitance meter. The C-Meter is a microprocessor based device that determines capacitance by measuring the RC time constant of the attached unknown capacitance and the electronically selected internal resistance. The C-Meter is not only good for measuring capacitors, but performs well in the measure of stray capacitance of circuits, the interwinding capacitance of transformers, and practically any "C" because it does not use an A.C. signal as do meters that use the impedance method. Another invaluable device in the laboratory is the grid-dip meter. The grid-dip meter is an easy and simple means of determining the self resonant frequency and parasitic resonances of a pulsed circuit without any electrical connections. From the self resonance frequency, the approximate inductance of the circuit can be calculated. Identifying parasitic resonances can aid in the design of snubber networks and modification to the circuit

layout to reduce or eliminate unwanted "tank circuits". The grid-dip meter is also useful in measurement of the inductance of pulse transformer windings.

As mentioned in Section 4.3, the General Radio Type 1690 Dielectric Test Cell is used for measurement of the loss factor of dielectric films as well as determining the relative dielectric constant. Using the 1690 Test Cell in conjunction with a wideband oscillator and the General Radio Impedance Bridge, the frequency dependence of the films dielectric constant can be plotted. One test cell plate is movable with a calibrated micrometer adjustment. The micrometer is calibrated for air as a dielectric medium, thus, the relative dielectric constant of an unknown substance can be calculated from the effect of placing it in the test cell.

Electromagnetic radiation from repetitive pulse circuits is very often a major concern in systems with large amounts of semiconductor electronics. All of the component test circuits and the repetitive lasers are monitored for RF radiation with Narda Broadband RF meters. Two meters covering frequency bands from 1 MHz to 3 GHz and 3 GHz to 18 GHz respectively were purchased for these measurements. Average power level is measured with a thermal element in the probes of the Narda Radiation meters. No successful approach or device could be found to measure the peak broadband radiated power from a repetitive circuit. The main source of radiation from the repetitive pulsed circuits investigated is from the ionized gas of the switches. The common 11.4 cm (4.5") diameter ceramic thyratron operation

in a circuit at 1000 pps and 20 kW average power switched to the load radiates approximately 80 to 100 mW/m^2 in the 1 MHz to 3GHz band. The same circuit with a metal envelope thyatron radiates less than 2 mW/m^2 in the same range showing the effect of the metal envelope in shielding. Neither of these power levels is sufficient to cause concern for operators or shielding design. Power radiated from repetitive circuits with the gas switches shielded is below the detection range of the meters. Meters are available in the laboratory for the measure of X-ray radiation from the switches. High energy radiation from circuits operating at voltages less than 100 kV are attenuated by nearly any type of material. Transformer oil, in which most tests are conducted, is an excellent absorber of soft X-rays and no readings could be detected from submerged switches even with the most sensitive meters. Radiation from thyatrons operating in air is so greatly attenuated by the equipment housing, there was no health hazard.

In Section 4.4, the General Radio Model 1933A Precision Sound Pressure Level Meter is used to make the measurements necessary to calculate the amount of electrical energy the test capacitors convert into acoustical power. These measurements are also very important to the design of enclosures and noise insulation to meet sound level exposure standards.

Failure analysis requires the widest variety of diagnostic tools. As detailed in Section 4.5, scanning X-ray Computer Aided Tomography, CATSCAN, is an excellent means of nondestructive analysis on failed or afflicted

capacitors that show no external signs of damage. The CATSCAN is most often used in medical applications. Other nonintrusive diagnostic techniques are X-ray and neutron-radiograph photography. X-ray photography is used worldwide for numerous applications and is a means of looking inside thyratrons and capacitors to identify areas that should be investigated during an autopsy. The neutron-radiograph is used primarily in the quality control of nuclear weapon components but is an excellent means of determining the types of materials in a device under investigation. A skilled operator can identify elements such as molybdenum, nickel, etc., from the gray level of the radiograph for a specific exposure time.

Surface conditions of dielectric films, electrodes, and thyatron cathodes are examined with the Scanning Electron Microscope. Information from the SEM is valuable in determining emission characteristics and origins of damage. Analysis of material from breakdown products of dielectric film, condition of electrodes, and titanium hydride reservoirs are best done with computer-aided X-ray diffraction spectroscopy. Detection to the elementary level of carbon is possible with this method. This method is widely used for analysis of materials deposited onto laser windows and mirrors.

An instrument which is a real time saver when energizing a new circuit for the first time is an ultrasonic translator. The Hewlett Packard 80018 Ultrasonic Translator, originally designed for detecting high pressure

gas leaks, is also excellent for detecting the high frequencies generated by arcing and corona.

Temperature is probably the most important quantity next to electrical measurements. Dial thermometers are by far the best means of measuring temperature in high voltage circuits. This type of mechanical thermometer is easily calibrated in ice water and is absolutely impervious to the effects associated with high voltage pulsed circuits. When a very accurate temperature measurement is required as in the calorimetry in Section 4.3, a thermocouple/digital pyrometer is employed. These meters, however, will not operate (and in fact have a tendency to fail) if connected to an energized circuit.

3.4 GROUNDING AND SHIELDING

At very high peak powers, large transient voltages can be developed on relatively small impedances. During the course of this investigation, pulse currents of up to 50 kA at kilojoule energies were achieved. With di/dt approaching 10^{12} amperes/second, a few nanohenries of inductance can generate thousands of volts which will wreak havoc in sensitive diagnostic amplifiers. With the main point of this investigation being high current rate of rise circuits, the significance of this effect is enhanced. Repetitive peak powers achieved during this investigation can be very lethal and destructive to both instruments and operators. Proper design of the power distribution and grounding is imperative for safety and accurate data acquisition in a harsh electrical environment.

Conduction is the most common transport mechanism of electromagnetic interference in repetitively pulsed circuits. Very rarely is interference caused by radiation in a properly grounded circuit. An approach that will eliminate conducted electrical noise and which does not present electrical hazards must be employed. The word "ground" in pulse circuits is almost meaningless. Skin effect resistance and inductive drop ($L \cdot di/dt$) in short pulse, high current circuits does not allow a large area ground reference such as a ground plane. There are two types of grounds considered in the laboratory: {1} power mains ground and {2} the instrument ground. Let us consider the power distribution ground first. A "grounded conductor" refers to the neutral A.C. line which is grounded at various points throughout the distribution network. It must be remembered that the neutrals carry return current. "Grounding conductors" refers to a ground wire, usually green, that is carried along with the live (hot) and neutral line in a power mains. The "grounding wire" does not carry current except in a fault condition, thus its purpose is for the safety of the operators. Therefore, since the neutral carries current and the grounding conductor is for fault protection, it is neither safe or beneficial to use either as the measurement ground reference.

The second ground considered is the diagnostic or instrumentation ground. Most often this is defined by equipment that uses single ended inputs such as the BNC connector. Equipment that uses a single ended input, by

virtue of construction and safety, ties the instrument signal ground to the chassis ground and to the grounding conductor (green wire) of the power mains. This is the primary source of low impedance "ground loops" and is the reason for the small discharge between the coaxial cable outer conductor and the instrument chassis. The most common way of eliminating ground loops is by breaking the grounding conductor where the instrumentation connects to the power mains, cutting the green wire. In many cases this is satisfactory but, in the case of a live (hot) to green wire fault at a remote location from the system "single point ground"; will result in the local ground being elevated to line voltage. It is thus necessary to devise a grounding scheme that is both safe for the operator and consistent with good measurement practices. In order to design such a system, the sources of electrical noise and ground loops must be examined.

Sources of EMI (electromagnetic interference), or noise, are almost always related to the A.C. mains. The most common of these problems is voltage differential along the neutral line in a power mains bus system resulting in differences in local ground potential. Voltage differences between the A.C. neutral potential at instrumentation and the neutral potential at the experiment is caused primarily by IR drop. Referring to Figure 3.4.1 a voltage drop is unavoidable between points 1 and 2. If the impedance looking back into the power mains from the experiment is lower than the impedance looking back into the oscilloscope to the mains, then an A.C. noise signal will appear on the

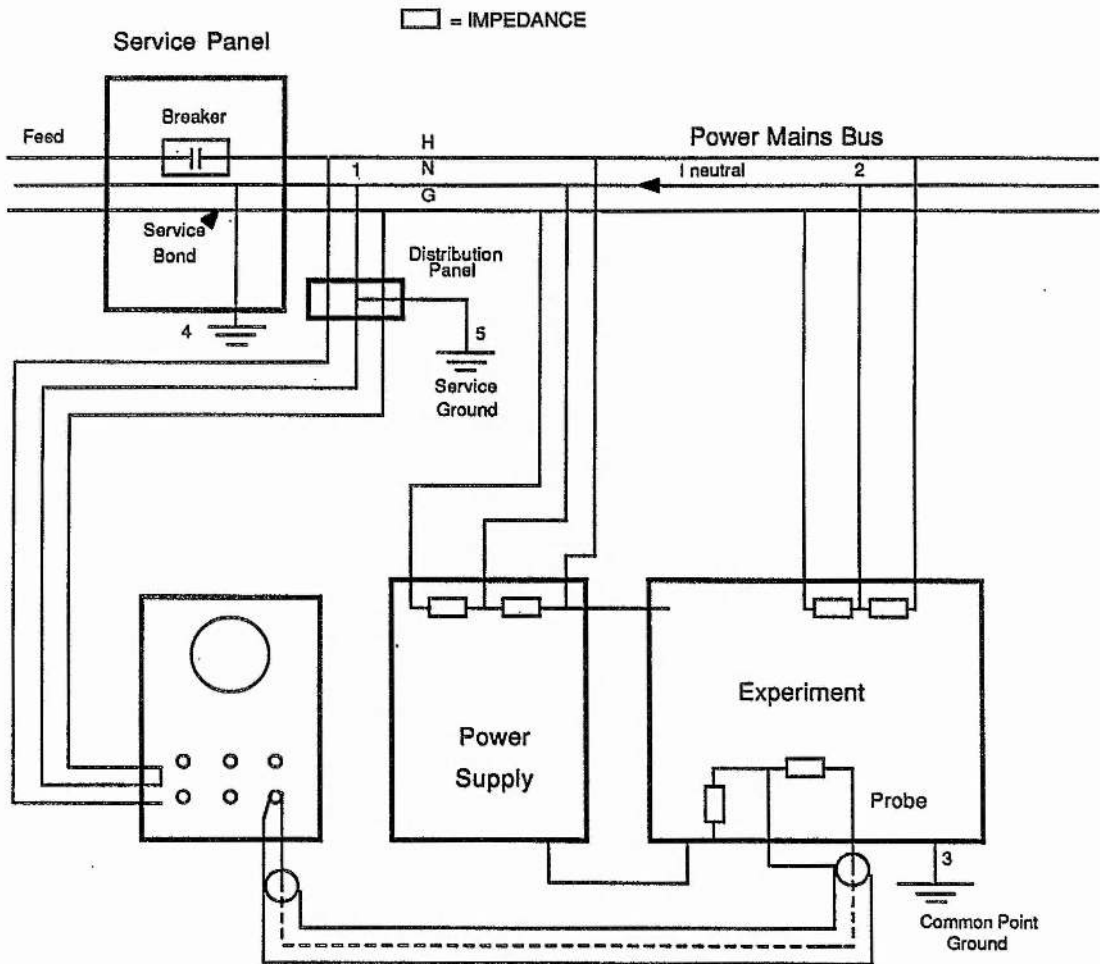


Figure 3.4.1 Spurious signals from power distribution wiring techniques.

oscilloscope. This signal usually takes the form of a distorted sinusoidal waveform of power mains frequency. Coming from a relatively low impedance, the signal cannot be "shorted" out and will appear on the oscilloscope even with the input grounded, which leads to the common misconception that it is caused by electromagnetic radiation. The second

common source of EMI is from local ground potential difference. Again referring to Figure 3.4.1, it is reasonable to assume that the impedance between points 3, 4, and 5 are not zero and are often quite high because the only electrical path between them is the laboratory floor. With the oscilloscope being grounded at point 5, differences in local ground potential are the source of EMI. As with the neutral voltage drop, differences in potential between the grounds will appear on the oscilloscope as a distorted A.C. signal. Both of these EMI sources can result in signals of several hundreds of millivolts. Interference of this nature tends to distort data and overwhelm very small signals such as those from thermocouples. The first inclination is to cut the ground at point 5 in Figure 3.4.1. This will most certainly eliminate the problem and in the event of a massive high power load fault in the experiment, might also eliminate the operator.

To solve the signal-versus-safety dilemma, a common source transformer is incorporated to feed both the instrumentation and the experiment. This technique will eliminate the effects of A.C. mains interference caused by neutral voltages and ground differences, leaving only fault and pulse currents as a source of EMI. Figure 3.4.2 shows a simplified single phase A.C. wiring diagram for the laboratory. The actual laboratory used three phase power but the principle is the same.

First, it is noted that all neutral current flows into the power mains, thus avoiding any neutral voltage difference as with the bus configuration. Second, having a

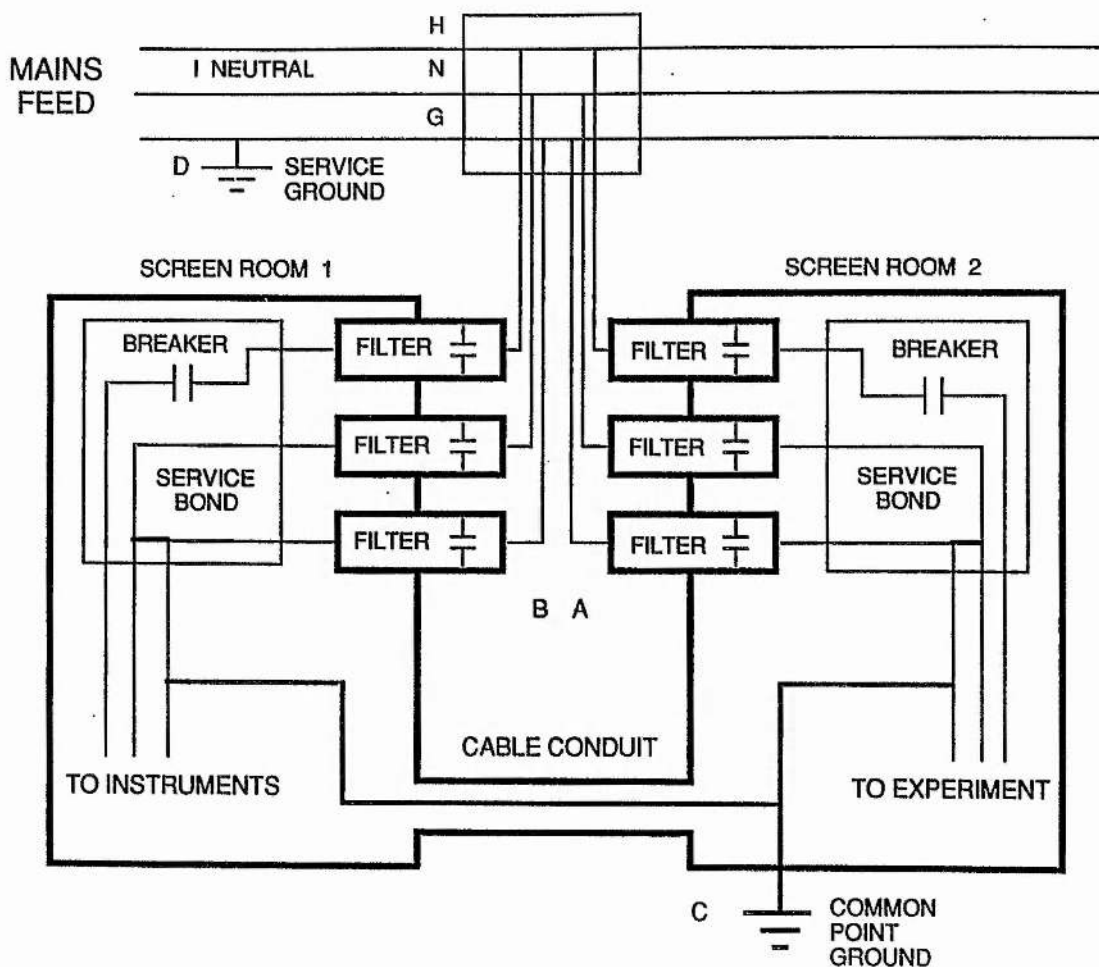


Figure 3.4.2 Power distribution diagram for the laboratory.

common point ground at C, (Figure 3.4.2) for both experiment and instrumentation will eliminate the difference in ground potential since no current flows in the grounding conductor connecting Screen Room 1 with Screen Room 2. Test of this plan is done by disconnecting the green wire at the breaker panel in the screen rooms and detecting no EMI. Effects of high current discharges on conducted interference are reduced further by using a common point ground as depicted in Figure 3.1.1 and the use of low pass line

filters on the power input to the screen rooms. Looking back into the power mains from points A and B in Figure 3.4.2, any stray pulse currents will see a high impedance of the low pass filters. In addition, by using a multiple secondary power transformer for the common power source, another stage of isolation is included. Including the power line filters will induce EMI from the displacement currents of the filter capacitors. By design, these are high loss filters that barely pass power line frequencies. This results in a "larger-than-normal" capacitive current. In the laboratory, filter leakage current was found to be 900 mA and resulted in a ground differential of about 55 uV between the screen rooms. Identifying this source of EMI allows alternative steps to be taken to ensure accurate data.

Even though radiated noise was not an anticipated problem, all pulse circuits were enclosed in oil filled metal tanks. However, this was done more for insulation and cooling purposes rather than for shielding. To avoid ground loops, no connections between the tanks and the enclosed circuitry were allowed. Likewise, the grounds from the diagnostics, power supplies, and ancillary equipment were isolated from the development tank and the screen rooms. Copper pipes were used to connect the metal enclosures to screen rooms which enclosed the development tank and the diagnostic equipment. Referring to Figure 3.1.1, the diagnostics are enclosed in a screen room as is the component development tank. Each charging system is enclosed in its own steel tank and connected to the

component development tank via copper conduit. Power supplies are enclosed in the usual cases supplied by the manufacturer. Both power supplies have transformer isolated "floating" outputs, thus eliminating any ground loops. Power supply grounds are carried through the copper conduits and grounded at the common point along with the electrical service ground. Finally, the entire shielding enclosure is grounded at the common point. A photograph of the laboratory showing the two screen rooms, the main power supply, and the copper conduits is seen in Figure 3.4.3.

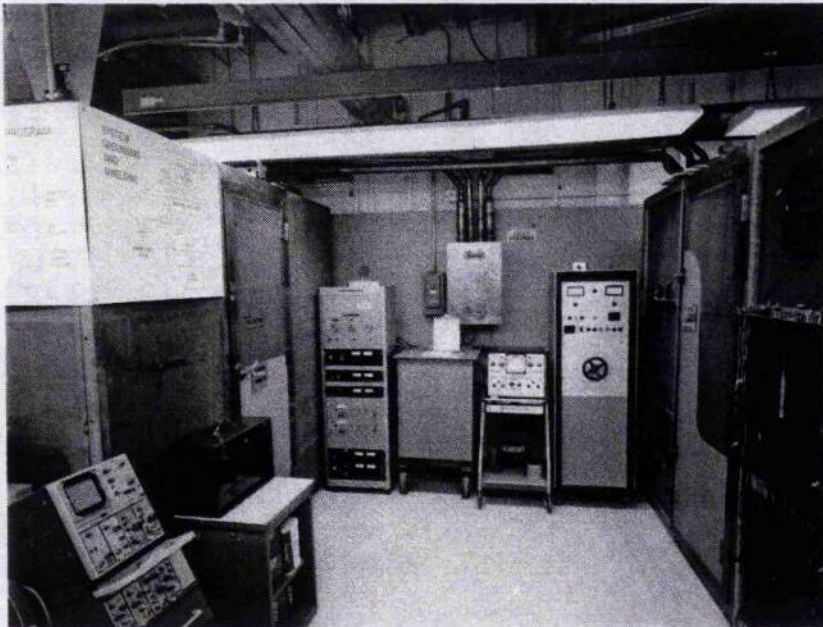


Figure 3.4.3 High Repetition Rate Component Development Laboratory.

Note that the screen rooms are isolated from the tile floor with 8 layers of 31 mm polyethylene. Ancillary equipment such as power supplies were selected with transformer

coupled outputs to evade ground loops. All primary power for the experimental circuit is derived from the Screen Room 2 service panel and all diagnostic equipment power from Screen Room 1. Finally, as mentioned above, both screen rooms were fed from a single power transformer as a common source. This transformer has one primary and three secondary windings for the two screen rooms and an for general laboratory power for lights and power tools.

Connections of all low voltage A.C. and D.C. power (<2000 volts) were made via twisted pair conductors. All lines have both common-mode and differential-mode rejection filters on the sending and receiving ends. High voltage connections were made via coaxial cables with common mode and capacitive filters on the receiving end. No transient suppressive devices such as metal-oxide varistors were used anywhere in the laboratory due to their inherent short life in repetitive pulse circuits.

Final signal quality of the laboratory is such that when observing the current pulse from a circuit operating at 1000 pps, 65 kV, 38 kA, with a 120 nS pulsewidth, the 55 uV EMI signal from the line filter leakage currents can be detected to be modulating the 38 volt signal from the CVR. The quality factor pertaining to transmission of data is the signal-to-noise ratio. The IEEE Standards dictionary defines the general signal-to-noise ratio as "the ratio of the value of the signal to that of the noise". To remove the ambiguity of the general definition, this ratio will be expressed in terms of peak-to-peak amplitudes throughout this thesis. Using the peak-to-peak signal to peak-to-peak

noise ratio interpretation, the noise level is over 100 dB down for diagnostic signals greater than 5.5 volts.

References for Chapter 3

Glasoe, G.N., and Lebacqz, J.V., eds., Pulse Generators, New York, McGraw-Hill, 1948.

Muehlenweg, C., "Low Inductance Current Viewing Resistors for Hydrogen Thyratrons," 3rd IEEE Pulsed Power Conference, Albuquerque, New Mexico, June 1981.

Muehlenweg, C. and McDuff, G., "Measuring Fast Pulse Currents Using Low Inductance Current Viewing Resistors and di/dt Probes," Workshop on Measurements of Electrical Quantities in Pulsed Power Systems, National Bureau of Standards, Boulder, CO March 2-4, 1980.

Sarjeant, W.J., "Energy Storage Capacitors," Power Conditioning Technology, Vol. 1, LA-UR-79-1044.

CHAPTER 4

CAPACITORS

4.1 CAPACITANCE

A capacitor is simply two conductors separated by an insulator. Capacitance may be defined by the rate of change of charge divided by the rate of change of voltage

$$C = \frac{(dQ/dt)}{(dV/dt)} \quad \text{farads (4.1.1A)}$$

or, more conventionally, by the equations

$$C = \frac{\Delta Q}{\Delta V} = \frac{\epsilon_0 \epsilon_r A}{d} \quad \text{farads (4.1.1B)}$$

where we have ϵ_0 = dielectric constant of free space,
 ϵ_r = relative dielectric constant,
 A = the area of the conductors, and
 d = the spacing between the conductors.

Countless numbers of books, articles, conferences, and journals are devoted to the study of dielectrics so a comprehensive critique will not be addressed in this thesis. However, a brief synopsis of the basic theory of dielectrics will be presented as a background review for the investigations reported.

When an electric field is impressed across a dielectric, the medium becomes polarized and the associated motion of charge carriers results in energy storage and dissipation. There are two types of polarization, induced and permanent dipole alignment. Induced polarization is

characterized by the displacements of electrons and ions from their equilibrium positions and so long as they remain displaced energy is stored in the medium. Since induced polarization is an elastic process [Dekker, 1965], it is constant up to very high frequencies where atomic and molecular resonances are present.

Polarization due to the alignment of permanent dipoles is the major contributor to the dielectric constant [Sarjeant, 1979]. By definition, the polarization per unit volume is equal to the product of the electric field and the susceptibility and is written as

$$P = \chi * E \quad . \quad (4.1.2)$$

The susceptibility can be related to the relative dielectric constant by

$$\epsilon(\omega) = 1 + 4 \pi \chi(\omega) \quad . \quad (4.1.3)$$

The value of this constant is very sensitive to temperature; i.e. a large relative dielectric constant temperature coefficient. Temperature increases have a depolarizing effect on all materials. Therefore, for capacitors to operate in high repetition rate circuits, it is desired to have a dielectric with a small temperature coefficient. The relative dielectric constant is defined as

$$\epsilon(\omega) = \frac{D(\omega)}{E(\omega)} \quad , \quad (4.1.4)$$

where $D(\omega)$ is the dielectric displacement and $E(\omega)$ is the electric field. Separating the complex number $\epsilon(\omega)$ into

real and imaginary parts we can define the phase lag between the rate of change of displacement and the rate of change of electric field as the angle, δ . That is, as the electric field changes, the dipole alignment will lag this change by a phase angle. It should be noticed at very low frequencies, there is no contribution to the dielectric constant because the dipole movement can keep up with the changing field and at very high frequencies the dipole inertia will prohibit alignment at all. However, in between these two extremes the dipole alignment will always be out of phase with the field and this is the area of interest in discharge capacitors. The tangent of this phase angle, δ , is known as the dissipation factor, or simply $\tan \delta$.

There are about fifty common solid dielectrics used in capacitors and about a dozen fluids. In high repetition rate discharge circuits where very high average and RMS currents can be attained, there are only a few suitable dielectrics. Dielectrics for this duty must have a small temperature coefficient, that is, the dielectric constant should remain constant over a large range of temperatures. Temperature coefficients are expressed as a negative percentage. Low dielectric loss is another property essential for high repetition rate capacitors because, at large RMS currents, substantial heat can be generated on even the smallest of dissipative elements. This is all important in spirally wound capacitors because the only path of heat removal is by conduction out through the foil edges (Refer to Figure 2.1.1). Pulse capacitor dielectrics should also exhibit constant characteristics with frequency. Since

pulse capacitors are exposed to a wide range of high frequencies, fluctuations in dielectric constant and loss are not a desired characteristic. Frequency dependence of capacitance and loss further reduce the number of suitable dielectrics for high repetition rate applications. Loss characteristics are discussed in detail in Section 4.3. Lastly, many dielectrics exhibit an electric field dependence, usually given in data sheets as the "voltage coefficient". As with temperature, this parameter is commonly stated as a negative percentage. The magnitude of this effect depends on material properties and mechanical forces. Dielectric constant variations with electric field are determined empirically for the most part. Some capacitors, such as the spirally wound fluid impregnated type, exhibit electrical characteristic changes due to movement of the capacitor plates. This effect is addressed in detail in Section 4.4. The more common low loss dielectrics used in capacitors are listed in Table 4.1.1.

TEST CAPACITORS DATA

Many different capacitors were evaluated during the investigation. Only eight different types were found suitable for in-depth investigations for reasons of life, inductance, and size. The eight final test capacitors are referred to by letters A through H corresponding to a specific manufacturer. Different generations of capacitors are denoted by subscripts and in the case of manufacturer G two units were examined, a 1 nF and a 2.7 nF unit denoted as G1 and G2.7, respectively.

FILMS	DIELECTRIC CONSTANT (ϵ_r)	DENSITY (g/cm ³)	DIELECTRIC STRENGTH (kV/mm)
polypropylene	2.3	.905	378
polysulfone	3.0	1.42	275
polyethylene	2.2	.965	185
polytetra- fluoroethylene (Teflon)	2.1	2.2	60
polyvinylidene difluoride* (PVDF)	9.7	1.77	350
polycarbonate*	3.0	1.2	90
PAPERS			
reconstituted mica	1.6-8	1.6	63
paper (best)	6.0	1.0	158
CERAMICS			
barium titanate	500-6000		1.5
strontium titanate	500-9000		2.5
LIQUIDS			
transformer oil	2.2	.98	13
silicone oil	2.8	.97	13
*Not low loss			

Table 4.1.1 Common low loss dielectrics.

At the onset of this programme, each of the participating manufacturers was briefed and requested to deliver "best effort" units for an impartial and in-depth study. During the course of the study, feedback was provided to the manufacturers and new capacitors were designed to overcome the short-comings uncovered by the investigation. In one instance, three generations of a particular design were made. Design and materials used in the units will be discussed throughout this report but no company names will be mentioned so as not to endorse or denounce any of the manufacturers.

The first measurement made in the capacitor investigation was, naturally, capacitance. Capacitance was measured with a commercial meter and dynamically in a pulse discharge circuit. Results from the commercial meter coincided with the values stated on the capacitors, the case value. The meter determines the capacitance by charging the unit to 5 volts and discharging it through a calibrated resistor measuring the RC time constant. Dynamic capacitance measurements were made in a thyratron switched 1000 pps pulsed discharge circuit. Tests were conducted at the full rated capacitor voltage so the effect of voltage and frequency would be included in the measurements. The dynamic measurements are based on a charge/energy conservation principle. First, from the case ratings of the capacitor, the amount of charge, q , that is required to charge the test unit to the case full rated voltage is calculated, $q(\text{case}) = C(\text{case}) * V(\text{case})$. This value represents

the theoretical amount of charge stored in the capacitor. Second, the amount of charge delivered to the capacitor from the charging circuit is measured and recorded via a current viewing resistor (CVR), $q(\text{charge}) = i(\text{charge}) * t(\text{charge})$. The CVR is inserted between the output of the charge circuit and the test capacitor so as not to reflect charge system losses. Next, the peak voltage $v(\text{charge})$, on the test capacitor is recorded. The quantities, $q(\text{case})$ and $q(\text{charge})$ are compared. If the test capacitor has a voltage dependency, $q(\text{charge})$ will not equal $q(\text{case})$. So, from $i(\text{charge}) * t(\text{charge}) = C(\text{DCunknown}) * v(\text{charge})$, the variation in capacitance due to static voltage is found. All of the capacitors tested had a negative static (D.C.) voltage coefficient, that is $q(\text{charge}) < q(\text{case})$ and these values are listed in Table 4.1.2. A BaTiO_3 unit was used as the test device for calibration as it has a well documented voltage coefficient [Clark, 1962 and Manufacturer data]. The capacitor is discharged through a well characterized load and the load voltage, $v(\text{load})$ and load current, $i(\text{load})$ are recorded. From here the power dissipated in the load, $P(\text{load})$, is found and, by integrating with respect to time, the energy, $E_n(\text{cap})$, delivered to the load from the capacitor (minus switch losses determined earlier) is found. From $E_n(\text{cap}) = 0.5 * C(\text{ACunknown}) * v(\text{charge})^2$, a new value for the variation in capacitance due to discharging is determined. If $C(\text{ACunknown})$ is radically different from $C(\text{DCunknown})$ then the dielectric has a frequency dependence or as will be shown in Section 4.4, the capacitor has a physical phenomenon perturbing the value. For all the solid

dielectric units the values for C(ACunknown) and C(DCunknown) were equivalent within the 2% diagnostic accuracy. However, the film/oil units had very peculiar behavior. During the discharge, the apparent capacitance increased by as much as ten percent. From all existing dielectric data, this phenomenon could not be explained. Because a film/oil capacitor is not rigid in construction, it is suspected that movement of the conductors due to forces induced by the electric field is the cause of the change of capacitance during the discharge. In fact, this is the case and is addressed in detail in Section 4.4. A list of the measured voltage coefficients is given below in Table 4.1.2. Accuracy of these measurements is 2%, so values less than this are extrapolations. The variation of capacitance during the discharge is not constant but lies within the range stated in the above table. Sometimes the capacitors show almost no change in value during the discharge.

SUPPLIER	CASE VALUE (nF)	STATIC VOLTAGE COEFFICIENT	DYNAMIC VOLTAGE COEFFICIENT
A	1	-4%	-4%
B	1	<-2%	+7 to 10%
C	1	<-2%	+7 to 10%
D	1	<-2%	+7 to 10%
E	1	<-2%	+7 to 10%
F	0.96	-6%	-6%
G1	1	-4%	-4%
G2.7	2.7	-4%	-4%
H	0.56	-40%	-40%

Table 4.1.2 Voltage Coefficients for final nine test capacitors.

4.2 INDUCTANCE

The second electrical parameter of interest to high repetition rate capacitors is inductance. It is important for the designer to know this quantity especially in circuits which operate with large values of di/dt , as it will affect the circuit response. Often, the component with the largest inductive value in a fast discharge circuit will be the energy storage capacitor. Since capacitors are made with materials which have a relative permeability of 1, inductance is dependent on geometry alone. This implies that the inductance should be easily calculated from the dimensions of the capacitor in question. For the ceramic and the mica units this is the case, but for the spirally wound film units, it is far from it.

INDUCTANCE OF SOLID DIELECTRIC TEST CAPACITORS

Inductances of the solid dielectric capacitors are measured by two different methods and verified by calculations. Starting with the ceramic units (Figure 2.1.2), the inductance is calculated by modeling the capacitor as coaxial conductors. By enclosing the unit in a conductive shroud, or current return, the inductance of the assembly can be found from

$$\frac{L}{m} = \frac{\mu_0 \mu_r}{2\pi} \ln \frac{r_2}{r_1} \text{ Henry/meter, (4.2.1)}$$

where r_2 is the outer diameter of the current return shroud and r_1 is the outer diameter of the capacitor terminal conductor. For the three test ceramic capacitors,

calculated inductance values ranged from 10 to 25 nH. (A complete list of inductance values for all the capacitors is found at the end of this section.) To verify the first calculations, the inductance was measured with a vector impedance meter. The vector impedance meter measures the magnitude and phase angle of the device under test from 50 kHz to 250 MHz. All of the ceramic units had a self resonance between 25 and 35 MHz which translates into an inductance of 10 to 25 nH depending on the capacitor under test. As an added check, the inductance is also calculated from off-resonant readings. From the capacitance, the impedance magnitude, and the phase angle, the inductive component is found. Inductance values determined from the vector impedance meter were consistent within 20% of the values calculated from the capacitor dimensions. The large error is a result of the very small values of inductance and stray effects that distort the impedance meter values. However, 20% of ten nanohenry is an acceptable uncertainty for general design purposes.

As a third verification, the inductance of the ceramic capacitors was calculated from electrical measurements of a pulsed discharge circuit. Modeling the 1000 pps circuit used to measure the capacitance (Section 4.1), the equivalent circuit in Figure 4.2.1 is derived. Referring to Figure 4.2.1 the total discharge circuit inductance is determined mathematically from the current waveform, $i(t)$. Taking into account the physical size, the type and layout of connections, and the complexity of test circuit modification, four to six test capacitors are mounted in a

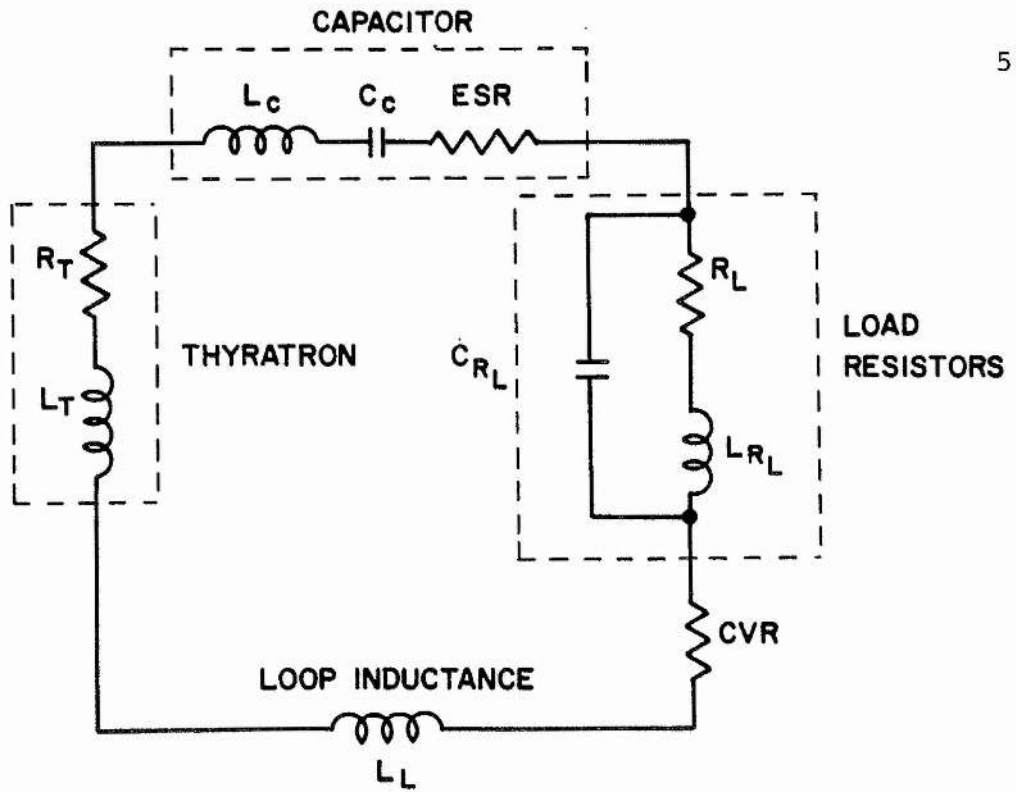


Figure 4.2.1 Lumped equivalent of the discharge circuit.

low inductance housing in the test circuit, C_c in the model. Having previously determined the voltage dependence (Section 4.1) of the ceramic capacitors, this is incorporated into the model as a $C_c(v)$ for these units. The test circuit is operated at full rated voltage and $i(t)$ is recorded by the digitizers. Three of the test capacitors are removed and the void is filled by a flux excluder. The effect on the total loop inductance of removing half the capacitors will be dominated by the capacitors' self inductance. Again $i(t)$ is recorded and compared to the current waveform of the six units. This method has two important features. First, the charge voltage on the capacitor is not critical to the measurement because $C_c(v)$ is known, and it is the frequency component that contains the information. Secondly, time, is the parameter that can be measured most accurately. Subtracting the two current waveforms the difference in the

period of oscillation is found and substituting this number into the equation for $i(t)$, the difference in total loop inductance is determined. Dividing the change in the total loop inductance by three, gives the inductance of the capacitor in question. Only two of the three types of ceramic units were checked in this way and the results were within 25% of the values calculated from the other two methods.

Inductances of the mica paper capacitors are found in much the same way as the ceramic units. Remembering that the mica units consist of many series/parallel capacitive packs, direct calculation of inductance from physical dimensions is not possible. Once again the vector impedance meter was employed. Wrapping the mica capacitors in aluminum foil as a current return shroud minimized the effect of stray and connection inductance. Several different mica designs were examined and the inductances ranged from 80 to 150 nH depending on the design. The inductance of the mica units is only weakly dependent on the capacitance value over a fairly large range. X-ray photographs were taken of the mica capacitors and it was easily spotted why one had a lower inductance than the others. The lower value corresponded to the design with the tightest coupling between the internal current path and the external current return. The mica manufacturer was consulted and a new set of mica capacitors were supplied. By decreasing the capacitance of the individual pack, increasing the number of parallel packs, and rearranging the pack layout the inductance was found to be reduced to lie

within the same range as that of the ceramic capacitors, i.e. 25-30 nH. Even though the new mica capacitor has over ten times the volume of an equivalent ceramic unit, the inductance is approximately the same because of the multiple current paths of the many parallel packs and their relation to the external environment. Because capacitors with inductances greater than about 100 nH are not useful for operation at high di/dt , the number of viable mica units was reduced to a single design. For verification, the same "in circuit" test is performed on the mica units. Pulse discharge measurements gave values within 30% of the vector impedance meter. The larger error was due to the large size of the mica units and the less efficient flux exclusion in the test circuit when three of the capacitors were removed. However, this accuracy is satisfactory.

INDUCTANCE OF SPIRALLY WOUND IMPREGNATED FILM CAPACITORS

Four manufacturers provided their best dielectric film, fluid impregnated capacitors to meet the following specifications.

Capacitance: 1 - 2 nF

Voltage Rating : 20 - 30 kV

Repetition Rate: < 2000 pps

Lifetime: $>10^9$

Inductance: smallest possible

Discharge Current: 1000 amperes

RMS Current: 10 amperes

Two manufacturers provided capacitors in tubular cases and the others provided rectangular packages.

From the basic construction of the spirally wound units the complexity of the inductive term is obvious. In Figure 2.1.1 a cross section of a spirally wound capacitor pack is illustrated. At low frequencies, where the conductor or plate thickness is much less than the skin depth, the pack behaves rather like a set of nested coaxial cylinders. Current flow is through the plates, through the swaged extended foil region and out via the leads. However, at frequencies where the skin depth is approaching the conductor thickness, a strong frequency dependence emerges governing the electrical characteristics of the pack.

Transmission line characteristics of spirally wound capacitors have been described for A.C. response by Tenney [1965] and Los Alamos National Laboratory report LA-3617. Both references are totally theoretical in nature and are not supported empirically. These derivations, as most computer models, describe the electrical characteristics of the device in great mathematical detail but no effort is made to relate the theory with device design or even measurable quantities.

The first spirally wound units to be investigated are from Company B and are designated B_1 . In section 4.5, Figure 4.5.3, construction of the cylindrical spirally wound test capacitors is pictured. Knowing that the inductance characteristic of a capacitor depends on geometry, the construction details are examined first. The contribution to inductance of leads and internal connections of the capacitor is straightforward in analysis and is not discussed. The 6 nF pack for the B_1 unit has a winding

aspect ratio, pack O.D. to I.D. of 8:1. Considering a single pack such as depicted in Figure 2.1.1 and enclosing it in a cylindrical current return, the outer winding forms a coaxial system with the return. The outer winding shields the inner windings from coupling to the current return so the return/outer winding can be treated as a separate system. Inductance for the return/outer winding is described by Equation 4.2.1 and the capacitance of the winding is described by Equation 4.1.1. Neglecting the capacitance between the return and the outer winding is justified by connecting the outer conductor of the winding to the return and charging the inner conductor as seen in Figure 4.2.2.

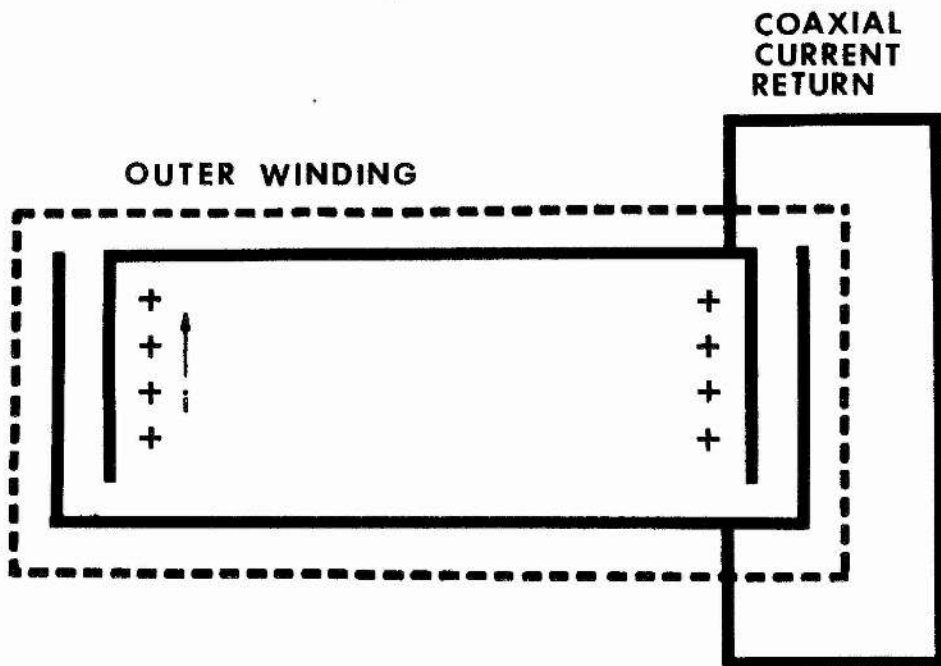


Figure 4.2.2 Model of outer winding and current return of a spirally wound capacitor pack.

The outer winding of B_1 has a capacitance of 250 pF, 4% of the pack total. Capacitance between the pack and the current return is 12 pF. Inductance of the coaxial assembly of the pack from B_1 together with the coaxial return is 912 pH. Current flow in outer winding region is in the axial direction.

Because of the skin effect, current is not allowed to flow out of the inner windings through the foil edges in the axial direction but must follow the spiral to the outer winding. This characteristic makes the inner windings behave as a transmission line. When a capacitor pack is unrolled on a flat surface and viewed in cross-section, it appears as depicted in Figure 4.2.3, a simple transmission line.

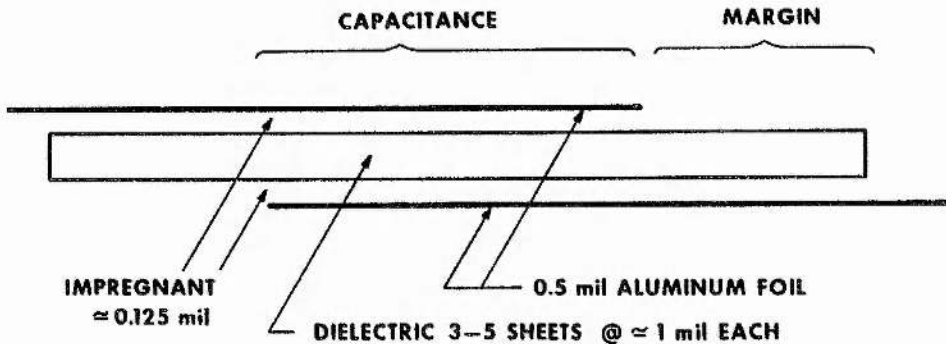


Figure 4.2.3 Cross-section of a winding of a spirally wound capacitor pack.

Unrolled dimensions of the B_1 polypropylene film/silicone oil pack are as follows: length of 2.95 meters, active width of 0.0112 meters, and a plate spacing of $108 * 10^{-6}$ meters. From these dimensions the characteristic impedance of the pack is calculated to be 1.89 ohms and the inductance/length

is 21.8 nH/meter. As mentioned above, each capacitor has 6 of these packs in series giving a total impedance of 11.3 ohms for the capacitor. If the pack behaves predominantly as a transmission line, then the inductance of the total capacitor can be calculated from $L = CZ^2$, where C is the case value and Z is the transmission line impedance (calculated from the unrolled pack) times the number of series packs. From this equation a calculated lumped equivalent inductance for the B₁ capacitor is 130 nH. Thus the conclusion might be drawn that by knowing the winding dimensions and dielectric, the inductance of the capacitor could be calculated. For capacitors such as B₁, with a large winding aspect ratio, this is true. However, as will be shown, the physical dimensions of the winding have a large effect on the electrical characteristics of a capacitor.

For a winding to exhibit transmission line characteristics, the length of the winding must be longer than the active width. Assume, that for lengths greater than ten times the active width, the windings behave as a transmission line and, for lengths less than this, the winding is predominantly capacitive. For the B₁ unit, this "transition section" from capacitive to transmission line characteristics is approximately 10 cm or 1.5 turns. (Remember the outer-most winding behaves as a coaxial capacitor and has only axial current flow.) This "transition section" is the 1.5 turns between the outer-most layer of the pack and the point where pack characteristics become transmission line dominated. Current

in the transition section will have both an axial and spiral component. Therefore, the model of the B_1 spiral pack consists of the 2.5 turns that appear as a 690 pF coaxial capacitor and all subsequent layers behave as a 1.9 ohm transmission line 2.83 meters long. From these assumptions, it is clear that such a winding behaves primarily as a transmission line much as the impedance calculation above implies. In view of this, a lumped equivalent model of the B_1 capacitor can be derived.

From these assumptions a 1 nF, 25 nH capacitor was designed. Manufacturer B was selected to construct the unit. This capacitor had a small inside to outside pack dimension ratio, a larger active width, and a larger diameter. It was designed so that the length of the winding was equal to ten times the active width to minimize the transmission line effect. This unit was subjected to the same test as before and the results are listed in Table 4.2.1 as device B. With the assumptions listed above, a capacitor was designed to meet a certain inductance specification and the designed calculations were verified by experiment. Three generations of spirally wound capacitors are shown in Figure 4.2.4. The third generation, labeled with a 3, is the 1 nF, 25 nH unit described above.

Having derived a method for calculating the inductance of the spiral units, the vector impedance meter was consulted for verification of calculations. Spirally wound units are much more complex than two plates separated by a dielectric such as the ceramic units; this additional complexity shows up in the impedance measurements. All the

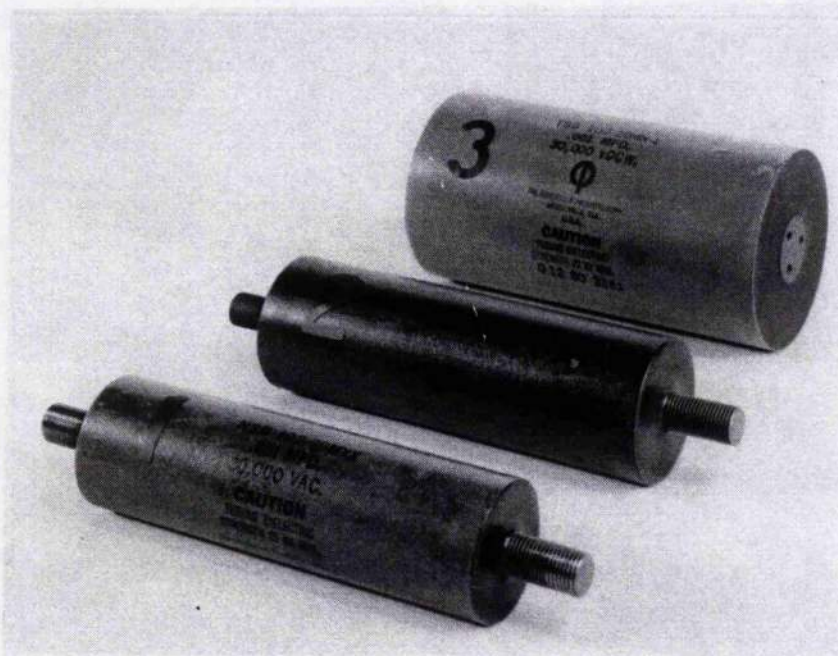


Figure 4.2.4 Three generations of spirally wound dielectric film capacitors.

film/oil capacitors exhibited several self resonances over the range of the meter. First resonances were in the range of 11 to 16 MHz, corresponding to inductances from 100 to 200 nH which is consistent with the calculated and in-circuit measured inductances.

The test circuit is modified to accommodate the varying packages of the film/oil capacitors for each of the measurements. Procedures for the measurements were conducted as previously described to maintain consistent experimental data.

During the course of the investigation, many capacitors were evaluated and many changes in design were implemented. Table 4.2.1 reflects the changes as denoting the earlier units with numeral subscripts. The final or only generation

is denoted by no subscript. For example, manufacturer B supplied three generations of capacitors during the investigation. These are denoted as B₁, B₂, and B, where the latter is the final test device. The number of iterations from a particular supplier is determined by life, inductance, voltage and temperature stability, and other factors. Some capacitors such as those from supplier G, had no changes. Results for the inductance investigation are listed in table 4.2.1.

SUPPLIER	CASE VALUE (nF)	INDUCTANCE (nH)		
		CALCULATED	Z-METER	IN CIRCUIT
A ₁	.5	-	69	86
A ₂	1	-	123	144
A ²	1	-	31	24
B ₁	.5	130	155	128
B ₂	1	125	155	125
B ²	1	20	41	25
C ₁	1	141	190	185
C	1	140	152	177
D	1	63	71	88
E	1	164	188	189
F	1	22	26	30
G ₁	1	18	25	26
G _{2.7}	2.7	18	25	29
H	1	22	31	36

A = MICA; B,C,D,E = FILM/OIL; F,G,H = CERAMIC

Table 4.2.1 Inductance values for many of the test capacitors.

There are three ceramic types not listed because these units had lifetimes shorter than that required to make the

capacitance and inductance measurements. With the inductance values in Tables 4.2.1 combined with the capacitance values of Table 4.1.2, we are left with only the determination of the equivalent series resistance of the test capacitor to complete the electrical model presented in Chapter 2.

SUMMARY

Ceramic capacitors of the types investigated, when mounted in a cylindrical current return, can be treated as a coaxial assembly for the measurement and calculation of inductance. Inductance of the ceramic capacitors is verified by three independent methods. Mica paper capacitors have such complex geometries that only direct measurements are a viable means of inductance determination.

Spirally wound units with extended swaged foils are modeled as a coaxial assembly and a transmission line. Criteria for treating the spirally wound capacitor as a set of nested coaxial cylinders are determined and verified. Based on the assumptions,

$$l - l_{out} < 10 w_a \quad \text{capacitive dominated}$$

$$l - l_{out} > 10 w_a \quad \text{transmission line dominated}$$

where we have l = total winding length,

$$l_{out} = \text{length of outer turn, and}$$

$$w_a = \text{active foil width}$$

it is possible to design or calculate the inductance of a spirally wound pack from its physical dimensions. Outside the boundary conditions, the spirally wound pack must be treated as a capacitor consisting of three separate sections:

1} A coaxial capacitor consisting of the outer-most turn of the spiral; 2} a capacitor consisting of the number of turns inward from the outer layer for a length not to exceed ten times the active foil width; and 3} as a transmission line for all subsequent turns inward.

4.3 THE EQUIVALENT SERIES RESISTANCE, ESR

In high repetition rate pulsed circuits, component losses are a major design consideration [McDuff, Nunnally, Rust, Sarjeant, 1980; Thompson and Mauldin, 1983; Sarjeant, 1984]. Accurate means of calculating the power dissipated by a pulse capacitor is essential for determining the electrical efficiency and in designing cooling systems for removal of the associated heat. In high voltage systems, dielectric loss can be a major contributor to power dissipation. Total energy dissipation in a capacitor is the sum of dielectric, tab, corona, lead connections, and skin effect resistive losses. Dielectric loss [Clark, 1962] is dependent on temperature, voltage, and frequency which adds to the complexity of determining an accurate value. From the circuit designer's point of view, ESR involves cooling requirements, packaging, and component layout. Also, with the ever increasing interest in extraterrestrial application where ejection of heat at low temperatures by radiation is both awkward and requires much space, efficiency is of utmost importance. For the capacitor designer, a knowledge of ESR is important to the construction techniques used. Thermal design of the unit is dependent on the amount of heat requiring rejection. Ensuring that the internal

temperature does not exceed a predetermined level is essential for long life. Temperature control may be as easy as the addition of radiating fins or as complex as active cooling with the windings.

It was found during this investigation that the loss in a capacitor is interdependent on many variables. Accounting for all the dependencies in a model or low voltage simulation is close to impossible because of the voltage and frequency nonlinearities. Several methods of ESR determination were investigated, and for a limited range of conditions, most give accurate results. The only method found that accounts for all the parameters affecting the total loss of a capacitor is the calorimeter.

Several electrical methods are commonly used to measure the ESR but all are burdened with certain assumptions and restrictions that limit the accuracy over a broad operational parameter range. An examination of the common electrical methods is made and the limitations of each are discussed below. After the electrical methods, there follows an approach which gives accurate results regardless of frequency and voltage effects.

4.3.1 DISSIPATION FACTOR AND "TAN δ "

Classically the loss for a dielectric is described by the Dissipation Factor or "tan δ ". An equivalent AC circuit [Seacat, 1973] for a capacitor can be described by a parallel RC network having real and reactive components. The angle, δ , is measured between the total current vector

and the capacitive current component. Pictorially the dissipation factor can be described as seen in Figure 4.3.1.

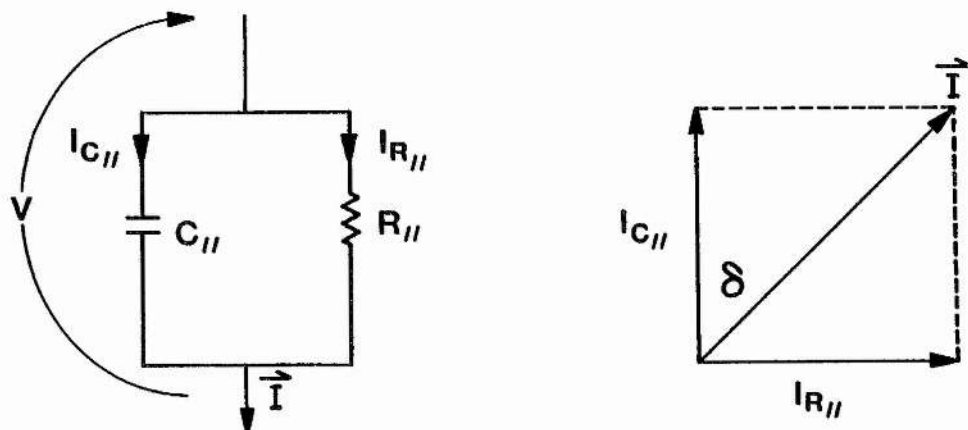


Figure 4.3.1 Low frequency equivalent circuit and resultant vector diagram used for defining $\tan \delta$.

By definition, we have

$$\tan \delta = \frac{I_{R//}}{I_{C//}}, \quad (4.3.1)$$

and knowing

$$V = X_{C//} I_{C//} = R_{//} I_{R//}, \quad (4.3.2)$$

we find

$$\tan \delta = \frac{1}{\omega R_{//} C_{//}}. \quad (4.3.3)$$

The parallel resistance can be related to the equivalent series resistance by the equation

$$R_{ESR} = \frac{R_{//}}{1 + \frac{1}{\tan^2 \delta}}. \quad (4.3.4)$$

Dissipation factors are usually determined in test samples of dielectrics in specially designed test fixtures such as the guard ring capacitor. A General Radio Model 1690 Dielectric Test Fixture is used to measure the $\tan \delta$ of the dielectrics used in the capacitors under investigation. Several conditions are made in defining the dissipation factor. These are: {1} the applied voltage is sinusoidal; {2} the dielectric exhibits no nonlinearities; {3} lead and connection resistances are neglected; and {4} the inductance of the capacitor is neglected.

For most low voltage/frequency AC applications, the $\tan \delta$ measurements will yield results with only a few percent error if the applied excitation is of the approximate frequency to which the dielectric in question will be subjected in use. In particular, in small value capacitors (1-100 nF) the inductance is often equal to or larger than the capacitance. However, in high repetition rate pulsed circuits where the pulse widths are short, the inductance of the capacitor as described in Section 4.2, can not be ignored. This is easily demonstrated mathematically in a simple example. Assume we have a capacitor with no loss, just capacitance and inductance. The equivalent circuit and resultant vector diagram is seen in Figure 4.3.2. When measuring the value of the capacitive reactance, or capacitance with an impedance bridge, the measured value is represented by $X_{C_{MEAS}}$ in Figure 4.3.2.

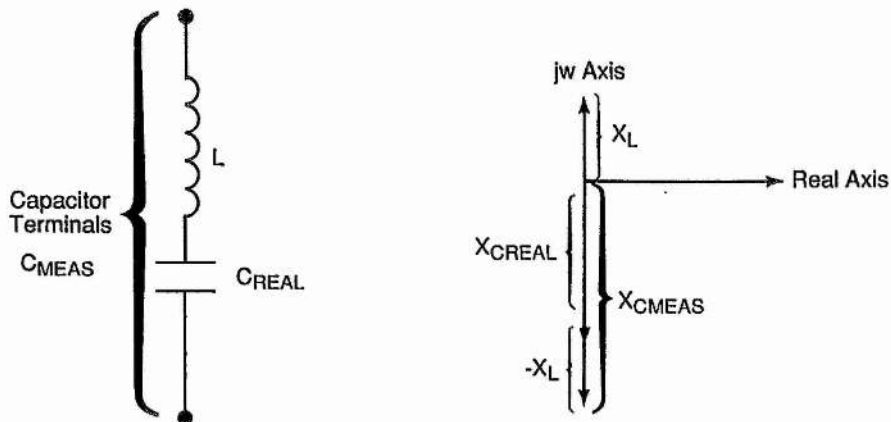


Figure 4.3.2 Effect of lead inductance on measured value of capacitance.

Accounting for the inductive component we can write

$$X_{C_{REAL}} = X_{C_{MEAS}} + X_L \quad (4.3.5)$$

Substituting the AC steady state values and simplifying we get

$$C_{REAL} = \frac{C_{MEAS}}{1 + \omega^2 LC_{MEAS}} \quad (4.3.6)$$

where C_{MEAS} is the measured value of capacitance and C_{REAL} is the actual capacitance. It is seen that the inclusion of the lead inductance, which is never zero, adds to the value of the real capacitance, C_{real} . Therefore, only when the excitation frequency is sufficiently low, such that the contribution of the lead inductance is small can the above method of dielectric loss yield an accurate value.

4.3.2 TEMPERATURE AND FREQUENCY EFFECTS

Temperature increase has a depolarizing effect on material properties. In dielectrics with a Curie point, when this temperature is reached, the material dipole moment all but vanishes along with the susceptibility. In dielectrics chosen for pulse capacitors, the dissipation factors usually increase smoothly with temperature as seen in Figure 4.3.3.

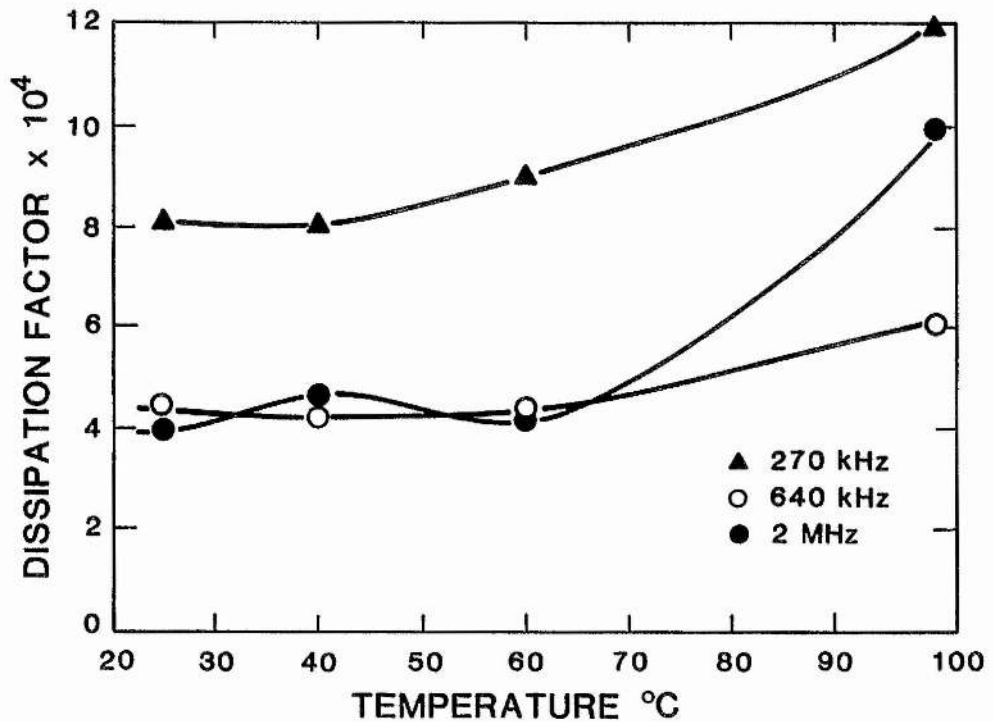


Figure 4.3.3 Temperature dependence of dissipation factor in capacitor grade Teflon.

Unlike the temperature dependence, dissipation factor exhibits a strong frequency dependence in certain ranges. This characteristic can be tailored to fit specific needs by the addition of fillers to the polymer resin films. Plots

of $\tan \delta$ for Teflon and Teflon with several fillers can be viewed in Figure 4.3.4. Likewise, ceramic [Yamaji and Waku, 1972] and mica [Clark, 1962] dielectrics exhibit similar properties and can be custom designed for specific requirements. It is easy to see that the optimum dielectric would have a dissipation factor that is independent of temperature and frequency effects.

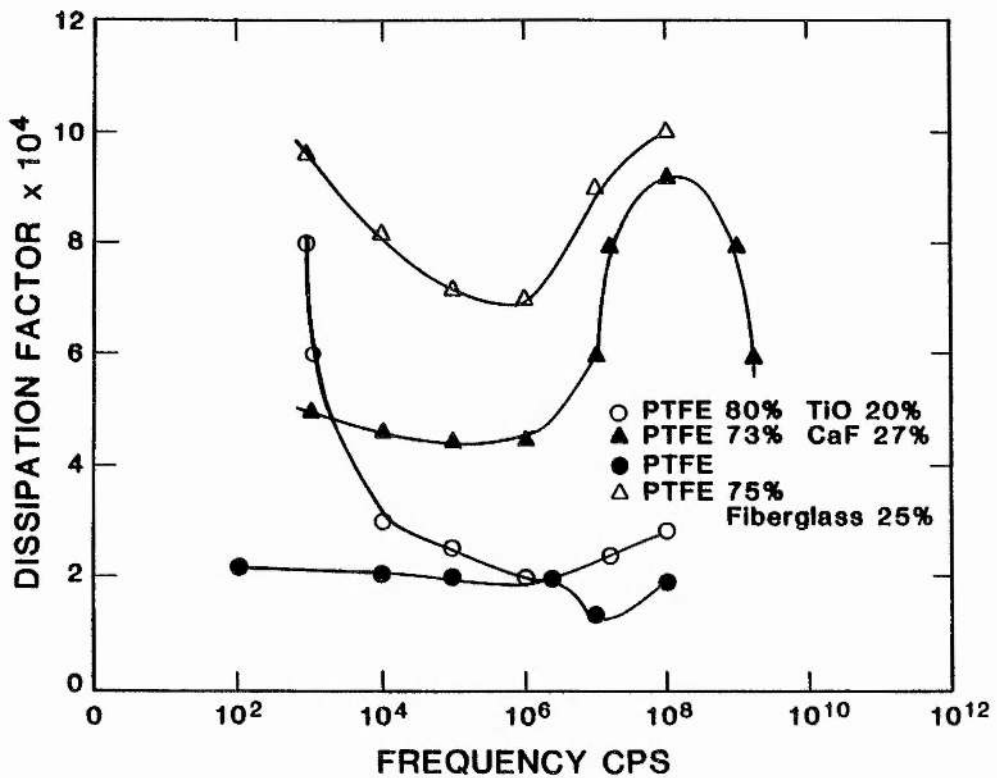


Figure 4.3.4 Dissipation factor as a function of frequency for Teflon and Teflon compounds.

4.3.3 ELECTRICAL METHODS

To investigate the total loss of capacitors electrically, a lump model proves sufficient for most engineering calculations. Working from the lumped equivalent high frequency model of the discharge circuit as

described in Section 4.2 it is quite simple to calculate the ESR. Having the digitized waveform for $i(t)$ and $V(c)$, a computer program was written to calculate the value of ESR. This method of loss determination is calibrated with a low voltage, high loss capacitor of a known (0.25 ohms) equivalent series resistance. The calibration procedure consists of taking ESR data with the known loss capacitor, then adding a 0.25 ohm resistor in series with the unit and retaking the data. After several iterations, the ESR can be determined when the measured value doubles. This empirical determination was successful on the 50 volt test unit. However, when a low loss capacitor of any type is checked with this technique an insurmountable problem arises. It was quickly realized that the high voltage diagnostics did not have the dynamic range to detect milliohms in a circuit operating at many tens of kilovolts and many kiloamperes. Assuming that the probes would be accurate over this range, the digitizer has only a 40 volt resolution at 20 kV and 1.9 ampere resolution for the 1000 ampere pulse. With this minimum resolution, resistance can be resolved down to 50 milliohms which is many times larger than the ESR of the capacitors in question.

ESR METERS

Commercial ESR meters usually use a four terminal technique also known as the Kelvin method. A four terminal meter consists of an A.C. current source of fixed low impedance and a high impedance voltage meter. When the voltmeter is phase locked to the AC excitation signal the

voltage reading is proportional only to the real component of the impedance of the device under test. Details of this method have been described in numerous basic electronics texts and will not be discussed. The major drawback to this type of measurement is that it is prohibitively expensive to construct a constant impedance broadband AC source at the voltages of interest. All commercial meters work at voltages less than 50 volts and fixed frequencies, usually 1 kHz or 100 kHz.

SERIES RESONANCE METHOD OF ESR DETERMINATION

One of the most common methods of ESR determination [Haywood, no date; Sarjeant, 1979] employs a RF power oscillator driving the capacitor in question at its first self resonant frequency. If the output impedance of the oscillator is much less than the ESR of the capacitor then an accurate value can be obtained for that particular frequency. There are, however, four major weaknesses to this method. These are: {1} often the major frequency component of the discharge circuit in which the capacitor will be used is nowhere near to its first self resonance; {2} the power required to drive the zero impedance at series resonance is large; {3} making an oscillator with an impedance lower than the ESR of low loss capacitors is a major achievement in itself and {4} in the case of spirally wound units, there is rarely a true series resonance.

CIRCUIT ENERGY INVENTORY

As the name implies, in this method, ESR can be calculated by taking an inventory of the energy around the discharge circuit. This method is described at length by McDuff, Nunnally, Rust, and Sarjeant [1980]. The principle of this technique is to use large magnitude circuit parameters that can be measured accurately to calculate where the energy is stored and dissipated in the discharge circuit. Briefly, by measuring the total energy delivered to the storage capacitor, $1/2 CV^2$, and subtracting the energy dissipated in the switch and the load, the difference is the energy dissipated in the capacitor. This technique allows the ESR to be measured in completed hardware and there is no issue of voltage, frequency, and thermal effects. However, this method does not account for electromagnetic or acoustic radiative losses. Scrutinizing, this technique revealed two significant limitations. First, to obtain an accurate result, the dynamic range of the measurements must involve at least six decimal places in order to detect sub-milliohms in a circuit operating at tens of kilovolts and kiloamperes. The second factor discovered, is that the resistance of the connections in the test circuit had a greater influence than predicted. It was found that the connections of the capacitor in the circuit contribute up to 50% of the energy dissipated. When adding the dissipation of the probes to the circuit, an artificially high value is obtained. A larger than actual value could be considered the worst case but for some applications (extraterrestrial) where every milliwatt

counts, it is not acceptable. This investigation determined that while the ESR of the test capacitor could be measured by this method, the capacitor would not be suitable for high repetition rate circuits.

VECTOR IMPEDANCE METER

The last, and by far simplest, electrical method which will be discussed is the vector impedance meter. Instead of placing the capacitor in series resonance, the capacitor is connected in parallel resonance where the impedance is maximum. This can be done with standard components or with the Hewlett Packard Vector Impedance Meter. At parallel resonance the ESR of the circuit determines the Q. As with other low voltage methods, dielectric nonlinearities are not taken into account.

As it was plain to see by this point, ESR determination of low loss capacitors via electrical methods is too complex to be of real use. After an in depth search, it was decided that the only truly accurate way to include all aspects of capacitor losses is to use calorimetric methods.

4.3.4 CALORIMETER/PULSE MODULATORS

Initially, it was not anticipated that combining a calorimeter in a pulse modulator would be a major undertaking. However, as it was subsequently realized, the losses in a well designed low loss capacitor are much smaller than predicted by the electrical methods or values previously reported. Also, the environmental conditions have a great effect on the calorimeter when such small

powers are being investigated. Because the main interest is in pulse widths of 50 nS to 2 uS, the inductance of the discharge circuit must be kept at a minimum. Close physical proximity of the components in the low inductance discharge circuit gave rise to a real thermal isolation dilemma. It was found that not only did thyratron dissipation affect the temperature measurement in the calorimeter but the ambient room temperature as well.

The final apparatus consisted of the standard RLC discharge circuit as described in Section 3.1. A schematic/pictorial of the experimental calorimeter modulator is illustrated in Figure 4.3.5. Referring to this

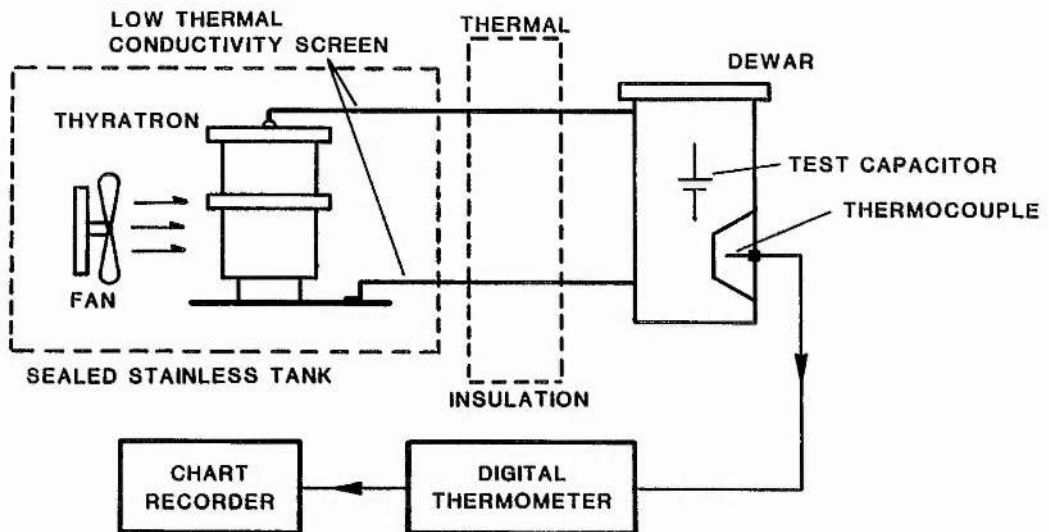


Figure 4.3.5 Modulator/calorimeter schematic diagram.

figure, heat from the stainless steel tank is exhausted outside via special ducting so as not to influence the room temperature. Electrical connections from the dewar are made of high thermal resistance screen so as not to transfer heat

from the modulator to the dewar. The dewar itself is also insulated from the modulator tank by six layers of 0.125-inch thick asbestos. These precautions reduced the perturbations caused by the thyratron and the ancillary circuitry. The long term stability of the calorimeter was such that over any 30 minute period, the temperature inside the dewar was found to be constant ($<0.055^{\circ}\text{C}$ fluctuation). Over a 24-hour period, the temperature would vary by $\pm 1.2^{\circ}\text{C}$ tracking the daily rise and fall of ambient temperature. This characteristic set the upper bound of the length of the test period to 30 minutes. Before describing on the rest of the experiment, a brief explanation of the calorimetric measurement is in order.

From basic thermodynamics, we have

$$C = \frac{H}{m(T_2 - T_1)}, \quad (4.3.7)$$

where we have m = mass of the calorimeter medium,

C = specific heat of the calorimeter medium,

H = heat added to systems in calories,

T_1 = initial temperature in $^{\circ}\text{C}$, and

T_2 = the final temperature in $^{\circ}\text{C}$.

Measuring the temperature rise of the mass contained in the dewar, the power input, P , of the system can be calculated by

$$P = \frac{Cm(T_2 - T_1)}{t} \quad 4.185 \text{ Watt-sec}, \quad (4.3.8)$$

where t is the time for which power is input to the system. Once the input power is found, it is a simple calculation to find the ESR. As mentioned above, the length of the measurement period was limited to 30 minutes by the nominal $0.055\text{ }^{\circ}\text{C}$ change in the calorimeter temperature. Many calibration tests were made to fully characterize the behavior of the calorimeter.

Sulfurhexafluoride was selected from several gases and fluids for use as the calorimeter medium. Nature was kind in providing SF_6 with a mass and specific heat of the appropriate value to allow a sufficiently large temperature rise in the system during the test period and also providing the electrical insulation required. By judicious choice of the calorimetric medium, the effect of heat loss from the dewar and heat input from extraneous sources can be eliminated. Current from the current viewing resistor was recorded by the computer controlled waveform digitizer/data acquisition system to make the ESR calculation. The repetition rate was initially 1000 pps and is adjusted slightly so that the RMS current in the test unit is exactly 10 amperes. Ten amperes was chosen because it is convenient for calculations, large enough to produce enough heat to be measured, and is a typical current rating of the type of capacitor under investigation. Discharge pulse shape was a half-cycle sinusoid with a base width of 70 ns with 25% current reversal in the first test and 1.5 μs with 80% reversal in the second.

To calibrate the calorimeter, the test capacitor is moved into the stainless tank and a 1% tolerance, 0.05 ohm

resistor network is connected in the dewar. Temperature rise data is taken for the standard test period and the power input to the calorimeter is calculated. As a secondary calibration, the same resistor network is driven by a constant power low voltage source at the power calculated from both pulsed measurements of the resistor and a test capacitor. Discrepancies between the temperature measurements from the capacitor and both resistor calibrations are found to be ± 20 and $\pm 40\%$. Despite the fact that the absolute accuracy was poor, the impact in the design of a large energy storage network is small due to the minuscule ESR values. For example, for a capacitor with 0.316 milliohms ESR at 10 amperes RMS, variance in the power dissipation due to measurements inaccuracy is 20 to 40 mW. A bank of one hundred such capacitors would weigh 160 lbs and dissipate 2 to 4 watts, or about 25 mw/lb. This error is still an order of magnitude less than can be measured with any other method investigated. Measurement procedures were determined empirically during calibration. After the capacitor was installed and the dewar filled, the entire modulator with all ancillary power applied (except high voltage) was allowed to equilibrate for 24 hours before data was collected.

Nine capacitors were tested from eight manufacturers which produce capacitors specifically for service at high repetition rates. The results can be found in Table 4.3.1 along with various electrical parameters of interest. Four are film-fluid impregnate, three ceramic, and one reconstituted mica. Of the four film-fluid types, two are

comprised of polypropylene/silicone oil, one Teflon/silicon oil, and one polysulfone/fluorocarbon fluid. The film capacitors are represented in the table by manufacturers B, C, D, and E; the ceramics by F, G, and H; and the mica, by Manufacturer A.

SUPPLIER	CASE VALUE (nF)	ESR 80nS (mΩ)	ESR 1.5 uS (mΩ)
A	1	0.617	0.747
B	1	0.480	2.940
C	1	0.445	0.274
D	1	0.316	0.125
E	1	0.645	0.099
F	1	1.100	1.220
G1	1	1.470	1.532
G2.7	2	1.690	1.450
H	.5	1.540	FAILED

A = MICA B,C,D,E = FILM/OIL F,G,H = CERAMIC

Table 4.3.1 ESR of the nine final test capacitors.

Inspecting Table 4.3.1 it is seen that the ESR values are relatively constant except for the entry from Manufacturer B. Autopsies of the B capacitor revealed that this unit had a film wick incorporated for impregnation. Loss characteristics for the wick is referenced in [Clark, 1962] and found to have a peak in the dissipation factor around 1 Mhz. The manufacturer also emphasized that this capacitor was designed for 100 nS pulse width operation and that the loss should increase by an unknown amount in lower frequency circuits. The ESR in the mica and ceramic

capacitors remained constant for both frequencies of interest which is consistent with data published by Yamaji and Waku, 1972, and by Clark, 1962.

4.4 MECHANICAL FORCES

Anyone who has ever been around a repetitive pulse modulator is familiar with the boisterous whine associated with its operation. This brings to light a very important issue, simply stated, any noise you can hear, has some serious mechanical forces as its source. Noise generated by modulators is not only annoying, but can present an added engineering task in its reduction to meet safety standards. Three main sources of noise generation in a pulse circuit are electrostriction, magnetostriction, and acoustic shock due to gas discharge. Since capacitors are non-ferrous and hopefully do not experience gas discharges, electrostriction is the only process to be considered. Electrostriction is defined as the property of a dielectric to deform under the influence of an electric field. Materials that have a reversible electrostrictive property are known as piezoelectric. In capacitors, electrostriction is important not only in noise control but impinges upon the design and life of the device. Many capacitor failures are related to material fatigue caused by the repetitive forces generated within the component. Sometimes mechanically related failures are due to disturbances in the physical condition of the capacitor such as wrinkles in thin foil conductors which result in electric field enhancement and high local dielectric stresses. In particular, spirally wound fluid

impregnated capacitors may display a change in value due to electrostrictive movement.

FORCES IN SOLID DIELECTRIC CAPACITORS

Consider the ceramic capacitor seen in Figure 4.4.1.

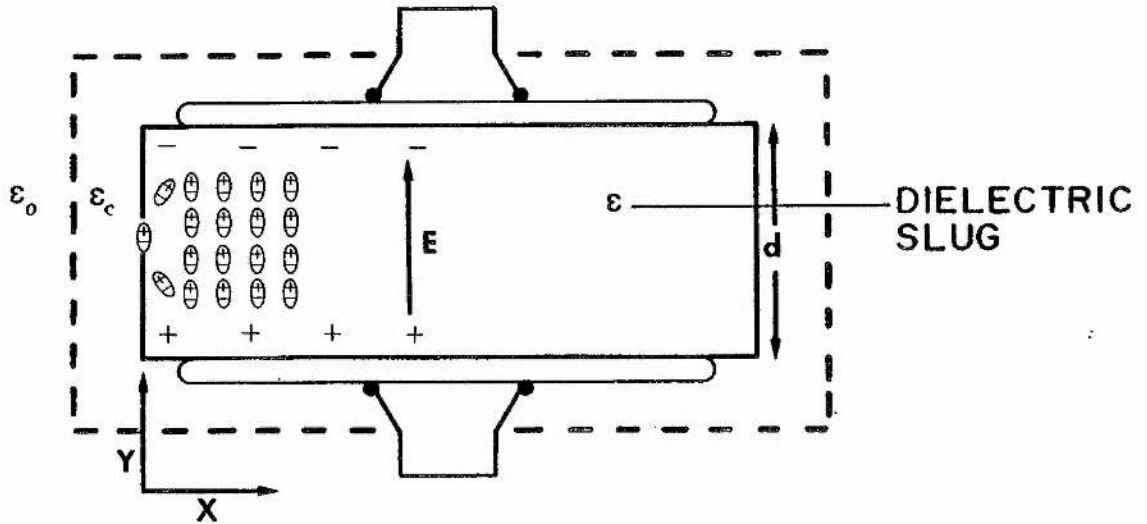


Figure 4.4.1 Diagram for force analysis in ceramic capacitors.

When a voltage is applied the dipoles align in the direction of the electric field, E . Neglecting the fringe fields on the edges of the capacitor for now, the attractive force between the plates is

$$f(y) = \frac{1}{2} V^2 \frac{dC(y)}{dy} = -\frac{1}{2} \frac{\epsilon AV^2}{d^2} \quad (4.4.1)$$

where we have A = capacitor plate area,

V = charge voltage,

$\frac{dC(y)}{dy}$ = capacitance position dependence function.

This force is due to opposing charges, and is in the $-y$ or axial direction resulting in a compressive force. It should also be noted that the force is proportional to the relative dielectric constant of the material between the plates.

It can be seen from Equation 4.4.1, that if the dielectric contains impurities (which is always the case), with a relative dielectric constant greater than the base material these impurities will be acted on with a greater force. Simply stated, forces on the dielectric will try to pull the higher dielectric constant material into the capacitor and expel the lower dielectric constant material. A mathematical derivation of the forces on a dielectric is found in Appendix 2. Since the charge voltage is related to the electric field in the dielectric, then the above statement can be modified to say that the higher dielectric constant materials will be attracted toward the high field points, i.e. the edges of the capacitor plates. Thus, high purity and stress relief on conductor edges (Figure 2.2.2) are important in capacitor design. Internal forces result if the dielectric contains impurities or has breakdown products that have a different dielectric constant than the base material. These internal stresses in a solid dielectric can lead to fractures. For example, neglecting electrostrictive effects, the 1 nF ceramic capacitor G1, will have a total axial pressure of 72.3 kPa (10.5psi) exerted on the dielectric when fully charged. These forces are important considerations in the design of the dielectric material. Crystal orientation, compliance, stiffness, and

stresses must all be taken into account in the design to achieve mechanical strength and long life. This complex problem gets even more complex when accounting for the electrostrictive nature of most ceramic crystalline structures.

ACOUSTIC POWER GENERATION

Total power delivered to or from a capacitor is the sum of the time rate of change of electrical energy plus the product of the force and the time rate of change of dimensions, Equation 4.4.2. The first term is related to the electrical energy stored and the second to the mechanical energy stored in compressing the dielectric.

$$\text{POWER} = \frac{d \text{ Energy Elect.}}{dt} + F(x,y,z) \frac{d(x,y,z)}{dt} \quad (4.4.2)$$

Since dimensional change is very small, the second term is insignificant except for very small time intervals or pulse widths. When a capacitor is discharged slowly, say greater than 1 μs , very little mechanical power is transferred to the environment. However, in short pulse discharges this term becomes significant and the power transferred to the environment takes the form of heat and acoustic pressure waves. It is very important to note, from Equation 4.4.2, the total loss in a ceramic capacitor, has a pulsewidth dependency due to mechanical forces as well as material properties.

Calculation of the transfer of mechanical power to the environment is described [Mason, 1964] by nine time dependent linear equations relating stress, strains, polarization, mass, electric fields, and compliance in three dimensions. Solutions depend on the electrical inputs and the physical characteristics of the dielectric. These values are available for material similar to that used in capacitor H. Values for mechanical coefficients for units F and G are not available from the manufacturer nor is the exact material description other than "SrTiO₃ plus other ingredients."

Determining the electro-mechanical coupling coefficient is complicated further by the physical layout and mass damping of the discharge circuit. Mounting ceramic capacitors in a semi-rigid structure, i.e. at least one deformable connection, will allow the unit to deflect due to electrically induced forces. Rigid mounting will increase the stress on the capacitor by not allowing for deformation due to electrostriction. Rigid mounting of all the ceramic test capacitors lead to an early failure due to fracture of the dielectric material or breaking of the internal connections between the metallization and the terminal lugs. At least one terminal of a ceramic dielectric capacitor used in a short pulse circuit should have some form of stress relief when mounted. Thickness of the conductors should be chosen for stress relief rather than electrical properties because, in short pulse circuits, the skin effect will limit the area of the conductor used. Electrical connections made with very thin (foil) conductors

are recommended for the longest reliable life of the capacitors. Transmitted mechanical pressure waves are negligible as far as damage to adjacent components is concerned but must be considered in the design of the acoustic insulation.

ACOUSTIC MEASUREMENTS

The main interest in this investigation is not of the molecular interaction in dielectrics but in the development of long-life capacitors for high repetition rate circuits. Two items of concern when designing a circuit with ceramic capacitors are the mechanical mount and acoustic insulation necessary to keep the generated noise to a tolerable level. Measurements are made to derive a general factor of noise generation that could be used in designing acoustic insulation for future modulators. A General Radio Effective Sound Pressure Level, SPL, meter with A weighting is used for the measurements. Sound pressure level with A weighting is the accepted industry standard for noise control. Pressure readings are fairly uniform in the experimental screen room except at positions well below the top of the oil tank towards the floor where the level begins to drop off. Pressure wave uniformity is such that the directivity factor induced by the oil tank can be neglected. The SPL meter microphone is mounted on the inside wall of the experimental screen room approximately one meter from the surface of the oil. The SPL is recorded for groups of eight capacitors each of Types F, G1, G2.7, and H positioned 40 cm below the surface. Measurements are made inside the screen

room with the door closed at 1000 pps at the full rated voltage of the capacitors under test.

The noise generated is of multiple frequencies due to interference effects in the oil and the room, so the data can be analyzed as described by classical ray theory [Sabine, 1922] of diffuse noise. Using this approach simplifies the analysis and has been found to give fairly accurate results in the area of architectural acoustics. After the circuit is switched on, there is a period in which the sound level grows in a closed volume until the rate of generation equals the rate of absorption. The screen room being fairly "live", that is, having a small coefficient of absorption, α , the time to equilibrium is on the order of a few seconds. The thyratron test circuit used throughout the capacitor investigation generated a 66 dBA SPL with the discharge capacitors heavily muffled. Sound pressure levels and intensities for groups of 8 ceramic capacitors, Types F, G1, G2.7 and H are listed in Table 4.4.1. Using capacitor G1 as an example, the effective pressure, P_{eff} , is calculated from the SPL in Table 4.4.1 by $SPL = 20 \log P_{eff}/P_0$ where P_0 is the 0 dB reference pressure of 0.00002 Pascal. From the pressure, the sound intensity, I_{air} , can be calculated for random diffuse noise as $I_{air} = P^2/8\rho_0c$ in watts/m² where ρ_0c is the characteristic impedance of air at room temperature in rayls. The sound intensity in the oil is calculated from $I_{oil} = I_{air} * -\Psi$, where Ψ , is the sound intensity transmission coefficient. The sound intensity transmission coefficient from oil to air is -29.4 dBA [Kinsler, 1950]. The sound intensity in the oil is listed in

the last column of Table 4.4.1. The power required to generate the room intensity of 73 dBA is given by

$$W_{oil} = I_{oil} \alpha S = 905 \text{ uW} \quad (4.4.3)$$

where we have S = inside surface area of tank in m^2 ,

α = absorption coefficient in Sabines/ m^2 ,

SUPPLIER	SPL (dBA) (ref.00002Pa)	INTENSITY ($W/m^2 * 10^{-6}$) (air)	INTENSITY ($W/m^2 * 10^{-3}$) (oil)
F	74	3.024	2.634
G1	73	2.404	2.094
G2.7	74	3.024	2.634
H	89	95.71	83.36
Test Circuit	66	.4796	.4177

Table 4.4.1 Measured SPL and intensity of groups of 8 ceramic capacitors.

To confirm this calculation, the sound pressure level in air of 86.9 dBA is calculated for the screen room based on a 905 uW source comprised of the capacitors and test circuit. The test circuit is raised out of the oil and operated at full power in air and a SPL of 83 dBA is measured. The discrepancy in the calculated and measured SPLs is attributed to the estimation of the absorption coefficient of the screen room. The value for the absorption coefficient, α , used in the calculation of SPL for the circuit in air is for the bronze screen of 60% transparency commonly used in construction. The screen room which houses the experiment has a double layer of copper of 40%

transparency. However, for the purpose of defining a general conversion factor the correlation between calculations and empirical data is satisfactory. One interesting comment, according to Kinsler [1950], a loud scream requires about 1 mW for generation and the noise generated by the capacitors is about as loud.

Subtracting the contribution of the test circuit and using Equation 4.4.3, the acoustic power generated by the capacitors is calculated at 721 uW. Thus, each capacitor acts as a 90 uW acoustic source, assuming each capacitor contributes equally to the power. This assumption is reasonable because all the test units are mounted in identical fashion and the radiated power is a linear function contributing to the total loss of the capacitor. The pulsewidth of the test circuit for the acoustic measurements is 80 nS, the same as in the ESR measurements in Section 4.3. The total power dissipated in capacitor G1 in the test circuit, from Table 4.3.1, is 147 mW, of which 0.062% is converted into acoustic power. The overall electro-acoustic power conversion, EAC_{noise} , is defined as acoustic power output per capacitor divided by electrical power input per capacitor. Table 4.4.2 lists all the values of EAC_{noise} for the nine final test capacitors. This factor is dependent on all the factors affecting loss discussed in Section 4.3 as well as the rate of discharge. The mass, rigidity, absorption properties, and physical layout of the pulse circuit as well as the size of the enclosure housing the circuit, also affect the acoustic conversion efficiency.

The test circuits are designed to simulate the mechanical design and layout of a high repetition rate excimer laser. The conversion factors for the type G and H capacitors were used in the design of a 400 mJ/pulse 500 pps thyatron switched XeCl laser predicting a SPL of 59 dBA. The sound pressure level at a distance of a few centimeters from the surface of the laser modulator enclosure was measured at 53 dBA when operating into a gas load (see Chapter 6). The lower measured level is attributed to the very large volume and the unknown acoustic characteristics of the laboratory housing the laser. The pulsewidth of the discharge in the laser was 200 ns compared to 80-90 ns of the test circuit and the mechanical layout was much more complicated; also exact values for absorption coefficients, again, are not readily available.

The analysis of the conversion of electric to acoustic power was performed on the ceramic capacitors because of the simple geometry, the pronounced electrostrictive effect, and availability of data. Doing the same for the mica paper capacitors is not as straightforward due to their complex structure. Based on the analysis of the ceramic capacitors, only acoustic measurements were conducted on the final design mica unit. Over half the weight of the mica paper capacitor is due to the high temperature potting compound in which the capacitor pack assembly is encapsulated. The potting compound cures to a semi-elastic state and has a high coefficient of absorption. Of the 14 different capacitors tested, the encapsulated mica unit was by far the quietest. The added mass of the case and the acoustic

properties made the mica SPL just 2 dBA greater than the circuit level of 66 dBA. Units tested that had a lighter weight case had a slightly higher acoustic output. From the SPL measurements, it is difficult to assign a quality factor to the mica units in terms of electrical to acoustic energy conversion when the accuracy of the SPL meter is ± 1 dBA.

SPIRALLY WOUND IMPREGNATED FILM DIELECTRIC CAPACITORS

The same analysis applied to solid dielectric capacitors can be applied to the dielectric film oil impregnated units with a few exceptions. In the case of the spiral units, the dielectric film is essentially suspended in a dielectric fluid that is free to move within the case. Also, coupling of acoustic pressures from the spiral packs to the external environment is a complex route dependent on winding tensions, pack connections, and case material. As with the mica units, only the SPL is measured for the oil impregnated capacitors to derive the factor for electro-acoustic conversion for circuit design considerations. A complete list of the acoustic outputs, percentage of loss contributed to acoustic energy conversion, and conversion efficiency from electrical to acoustic power is seen at the end of this section.

A unique mechanical property of the oil impregnated units was discovered during this portion of the capacitor investigation. Most of the units tested showed a large capacitance change with applied voltage. At first it was thought that this was due to voltage stress as defined by the voltage coefficient of capacitors as described in Table

4.1.2 in Section 4.1. Several references [Clark, 1962 and Manufacturer Data] were consulted and the known dielectric voltage coefficients could not account for the large changes. The answer to this ambiguity came when it was noticed that the voltage dependence varied with the production batch. All incoming capacitors were engraved with a serial number unique to the particular order. A capacitor of a certain production batch would have a different voltage coefficient than an "identical" unit from a different production batch. This indicated that the measured "voltage coefficient" for the oil impregnated capacitors is more dependent on a mechanical parameter than an electrical property of the dielectric. The capacitance at full voltage of all the first generation capacitors is randomly distributed within $\pm 10\%$ of the case value. This variation is attributed to the winding control of the capacitor packs. Small variations in capacitor dimensions due to winding tension, thickness of fluid layer, and foil alignment do not affect the final value of the capacitor greatly. However, winding tension and fluid layer thickness determined by impregnation, are found to affect the position dependence, $C(y)$, of the capacitor during charging and discharging. If the capacitor is loosely wound and the foils are allowed to move with respect to the dielectric film, during a charge-discharge cycle substantial capacitance change is possible.

Consider the average relaxed winding layer for a polypropylene silicone oil capacitor pack diagrammed in Figure 4.2.3. The capacitor plates (aluminium foil) are

12.7 μm (0.5 mil), the total dielectric thickness is 102 μm (4 mils), and the nominal fluid thickness is 3.18 μm (0.125 mil). The relative dielectric constant of polypropylene is 2.3 and silicone oil is 2.8. The total capacitance is made up of three series capacitors assuming uniform impregnation. The position dependent capacitance, $C(y)$ per pack is given by

$$C(y) = \frac{\epsilon_0 \epsilon_1 \epsilon_2 A}{d \epsilon_2 + 2 \epsilon_1 \left(\frac{y-d}{2}\right)} \quad (4.4.4)$$

where we have A = plate area,

y = plate separation,

d = dielectric film thickness

ϵ_1 = film relative dielectric constant, and

ϵ_2 = fluid relative dielectric constant.

As described in Equation 4.4.1, as the capacitor is charged, the electric force compresses the dielectric and tries to squeeze out the dielectric fluid. The effect of this force is seen mainly in the outside layers of the common film/oil capacitor where the winding tension is normally less. With the spiral construction, the majority of the capacitance is in the outside layers. Thus, the area of the capacitor pack that is most affected by electrical forces, also has the largest percentage of the pack capacitance. Using the same procedure as used in the voltage coefficient measurements in Section 4.1, the time varying capacitance of the first

generation film/oil units is measured. A typical capacitance versus time graph for a 200 nS discharge of four type B₁ capacitors is seen in Figure 4.4.2. To increase the signal to noise ratio of the measurements, four units from the same production batch were tested simultaneously assuming all are similar in construction. Internal windings of extended foil swaged and soldered packs are essentially sealed off on the ends and the forces are balanced in the inner windings. The only path of fluid movement for pressure relief is of high impedance in the direction of the spiral.

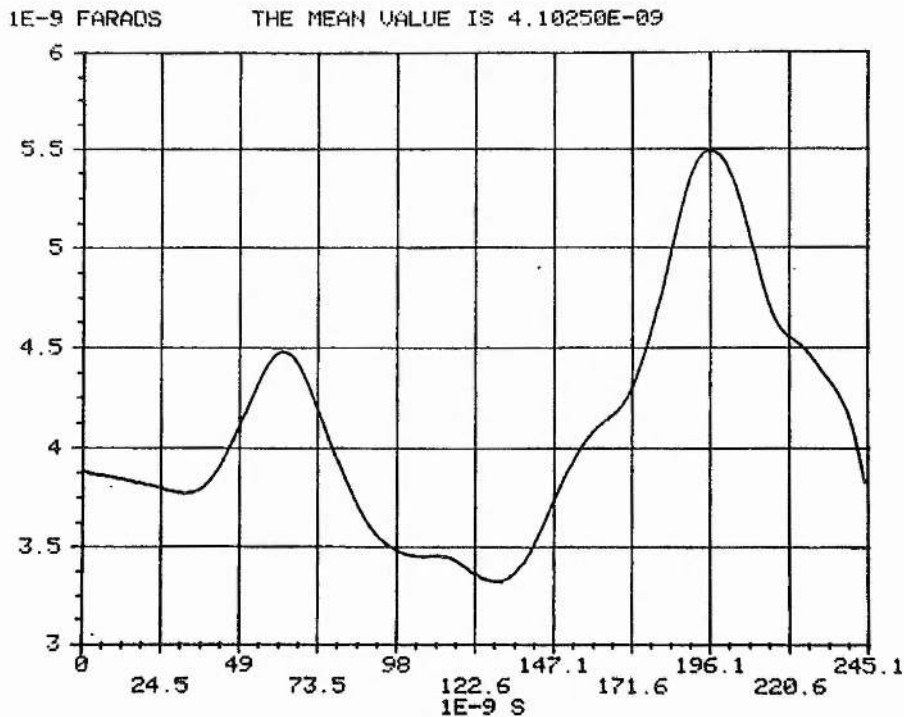


Figure 4.4.2 Time varying capacitance of a normal dielectric film oil impregnated capacitor during the discharge.

To confirm the hypothesis that winding characteristics are responsible for the apparent voltage dependence, the same tests are conducted on a set of capacitors wound with constant tension. These capacitors showed a much reduced voltage coefficient from the previous generation. The new measured voltage coefficients could be related to dielectric properties given by Clark, 1962. Introducing this change confirmed that mechanical forces do affect the value of the capacitance in dielectric film fluid impregnated capacitors. Not only did constant tension windings reduce the voltage dependence of the capacitor value but the life increased as well. Reducing movement within the capacitor reduces material fatigue and probably contributes to a longer life in the polypropylene film capacitors. Teflon film capacitors showed the same dependence on winding tension as the polypropylene but did not show the increase in life. This could be attributed to smaller stiffness value of and better wetting properties (less surface tension) of Teflon but this is not confirmed. Even though the percentage change in capacitance due to mechanical forces is small, it must be considered when the electrical efficiency and performance of a pulse modulator is a critical issue.

SUMMARY

It is concluded that mechanical forces induced by electrical fields are important to both the design of high repetition rate modulators and to the life of pulse capacitors. The most important parameter pertaining to modulator design is the electrical to acoustic power

conversion. A complete list of the acoustic power output per capacitor is presented in Table 4.4.2. Tests were conducted in a 80-90nS 1000 pps discharge circuit at the full rated voltage of the capacitor. The third column lists the amount of total capacitor loss that was converted into acoustical power. Values for the electro-acoustic power conversion factor EAC_{noise} are listed in column four where

$$EAC_{noise} = \frac{\text{Acoustic Power Output/Capacitor}}{\text{Power Input/Capacitor}} \quad .(4.4.5)$$

The acoustic output for the mica and film/oil capacitors is largely dependent on the volume and material of the case and the winding technique of the particular device. General descriptions of the mica and oil-filled units can be found in Section 2.2 along with a photograph of the test capacitors.

The main influence on the life of the capacitors is the electric field induced force. As described by Equation 4.4.2, the force exerted on a dielectric is proportional to the dielectric constant. If impurities or products of electro-chemical breakdown have a dielectric constant greater than that of the bulk material, these compounds will be attracted to the high field regions of a capacitor. Many of the organic electro-chemical damage products of polymer films used in capacitors have dielectric constants greater than the undamaged material. Some of these damage products (such as acetylene gas) are quite mobile in the fluid impregnate. Products that are free to move will concentrate

on the foil edges, giving rise to severely distorted and locally intense electric fields.

NOTE: Data and results for the H type capacitors are highly questionable because these units would fail faster than the data could be recorded.

SUPPLIER	ACOUSTIC OUTPUT POWER/CAP (uW)	% TOTAL LOSS	EAC _{noise} (* 10 ⁻⁶)
A	13.2	.021	.016
B	22.5	.046	.018
C	22.5	.051	.018
D	48.8	.154	.039
E	34.1	.052	.027
F	120.	.109	.096
G1	90.5	.062	.072
G2.7	120.	.071	.096
H	4400	2.9	3.52

A = MICA B,C,D,E = FILM/OIL F,G,H = CERAMIC

Table 4.4.2 Acoustic parameters for nine test capacitors.

4.5 LIFETIMES AND FAILURE MECHANISMS

Knowing a component's electrical characteristics allows the engineer to design accurately the physical dimensions of a high di/dt pulsed circuit. Being able to design a circuit with predictable response greatly reduces the time and effort required in the development of advanced pulsers. At this point in the investigation, the electrical parameters of inductance, capacitance, and equivalent series resistance are well understood. Having the ability to

design repetitive short pulse circuits with great detail is of no real value if there are no components suitable for the duty. As described in Chapter 1, the goal of this effort is to develop pulsed components not only with known and understood characteristics, but with lifetimes of 10^{10} discharges. Because there is practically no information on the life and failure mechanisms for components used in short pulse repetitive pulsers, it is necessary to generate a data base. In order to collect reliable life data, the test circuits must not only simulate the conditions that the component will see in the end use but operate without failure for periods longer than the components under test. This is somewhat of a paradoxical situation since the goal of this programme is to develop the components that are needed in the test circuits. However, it is not as difficult as it first appears. All of the ancillary equipment such as timing, triggers, and bias supplies can be designed such that they operate well within their specifications (i.e., without undue stress). With careful layout and proper selection, the switch limitation can be overcome to some extent but a large portion of the switch development occurs simultaneously with the capacitor testing. After eight years, the original test circuit has accumulated over 38,000 high voltage hours. In the last 24,000 hours, the only failures have been components under test. During the eight years of testing, 292 capacitors failed in life test. Statistical data which is of prime engineering importance is collected for all of the tests and most of the test capacitors were dissected for failure

analysis. A brief review of the statistical variation of the Weibull method for life test analysis is discussed below. The remainder of the section will review the pertinent results of the capacitor life test.

WEIBULL DISTRIBUTION OF FATIGUE LIFE

The Weibull distribution, even though not widely accepted, was chosen for statistical analysis of the life test data. Extreme value distribution for analysis was first proposed by R.A. Fisher and L. Tippett [Fisher and Tippett, 1928]. W. Weibull [Weibull, 1951] proposed a method of relating extreme value distributions for the analysis of fatigue data. The basic assumption of this analysis, is that fatigue failures are due to extreme values, that is, caused by the weakest link. From a component testing standpoint, this method of analysis, regardless of the theoretical basis, has been shown to be useful in the prediction of component performance based on life test data.

Based on the above assumptions, the failure rate of a group of components is represented by the distribution

$$F(N) = \frac{b}{(N_a - N_o)} \left(\frac{(N - N_o)}{(N_a - N_o)} \right)^{b-1} e^{-\left(\frac{N - N_o}{N_a - N_o} \right)^b} \quad (4.5.1)$$

where we have N = component life,

N_a = characteristic life occurring at 63.2%
failure point of the components,

N_o = minimum component lifetime, and

b = the Weibull slope parameter.

It should be noticed that if $b = 1$, $F(N)$ is a simple exponential distribution and if b is approximately 3.5 it is a normal distribution. It can be shown [Weibull, 1961] that the above distribution can be rewritten for the fraction of component failures at life N as

$$F(N) = 1 - e^{-\left(\frac{N - N_0}{N_a - N_0}\right)^b} \quad (4.5.2)$$

where $F(N)$ is the percentage failure. Equation 4.5.2 is now in a form that is easily computed and put into graphical form. This distribution, for capacitor lifetimes, is plotted versus number of discharges or shots. The Weibull parameter b , is defined as the slope of the plot of $F(N)$ in Equation 4.5.2. Thus the larger the b parameter the steeper the plot of $F(N)$ and the lower the dispersions of failures. Failure dispersions can be directly related to quality control in the manufacturing process. Simply stated, the larger the Weibull slope parameter, the more consistent the component characteristics and thus the more predictable the component lifetime. In this investigation the Weibull slope parameter is used as a quality factor for the capacitors tested. Combining it with the mean-time-to-failure and discharge parameters, yields the three quantities used to predict the capacitor life and reliability.

Using Equation 4.5.2, a program was written for the Tektronix data acquisition system to record the component failure times and plot the Weibull distribution. Sample outputs are found at the end of this section. Normally, eight capacitors were tested simultaneously to maximize the

data acquisition rate. In some cases as few as six and as many as 16 were tested simultaneously depending on the desired circuit parameters. Each life test was repeated (except for high energy density mica) at least once for verification. Life test for some of the early film/oil units lasted only a few minutes at kilohertz repetition rates so these tests were repeated until the supply of the test units was exhausted. In the case of capacitors from supplier G, a life test requires nearly two months of 24 hour a day operation so these tests were repeated only once if corroborative results were obtained.

PREVIOUS INVESTIGATIONS

Information on power factor correction capacitors used in electrical power distribution is available in great quantity from General Electric and Westinghouse. Life of these capacitors is usually terminated by lightning strike and lifetimes of over 30 years have been recorded. Reliability of power factor correction capacitors was achieved by the same brute force method used in the test circuits. Because size or weight is not a major factor in this type of service, the units are designed to operate at dielectric stresses of less than 11,800 volts/mm (300 volts/mil). Included in this data base is a considerable amount of data on failures due to overvoltage and high power transients.

A considerable amount of work has been performed investigating the life and reliability of low repetition rate, single shot high energy density capacitors [Boicourt,

1968, 1970, 1975]. These units have lifetime requirements of only a few thousand shots but a demanding energy density specification. Capacitors of this type are primarily used in the generation of intense plasmas in confinement experiments and in Marx generators driving particle beams.

The first comprehensive repetitive (<300 pps) work was performed [Parker, 1976 thru 1980] at Hughes Aircraft in the development of high energy density capacitors for modest voltages and lifetimes for airborne applications. Requirements of this program were light weight, highly reliable high power capacitors with lifetimes on the order of a few million shots. The work of Boicourt and Parker set the standards for modern high energy density capacitor design. Numerous other researchers have investigated life and reliability of capacitors but, for the most part, they are extensions of the work by Boicourt and Parker.

Fluid impregnated dielectric film capacitors fail due to about 20 common mechanisms. Most of these mechanisms can be directly related to shortcomings in the quality control in manufacturing and winding and impregnation techniques [Boicourt, 1968]. It has been shown [Parker, 1980; Boicourt, 1975] that the manufacturing quality control can be improved to the point where the dominant failure mechanism is due to the electric field. Bulk dielectric, foil edge, and margin flashover are the three prime failures due to high electric stress. Margin flashover can be eliminated by better impregnation and by increasing the margin length. Increased margins result in a smaller volume density but in many cases this can be negated by proper

design. Random failures (not associated with foil edges) in the film volume between the capacitor conductors, bulk failures, can be reduced by using multiple layers of high purity film. However, bulk failures can never be completely eliminated. It is generally accepted that, with improved manufacturing techniques, the maximum electric field at which a capacitor can be operated is limited by failures caused by corona at the foil or conductor edges. This statement is true for all capacitors. The foil commonly used in spirally wound capacitors is cut on a shear. Shearing leaves the foil edge jagged with sharp protrusions on one side. These sharp edges result in tremendous field enhancement factors [Alston, 1968] and reduces the corona inception voltage. A detailed theoretical study of field enhancement in spirally wound capacitors is treated in [Bickford and Springer, 1981]. Corona at the foil edges leads to dielectric deterioration [Krasucki, Church, Garton, 1962] and failure. Parker proved in practice, by reducing the electric field enhancement at the foil edge, that the energy density, life, and reliability of pulse discharge capacitors can be improved. Alternative methods to shearing such as laser, and e-beam cutting were investigated by Parker [1977]. Techniques such as rolling, plasma erosion, chemical etch, and spark discharge machining [Parker, 1980] were also researched as to the efficacy in "rounding off" the rough foil edge. Parker concluded that laser cutting followed by a chemical etch produced the smoothest edge with the highest corona inception voltage. By reducing the corona inception voltage, the average electric field

impressed on the dielectric can be increased to obtain a higher energy density. Laser cut chemical etched foil is relatively inexpensive to produce and had attained widespread availability in the United States by 1981.

SPIRALLY WOUND FLUID IMPREGNATED CAPACITOR DATA

The first generation capacitors were procured to satisfy the specifications listed in Section 4.2. A general electrical specification was used to establish the state-of-the-art in commercially available repetitive capacitors. No recommendations were made to the manufacturers as to the design or construction other than that the units should be a best effort. Four manufacturers supplied ten units each in the first iteration. The first set of capacitors was tested in the thyatron switched, 1000 pps test circuit shown in Figure 3.2.1. Waveforms for the thyatron anode voltage and the discharge loop current are shown in Figure 4.5.1 for a 30 kV capacitor. Discharge parameters were adjusted to be as close as possible to; 100 ns pulsewidth, 1000 amperes peak, 10 amperes RMS with less than 10% current reversal.

Life test results from the first generation capacitors were very discouraging. The test procedure was to start the test circuit at 1000 pps repetition rate and then increase the charge voltage on the capacitor to the case rating. Over fifty percent of the first capacitors tested failed below the case peak voltage rating. Capacitors from Manufacturer B performed the best with only two units failing below rated voltage. The average lifetime, MTTF, or

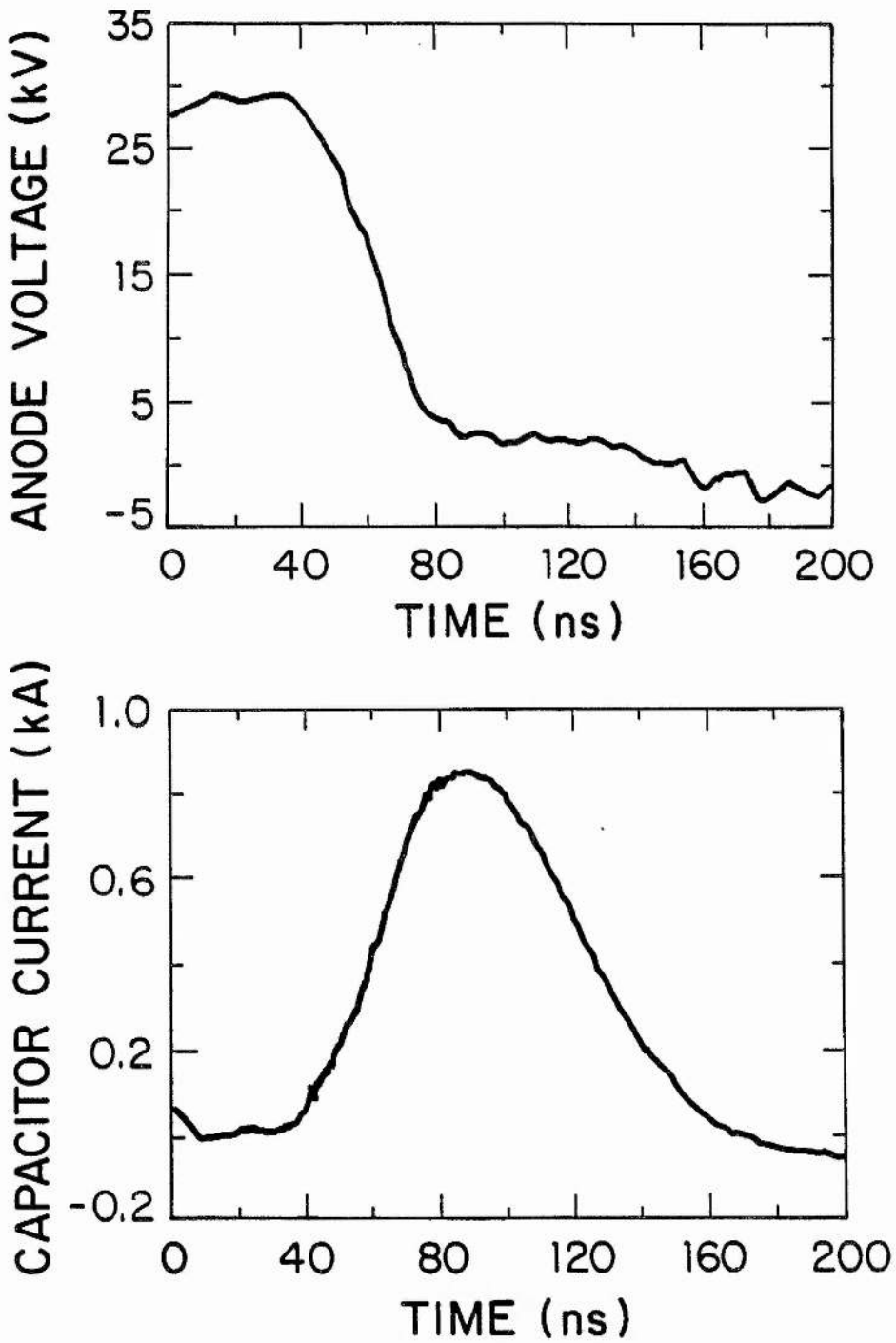


Figure 4.5.1 Test circuit waveforms for short pulse capacitor life test.

Mean-Time-To-Failure, for the first capacitors from vendor B was $6 * 10^5$ shots (12 minutes). All of the failed units underwent the autopsy procedure. As well as could be

determined, 60% of the failures were due to margin flashover, 30% to edge failures, and 10% were destroyed beyond diagnosis. A high edge failure rate was anticipated but the margin flashover failures were totally unexpected. The margin failures can be rationalized by the large dV/dt (of the order of 10^{12} volts/second) and the associated dynamic electric fields causing breakdown in the fluid impregnate. It has been proven experimentally [Rohwein, 1981] that repetitive stressing causes low level ionization around electrodes in insulating oils which lead to bubble formation, partial discharges, and finally breakdown. Measurements indicate that pulse rates of only 5 pps will reduce the dynamic breakdown voltage in bulk transformer oil by a factor of two over the D.C. level [Rohwein, 1981]. In a spirally wound capacitor, this effect is complicated by surface tracking and the variable quality of impregnation. The data from the first capacitors was so scattered in values that it was useless. Learning from this experience, the capacitor specification was amended to require the units to have double width margins and the vendor to supply a description of materials used in the units. The next set of capacitors consisted of ten units each with sheared aluminium conductors. These capacitors are referred to as the "first generation" throughout this thesis. Testing was resumed with substantially better results. Of the next set of capacitors, 2.5% were considered infant mortality, that is, failed below rated voltage and are not considered in the statistics. As well as could be determined from the remains, approximately 75% failed due to dielectric failure

at the foil edges and 25% due to damage caused by arcing between series packs. All of the first generation capacitors consisted of six compression bonded 6 nF packs connected in series. Compression bonding results in a nonuniform connection between the packs and point contact resistances due to oxides on the aluminium foil conductors. Under rapidly changing field conditions, arcing between the packs and damage to the windings occurred primarily on the outer surfaces of the pack where the dv/dt and di/dt were greatest due to the low inductance characteristics (Section 4.2) of the outer layers. To confirm this failure mechanism, several used, but not failed, capacitors were dissected. A good example of interpack arcing is seen in Figure 4.5.2. In this figure, arcing on the edges between

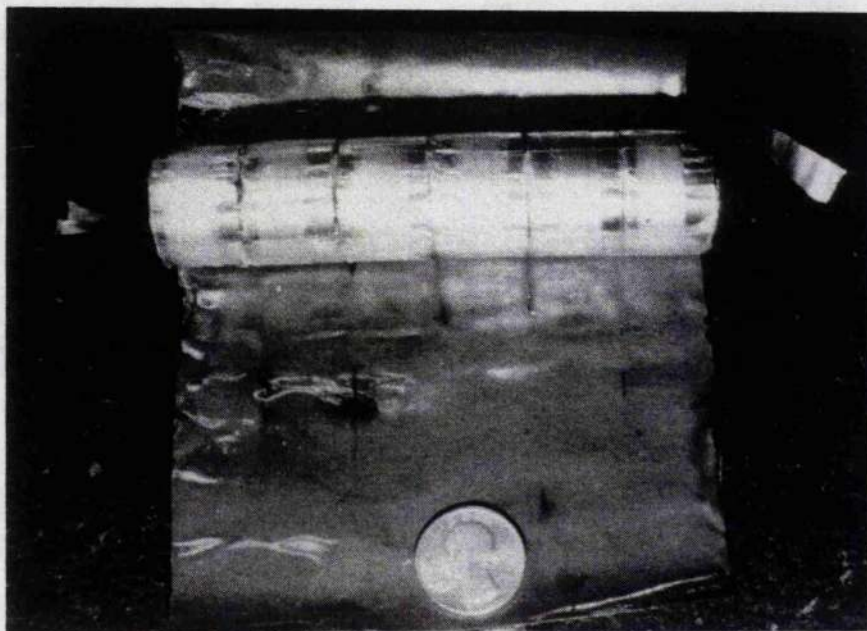


Figure 4.5.2 Damage caused by arcing between compression connected capacitor packs.

packs resulted in the burning of the insulating paper wrapped around the capacitor pack assembly and melting of the 0.0127mm aluminium foil and polypropylene dielectric. An important feature to note is that the far left end of the capacitor in the photograph was connected to the anode of the thyatron, the highest dV/dt point in the test circuit. The capacitor specification was again amended so that the pack connections were required to be soldered to reduce the number of failures caused by interpack arcing. Forty updated first generation units were received and 31 failed in testing. The average life of the new units, from all four manufacturers, increased by a factor of two with the inclusion of soldered pack connections. Of the 31 failures, 9.7% (3 units) were considered infant mortality. The infant mortality rate is higher in the soldered packs construction than in the compression bonded type because of the heat associated with the added soldering step. Neglecting the infant mortalities, all remaining units failed due to dielectric breakdown at the foil edge. During the autopsies of the second set of first generation capacitors, an important feature was noticed. The capacitor pack adjacent to the highest dV/dt terminal always sustained the greatest damage. Referring to the pictorial diagram of the simple cylindrical style capacitor in Figure 4.5.3, a typical failure of the updated first generation capacitors is illustrated. The upper terminal in the diagram is connected to the anode of the thyatron ($dV/dt > 10^{12}$ volts/sec) and is charged to 30 kV. Packs are numbered sequentially from the high to low dV/dt terminal. Of the 28

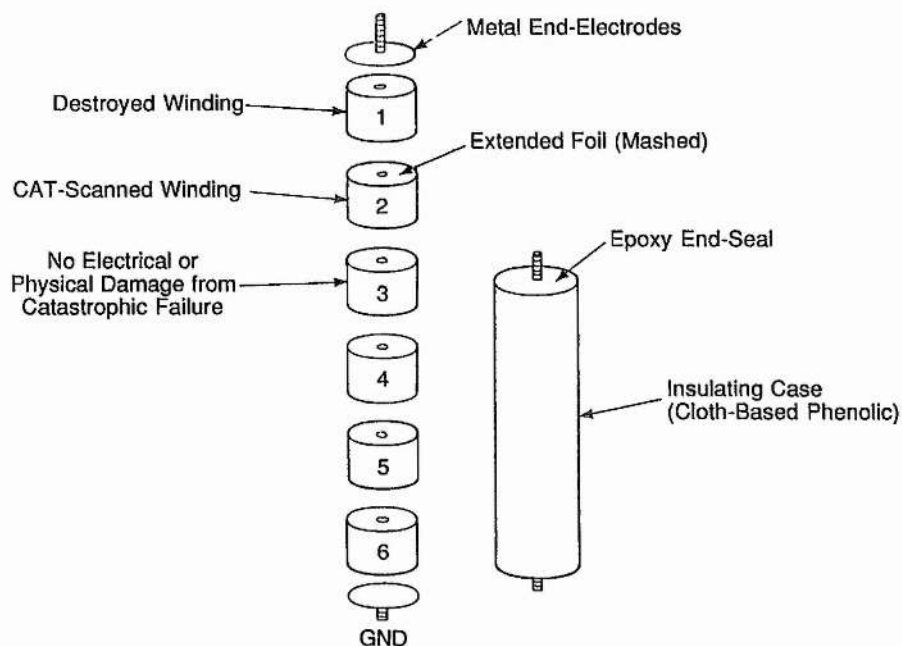


Figure 4.5.3 Damage pictorial of 30 kV 1 nF test capacitor.

(non-infant) failures, the pack in position #1 was always the source of the primary breakdown. Also, the point of the initial breakdown was always in the outer winding layers. Often, pack 2 in the diagram was damaged, but never to the extent of pack 1. Several units had some damage in the #3 pack but packs 4, 5, and 6 remained unharmed. Usually, the first pack was destroyed beyond recognition, but the second and third packs appeared undamaged under visual inspection. Packs that had no apparent damage were first examined with an ohmmeter for D.C. continuity and then with a capacitance meter. If internal damage was suspected, the pack was subjected to diagnosis with scanning X-ray Computer-Aided-Tomography, CAT-SCAN. A photograph of a CAT-SCANNED pack is seen in Figure 4.5.4. This particular pack was in the #2 position in the series string and measured 21 ohms D.C. resistance.

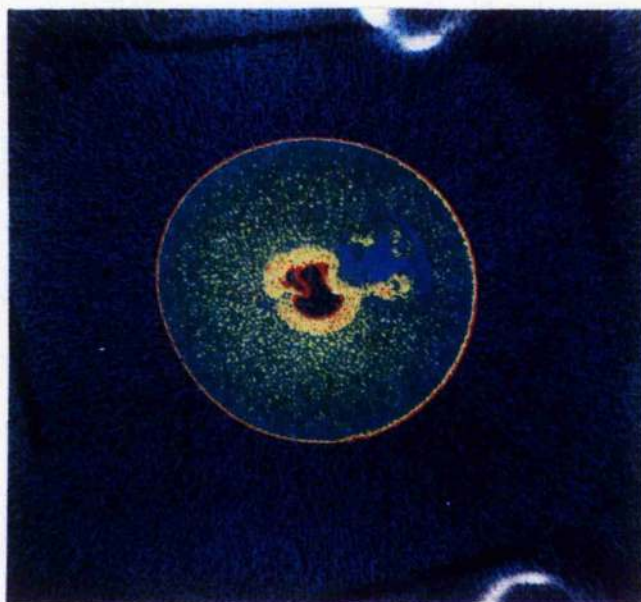


Figure 4.5.4 CAT-SCANNED capacitor pack.

It is seen that the pack in Figure 4.5.4 failed near the start of the winding. This conflicts with the previous statement that all capacitors failed on the outer winding layers. The internal damage seen by the CAT-SCAN is not the cause, but the results of an outer layer foil edge breakdown in pack #1. When the #1 pack shorted, the voltage stress on the remainder of the capacitor increased by 16.7%. At this point the capacitor had not failed catastrophically. Capacitor packs of the type shown in the figure are wound on a removable bobbin very similar to a paper clip. Using the "paper clip" bobbin often causes a wrinkle in the start of the pack winding as can be seen in Figure 4.5.4. This wrinkle is a site of an electric field enhancement which results in a dielectric breakdown. Usually, by the time the #2 pack sustains major damage a catastrophic failure occurs

(case explodes) and the test is automatically terminated. All the capacitors of the updated first generation failed in this general sequence. Examination of destroyed, damaged, and new packs revealed many wrinkles associated with the use of the clip type bobbin. Even though start wrinkles are not attributed directly to the capacitor failure, the specification is again updated to require the capacitor pack to be wound on a nonremovable tubular bobbin. Test of the internal bobbin design was performed with a sample of 15 capacitors from manufacturer B instead of the usual four vendor 40 unit set for cost reduction. Lifetimes of the tubular bobbin units is substantially the same as the clip bobbin type but now all damage to the packs occurred on the outer layers.

With three updates to the original first generation specification, the MTTF has been improved to $1.1 * 10^6$ shots, substantially less than the 10^{10} shot goal. However, the dominant failure mechanism has been reduced to the previously reported capacitor limit for low repetition rate service. Sometimes a capacitor will fail and the source of the failure cannot be determined from the charred remains. For this reason, in each batch of capacitors, a few units were removed at various points in the test period for analysis. Partial discharge analysis, which is used in a variety of insulation testing procedures, was investigated as a possible diagnostic tool. The partial discharge signature for the used capacitors was recorded and the units returned to the test circuit. This technique proved nearly 100% accurate in predicting infant mortality failures but

revealed no conclusive evidence for life prediction. After a great effort was expended in partial discharge analysis, a more basic approach was taken.

Fluid impregnate from the used units was sent for chemical analysis and the packs were unwound under a binocular microscope for visual inspection. It is postulated that a few of the unidentified failures are due to bulk dielectric breakdown but there was no evidence to support this. Damage at the foil edge, even in slightly used capacitors, was clearly visible in the microscope and by half the MTTF, the damage could be seen easily with the unaided eye. Finding evidence of bulk dielectric damage was substantially more difficult. Each capacitor of the first generation contained 36 meters of 0.0191 mm polypropylene film that must be inspected under the microscope. After seemingly endless visual inspection a site of bulk dielectric damage was located. Figure 4.5.5 shows a diagram of the damage due to electric field observed in the polypropylene dielectric. A photograph (50X) of the damage at the foil edge, and a photograph (3000X) of the site of bulk dielectric damage depicted are shown. The debris along the foil edge was analysed with X-ray diffraction techniques and found to be nearly pure carbon. Traces of silicon and complex carbon chain molecules, most likely from the oil and left over polypropylene, were detected in scant quantities. The same analysis is performed on the site of bulk dielectric damage with similar findings. The carbon deposit in the second photograph was captured inside the 0.019 um thick polypropylene. The gas bubble around the deposit was

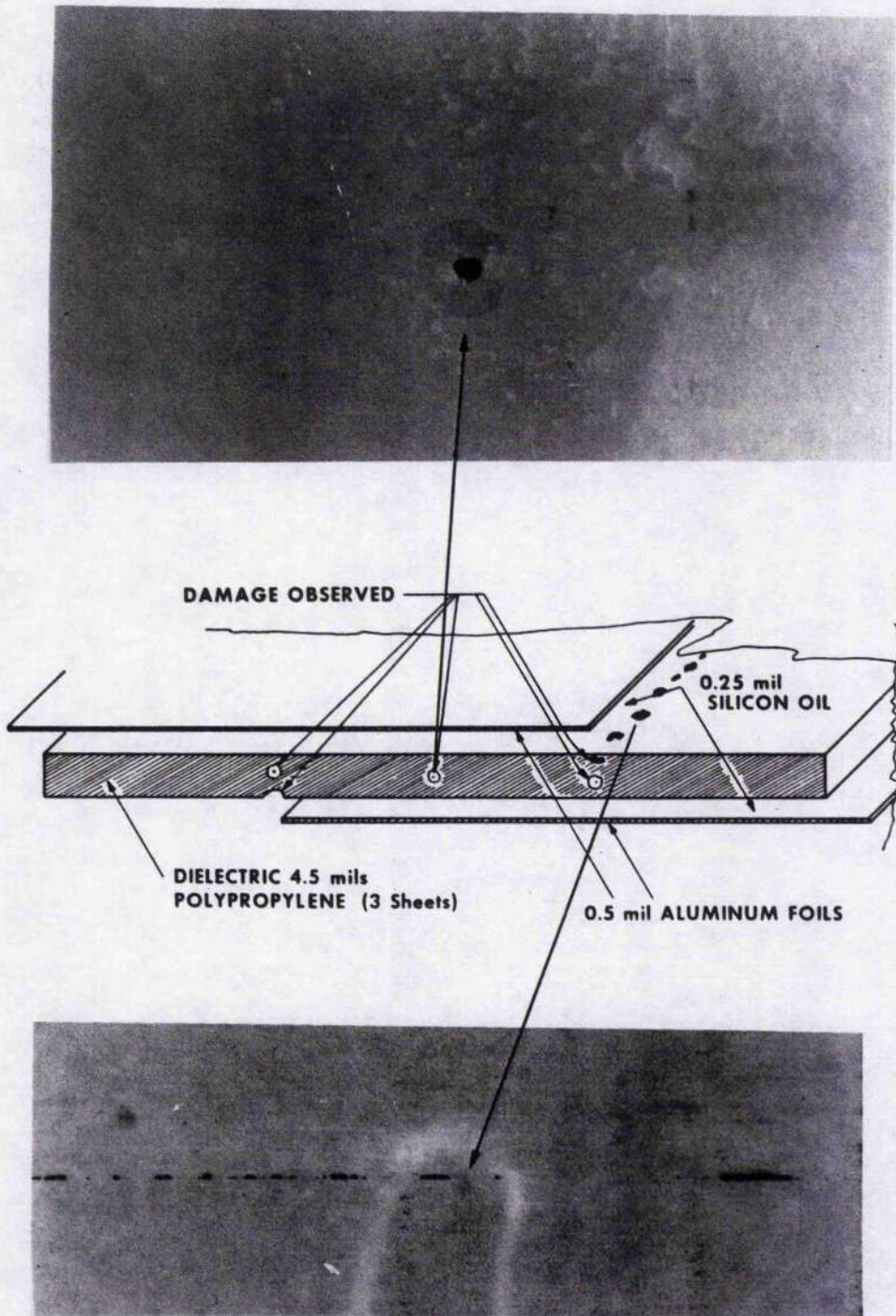


Figure 4.5.5 Dielectric damage in spirally wound silicone oil polypropylene capacitors.

acetylene. The deposit is approximately 2.3 um in diameter and the acetylene bubble 8.3 um in length. The carbon is thought to be formed by partial discharges in a void of low relative dielectric constant gas (air) in the polypropylene film and the acetylene is a breakdown product of polypropylene. Several such sites of bulk dielectric damage were found during the capacitor autopsies. Chemical analysis of the silicone fluid showed a high concentration of dissolved acetylene gas confirming the finding from the x-ray diffraction data of the captured bubble.

Gas generation solved the question as to why a capacitor fails catastrophically, i.e. explodes. Energy stored in the total discharge circuit was 3.6 joules with 8 capacitors. This is far too little energy to rupture a 3.2 mm phenolic or a 4.76 mm PVC capacitor case. To verify that the catastrophic failure is caused by internal gas pressure, a special capacitor was constructed with a mechanical "over-pressure" plug. Pressure rating of the plug was 240 kPa (35psi). The capacitor was installed in the test circuit and after about 20 minutes of 1000 pps operation the plug blew out. Interestingly, the capacitor did not fail for another few minutes and a tiny string of dark bubbles exited the hole in the capacitor where the plug had been. When failure did occur, the unit simply shorted with no explosion.

Initially, all the suppliers had provided capacitors of polypropylene film impregnated with silicone oil. This was because of the low loss nature of polypropylene and the

hazard-free silicone oil. Likewise, all the units thus far used aluminium cut by shearing. Having reduced the failure mechanisms to edge and bulk failures, a last set of 30 first generation capacitors was ordered with the new specification of laser-cut, chemically etched foil. Only two vendors were chosen at this point for reasons of quality and cooperative attitude.

So far all testing was done at 1000 pps at approximately 6 amperes RMS per capacitor. Case temperature of the capacitors was monitored throughout all testing with no variations noted. Since the failure of the first generation capacitor was fairly well characterized, the next series of tests were operated at 250, 500, 750, 1000, and 1666 pps repetition rates. This gave RMS current values of 3, 4.25, 5.2, 6, and 7.76 amperes which resulted in a difference in capacitor power dissipation of almost a factor of 7. Twenty eight of the capacitors were tested and 20 failed. The Weibull statistical plots for this group of tests are found at the end of this section. The failures were plotted versus repetition rate and the graph is shown in Figure 4.5.6. Changing to laser-cut, chemically etched foil doubled the life of the first generation capacitors but did nothing to change the failure mechanisms. Of the 20 capacitors failed in this series of tests, only one could not be attributed to edge failure of the outer winding. During this series of tests, no difference in temperature of the capacitor case was detected. This is consistent with power dissipation calculated from the ESR values listed in Table 4.3.1. Since the life was essentially constant from

750 to 1666 pps, a thermal cause such as dielectric shrinkage is ruled out as the source of the repetition rate dependence.

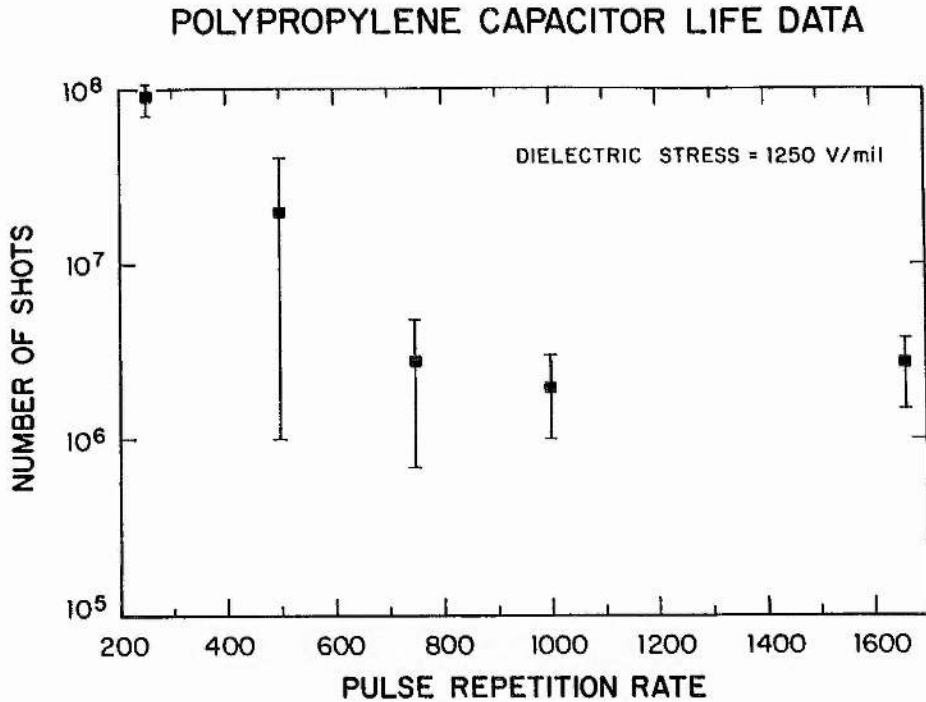


Figure 4.5.6 Life versus repetition rate for polypropylene spirally wound capacitors.

An effect of repetitive pulsing on the strength of dielectric fluids [Rohwein,1981] is ruled out because none of the capacitors failed due to margin flashover. The repetition rate dependence can only be attributed to mechanical fatigue of the capacitor materials. As discussed in Section 4.3, the mechanical force is proportional to the rate of change of the electric field. Very little data on mechanical fatigue for polypropylene suitable under short duration stress was located. The American Society for Material Testing, ASTM, has a standard test procedure for measurement of the flexural strength of polymers. Flexural

strength is defined as the minimum pressure that will result in mechanical failure of a body as prescribed by ASTM standard D790-49T. This test is a "single shot" test to failure of a standard size bar of material. The magnitude of the flexural strength is dependent highly on the crystalline structure of the polymer under test. Percentage of crystalline structure of a polymer is dependent on manufacturing processes and proportional to the number of flexure cycles to which the material is exposed. With this in mind, the more immediate issue is the life of the test capacitor which, thus far, falls almost 4 orders of magnitude below the goal set at the onset of the programme.

Polypropylene film capacitors are found to have two major shortfalls: 1} generation of gas which leads to catastrophic failure and 2} a strong dependence of lifetime on repetition rate and dV/dt . The last aspect, dV/dt , is best illustrated in the use of the original test capacitors in pulsed circuits with with low dV/dt and di/dt . Six capacitors were installed in a discharge circuit operating at 1000 pps, a pulse width of 1 mS, and with 100% current reversal at full rated capacitor voltage. Life of these capacitors in the test circuit is less than 10^6 shots but in the low dV/dt circuit, a failure has not occurred in seven years of service and more than $3 * 10^{10}$ shots. Because of the problems associated with polypropylene, alternative dielectric films were examined. Polytetrafluoroethylene or Teflon, has several preferred mechanical properties, listed in Table 4.5.1, and was selected as the dielectric for the second generation capacitors. The much greater flexural

strength allows Teflon to experience more flex cycles with less crystallization and the low surface friction coefficient allows the material to wet better in the impregnation process. Dielectric constants are similar in

MATERIAL	FLEXURAL STRENGTH (kPa)	SURFACE FRICTION COEFFICIENT
POLYPROPYLENE	54.8	0.81
TEFLON	13.7×10^6	0.22

Table 4.5.1 Mechanical stress properties of polypropylene and Teflon.

value but the lower dielectric strength of Teflon results in a slightly larger capacitor. Also, electrical breakdown of Teflon should not result in gas production since this material is not combustible [Clark, 1962]. Based on the updated capacitor specification of: 1} double width margins, 2} soldered pack connections, 3} nonremovable tubular bobbins, and 4} laser-cut chemical etched foil, a second generation capacitor with Teflon film dielectric was procured. These units were initially tested at 1000 pps in the 100 nS test circuit. After 1000 hours (3.6×10^9 shots) with one failure, the test was terminated. The single failure out of 7 capacitors occurred at the foil edge of the pack in position 4 (Figure 4.5.3) near the start of the winding. Breakdown at this position is attributed to a random dielectric failure due to a site imperfection in the dielectric or winding.

The test was terminated because simply changing the dielectric to Teflon resulted in a 1000 times improvement in lifetime. This radical improvement may be attributed to the more flexible characteristic and better impregnation properties of Teflon. However, this hypothesis is not substantiated and is left for future investigations. Temperature of the second generation capacitors was constant over the full test period. Again, from the ESR measurements (Section 4.3) and loss data [Clark, 1962] no large temperature increase was anticipated.

As a simple side experiment, a mylar/paper capacitor was made as a sample by Vendor B and operated in the test circuit. Mylar/paper is an extremely lossy dielectric combination and is not suitable for repetitive service.

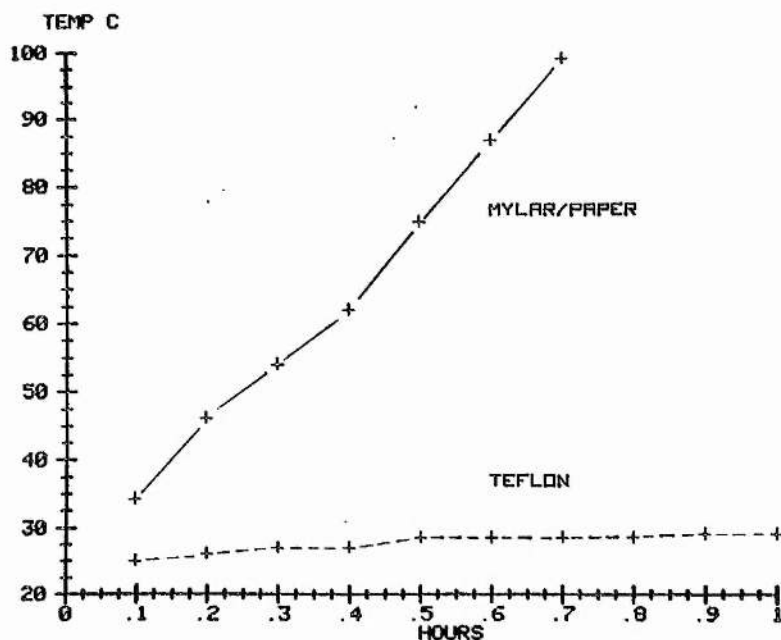


Figure 4.5.7 Case Temperature for a mylar/paper and a Teflon dielectric capacitor.

Case temperature data for both capacitors in the 1000 pps test circuit was recorded and is graphed in Figure 4.5.7. The Teflon capacitor temperature tracked the test circuit oil exactly.

With greatly improved lifetimes, the Teflon capacitors are well suited for high repetition rate service. However, the inductive component is still too large for use in high di/dt circuits. The remainder of the development on spirally wound fluid impregnated units centered around reducing inductance. The final "third generation" design is described in Section 4.2 and all three generations from one vendor are seen in Figure 4.2.4. The third generation had lifetimes in excess of 5×10^9 shots but a volume and energy density that severely limited its use. A much more compact package for capacitors of the 1-4 nF, 30-50 kV size can be fabricated in a solid dielectric.

SOLID DIELECTRIC CAPACITOR LIFE

Life and failure analysis of the solid dielectric capacitors, ceramic and reconstituted mica paper, is trivial when compared with the complex nature of the spirally wound units. In both cases, flashover of the dielectric is the only electrical failure mechanism. Reliability of these types of pulsed capacitors is governed solely by design of the case and manufacturing quality control. Documented lifetimes of 25 years have been recorded for mica capacitors operating at low stress. This type of capacitor was used in communication circuits of the lunar missions nearly twenty years ago. However, as with the spirally wound capacitors,

very little comprehensive data is available on solid dielectric units in short pulse circuits.

Of the four ceramic units initially tested, MTTF varied from 10^4 to 4.3×10^9 shots. The shortest lived units failed due to separation of the terminal from the metallization on the ceramic slug. This type of failure found in units from Vendor H was caused by electrostriction and a poor adhesion process. Shot life of the two other designs of ceramic capacitors averaged about 5×10^7 shots. The life of these capacitors is limited by breakdown between the case and the dielectric slug. Breakdown in this region is attributed to voids (most likely trapped air) between the encapsulating case and the dielectric slug (Figure 2.1.2). This is substantiated by the fact that the capacitors have longer lifetimes in an oil environment than when operated in air. When a ceramic capacitor is submerged in oil, a small amount is wicked into the areas between the case and dielectric slug, thus filling most voids.

One particular design, from vendor G, surpassed all other ceramic styles with a MTTF of $>4 \times 10^9$ shots. A graph of the Weibull statistics for the G2.7 units is seen in Figure 4.5.8. All previously tested capacitors had Weibull slopes of less than 3. Every Vendor G unit failed due to flashover between the case and the dielectric. Alarmingly, only one of the ceramic manufacturers showed any interest in the results of the testing even though test data and autopsy analyses were sent to all the manufacturers. Vendor G responded to this information with the explanation that the entire manufacturing process is automated and any change at

all would require great expense in both equipment modification and loss of revenue due to lost production.

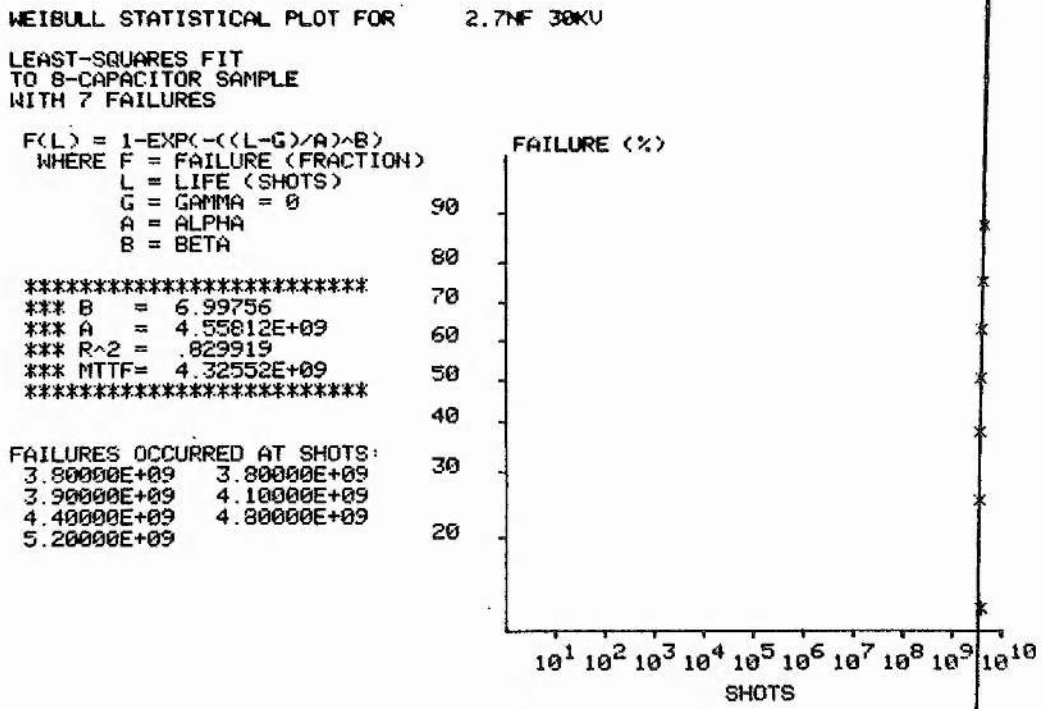


Figure 4.5.8 Weibull statistical plot for capacitors G2.7.

With no means of producing real device modifications, data acquired in the investigation of ceramic units is of engineering and design use only. A complete list of life data is seen at the end of this section.

Interaction with reconstituted mica paper capacitor manufacturers was even more astonishing than with the ceramic makers. Of four manufacturers solicited to participate in this development program, only one, Vendor A, responded. Unlike the ceramic capacitors, change in design of mica units is readily accomplished. Mica capacitor design is fairly well understood by the manufacturer as far as voltage holdoff and life are concerned. Encapsulation is

generally accepted as the primary life limiting factor for this type of capacitor in pulsed service. This has been documented for high repetition rate low di/dt service in radar development studies from the 1940's and 1950's at the Evans Signal Laboratory [Schneider]. Findings in this investigation concurred with this limitation as the only failures noted were due to margin flashover. In the mica design, this problem is easily overcome by extending the margins and proper encapsulation. After just a few iterations, a capacitor with life of $>10^{10}$ shots was developed and tested. The breakdown mechanism for this type of failure is thought to be similar to that of the loss of dielectric strength in transformer oil [Rohwein,1981]. Thorough investigation of this phenomenon is beyond the scope of this investigation and is left to future research. Achieving the life goal of 10^{10} shots was quite easy to achieve with the mica units and the main effort was focused on increasing the energy density. With mainly innovation on the part of the manufacturer, the energy density of the mica paper capacitors was increased to that of the ceramic types. No statistical data were collected on the mica units because in the final design there were no failures. Completing 10^{10} shots in the test circuit required over 3000 hours at 1000 pps and, normally, several thyratrons were consumed. Only one life test of five mica units was performed. This test was terminated at 2777 hours of high voltage operation with no capacitor failure. The excessive cost of this test prohibited a duplication to provide verification of results.

SUMMARY

This section summarizes the major aspects of the life test and failure analysis performed in the pulsed capacitor investigation. Certain details such as voltage stress and case design have been intentionally neglected to protect certain information considered to be proprietary by the manufacturers concerned. It should be remembered that all testing was performed at the capacitor rated voltage. Reducing the electric stress on the dielectric can extend life considerably. A case in point, the operating voltage for ceramic capacitor from vendor G was increased by 15% in the test circuit with the result of a reduction in life of nearly 10000 fold. Likewise, when the voltage stress is reduced by 15%, the capacitor life will far exceed the 10^{10} shot mark. From an engineering standpoint, this information is quite useful in predicting life of pulse modulators. Many studies have defined mathematical scaling relations for electric stress versus life for a particular capacitors but no unified theory exists. Scaling laws are derived empirically and exist for a variety of capacitors such as tantalum and low voltage ceramic disc types.

A summary of the life test results is listed in Table 4.5.2 for the best of each generation of capacitors. Units with extremely short life or special units made to investigate a particular aspect of capacitor design are omitted. Capacitors B₁, C, D, and E₁ are silicone oil polypropylene spiral wound consisting of six series packs.

SUPPLIER	VALUE (nF)	ENERGY DENSITY (J/kg)	MTTF ₅ (*10 ⁹)	WEIBULL SLOPE "b" (average)	DIELECTRIC STRESS (V/mm)
A	50	7.5	>10	-	21,653
B ₁	1	.77	.003	1.76	47,244
B ₂	1	.70	3.8	2.44	29,525
B ₃	1	.15	>5	-	29,525
C	1	.35	.003	.76	31,496
D	1	.39	.003	.66	31,496
E ₁	1	.21	.003	1.83	47,244
E ₂	1	.15	>5	-	29,525
F	1	5.1	0.56	.69	2,952
G1	1	8.1	4.76	7.01	2,952
G2.7	2.7	6.2	4.32	6.99	2.952
H	.5	4.9	-	.11	1,574

A = MICA B,C,D,E = FILM/OIL F,G,H = CERAMIC

Table 4.5.2 Life test results for the best of each generation of high repetition rate capacitor.

The third generation Teflon/oil impregnated unit, B₃, and second generation unit E₂, were the low inductance design derived in Section 4.2 and were not thoroughly tested because of the poor energy density. The ceramic used in types G and H is a variation of SrTiO₃ and type H is BaTiO₃. Data in Table 4.5.2 for the solid dielectric capacitors is good for any repetition rate less than 1666 pps. No dependence of life on repetition rate was detected in the solid dielectric capacitors. The 50 nF mica capacitor A in this chart was of the final design high energy density unit developed during this investigation. Because of design trade-offs, the high energy density design can not be made

in values much less than 40 nF. The larger size of the 50 nF mica capacitor, is equal to the size required to connect 50 nF worth of ceramic capacitors in parallel. Tests of the 50 nF mica unit have not resulted in a failure and this unit is considered to be the longest lived, highest reliability capacitor studied in this investigation.

It has been demonstrated that, with improved manufacturing techniques the life and reliability of spirally wound fluid impregnated capacitors can be greatly improved. Starting from a general electrical specification and adding: 1} double width margins, 2} soldered pack connections, 3} nonremovable tubular bobbins, and 4} laser cut chemical etched foil, a three-fold increase in life is possible. Advancing further with this same design, selecting Teflon as a dielectric resulted in an increase in life of three orders of magnitude and strengthened the theory that the short life and repetition rate dependence of the polypropylene capacitor is due to mechanical fatigue. As discussed in Sections 4.1 and 4.2, the inductance and voltage dependence of the capacitor can be controlled by proper winding techniques.

References for Chapter 4

- Alston, L.L., "High Voltage Technology", Oxford, London, 1968
- Bickford, K.J. and Springer, T., "Field Grading in Capacitor Margins," Abridged in 3rd IEEE Pulsed Power Conference, Albuquerque, New Mexico, 1981 and Los Alamos National Laboratory Internal Report, 1982.
- Boicourt, G.P., "Problems in the Design and Manufacture of Energy Storage Capacitors," Los Alamos Scientific Laboratory, LA-4142, June 1968.
- Boicourt, G.P. "Problems in the Design and Manufacture of Energy Storage Capacitors," Los Alamos Scientific Laboratory, LA-4142-MS, June 1970.
- Boicourt, G.P., "The Diagnosis of Underdrying in Paper Castor Oil Capacitors," Los Alamos Scientific Laboratory, LAUR-75-2128, 1975.
- Clark, F.M., Insulating Materials for Design and Engineering Practice, John Wiley & Sons, New York, 1962.
- Dekker, A.J., Solid State Physics, Prentice-Hall, 1965.
- Fisher, R.A. and Tippet, L.H.C., "Limiting Forms of Frequency Distribution of the Longest or Smallest Member of the Sample," Proceedings, Cambridge Philosophical Society, 1928.
- Haywood, J., Capacitor Specialist, Technical Note.
- Kinsler, L.E. and Frey, A.R., Fundamentals of Acoustics, Wiley & Sons, 1950.
- Krasucki, Z., "Factors Controlling the Life of Power Capacitors," CIGRE Rep. 138, 1962
- Mason, W.P., ed., Physical Acoustics, Academic Press, 1964.
- McDuff, G., Nunnally, W., Rust, K., and Sarjeant, W.J., "Diagnostic and Performance Evaluation of Multikilohertz Capacitors," Special Symposium on High Energy Density Capacitors and Dielectric Materials, 1980 CEIDP Conference, Boston, Massachusetts, October 28, 1980.
- Nunnally, W.C., Kristiansen, M., Hagler, M., "Differential Measurement of Fast Energy Discharge Capacitor, Inductance, and Resistance," IEEE Transactions on Instruments and Measurements, Vol. 24, No. 2, June 1975.

- Parker, R.D., "Capacitors for Aircraft High Power," Air Force Aero Propulsion Laboratory, Technical Report AFAPL-TR-77-40, 1977.
- Parker, R.D., "Pulse Discharge Capacitor Weight Minimization by Peak Foil Edge Fields," First International Pulsed Power Conference, Lubbock, Texas, 1976.
- Parker, R.D., "Effect of Foil Edge Modifications and Configurational Changes on Energy Storage Capacitor Weight," IEEE Trans. on Parts, Hybrids, and Packaging, Vol.PHP-13, No.3, Sept. 1977.
- Parker, R.D., "High Power Capacitor Technology," 14th Pulsed Power Modulator Symposium, Orlando, Florida, 1980.
- Rohwein, G.J., "Partial Discharge Testing of Bulk Transformer Oil," 3rd IEEE Pulse Power Conference, Albuquerque, New Mexico, 1981.
- Sarjeant, W.J., "Energy Storage Capacitors," Power Conditioning Technology, Vol. 1, LA-UR-79-1044.
- Sarjeant, W.J., "Advanced Topics in High Voltage Engineering," University of New York at Buffalo Press, 1984.
- Seacat, R., Principles of Electrical Engineering I & II, Texas Tech University Press, 1973.
- Tenney, F.H., "AC Response to Spirally Wound Capacitors," Princeton University, September 1965.
- Thompson, M.C. and Mauldin, G.H., "Test Techniques for Model Development of Repetitive Service Energy Storage Capacitors," LA-UR-83-3634.
- Weibull, W., "A Statistical Distribution Function of Wide Applicability," Trans. Am. Soc. Mech. Engrs, Vol. 73, 1951.
- Weibull, W., "Fatigue Testing and the Analysis of Results," Pergamon Press, New York, 1961.
- Yamaji, A. and Waku, S., "Studies of Boundry Layer Dielectrics," Review of the Electrical Laboratories, Vol. 20, No. 7-8, July-August 1972.

ATTACHMENT I

Weibull plots and statistical life data for the five repetition rates plotted in Figure 4.5.6. All capacitors are first generation silicone oil/polypropylene spirally wound units.

POLYPROPYLENE 250PPS

LEAST-SQUARES FIT
TO 6-CAPACITOR SAMPLE
WITH 2 FAILURES

$F(L) = 1 - \exp(-((L-G)/A)^B)$
WHERE F = FAILURE (FRACTION)

L = LIFE (SHOTS)

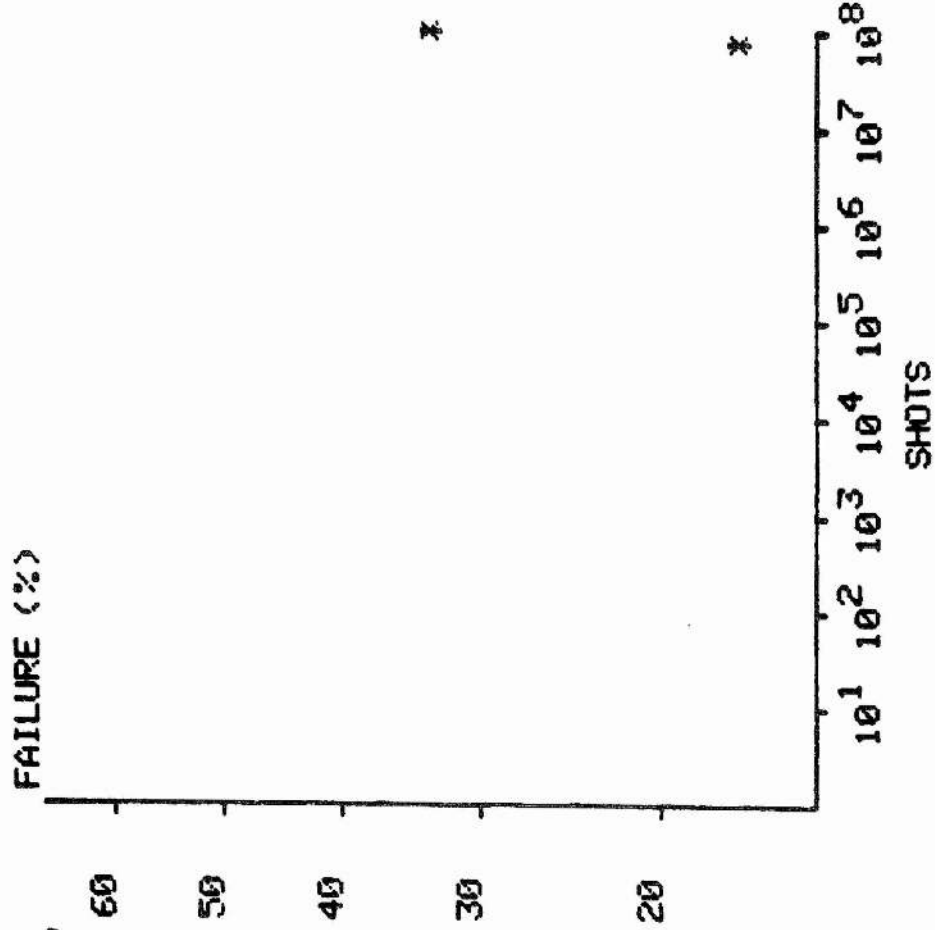
G = GAMMA = 0

A = ALPHA

B = BETA

*** B = 2.74191
*** A = 1.37630E+08
*** R^2 = .998437
*** MTTF = 1.20410E+08

FAILURES OCCURRED AT SHOTS:
7.40000E+07 9.90000E+07



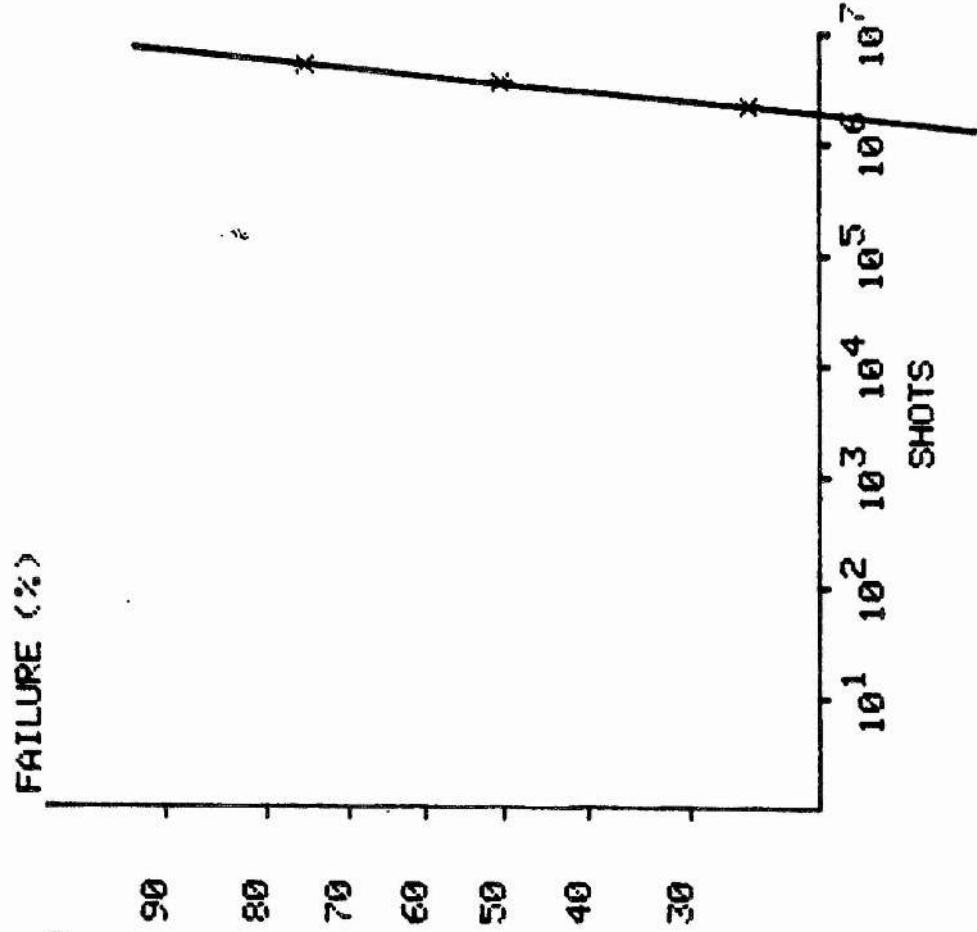
POLYPROPYLENE 500PPS

LEAST-SQUARES FIT
TO 4-CAPACITOR SAMPLE
WITH 3 FAILURES

$F(L) = 1 - \exp(-((L-G)/A)^B)$
WHERE F = FAILURE (FRACTION)
L = LIFE (SHOTS)
G = GAMMA = 0
A = ALPHA
B = BETA

*** B = 1.8308
*** A = 4.21285E+06
*** R^2 = .992415
*** MTTF = 3.44852E+06

FAILURES OCCURRED AT SHOTS:
2.10000E+06 3.60000E+06
4.90000E+06



POLYPROPYLENE 750PPS

LEAST-SQUARES FIT
TO 6-CAPACITOR SAMPLE
WITH 5 FAILURES

$F(L) = 1 - \exp(-(L-G)/A)^B$
WHERE F = FAILURE (FRACTION)

L = LIFE (SHOTS)

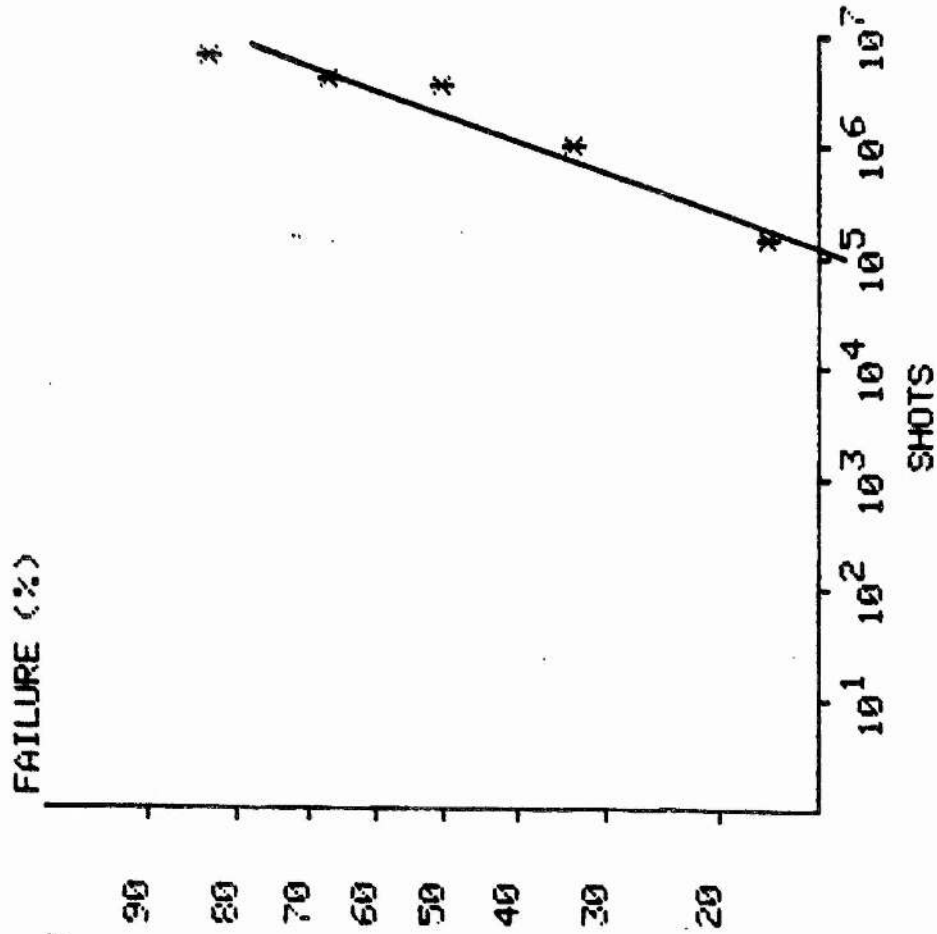
G = GAMMA = 0

A = ALPHA

B = BETA

*** B = .555614
*** A = 3.72444E+06
*** R^2 = .919565
*** NITF = 1.92565E+06

FAILURES OCCURRED AT SHOTS:
140000 990000
3.50000E+06 3.90000E+06
6.10000E+06



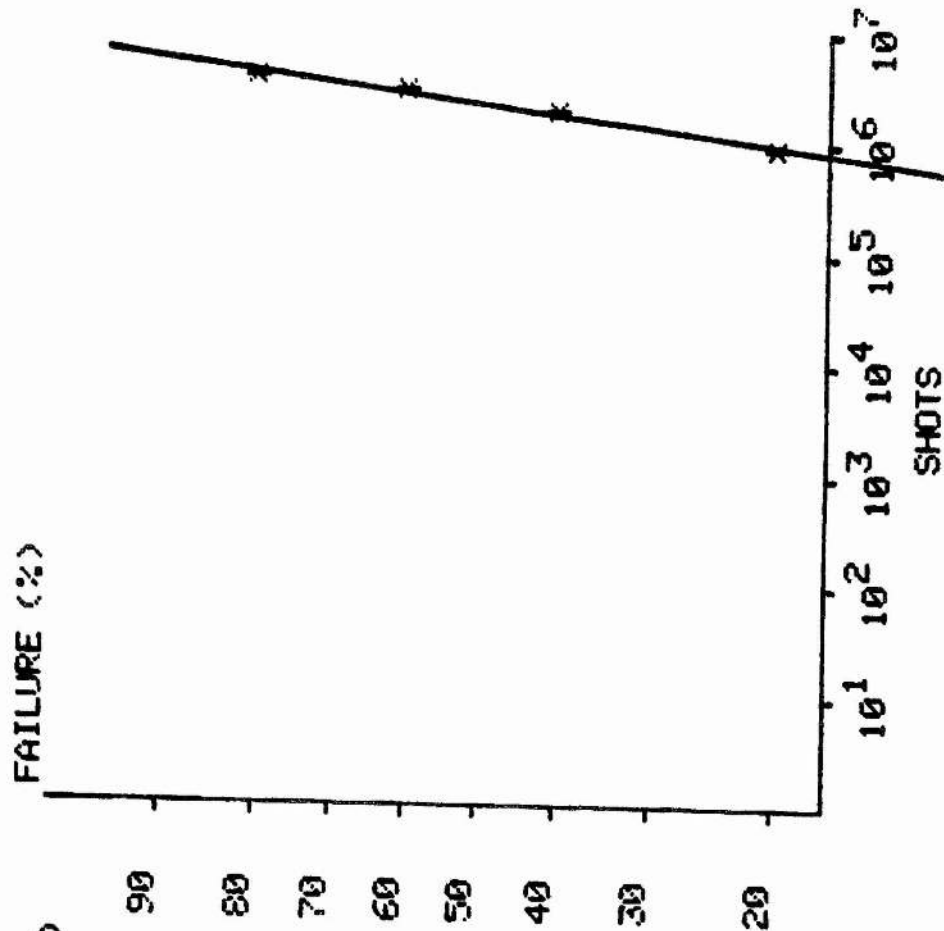
POLYPROPYLENE 1000PPS

LEAST-SQUARES FIT
TO 5-CAPACITOR SAMPLE
WITH 4 FAILURES

$F(L) = 1 - \exp(-((L-G)/A)^B)$
WHERE F = FAILURE (FRACTION)
L = LIFE (SHOTS)
G = GAMMA = 0
A = ALPHA
B = BETA

*** B = 1.3809
*** A = 2.81397E+06
*** R^2 = .977939
*** MTF = 2.15800E+06

FAILURES OCCURRED AT SHOTS:
900000 1.90000E+06
2.80000E+06 3.60000E+06



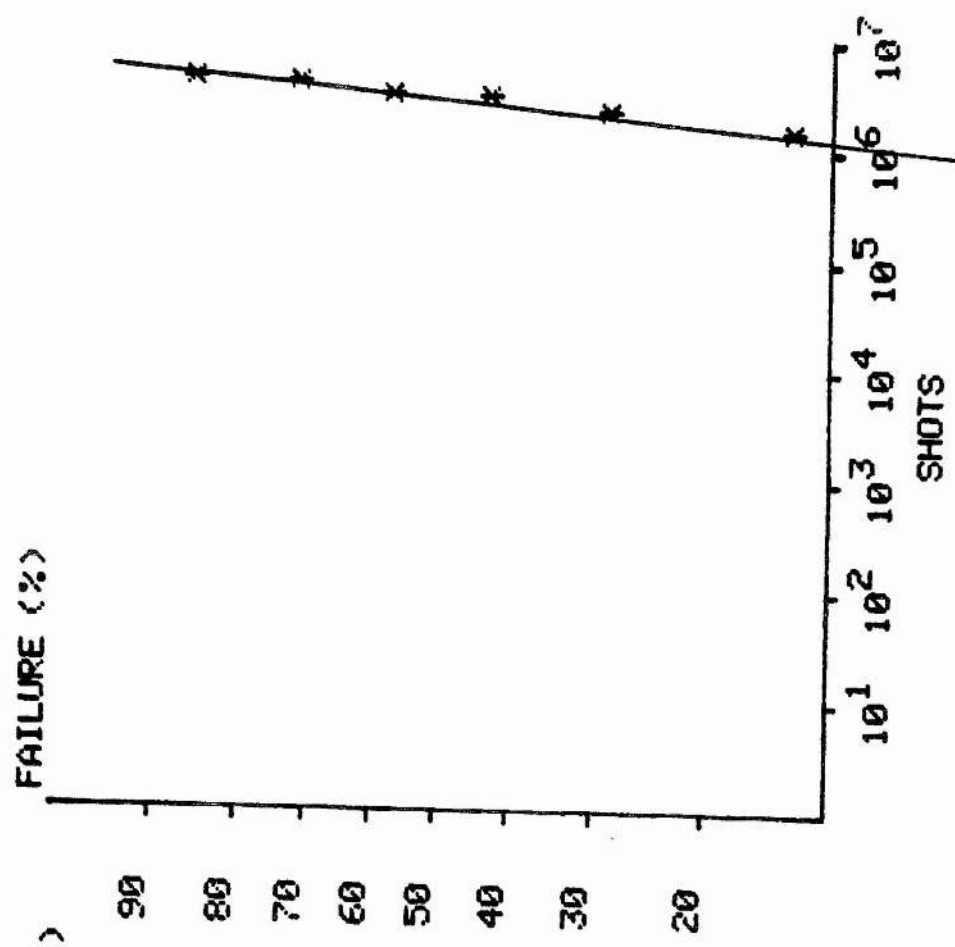
POLYPROPYLENE 1666PPS

LEAST-SQUARES FIT
TO 7-CAPACITOR SAMPLE
WITH 6 FAILURES

$F(L) = 1 - \exp(-((L-G)/A)^B)$
WHERE F = FAILURE (FRACTION)
L = LIFE (SHOTS)
G = GAMMA = 0
A = ALPHA
B = BETA

*** B = 2.43809
*** A = 3.35208E+06
*** R^2 = .973645
*** MTF = 2.88422E+06

FAILURES OCCURRED AT SHOTS:
1. 50000E+06 2. 20000E+06
2. 90000E+06 3. 00000E+06
3. 80000E+06 4. 10000E+06



CHAPTER 4A
DEVICE FOR DETECTING IMMINENT FAILURE OF
HIGH-DIELECTRIC STRESS CAPACITORS

Attached is a copy of the U.S. patent describing an electronic circuit that can detect the imminent failure of a high-stress, spirally wound fluid impregnated film capacitor. This technique was originally devised as a means to prevent a catastrophic failure of a fluid filled capacitor. A catastrophic failure usually resulted in a large amount of charred capacitor remains being deposited in the oil tank.

The circuit was optimized for use at power line frequencies as a measure to protect power factor correction capacitor banks in high voltage power distribution. In large distribution networks, it is common to have several hundred power factor correction capacitors in a single bank. An explosion of a capacitor in a large bank can inflict severe damage to surrounding units and cause a loss of revenue due to down time and increased power factor. As described in the patent, the technique will work on a single unit or a bank of parallel capacitors. In 1982, the right to manufacture of the device described was licenced to C. Itoh, Inc., a Japanese firm.

[54] **DEVICE FOR DETECTING IMMINENT FAILURE OF HIGH-DIELECTRIC STRESS CAPACITORS**

4,104,687 8/1978 Zulaski 361/17
 4,219,856 8/1980 Danfors et al. 361/15

[75] **Inventor:** George G. McDuff, Los Alamos, N. Mex.

"TTL Cookbook", pp. 47, 61, 75, 91, and 111, Don Lancaster, copyright 1974, by Howard Sams & Co., Inc.

[73] **Assignee:** The United States of America as represented by the United States Department of Energy, Washington, D.C.

Primary Examiner—Gerald L. Brigance
Attorney, Agent, or Firm—William W. Cochran, II; Paul D. Gaetjens; Richard G. Besha

[21] **Appl. No.:** 204,121

[57] **ABSTRACT**

[22] **Filed:** Nov. 5, 1980

A device for detecting imminent failure of a high-dielectric stress capacitor utilizing circuitry for detecting pulse width variations and pulse magnitude variations. Inexpensive microprocessor circuitry is utilized to make numerical calculations of digital data supplied by detection circuitry for comparison of pulse width data and magnitude data to determine if preselected ranges have been exceeded, thereby indicating imminent failure of a capacitor. Detection circuitry may be incorporated in transmission lines, pulse power circuitry, including laser pulse circuitry or any circuitry where capacitors or capacitor banks are utilized.

[51] **Int. Cl.** G08B 21/00

[52] **U.S. Cl.** 340/635; 340/661; 361/17

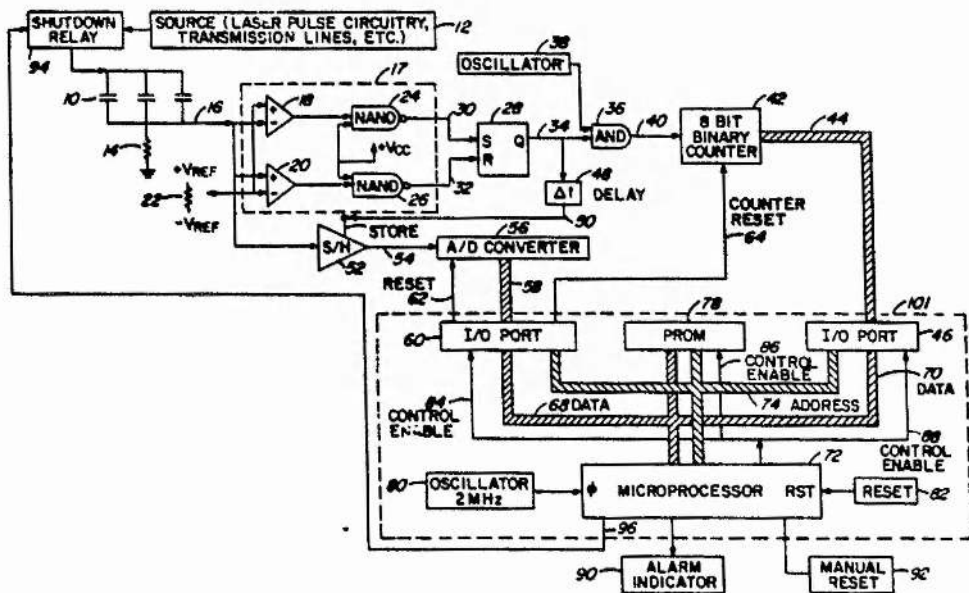
[58] **Field of Search** 340/635, 661, 653; 361/15, 16, 17, 272, 275; 324/60 C

[56] **References Cited**

U.S. PATENT DOCUMENTS

3,562,586	2/1971	Carter et al.	361/16
3,657,602	4/1972	Boehm et al.	340/635
3,735,250	5/1973	Masui	340/661
3,859,564	1/1975	Zulaski	361/17
3,984,734	10/1976	Becker	361/17

8 Claims, 5 Drawing Figures



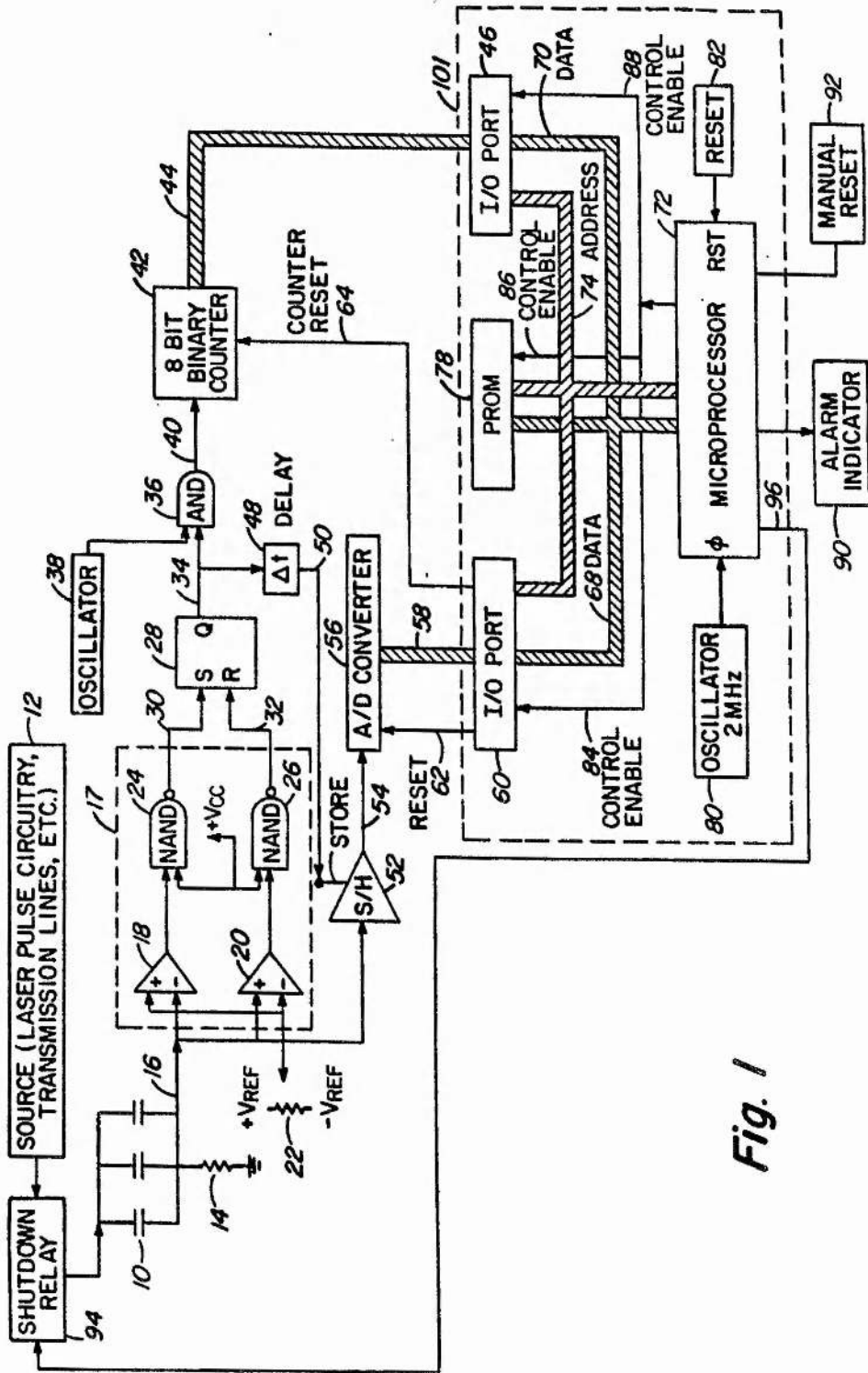


Fig. 1

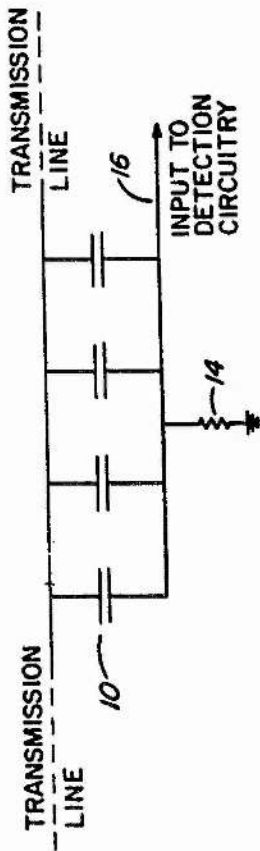


Fig. 2

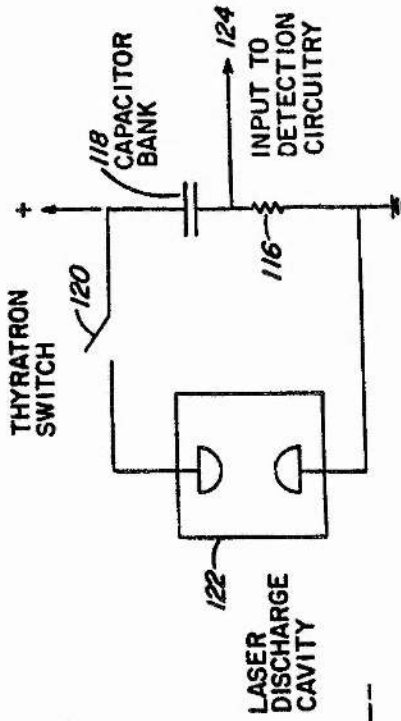


Fig. 4

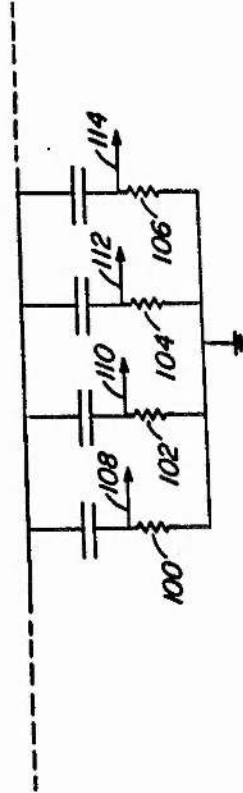


Fig. 3

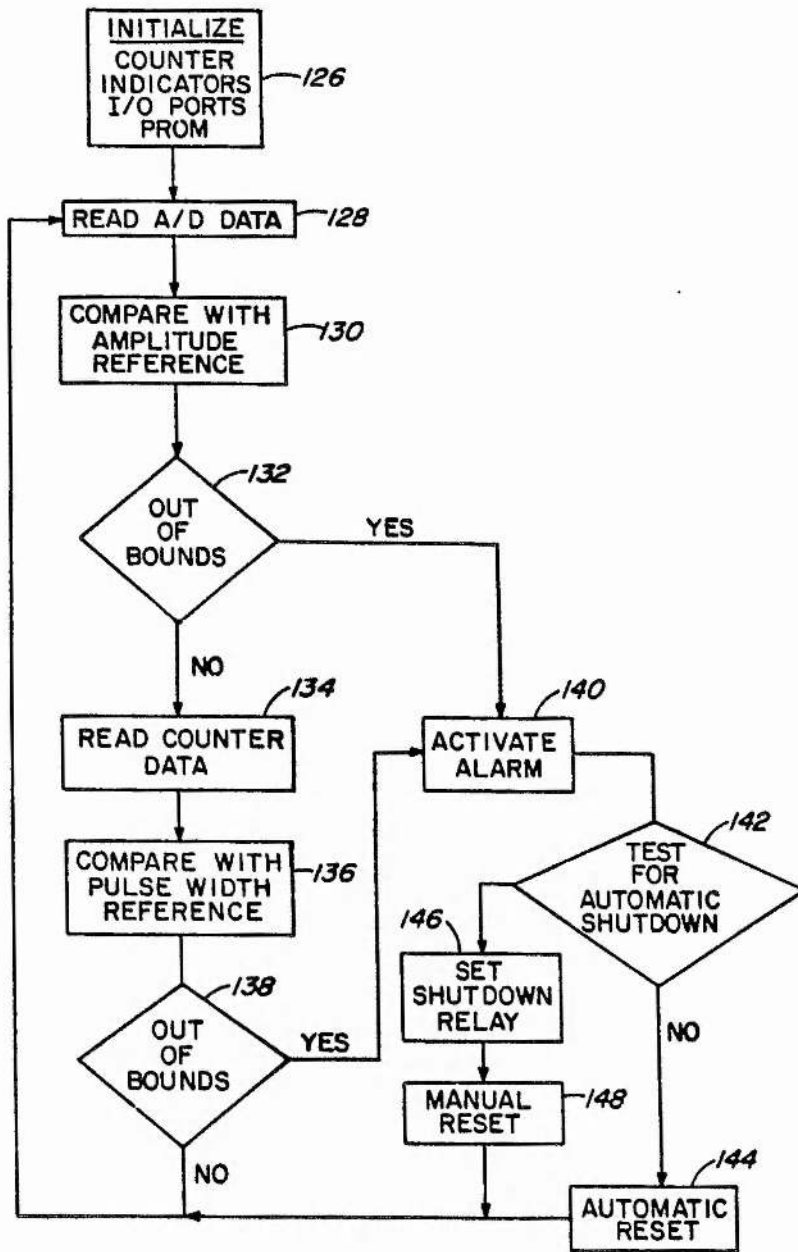


Fig. 5

DEVICE FOR DETECTING IMMINENT FAILURE OF HIGH-DIELECTRIC STRESS CAPACITORS

BACKGROUND OF THE INVENTION

The present invention pertains generally to measuring and testing devices and more particularly to a device for detecting the imminent failure of a capacitor. This invention is the result of a contract with the Department of Energy (Contract No. W-7405-ENG-36).

High-dielectric stress capacitors are employed in many applications where reliability is an extremely important factor. For example, electric power transmission and distribution lines use capacitor banks to correct problems of power lag due to inductance effects of the transmission line. Downtime resulting from capacitor failure can be expensive, e.g. as much as \$16,000 per second. Consequently, it is advantageous to know of the imminent failure of a capacitor bank under such circumstances to expedite replacement and minimize downtime and loss of profits.

Additionally, many pulse power systems utilize capacitor banks as a discharge source which also require high reliability. For example, high energy pulsed gaseous lasers such as used in molecular isotope separation systems and high energy laser fusion systems require banks of high-dielectric stress capacitors. Utilization of lasers in industrial applications necessitates high reliability of the pulse power systems to minimize downtime and maximize profits.

Although capacitors can be designed to reduce dielectric stress and consequently reduce corona inception problems and mechanical failure due to electrical stress, such capacitors are much larger than high-dielectric stress capacitors and are considerably more expensive to construct. Moreover, such capacitors are subject to eventual failure due to either the above reasons or chemical processes which occur within the capacitor. Consequently, capacitor design can not overcome the problems associated with reliability.

SUMMARY OF THE INVENTION

It is therefore an object of the present invention to provide a device for detecting imminent failure of a high-dielectric stress capacitor.

It is also an object of the present invention to provide a device for detecting imminent failure of a high-dielectric stress capacitor which is reliable in operation.

Another object of the present invention is to provide a device for detecting imminent failure of a high-dielectric stress capacitor which is easy, simple, and inexpensive to implement.

Additional objects, advantages, and novel features of the invention are set forth in part in the description which follows, and will become apparent to those skilled in the art upon examination of the following or may be learned by practice of the invention. The objects and advantages of the invention may be realized and attained by means of the instrumentalities and combinations particularly pointed out in the appended claims.

To achieve the foregoing and other objects and in accordance with the purposes of the present invention, as embodied and broadly described herein, the present invention may comprise a device for detecting imminent failure of a high-dielectric stress capacitor comprising: means for applying a variable magnitude current to said capacitor, means for detecting the pulse width and magnitude of said variable magnitude cur-

rent, means for comparing said pulse width and magnitude of said variable magnitude current with an average pulse width and average magnitude for a plurality of current pulses of said variable magnitude current, means for producing an alarm signal whenever said pulse width varies from said average pulse width by a first predetermined amount, means for producing an alarm signal whenever said magnitude exceeds said average magnitude by a second predetermined amount.

The present invention may also comprise, in accordance with its objects and purposes, a device for detecting imminent failure of a high-dielectric stress capacitor employed with a variable magnitude current comprising: means for sampling the current pulse width of said variable magnitude current, means for storing and averaging said current pulse width for a plurality of pulse cycles, means for comparing each current pulse width with an average current pulse width for a plurality of pulse cycles, means for producing a pulse width alarm signal whenever said current pulse width varies from said average current pulse width by more than a first predetermined amount, means for sampling said current magnitude of said variable magnitude current, means for storing and averaging said current magnitude for a plurality of pulse cycles, means for comparing each sample of said current magnitude with an average current magnitude for a plurality of cycles, means for producing a current magnitude alarm signal whenever said current magnitude exceeds said average current magnitude by more than a second predetermined amount, whereby said current magnitude alarm signal and said pulse width alarm signal indicate imminent failure of said high-dielectric stress capacitor.

The present invention is therefore capable of detecting the imminent failure of a high-dielectric stress capacitor to expedite the replacement and thereby minimize downtime of the system in which the capacitor is being utilized. In industrial applications where reliability is an extremely important factor, such a system can minimize losses and maximize profits.

The accompanying drawings, which are incorporated in, and form a part of, the specification, illustrate various embodiments of the present invention and, together with the description, serve to explain the principles of the invention.

BRIEF DESCRIPTION OF THE DRAWINGS

FIG. 1 is a schematic diagram of the preferred embodiment of the invention.

FIG. 2 is a schematic diagram of one embodiment for monitoring capacitors employed in a transmission line.

FIG. 3 is another embodiment for monitoring capacitors employed in a transmission line.

FIG. 4 is another embodiment for monitoring capacitors used in a laser pulse power system.

FIG. 5 is a flow diagram of the operation of the microprocessor illustrated in FIG. 1.

DETAILED DESCRIPTION OF THE PREFERRED EMBODIMENT OF THE INVENTION

FIG. 1 discloses the device of the preferred embodiment of the invention. A capacitor bank 10 is implemented with a source 12, such as laser pulse circuitry, transmission lines, etc. Examples of implementation of the capacitor bank with the source are shown in FIGS. 2-4. Current viewing resistor 14 is a low resistance

precision resistor connected between the capacitor bank 10 and ground. The variable magnitude current being monitored is applied via line 16 to operational amplifiers 18 and 20 of high speed comparator 17 which comprises a Signetics NE522.

Operational amplifier 20 amplifies the monitored variable magnitude current signal while operational amplifier 18 amplifies and inverts the variable magnitude current signal. A reference voltage source is applied via potentiometer 22 to the positive and negative inputs of operational amplifiers 18 and 20, respectively. In this manner, the inverted current waveform produced by operational amplifier 18 is added to the reference voltage while the noninverted current waveform produced by operational amplifier 20 is reduced by the reference voltage. The output of operational amplifier 18 is then applied to nand gate 24 while the output of operational amplifier 20 is applied to nand gate 26. A dc control voltage, V_{cc} , is also applied to nand gates 24 and 26. Nand gate 24 produces an output whenever either input is negative. Since V_{cc} is always positive, nand gate 24 produces an output signal which sets flip flop 28 whenever the output of operational amplifier 18 is negative. Similarly, nand gate 26 produces an output to reset the flip flop 28 whenever the output of operational amplifier 20 is negative. For positive voltage waveforms applied to operational amplifiers 18 and 20 via line 16, the voltage reference signal produced by potentiometer 22 varies the point on the waveform where the set and reset signals are produced by outputs 30 and 32. Of course, waveform variations are most prevalent at the widest point of the waveform. Consequently, the voltage reference signal is normally small compared to the peak voltage of the voltage waveform being monitored.

The output of flip flop 28 therefore constitutes a pulse having a pulse width representative of the waveform of the monitored variable magnitude current signal. The output pulse produced by flip flop 28 is then applied to and gate 36 which is clocked by a high speed oscillator 38 to produce a series of pulses at output 40 representative of the pulse width of output 34. Output 40 is applied to 8-bit binary counter 42 which counts the number of clock pulses representative of the pulse produced at output 34. This quantity is applied via 8-bit parallel data bus 44 to in/out port 46, which comprises a Mostek 3881.

The pulse produced by flip flop 28 is also applied to time delay 48 which produces a pulse at output 50 which is delayed by a predetermined interval, Δt , from the leading edge of the pulse produced at output 34. Output 50 is applied to the "store" input of sample and hold device 52 which comprises an Intersil SMH-IC-1. The store signal is delayed by a predetermined interval, Δt , so that the monitored variable magnitude current is sampled in the same location for each pulse waveform. The monitored variable magnitude current is applied to the input of sample and hold device 52 and is sampled at a predetermined location measured from the beginning of the waveform for each pulse waveform, set forth above.

The output 54, which is a signal representative of the magnitude of the monitored variable magnitude current is applied to A to D converter 56 which converts output 54 to a digital signal. A to D converter 56 produces a digital signal representative of the magnitude of the monitored variable magnitude current which is applied to in/out port 60 via 8-bit parallel data bus 58. The

in/out port 60 comprises a Mostek 3881. In/out port 60 produces reset signal 62 which is applied to A to D converter 56 and counter reset signal 64 which is applied to the 8-bit binary counter which functions to reset these devices to zero once the current information has been stored.

Data stored in in/out ports 60 and 46 are applied to microprocessor 72 via data buses 68 and 70 which comprise 8-bit parallel data buses. Programmable read only memory (PROM) 78 provides the program control (set forth in FIG. 5) to control microprocessor 72 and to program address information provided by data bus 74. The 2 MHz oscillator 80 and reset device 82 also supply necessary information to microprocessor 72 for proper operation. The microprocessing circuitry 101, FIG. 1, comprises a Mostek Z-80 microprocessor chip available from Mostek Corporation.

Control enable signals 84, 86, and 88 are generated by microprocessor 72 to initiate operation of the device. Alarm indicator 90 produces an audible and/or visual indication of the imminent failure of a capacitor in capacitor bank 10. An automatic shutdown signal can also be produced by microprocessor 72 at output 96 which is applied to shutdown relay 94 which functions to disable application of current to the capacitor bank 10 from the source 12.

FIG. 2 is a schematic illustration of one manner of implementing the current reviewing resistor 14 with the capacitor bank 10 employed in a transmission line. Current viewing resistor 14 monitors changes in current for all of the capacitors in capacitor bank 10 via output 16.

FIG. 3 is a schematic illustration of the manner of implementing a plurality of current viewing resistors 101-106. Each of the outputs 108-114 utilizes a separate circuit such as shown in FIG. 1 to monitor each of the capacitors separately, or can be combined to produce a single output. Additionally, one microprocessor chip can be used with a plurality of monitoring circuits.

FIG. 4 illustrates implementation of a current viewing resistor 116 in a pulse discharge circuit for a laser. In operation, the capacitor bank 118 is discharged through thyatron switch 120 to the laser discharge cavity 122. Current viewing resistor 116 monitors the pulse wave shape of the discharge from capacitor bank 118 via output 124, which is connected to a detection circuit, such as shown in FIG. 1.

FIG. 5 illustrates the operation of the microprocessor unit illustrated in FIG. 1 comprising elements 60, 78, 46, 80, 72, and 82. In operation, the 8-bit binary counter 42 is initialized by counter reset 64. Similarly alarm indicator 90, in/out ports 60 and 46 and programmable read only memory 78, are all initiated by signals from microprocessor 72 as shown in block 126 of FIG. 5. Then, data is read from A to D converter 56 via in/out ports 60 by microprocessor 72. Microprocessor 72 then compares data read from the in/out port 60 with amplitude reference data stored and averaged within the microprocessor from previous reading cycles, as illustrated in block 130, FIG. 5. If the amplitude data read from A to D converter 56 and in/out port 60 falls within a predetermined range, microprocessor 72 then reads counter data supplied by 8-bit binary counter 42 via in/out port 46, as shown at block 134, FIG. 5. This counter data is then compared with pulse width reference data from previous reading cycles. As shown in block 138, FIG. 5, if the pulse width data falls within a predetermined range, the microprocessor 72 then completes the operational loop and proceeds to read A to D data from A to

D converter 56 via in/out port 60, as shown at block 128.

Of course, all of the operational sequences are programmed from programmable read only memory 78. When microprocessor 72 compares amplitude reference data and determines that the data being read falls outside of the predetermined range of acceptability, the "yes" branch of block 132 is followed and alarm indicator 90 is activated as shown by operational block 140. The device then tests for automatic shutdown as shown by operational block 142. If automatic shutdown is not desired, the "no" branch is followed to operational block 144 which automatically resets the circuit and proceeds with the operational loop back to operational block 128. If it is determined, however, that automatic shutdown should proceed the "yes" branch of operational block 142 is followed and shutdown relay 94, FIG. 1, is activated as shown by operational block 146, FIG. 5.

Shutdown relay 94 disconnects the capacitor bank 10 from the current source 12 to prevent explosion of the capacitor bank 10 and possible damage to surrounding equipment. Manual reset 92, FIG. 1, can reactivate the operational loop as shown by operational block 148, FIG. 5, if it is determined that shutdown was caused by circuit transients, etc. Additionally, it may be determined that sufficient advance warning has been given and operation should proceed with a faulty capacitor bank 10 until it can be replaced. Normally the test for automatic shutdown as shown by operational block 142, FIG. 5, is a recycling of the operational loop a predetermined number of times. For example, if the test for automatic shutdown is activated a preselected number of times within a preselected time period, automatic shutdown will proceed. This avoids automatic shutdown for intermittent circuit transients which occur on transmission lines on a rather frequent basis. As a result, alarm indicators 90 are activated instantaneously, but the circuit is not shutdown due to these transient signals.

The present invention therefore provides a device which is capable of detecting imminent failure of high-dielectric stress capacitors which are employed in numerous pulse power systems, transmission lines, etc. The device is capable of testing for circuit transients and automatically shutting down operation of the capacitor bank well prior to failure and/or explosion of a faulty capacitor. Additionally, this device can be implemented with inexpensive microprocessor units which are capable of performing the many numerical calculations and comparisons required to carry out the present invention in a simple and inexpensive manner.

The foregoing description of a preferred embodiment of the invention has been presented for purposes of illustration and description. It is not intended to be exhaustive or to limit the invention to the precise form disclosed, and obviously many modifications and variations are possible in light of the above teachings. For example, source 12 can also be monitored by microprocessor 72 to detect changes in source magnitude or pulse width to prevent improper activation of alarm indicator 90. The embodiment was chosen and described in order to best explain the principles of the invention and its practical application to thereby enable others skilled in the art to best utilize the invention in

various embodiments and with various modifications as are suited to the particular use contemplated. It is intended that the scope of the invention be defined by the claims appended hereto.

What is claimed is:

1. A device for detecting imminent failure of a high-dielectric stress capacitor comprising:
 - means for applying a variable magnitude current to said capacitor;
 - means for detecting the pulse width and magnitude of said variable magnitude current;
 - means for comparing said pulse width and magnitude of said variable magnitude current with an average pulse width and average magnitude for a plurality of current pulses of said variable magnitude current;
 - means for producing an alarm signal whenever said pulse width varies from said average pulse width by a first predetermined amount;
 - means for producing an alarm signal whenever said magnitude exceeds said average magnitude by a second predetermined amount.
2. The device of claim 1 wherein said first predetermined amount is approximately 0.1%.
3. The device of claim 1 wherein said second predetermined amount is approximately 5%.
4. The device of claim 1 wherein said means for applying said variable magnitude current comprises a transmission line.
5. The device of claim 1 wherein said means for applying said variable magnitude current comprises a laser system.
6. A device for detecting imminent failure of a high-dielectric stress capacitor employed with a variable magnitude current comprising:
 - means for sampling the current pulse width of said variable magnitude current;
 - means for storing and averaging said current pulse width for a plurality of pulse cycles;
 - means for comparing each current pulse width with an average current pulse width for a plurality of pulse cycles;
 - means for producing a pulse width alarm signal whenever said current pulse width varies from said average current pulse width by more than a first predetermined amount;
 - means for sampling said current magnitude of said variable magnitude current;
 - means for storing and averaging said current magnitude for a plurality of pulse cycles;
 - means for comparing each sample of said current magnitude with an average current magnitude for a plurality of cycles;
 - means for producing a current magnitude alarm signal whenever said current magnitude exceeds said average current magnitude by more than a second predetermined amount;
 - whereby said current magnitude alarm signal and said pulse width alarm signal indicate imminent failure of said high-dielectric stress capacitor.
7. The device of claim 6 wherein said first predetermined amount is approximately 0.1%.
8. The device of claim 6 wherein said second predetermined amount is approximately 5%.

* * * * *

CHAPTER 5

SWITCHES

5.1 GENERAL REPETITIVE SWITCHES

There are many switches capable of operation at repetition rates in the multi-kiloHertz realm. The most common triggered, high power switches are spark gaps and thyratrons. A non-triggered "switch," in which operation is based on the nonlinear properties of magnetic materials, also falls into this class. A "magnetic" switch is better described as a pulse compressor or pulse sharpener. Being a passive element, the "magnetic" switch experiences an impedance change determined by the nonlinear characteristics of the ferromagnetic core material. It is not a switch in the general definition of the term, but the use of magnetic material in the generation of very short high energy pulses is an important technique in high repetition rate modulator design. A detailed design of a magnetic switch used in a high power laser is given in the next chapter.

The quality of a switch may be judged by its ability to hold-off high voltage, conduct rapidly when triggered, and recover its hold-off properties after conduction. Recovery characteristics determine the upper bound at which a switch can operate repetitively. In plasma and arc discharge switches, the rate in which the plasma or arc can be cleared from the switch determines the recovery time. In a magnetic switch, the recovery is determined by how fast the core magnetization can be reset to its initial starting value. Usefulness of a switch in a short pulse, low impedance,

discharge circuit such as a laser modulator is limited by its peak current and di/dt capabilities. Each of these considerations for the particular types of switches is examined in the following sections.

5.2 SPARK GAPS

Spark gaps are by far the most versatile of all high power switches. They can be designed to operate in gases or liquids at voltages from a few hundred volts to many Megavolts and switch currents from milliamperes to Megamperes. Even though spark gaps can be designed to operate over enormous electrical ranges, any one particular design is usually limited to a very narrow dynamic range. That is to say, a spark gap designed to operate at 50 kV will probably not perform with equal electrical and life characteristics (if at all) at 40 kV in the same circuit. Because spark gaps are designed on an "as needed" basis, it is practically impossible to develop a testing procedure to establish a data base on performance and design techniques. Obviously, the design and fabrication of a spark gap to hold-off 200 volts would not involve the same methods or materials as a 2 MV device. Electrode materials, flow rates, and dielectric media such as gas mixes and liquids, further complicate a systematic analysis of spark gap technology. This along with the wide variety of geometries, i.e. point-plane, rail, coaxial, etc, make it impossible to form an organized comparison of spark gap technology with any other switching technique. For these reasons, a spark

gap evaluation is only good for the specific parameters at which the gap was designed to operate.

Theory of spark gap design and breakdown phenomena have been investigated for well over one hundred years in all parts of the world. J.C. "Charlie" Martin, of the Atomic Weapons Research Establishment in Aldermaston, England, is considered by many as the first researcher to derive basic concepts of high power switching that in many areas are still considered the standard in the field. The wide diversity of high power spark gaps could not possibly be addressed with any sort of continuity in this thesis. So in keeping with the theme of this work, spark gaps will be discussed only as pertains to short pulse generation at high repetition rates.

Spark gaps for repetitive modulators date back to the late 1800's. Early repetitive switches took the form of rotary spark gaps. The first non-experimental applications of repetitive spark gap modulators were for lighting, medical, and radio applications [Tesla, 1891,1898,1899]. In the pre-radar period of the M.I.T. Radiation Laboratory, the first systematic development of repetitive spark gaps for short pulse applications had its beginning. Rotary gaps [Lebacqz and White, 1946], and multi-electrode quenched spark gaps were developed for use in kilohertz modulators. J.D. Craggs of the Metropolitan-Vickers Electric Company, Ltd. announced the invention of the "trigatron", the first three electrode sealed spark gap in 1942 [Craggs, et.al., 1942]. The trigatron is still the most common type of spark gap used today.

The main concern of a repetitive spark gap design is clearing the metallic vapor from the gap after conduction. Sealed repetitive gaps either operate at extremely low powers or in very short bursts because of the concentration of residual metallic vapor. To achieve long duration of operation a flow system is added to the gap to force the clearing of residues. A diagram of a basic trigatron with a flow system is seen in Figure 5.2.1. The flow is directed

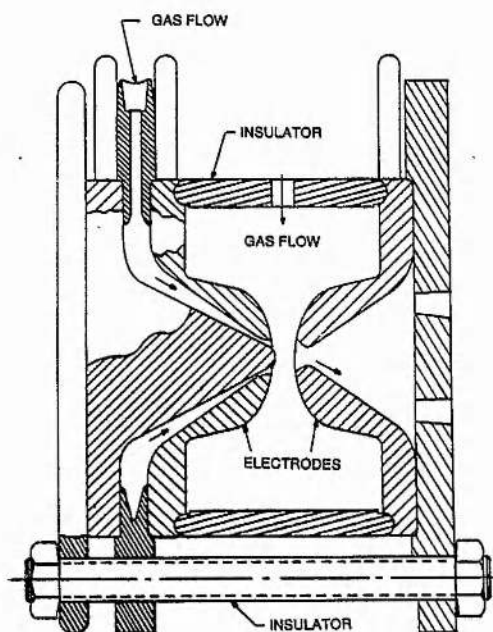


Figure 5.2.1 High repetition rate trigatron spark gap.

inward to increase the velocity and keep metal vapor from being deposited on the electrode insulators. Erosion products are exhausted through a hole in the anode, which has a low resistance countersink to maintain a uniform flow.

Trigatrons, rail gaps, and mid-plane triggered spark gaps were all investigated for the purpose of switching low impedance networks. The most suitable type of spark gap found for high repetition rate service was the gas blown

coaxial electrode device. The electrode arrangement of such a gap is seen in Figure 5.2.2. This particular gap [Veradyne, 1976] was specifically designed as a switch for a 1000 watt average power excimer laser [Butcher, et.al., 1982]. The coaxial gap was tested in burst mode at 50 kV, 50 kA, at a di/dt rate of over 10^{12} amperes/second. However, triggering was erratic and the gap was prone to prefire and fail to recover towards the end of the burst. When the gap was installed in a laser modulator [Butcher, et.al, 1982], it was required to switch a peak current of 24 kA with di/dt of $5 \cdot 10^{11}$ amperes/second. Life of the spark gap at a 500 pps repetition rate averaged about $2 \cdot 10^7$ shots (8 hours) before at least one of the electrodes had to be replaced due to erosion. Since the remaining modulator circuit components had predicted and proven lifetimes

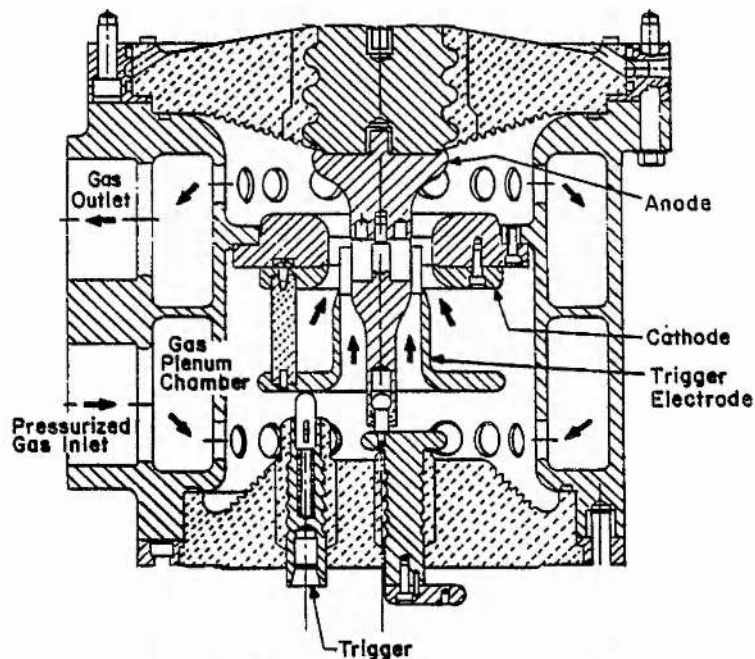


Figure 5.2.2 High repetition rate, coaxial electrode, gas blown spark spark gap [Veradyne, 1976].

of greater than 4×10^9 shots, this equates to a minimum 200 sets of electrodes and over 800 hours of replacement time over the estimated life of the laser. Since the switch was the shortest lived component of the modulator, an assessment of the lifetimes of repetitive spark gaps and life limiting mechanisms was undertaken.

Spark gap erosion has been investigated more than any other parameter in high power switching. This is partly due to the fact that each spark gap application usually has a unique spark gap that was designed specifically for that job and life information is desired for some logistic reason. The other reason is that erosion measurements are fairly simple to obtain. Spark gap erosion is a complex function of many variables and is not completely understood [Kristiansen and Hagler, 1978]. Surveys of repetitive spark gaps were made by P.N. Mace [1982] and by T.R. Burkes [1976, 1987]. Results of these studies revealed a very interesting fact with regard to erosion. Regardless of the electrode material or electrical operating conditions, at best, electrode material is eroded at an average rate of 50 micrograms per coulomb of charge transfer through the gap. This means that if a particular application requires a switch to transfer 100 Megacoulombs (not unreasonable in a high repetition rate modulator) the electrodes would have to have some 5 kg of material available for erosion.

Development of spark gaps for operation at high repetition rates was quickly abandoned due to the extremely short life. With no apparent means of circumventing the

natural limitations of material erosion, an investigation into longer lived switches was begun.

HISTORICAL COMMENT: It has been written [Menown, 1976] that every generation reinvents the wheel when it comes to high power switching. In the early days of radar, much work was concentrated on the development of long lived spark gaps. With the invention of the hydrogen thyratron, all work on spark gaps ceased. So much emphasis was placed on the thyratron that a periodic meeting, the Hydrogen Thyratron Conference, (later to become the Power Modulator Symposium) was established. One of the participants in the early days of high power switching related that "no matter how complex or hard to build the hydrogen thyratron was, it was better than working with spark gaps" [Schnieder, 1983].

5.3 THYRATRONS

The hydrogen thyratron was the longest lived, most reliable, highest power gain switch in the 1940's. Since its patent in 1918 [Langmuir, 1918], the hydrogen thyratron has become the most used switch in high power pulse generation. State-of-the-art thyratrons can have a dynamic switching range of over 100 in voltage and 100,000 in pulse current in a single device. Lifetimes of thyratrons in radar type modulator circuits have been demonstrated to exceed 50,000 hours [SLAC, 1974] with a total charge transfer of over 300 Megacoulombs [LANL, 1981]. With documented lifetimes of these magnitudes, the thyratron is,

as it was in 1942, the best candidate for use as a switch in a short pulse modulator.

The thyratron has two basic limitations that question its ability to switch low impedance circuits. These are peak current and di/dt . Both of these parameters are dependent on the emission properties of the cathode and the rate of plasma formation in the tube. Basic principles of thyratron operation have been published in three volumes of "Research Study on Hydrogen Thyratrons" [Germeshausen, Goldberg, and Riley] and in two books from the Soviet Union [Voronchev, 1958] [Fogel'son, et.al., 1974]. A comprehensive study into the ultimate limits of peak current and di/dt capabilities of a hydrogen thyratron was performed at E.G.&G. about 7 years ago [Turnquist, et.al., 1980]. These collections, along with over 500 hundred published research reports [Gundersen and McDuff] and two theses, provide a good foundation in the understanding of the hydrogen thyratron. With the huge amount of research conducted toward the development and use of hydrogen thyratrons, it is not reasonable to report on previous work in this thesis.

By far the most important aspect of thyratron technology, that has been overlooked in practically all the publications, is device construction. Plasma physics, electron dynamics, and electric field related phenomenon comprise only a small part of today's high power thyratrons. Materials compatibility, sealing, electrode processing, and thermal design constitute the major aspects of new device development. These "non-glamorous" issues in hydrogen thyratron technology have been addressed solely by the

manufacturers of this device. Because of the great investment of time and money by the manufacturers in the development of construction techniques, much of this information is closely guarded. All three major (free world) manufacturers of hydrogen thyratrons participated in this high power switch development programme. During the course of this investigation, many of the proprietary design techniques were made available to facilitate the development process with an understanding that it would be held in confidence. Therefore, in order to continue to protect this confidence and cooperative attitude of the manufacturers, no reference will be made in this thesis to the design or construction (other than that in Chapter 2) of the high power thyratrons. Rather, in keeping with the theme of this thesis, the application of the development devices and circuit techniques for short pulse modulators will be addressed.

Switch requirements for low impedance pulse modulators place strenuous requirements of current rate of rise on this element. Rates of rise of greater than 10^{12} amperes/second are not uncommon in this type of modulator. Spark gaps can easily meet this requirement but have very short lives. Until the advent of the excimer laser, there was no large demand for a high di/dt switch. As the laser was improved, the need for a long life switch became the major limiting factor. To overcome this limitation an effort was begun to develop circuit techniques and thyratrons for low impedance repetitive modulators.

The first step in the development programme was to establish the state-of-the-art in thyatron switching capability needed to define research objectives and goals for the programme. To do this, a series of tests was performed on "standard" thyatrons to ascertain their performance in low impedance short pulse circuits. Since triggering methods have a great influence on the electrical performance, [Germeshausen, et.al. 1953] [Fogel'son, et.al, 1974] [Menown, 1976] this was the first topic to be investigated. Tests of the effect of trigger impedance on the switch closure time (anode fall) and the switch jitter were performed on 5, 7.62, and 11.4 cm (2", 3", & 4.5") diameter triode and tetrode thyatrons. Various trigger configurations, i.e. bias voltages, bias currents, double trigger pulses in the case of the tetrode.etc. were examined at 1000 pps repetition rate. The effect on switching time and jitter was found to be a strong function of trigger impedance. Little effect due to trigger configuration was detected except in the case of extremely high di/dt ($>10^{11}$ amperes/second) where the application of two trigger pulses to the tetrode thyatron made a marked improvement in all switching parameters [McDuff, et.al, 1984 and 1985]. The result of these measurements for the 7.62 cm (3") tube is plotted in Figures 5.3.1 and 5.3.2. Plots of the data from the evaluation of the smaller and larger diameter tubes had similar curves but shifted in the x-direction. Where the curve of the anode fall times for the 7.62 cm (3") diameter tube is essentially flat below 100 ohms, this point occurs about 250 ohms and 33 ohms for the 5 cm (2") tube and 11.4

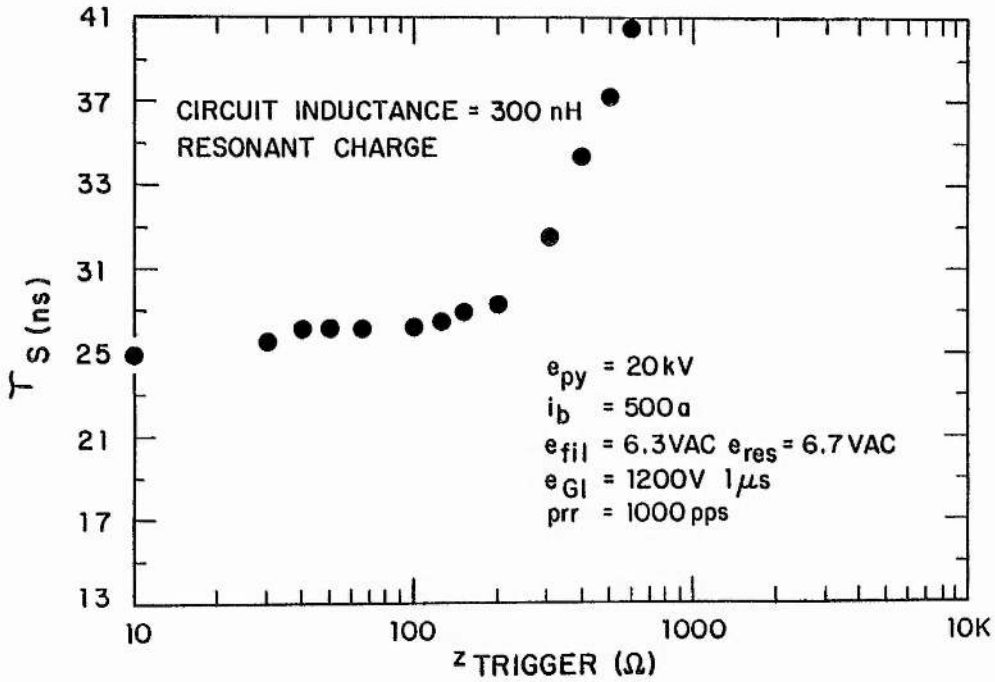


Figure 5.3.1 Anode fall as function of trigger impedance for a 7.62 cm (3") diameter thyratron.

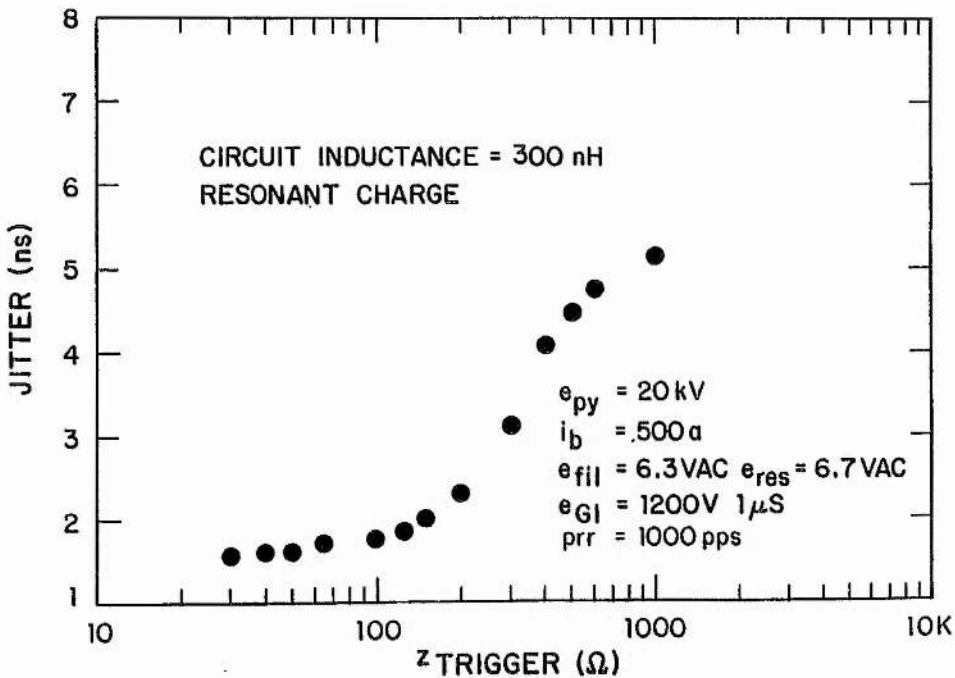


Figure 5.3.2 Switching jitter as a function of trigger impedance.

cm (4.5") tube respectively. The impedance of the driver at the knee of the curve is directly related to the volume of gas in the grid/cathode region. This relation is consistent with the basic triggering theory [Germeshausen, 1953]. A similar relation holds true for the jitter. Discharge parameters that were held constant during the tests are labeled on the figures. The current pulsewidth was 80 nS with a risetime of approximately 30 nS under the optimum switching conditions in the tests. A maximum di/dt in the test circuit of 2×10^{10} amperes/second was achieved. This is greater than most "radar" type thyratron applications but far below the need of short pulse modulators. Brief experiments at greater di/dt gave results consistent with those plotted in Figures 5.3.1 and 5.3.2.

Having established some guidelines for triggering, the effects of peak current and di/dt on the life of the thyratron was investigated next. In the first series of tests, the life as a function of peak current was examined. For cost containment in these experiments, only the 7.62 cm (3") diameter tubes were used. A plot of these data is seen in Figure 5.3.3. Trigger parameters for these tests were chosen at the optimum point from the data presented earlier. Again the fixed electrical conditions are labeled on the graph. To adjust the peak current, the impedance of the circuit was varied while maintaining a pulsewidth of 80 to 120 nS at the base. Each point on the graph represents a failed thyratron. Three tubes were tested at current levels of 2000, 1500, 1000 and 500 amperes. Only one tube failed at the 500 ampere level and the tests were terminated at

10^9 shots. Each thyratron was autopsied to determine the mechanism of failure. All failures were cathode related.

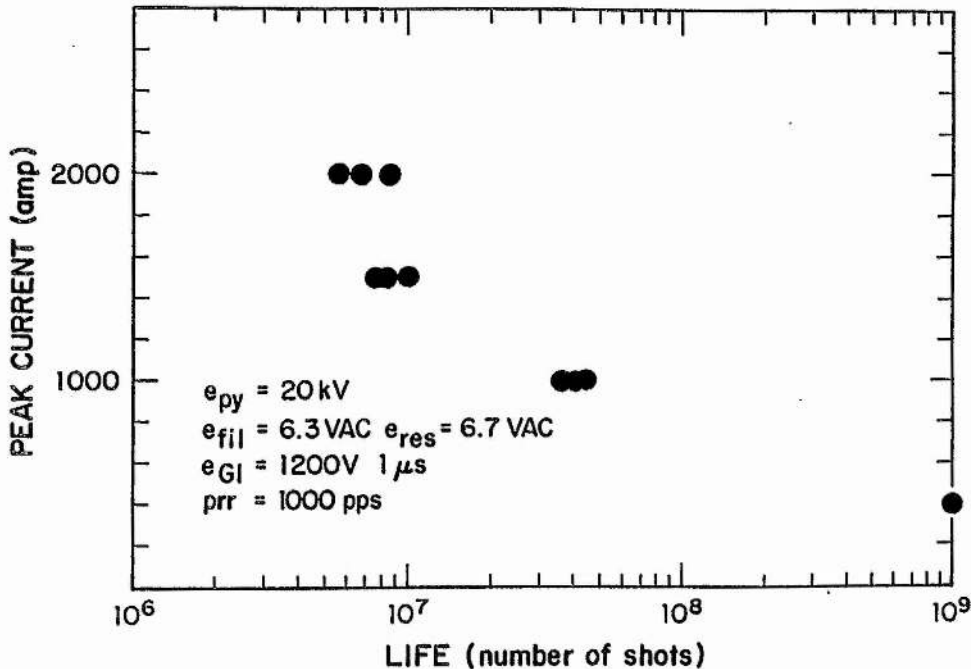


Figure 5.3.3 Thyratron life as a function of peak current for the 7.62 cm (3") diameter thyratrons.

In some cases, the oxide cathode coating had fallen off the nickel base and, in the high di/dt discharges, substantial arcing from the cathode to the grid had occurred. From this information, another series of tests was performed on the effect of di/dt on life of the thyratron. Results of these experiments, based partly on the data from the peak current tests, is displayed in Figure 5.3.4. To achieve a di/dt of between 10^{11} and 10^{12} amperes/second some of the data were taken in the laboratory test circuit and some in a commercial excimer laser. Because the 7.62 cm (3") diameter thyratron cannot switch peak currents great enough to achieve a di/dt greater than about 10^{11} amperes/second, these tests were performed with the 11.4 cm (4.5") diameter

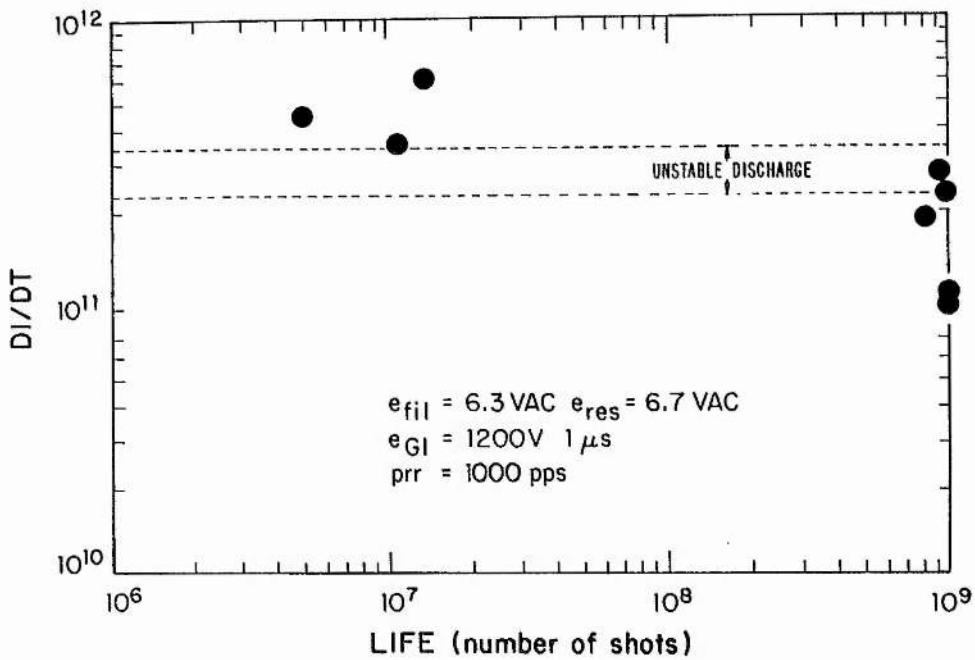


Figure 5.3.4 Life as a function of di/dt in a 11.4 cm (4.5") thyratron.

tubes. Results from these experiments showed that life has almost a step function dependence on di/dt . Below about 3×10^{11} amperes/second, life of the tubes was not greatly affected. Above this level lifetime dropped by a factor of one hundred. The value of this data is somewhat questionable because of the high peak currents, 7.5 to 10 kA, required to achieve the high di/dt . However, results of the autopsies showed a substantial increase in arcing between the cathode to grid and grid to anode in the tubes operated at di/dt of greater than 2×10^{11} amperes/second. Cathode to grid arcs are usually a consequence of insufficient electron emission from the cathode to sustain a plasma density capable of supporting the conducted current. Similarly, grid to anode arcs are due to insufficient plasma density to support conduction, resulting in a constricted discharge. Both these conditions result in an extremely large electric field

at the surface of the electrodes, which leads to field emission and a metal vapor arc [Gundersen, et.al. 1982, 1985]. Thyratrons of this type, operated at similar peak currents but very low di/dt , have lifetimes determined by the two normal "wear-out" mechanisms of cathode depletion and gas clean-up [Turnquist, 1976]. Current rate of rise is also highly dependent on the design of the grid and grid baffles and is reported to have an upper limit of 2 to 4×10^{11} amperes/second in a 35 kV single gap thyatron [Menown, 1976]. Even though the di/dt -life data is somewhat questionable in its accuracy, it is still a good baseline for circuit design that has been substantiated by other researchers.

With the data presented above, a substantial data base for operation of thyratrons in low impedance short pulse modulators was established. One last gap in the data base was thyatron power dissipation in a short pulse circuit. Thyatron power dissipation for microsecond pulsewidths and low di/dt is reviewed in many articles, the most complete being the work at the M.I.T. Radiation Lab [Glasoe and Lebacqz, 1946]. Because the theoretical understanding of loss mechanisms is not well understood at short pulsewidths, an empirical approach to power dissipation was taken. A method of energy inventory similar to the one described in Chapter 4, Section 3, was used to measure the energy dissipated in the elements in the pulse discharge test circuit. Stored energy in the discharge circuit was varied from 0.6 to 6 joules and plotted against the percentage of

energy dissipated by the thyatron and the load at 1000 pps. The results are seen in Figure 5.3.5. At stored energy of

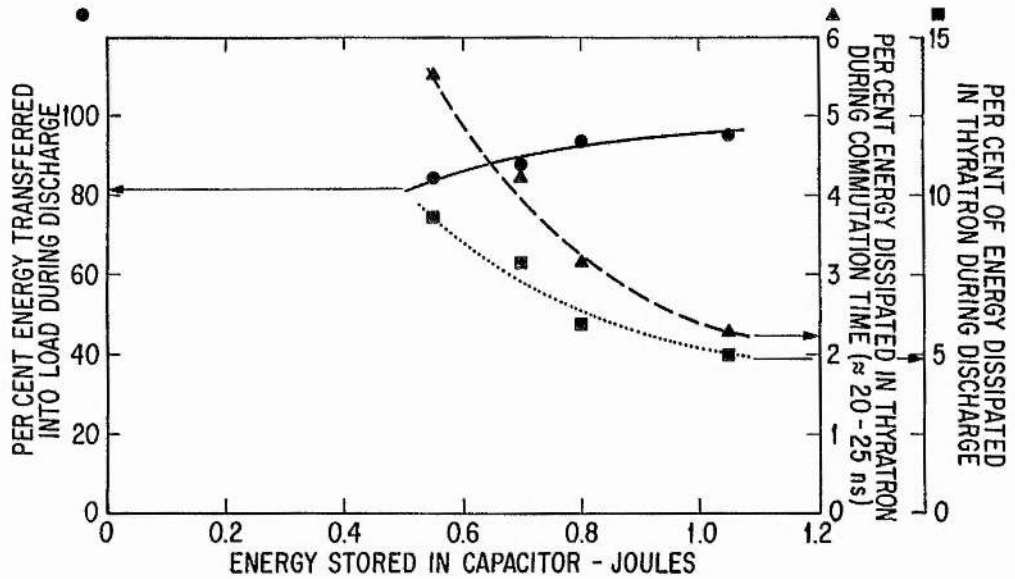


Figure 5.3.5 Energy dissipation in a thyatron switched, 120 ns pulsewidth, 1000 pps modulator.

about 1.5 joules, the dissipation during commutation becomes nearly constant at about 2% of the total stored energy. Likewise, the dissipation during the conduction period becomes nearly constant and is a function of the average switch current and the constant 150 volt conduction drop of a hydrogen thyatron. Above about 2 joules, total thyatron dissipation stabilizes at about 7% of the stored energy. Later experiments showed that this loss figure does not vary up to the maximum power handling capability of the thyatron.

Having determined the basic operating characteristics of hydrogen thyatrons in short pulse circuits and life limiting factors associated with peak current and di/dt , a future development plan was drafted. Since commercially

available thyratrons do not reliably operate with large current values at high repetition rates for prolonged periods, a dual development approach was taken. The first aim was to develop a method of operating several thyratrons in parallel from a single low impedance energy storage line. Parallel operation of thyratrons would provide a short term solution to the immediate problem of a high current switch. Second, a long term thyatron development programme was initiated since a quantum improvement in the di/dt capability of the thyatron was not likely to be made in the near future. Successful thyatron design from the long term programme must be mass producible if they are to be of any use. Because the development of a production thyatron is depends on the cooperation of the manufacturers, a major part of this programme was performed at the manufacturers' sites. No effort was expended into the development of a "new" type of diffuse discharge switch, such as a linear thyatron, because such a task would result in only a laboratory device that was not available on a wide-spread basis.

OPERATION OF THYRATRONS IN "HARD" PARALLEL

Thyratrons have been operated in parallel ever since their invention. In 1925, D.C. Prince operate several "new" mercury thyratrons in parallel in an inverter circuit at General Electric. Classical parallel operation has been accomplished by connecting a "ballast" element in series with the thyatron. The ballast element is usually a

resistor [Reintjes, 1952] or the more common "balanced reactor" [Lake, 1964] shown in Figure 5.3.6. The ballast

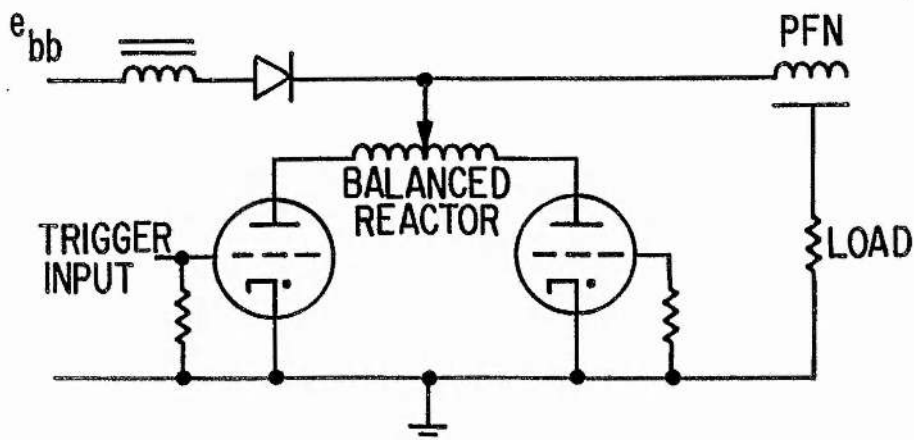


Figure 5.3.6 Conventional circuit for parallel operation of thyratrons [Glasoe and Lebacqz, 1946].

element prevented one thyatron from conducting before the other and thus "hogging" the discharge current. Using a ballast can be extended to as many thyratrons as desired. Ballast elements force current sharing by inserting a fixed impedance in series with the switch. In a low impedance circuit, where inductance must be kept to a minimum, this method is not practical. The use of resistor ballasting in high power circuits results in unacceptable losses. One method of avoiding the use of ballast elements is to use a separate energy store for each thyatron [Scoles and Snelling, 1978] [Brown and Smith, 1986]. Having a separate energy store for each thyatron works quite well in eliminating the "hogging" problem but usually adds a great number of components to the modulator, which can reduce the reliability. To minimize the number of modulator components, increase reliability, and reduce the repair time

in the event of a failure, the thyratrons must be connected to a single energy store in "hard parallel", that is, no form of impedance connected in series with the tubes to forces current sharing. The main advantage of a single parallel connection is the reduced complexity of the mechanical design of the energy storage network and switch mounting hardware. From an industrial process point of view, reliability and simplicity of construction are all important factors.

From previous experiments [McDuff, 1978] it was known that the anode delay time (time between the grid breakdown and start of conduction) could be controlled by the level of the control grid negative bias. With two thyratrons connected in "hard parallel" on the end of a 25 ohm network, the time at which the tubes conducted was controlled by means of a computer programmable bias supply [McDuff, 1981]. Forcing commutation by means of negative bias adjustments, even though completely successful, had several drawbacks. Adjusting the grid bias affects more than just the anode delay time. Recovery, switching (or anode fall time), and jitter are all affected by the level of the negative bias on the control grid. These and several other circuit problems [McDuff and Litton, 1982] made the method of bias control somewhat unstable. Having the control circuitry connected to the grid of the thyatron made the technique prone to electrical interference problems. Even though the scheme worked well enough, the unstable nature of the control encouraged the exploration of another technique. The next

method of commutation control was to provide separate triggers with adjustable delays to each of the thyratrons.

The trigger control technique is based on charge transfer. When the common energy storage network is charged to a predetermined voltage, V , it stores a fixed charge, Q . With a number of switches, N , each switch should pass Q/N amount of charge in the same time interval if the switches are sharing equally. A block diagram of the trigger control system is seen in Figure 5.3.7. Referring to this figure, the current through the thyatron is acquired by the

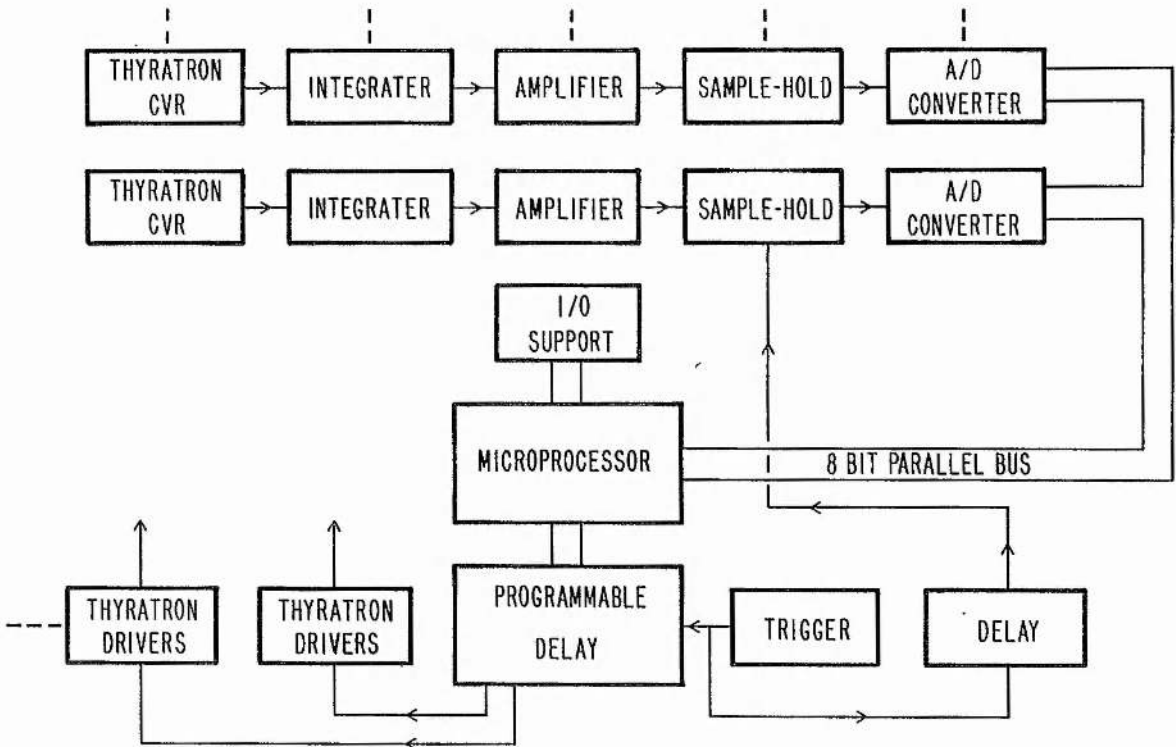


Figure 5.3.7 Trigger control system block diagram.

thyatron CVR (current viewing resistor). The current pulse is integrated to give Q , amplified, and fed to the pretriggered sample-hold circuit where the value of Q is stored. Next, a low speed A/D converter translates the

values of Q to an 8-bit digital word which can be understood by the microprocessor. The microprocessor averages all the values of Q and subtracts each Q from the average. If the difference between the average, Q/N , and the measured Q is within a preprogrammed range the microprocessor does nothing. If the difference is negative, the thyatron passing that Q is commutating too early; that is, that particular thyatron is passing more current than Q/N . Likewise, if the difference is positive, that thyatron is commutating too late and not passing its share of the total charge. A hybrid programmable delay, with 1 nS step resolution, is controlled by the microprocessor to adjust the delay of the trigger pulse to the thyatron drivers. Thus, the circuit forces each thyatron to pass the same amount of charge in the same preprogrammed time interval and current sharing is achieved. The major advantage of this method is that all control is done at a low level, isolated from all high voltages and possible interference. Also, this method works independently of the anode delay time of each tube. It was found during the testing, that the control circuit could correct differences in commutation times up to 200 nS. This "capture window" is large enough to make it possible to use a triode and a tetrode thyatron (large difference in anode delay) in the same circuit. Current sharing is controlled flawlessly at any voltage and repetition rate because the technique is based on the amount of charge each switch passes. If the control system was turned off allowing the thyatron drivers to all fire simultaneously, usually one thyatron would "hog" all the

current. With high speed microcomputers, the control circuit can perform the calculations and adjust the thyatron driver delay in less than 100 μ s. A high speed control circuit was not required in the three-tube circuit, shown in Figure 5.3.8,

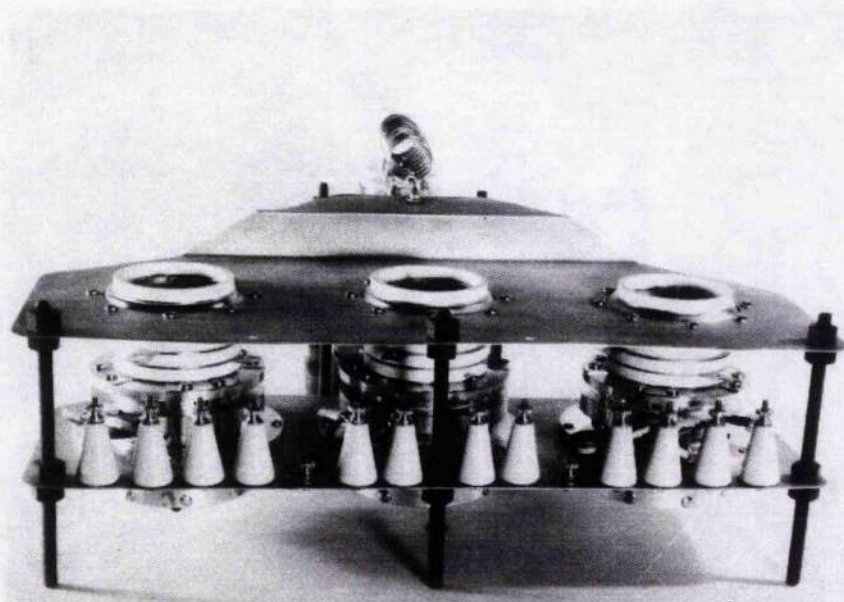


Figure 5.3.8 Three thyatron, 10 ohm "hard" parallel test circuit.

because a thyatron driver delay was only adjusted by the microcomputer a few times a day at kiloHertz repetition rates. It was discovered that once the timing had been set, the thyatrons would tend to stay in synchronization. The three-tube circuit would operate at 1500 pps, with uniform current distribution between all three thyatrons. Measurements showed that after the initial warmup drift in the anode delay time, the thyatron anode delay would remain within 4 nS during any 24 hour period.

Commutation control by thyatron trigger delay adjustment was found to be far superior to the control grid bias method in terms of stability and range of control. This technique was later extended to a five thyatron circuit with similar results. There was no practical limit found for this technique and it should work equally well for common or separate energy storage lines.

THYRATRON DEVELOPMENT PROGRAMME

As mentioned before, thyatron development depends upon the cooperation of the manufacturers to produce the devices. Anyone familiar with the complexity of high power thyatron construction will attest the futility of attempting to construct a device without the benefit of a large production facility. Even though the majority of the true device development was on the part of the manufacturers, the evaluation of the devices was performed as part of the component development effort reported in this thesis.

The original intent of the development effort was to expand the peak current and di/dt capability of high power thyatrons. However, as the work on circuit techniques for driving low impedance loads progressed, the emphasis in thyatron development changed from achieving higher currents and di/dt , to extending the operational lifetimes.

Low impedance circuits require meticulously careful design to minimize the inductive components and maintain a constant impedance from energy store to the load. When the load is time-varying or reactive such as a laser or pulsed magnet, this task becomes more difficult. Circuit

techniques have been developed to deal with non-linear time varying loads [Ball and Burkes, 1975] [Roark, et.al., 1978] [Nelson and McDuff, 1986]. But when the impedance drops to the tens of milliohm level, matching the load to the energy store in a high voltage circuit becomes impossible. Having a load that is much less than the driving point impedance of the energy storage network results in an underdamped circuit. In a thyatron switched circuit, this means large negative anode voltages. A standard thyatron can withstand only a limited amount of negative anode voltage immediately after the forward conduction. Too large a negative anode potential will result in an inverse arc, or arc-back, due to field emission from the surface of the anode. Arcing in a thyatron will increase the rate of gas depletion or "gas clean-up". Severe damage can occur if the inverse arc reaches the cathode surface and destroys the emissive material. Since there was no reliable method of matching circuit impedances to an ultra-low impedance load, a means of protecting the switch was sought.

The conventional way of protecting a thyatron from arc-back is to place an inverted thyatron in parallel with the forward conducting tube to conduct the negative going current. In a low impedance circuit this is not always possible because the addition of another thyatron will increase the inductance of the circuit beyond the acceptable limit. High voltage solid state rectifiers cannot be used because of the excessive inductance of the long series stacks and the relatively short life in short pulse circuits operating at high peak currents. Double-ended thyatrons

are one possible solution in some cases, but their intrinsically long recovery time is not well suited for very high repetition rates. Since it is not practical to eliminate the inverse voltage on the switch in a low impedance circuit, the new direction of the thyatron development programme was to devise a switch that withstands the inverse voltage.

In 1978 a new type of thyatron was announced at the Power Modulator Symposium at Buffalo, New York [Menown and Neale, 1978]. This device had a cavity or "hollow" anode that provides a source of electrons to support ionization in the reverse direction without arcing. (See Figure 2.2.2) Working with this new thyatron, an aggressive development, test and evaluation plan was undertaken. The first experiments were performed on a series of 11.4 cm (4.5") diameter oxide cathode ceramic thyatrons [McDuff, 1983]. After just two design changes, with the proper triggering method, lifetimes of greater than 2×10^9 shots in a laser circuit was demonstrated [McDuff, 1983] [McDuff and Rust, 1985]. Two of these thyatrons were designed into the laser modulator described in the next chapter (Figure 6.1.9). Lifetimes of these tubes were limited by cathode depletion. Autopsies revealed that practically all the tri-oxide cathode coating had been completely evaporated from the nickel cathode substrate. The rest of the thyatron showed wear normal for that amount of use. The hydrogen reservoir was in good condition, indicating that the life was not limited by gas clean-up. Two additional tubes were life tested with similar results.

The 2×10^9 shot lifetime was nearly 150 times longer than the next best thyratron tested to date. Because the life of the thyratron was limited by cathode emission, this became the focus of the development. A cathode material with inherently longer emission life is made of a tungsten sponge impregnated with a barium aluminate mix [Hull, 1939]. Incorporating a dispenser cathode into a new envelope design resulted in the metal-envelope series of compact high power thyratrons with extremely long lifetimes [Cook, 1960]. A special metal-envelope thyratron fitted with a hollow anode was constructed for evaluation. Three technical features were combined in the new device to give an outstanding performance. First was the special hollow anode design that allowed much greater reverse current than was previously possible. Second was the long life barium aluminate cathode which can support much higher electron current emission densities than an oxide coating type of cathode. The third and newest innovation in thyratron technology was the introduction of a triple-grid design [Kettle and Wheldon, 1976] into a hollow anode thyratron. Specially designed grids reduce the jitter, allow higher rates of rise of currents without arcing, and allow current densities greater than 10 kA/cm^2 in the grid apertures. Complete details of the operation and performance of this new class of tube is reported by McDuff and Rust [1985] and Pirrie et.al. [1986]. One of these thyratrons was used to test the final design of mica capacitor to nearly 10^{10} shots as described in Chapter 4, Section 5.

After three years of a cooperative development effort with the manufacturer of the hollow anode thyratrons, a life improvement of over 500 was achieved in thyratrons for low impedance circuits operated at high repetition rates. This new class of thyratrons is equal in every respect to its "solid" anode counterpart except it has the ability to conduct in the reverse direction with no deleterious effects on the device lifetime.

With the development of a thyatron, having lifetimes equal to those of the energy storage capacitors, it is possible, for the first time, to design a high repetition rate modulator capable of delivering tens of kilowatts to a low impedance load, with predictable lifetimes of 10^{10} shots. One such design, for a 200 watt average power, pulsed excimer laser, is detailed in the next chapter.

References for Chapter 5

- Ball, D.G. and Burkes, T.R., "Pulse Generation for Time Varying Loads," Dept. of Electrical Engineering, Texas Tech University, Thesis, 1975.
- Brown, A.J.W. and Smith, P.W., "A Multi-Parallel Thyatron, Repetitively-Pulsed Power Supply for High-Power Gas Lasers," Seventeenth Power Modulator Symposium, 1986.
- Burkes, T.R., "A Critical Assessment of High Power Switches," Naval Surface Weapons Center, Dahlgren, Virginia, 1976.
- Burkes, T.R., "A Critical Assessment of High Power Switches--1987 Revised Edition," Naval Surface Weapons Center, Dahlgren, Virginia, 1987.
- Butcher, R.R., Tennant, R.A., Erickson, G.F., Swisher, S.L., Willis, W.L., "A High Average Power Excimer Laser," Proceedings of CLEO, 1982.
- Cook, K.G., "A High Power Metal Envelope Deuterium Thyatron," Sixth Symposium on Hydrogen Thyatrons and Modulators, 1960.
- Craggs, J.D., Haine, M.E., Meek, J.M., "The Development of Triggered Spark Gaps with a Particular Reference to Sealed Gaps," Metropolitan-Vickers Electric Co., Ltd., Report C-331, Sept. 1942.
- Fogel'son, T.B., Vagin, L.N., Breusova, L.N., "Impulse Hydrogen Thyatrons," Soviet Radio, Moscow, 1974.
- Germeshausen, K.J., Goldberg, S., Riley, D.F., "Research Study on Hydrogen Thyatrons...Volumes I,II, & III," Edgerton, Germeshausen, & Grier, Inc. Boston Massachusetts, 1953, 1956, & 1957.
- Glaseo, G.N. and Lebacqz, J.V., eds., Pulse Generators, New York, McGraw-Hill, 1946.
- Gundersen, M., Guha, S., Cole, H., "A Study of Discharge Processes in Hydrogen Thyatrons," IEEE Tran. Plasma Sci., PS-10, 1982
- Gundersen, M., Kunc, J., Erwin, D., Braun, C., "Fundamental Processes in High Current Glow Discharge Switches," Fifth IEEE Pulsed Power Conference, 1985.
- Gundersen, M. and McDuff, G., "The Complete Thyatron Reference," To be Published, 1988.

- Hull, A.W., "The Dispenser Cathode," Physical Review, Vol.56, July, 1939.
- Kettle, L.J. and Wheldon, R.J., "A Triple Grid Thyatron," Twelfth Power Modulator Symposium, 1976.
- Kristiansen, M. and Hagler, M., "Spark Gaps" from A Critical Assessment of High Power Switches, T.R. Burkes Principle Investigator Naval Surface Weapons Center Report # NP30/78, 1978.
- Lake, R.E., "The Parallel Operation of Hydrogen Thyratrons," Eighth Symposium on Hydrogen Thyratrons, 1964.
- Langmuir, I., "Electric Discharge Controlling Device and Method of Operating the Same," U.S. Patent 1,289,823, Dec. 31, 1918.
- Lebacqz, J.V. and White, H.J., "The Rotary Spark Gap," from Pulse Generators, McGraw-Hill Book Co., 1946.
- Los Alamos National Laboratory, Operating Log for the WNR Fast Extraction Kicker Magnet, Group P-9.
- Mace, P.N., Personal Communication, 1982.
- McDuff, G., EG&G Los Alamos Monthly Report #18, 1978.
- McDuff, G., "Parallel Operation of Thyratrons in Low Inductance Discharge Circuits," 3rd IEEE Pulsed Power Conference, 1981.
- McDuff, G. and Litton, A., "Development and Evaluation of Systems for Controlling Parallel High di/dt Thyratrons," Fifteenth Power Modulator Symposium, 1982.
- McDuff, G., "Test and Evaluation of the CX-1574 Thyatron for Use in Excimer Lasers," EEV Technical Reprint, EEV Co. Ltd. Chelmsford, Essex, England, CMI 2QU, 1983.
- McDuff, G. and Rust, K., "Evaluation of Bidirectionally Conducting Thyratrons for Pulsed Excimer Lasers," IEEE Sixteenth Power Modulator Symposium, June 1984.
- McDuff, G. and Rust, K., "A Short Note on Hollow Anode Metal Envelope Thyratrons for High-Power High Repetition-Rate Lasers," EEV Technical Reprint, EEV Co. Ltd. Chelmsford, Essex, England, CMI 2QU, 1985.
- Menown, H., Lecture at Texas Tech University, 1976.
- Menown, H., "Gaseous Switches: The Past and Present State of the Art," Invited paper to the First International Pulsed Power Conference, Lubbock, Texas, 1976.

- Menown, H. and Neale, C.V., "Thyratrons for Short Pulse Laser Circuits," Thirteenth Pulse Power Modulator Symposium, June, 1978.
- Nelson, B. and McDuff, G., "Pulsed Forming Network Design Program for Linear and Time-Varying Loads for the IBM Personal Computer," Seventeenth Power Modulator Symposium, 1986.
- Pirrie, C., Menown, H., Nicholls, N., "Advanced Thyratrons for the Nineties," Seventeenth Modulator Symposium, 1986.
- Reintjes, J. and Godfrey, T., "Principles of Radar," McGraw-Hill Book Co., 1952.
- Roark, R.M., Parten, M.E., Masten, L.B., Burkes, T.R., "Pulse Forming Networks with Time Varying or Nonlinear Loads," Thirteenth Power Modulator Symposium, 1978.
- Schnieder, S. Personal communication, 1983.
- Scoles, G. and Snelling, R.J., "Operating Hydrogen Thyratrons in Parallel," Thirteenth Pulse Power Modulator Symposium, 1978.
- Stanford Linear Accelerator Center, Operation Log of the Beam Line Thyratron Modulators, 1974.
- Tesla, N., "Alternating Electric Current Generator," U.S. Patent 447,921 March 10, 1891 and "Method of Operating Arc Lamps," U.S. Patent 447,920, March 10, 1891.
- Tesla, N., "High Frequency Oscillators for Electro-Therapeutic and other Purposes," American Electro-Therapeutic Association, Buffalo, New York, Sept, 1898.
- Tesla, N., "Apparatus for Utilizing Effects Transmitted from a Distance to a Receiving Device Through Natural Media," U.S. Patent 685,955, Sept. 8, 1899.
- Turnquist, D., "Thyratron Life," E.G.&G. Tech Note, 1976.
- Turnquist, D., Friedman, S., Caristi, R., Merz, S., "The Effects of Inductance and Plasma Growth on the Current Rise Rate in Ultra-Fast High Power Hydrogen Thyratrons," Advanced Copy to be Published, 1980.
- Veradyne Corp., 330 Victory Blvd., Burbank, CA 91502, Series 50,000 Coaxial Spark Gap.
- Voronchev, T.A., "Impulse Thyratrons," Soviet Radio, 1958.

CHAPTER 6
HIGH REPETITION RATE MODULATOR DESIGN
FOR A
PULSED EXCIMER LASER

6.1 INTRODUCTION

The paramount motivation of this investigation is the engineering of repetitive lasers. This chapter coalesces the component and circuit design data presented in the previous chapters and applies it to the design of a repetitive modulator for driving a XeCl pulsed excimer laser. Each step of the design is examined in detail with important implications of engineering principles discussed. A general design procedure and the complete design calculations for a 200 watt average power excimer laser are presented in this chapter. Results from the modulator testing are given and compared with the values calculated for critical electrical parameters. In most cases, discrepancies between the calculated and measured parameters are resolved. Aspects of laser medium preionization do not directly pertain to the topic of this chapter and so they are not addressed. The flow system and gas clean-up processor used in the the laser is based on a design of the EDS laser described by Butcher, et.al.[1982].

The laser described was designed to meet the needs of a particular industrial process. This laser must operate continuously for a standard 8 hour work day six days a week. Lasing frequency, energy loading, laser head design, power output, and beam profile requirements are predetermined by

process needs and are reviewed only as pertaining to the modulator design.

NOTE: Specifications marked with an asterisk are "given" by process requirements and are fixed in value.

LASER DESIGN

The minimum specification of the laser needed for the industrial process is *500 pps with at least *0.250 joules/pulse. A lasing medium of *XeCl with a *Neon buffer gas is chosen to give a 308 nm output wavelength. Given a *2% light energy extraction efficiency, we have from

$$\frac{\text{Energy Out}}{\text{Extraction Eff.}} = \text{Energy Deposited in Gas.} \quad (6.1.1)$$

Substituting into Equation 6.1.1 we find a gas energy deposition of 12.5 joules is required. Given the maximum gas energy loading of *30 joules/liter-atmosphere (j/l-atm) we find the discharge volume pressure-product, VP, from

$$VP = \frac{\text{Energy Deposited in Gas}}{\text{Gas Energy Loading}}. \quad (6.1.2)$$

Solving, (6.1.2) we get

$$VP = \frac{12.5 \text{ j}}{30 \text{ j/l-atm}} = 0.41 \text{ l-atm} = 410 \text{ cm}^3\text{-atm.}$$

It is also given that the ratio of electric field to gas pressure, E/P, be equal to *3 kV/cm-atm and a laser gas conduction voltage drop, V_g , of *25 kV. The discharge gap pressure product, GP, is found from

$$GP = \frac{V_g}{E/P} = \frac{25 \text{ kV}}{3 \text{ kV/cm-atm}} = 8.33 \text{ cm-atm.} \quad (6.1.3)$$

Knowing the VP and the GP products we can find the discharge width-length product, WL from

$$WL = \frac{VP}{GP} = \frac{410 \text{ cm}^3\text{-atm}}{8.33 \text{ cm-atm}} = 49.2 \text{ cm}^2. \quad (6.1.4)$$

So the important product parameters for the laser design are:

$$VP = 410 \text{ cm}^3\text{-atm}$$

$$GP = 8.33 \text{ cm-atm}$$

$$WL = 49.2 \text{ cm}^2.$$

Charting the GP and WL products for various discharge gaps, gas pressures, discharge widths, and discharge lengths (Table 6.1.1) a laser head with suitable dimensions can be

G (cm)	P (atm)	W (cm)	L (cm)
1.0	8.33	0.5	98.4
1.5	5.55	0.75	65.6
>> 2.0	4.16 <<	>> 1.0	49.2 <<
2.5	3.33	1.25	39.4
3.0	2.77	1.50	32.8
3.5	2.38	1.75	28.1
4.0	2.08	2.0	24.6

Table 6.1.1 GP and WL products.

selected. Choosing a gap of *2 cm, from Table 6.1.1, the laser must operate at a gas pressure of 4.16 atmospheres. A * beam aspect ratio, G by W, of 2 is acceptable for this application making the beam 1 cm wide. Again, from Table 6.1.1, to maintain a WL product consistent with the laser requirements, a discharge length of 49.2 cm is required. Therefore, we have a discharge volume of $2 \times 1 \times 49.2$ cm operating at a pressure of 4.16 atmospheres with 12.5 joules of energy deposited into the gas at 25 kV. The last calculation for the laser design is the discharge time or "pump time". It is given that the pump power should be greater than $^*0.4$ Gigawatts per liter atmosphere of discharge volume, Gw/l-atm. Thus, the maximum pump time, t_p , is found from

$$t_p = \frac{\text{Energy Deposited in Gas}}{(\text{Pump Power}) (\text{VP})} . \quad (6.1.5)$$

Solving (6.1.5), we get

$$t_p = \frac{12.5 \text{ j}}{(0.4 \text{ Gw/l-atm}) (0.411\text{-atm})} = 78 \text{ nS}.$$

To deposit 12.5 joules into the gas at 25 kV we must have an energy storage capacitor of 40 nF. For an LC discharge of 78 nS duration, we find the maximum allowable inductance of the loop from

$$t_p = \pi \sqrt{LC} \quad , \quad (6.1.6)$$

where C is the energy storage capacitance. Solving (6.1.6) for L , we find the total inductance of the discharge loop, L_H , can be no greater than 15.5 nH.

THE MODULATOR CIRCUIT

At this point we must consider the requirement that the laser must operate a minimum of 8 hours a day for 6 days a week at 500 pps without maintenance. As discussed in Chapter 5, a hydrogen thyratron is the only viable switch to meet these life requirements. Since the inductance of a single thyratron circuit is far greater than 15.5 nH, a two capacitor circuit such as the one seen in Figure 6.1.1 must be used to achieve the small inductance requirement of the discharge loop. This circuit is often called the capacitor

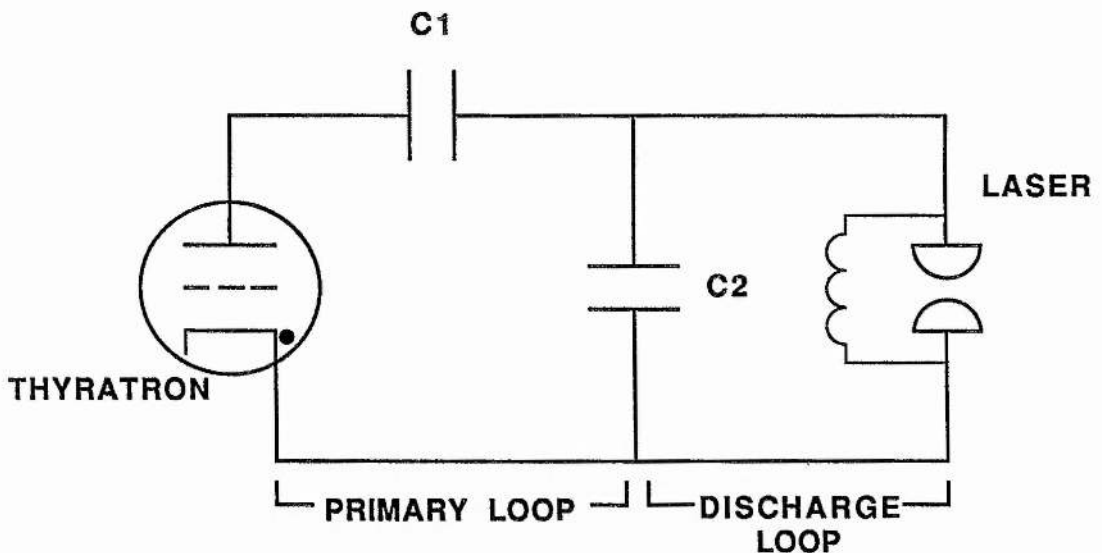


Figure 6.1.1 The capacitor pulse charge laser circuit.

ring-up circuit, the capacitive transfer laser circuit, or the capacitor pulsed charge circuit. Basically the circuit works on the basis that the laser is initially an open

circuit and acts as its own switch. Capacitor C_1 is discharged by the thyatron and charges capacitor C_2 in a time which is approximately equal to the time it takes for the laser gas to break down. The physical layout of the second loop must be made extremely compact thus, a low inductance. For these reasons, this is the most common circuit for driving a pulsed discharge laser.

DISCHARGE LOOP CIRCUIT DESIGN

From Equation 6.1.6, we found the total loop inductance of the laser head discharge circuit must be no greater than about 15.5 nH. The total loop inductance is the sum of the laser head gap inductance, L_H , the inductance of the capacitors, L_{C2} , and the inductance of the physical layout of the loop, L_D . The laser head is comprised of the electrodes and the current return path as illustrated in Figure 6.1.2. To prevent arcing from the pulsed electrode

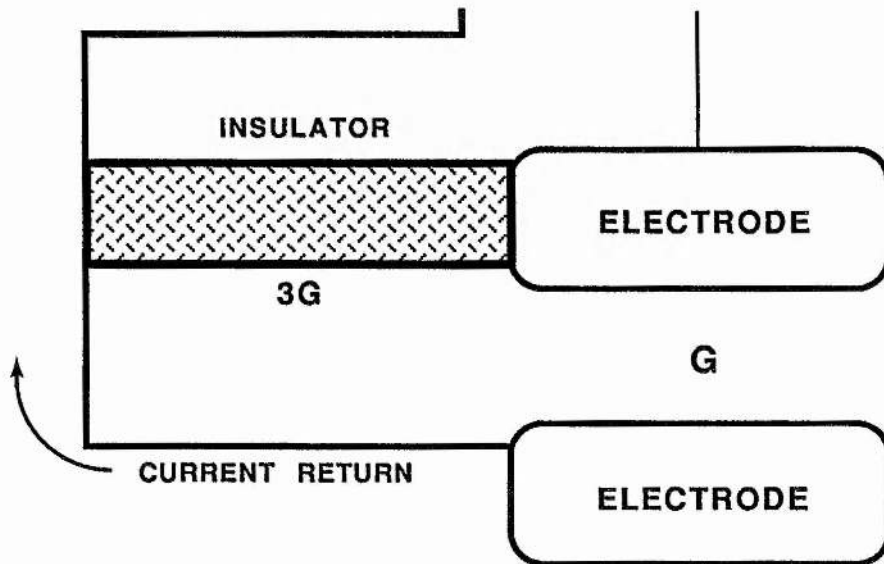


Figure 6.1.2 Illustration of laser head cross section.

to the current return, a distance of *three times the gap spacing is required. From Figure 6.1.2 the laser head inductance can be approximated by

$$L_H = \frac{\mu_0 A}{2l} = \frac{4\pi * 10^{-7} (0.02m) (0.06m)}{2(0.49m)} = 1.54 \text{ nH}, \quad (6.1.7)$$

where we have $A = G \times 3G$ from Figure 6.1.2. Subtracting the laser head inductance (6.1.7) from the maximum allowable loop inductance (6.1.6), we find the total capacitor and mounting hardware inductance must be no more than 14 nH. Knowing we require approximately 40 nF of energy storage capacitance and the laser electrode is about 50 cm long, to keep the inductance to a minimum, the capacitance should be distributed along the length of the electrode. From previous investigations (Chapter 4) we choose the 2.7 nF capacitor which is suitable in size and value to construct a 16 capacitor bank 48 cm long. This capacitor appears as G2.7 throughout this text. The value of the C_2 bank is 43.2 nF.

To minimize the inductance of the laser discharge loop a circuit layout in the configuration illustrated in Figure 6.1.3 is used. The electrode will be fed from eight points along its length from the bank of 16 capacitors (8 on each side). Since each capacitor will discharge into a small portion of the electrode, for analysis, we will break the electrode into eight equal sections of 6.26 cm in width. This is done to simplify the discharge loop inductance calculations. The layout and equivalent circuit of one eighth of the laser discharge loop is seen in Figure 6.1.3.

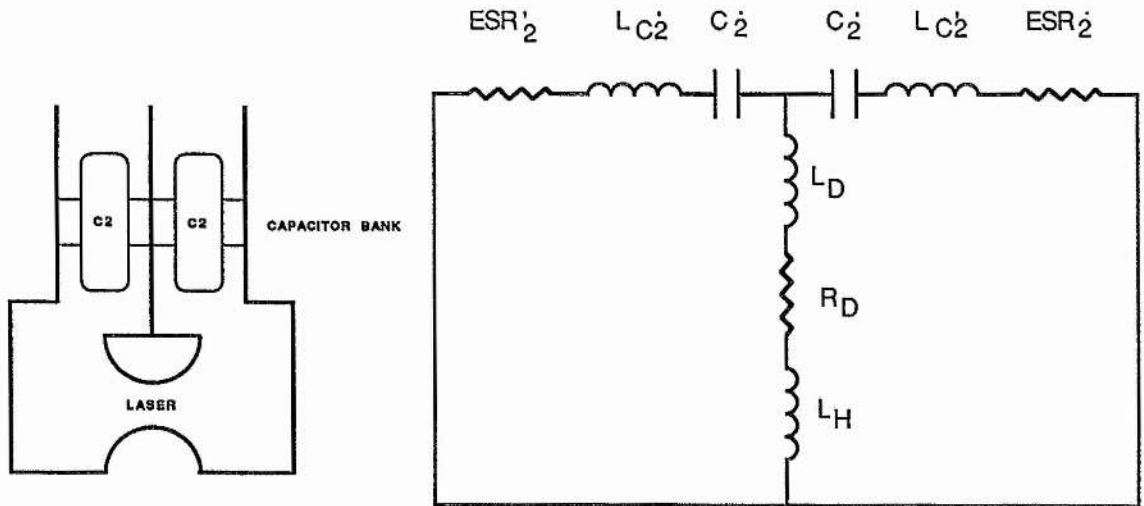


Figure 6.1.3 Layout for minimum inductance and equivalent circuit of the discharge loop.

Having eight feed points to the laser electrode will allow us to neglect the lateral inductance, that is, the inductance that opposes current flow down the length of the electrode. Referring to Figure 6.1.3, from Section 4.1 (Table 4.1.2) we find the capacitance of G2.7 to be 2.7 nF with a -4% voltage coefficient. From Section 4.2 (Table 4.2.1) we find the inductance of G2.7 is approximately 25 nH and from Section 4.2 (Table 4.3.1) we find the ESR is approximately 1.5 milliohms. The laser head inductance, L_H , was calculated earlier from Equation 6.1.7 leaving only the loop inductance, L_D , and the loop resistance, R_D , to be found to complete the equivalent circuit.

To calculate the inductance of the incremental piece of the laser discharge circuit, L_D' , we must first define its

physical description. The laser head discharge loop, accounting for the current returns, will take the physical shape depicted in Figure 6.1.4. To calculate the inductance of an increment of the discharge loop, we use the formula [NBS-C74, 1937]

$$L_D' = 0.00921 \left[(x+y) \log \frac{2xy}{h+w} - y \log (y + \sqrt{x^2 + y^2}) - x \log (x + \sqrt{x^2 + y^2}) \right] \\ + 0.0042 \left[\sqrt{x^2 + y^2} - \frac{x+y}{2} + 0.447(h+w) \right] \text{ uH.} \quad (6.1.8)$$

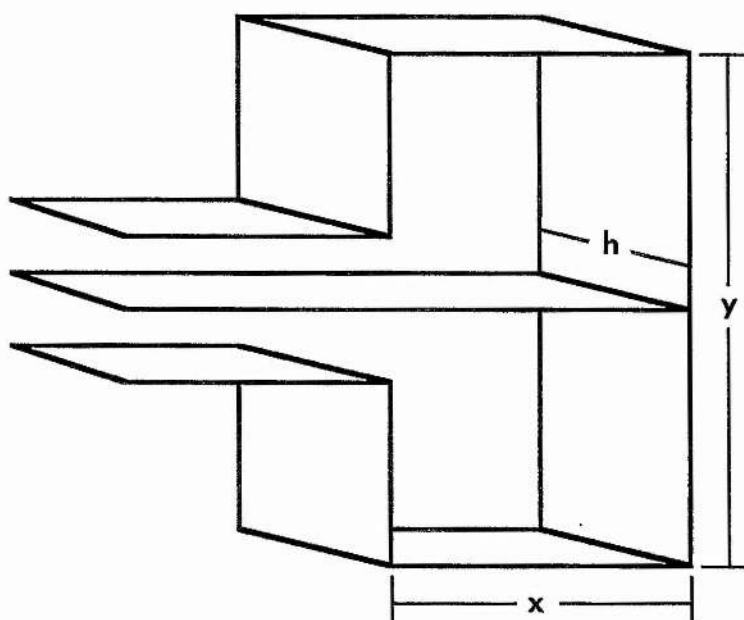


Figure 6.1.4 Diagram for defining terms in Equation 6.1.8.

Definitions for the terms x , y , and h of (6.1.8) are found in Figure 6.1.4. All dimensions in Equation 6.1.8 are in centimeters and are accurate when $2x \cong y$ and $x \cong h$. The term w is the skin depth of the discharge loop conductor and is found from

$$w = \sqrt{\frac{\rho}{\pi f \mu_0}} \quad , \quad (6.1.9)$$

where we have f = frequency of the current pulse in cps,
 ρ = the resistivity of the conductor, and
 μ_0 = the permeability of the conductor.

The resistance of the incremental discharge loop, R_D' , is calculated from

$$R_D' = \frac{\rho l}{wh} \text{ ohms/cm} \quad , \quad (6.1.10)$$

where h is defined in Figure 6.1.4 and l is the length of the current path for a single capacitor. Dimensions of the incremental discharge loop based on capacitor size and insulation requirements are: $x = 5\text{cm}$, $y = 12\text{cm}$, $h = 6.25\text{cm}$ (one eighth the electrode length) and $l = 22\text{cm}$. To solve Equation 6.1.8, we must find the value of the skin depth. The laser discharge loop will be made of nickel for chemical compatibility with the chlorine in the laser gas. Solving for the skin depth, w , for nickel at 30 MHz we get

$$w = \sqrt{\frac{7 \cdot 10^{-8}}{(4 \cdot 10^{-7})(30 \cdot 10^6)}} \frac{\text{ohm-m}}{(\text{h/m})(\text{Hz})} = 0.0024 \text{ cm.} \quad (6.1.11)$$

Solving Equation 6.1.8 we get

$$\begin{aligned} L_D' &= 0.00921[21.8 - 16.8 - 6.28] + 0.004[26 - 8.5 + 2.79] \\ &= 0.0694 \text{ uH} = 69.4 \text{ nH} \quad , \quad (6.1.12) \end{aligned}$$

for the inductance of the discharge path of one 2.7 nF capacitor comprising C_2 . Total inductance of the laser head is one sixteenth of L_D' because there are 16 parallel capacitors in the bank. The resistance of the loop is calculated from Equation 6.1.10 and 6.1.11 giving a resistance of the one eighth section of electrode of

$$R_D' = \frac{7 \cdot 10^{-8} (0.22)}{24 \cdot 10^{-6} (0.0625)} \frac{\text{ohm-m(m)}}{\text{m(m)}} = 10.3 \text{ m}\Omega . \quad (6.1.13)$$

As with the laser head inductance, the value R_D' is sixteen times the resistance of the entire laser head. We can now update the model of the discharge loop shown in Figure 6.1.3 to create the equivalent circuit in Figure 6.1.5. We must

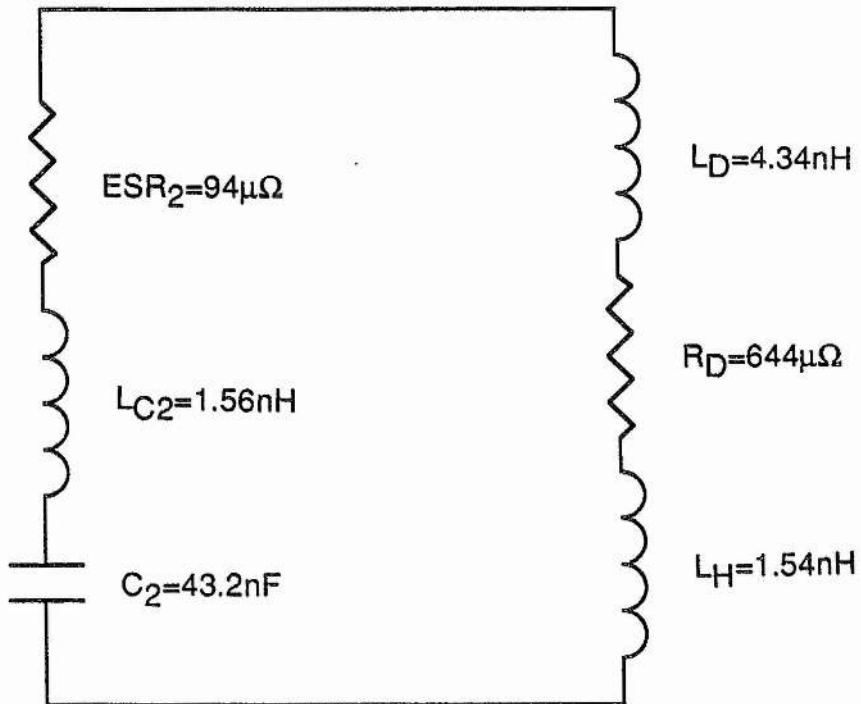


Figure 6.1.5 Final equivalent circuit of the laser discharge loop.

divide the values of ESR_2' , L_{C2}' , L_D' , and R_D' by 16 to get the the values for the entire length of the electrodes. Likewise, we must multiply the value of C_2' by 16 to get the value of the capacitor bank C_2 . The capacitance of the laser in the non-conductive state is only 2 pF and is neglected.

PRIMARY LOOP CIRCUIT DESIGN

The next step in the modulator design is the analysis of the primary loop. The purpose of the primary loop (Figure 6.1.1) is to charge the capacitor bank C_2 in a specific time within the electrical limits of the thyatron. The general equivalent circuit for the primary loop is seen in Figure 6.1.6. Inspecting Figure 6.1.6, we have already

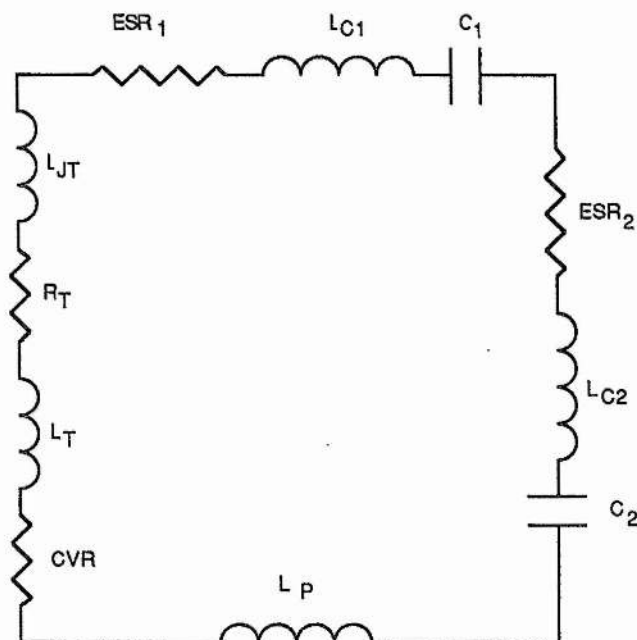


Figure 6.1.6 Proposed equivalent circuit of primary loop.

determined the values corresponding to the C_2 capacitor bank. It is left to determine the values of: the thyatron

inductance, L_T ; the thyatron resistance, R_T ; the CVR resistance, CVR ; the CVR inductance, L_P ; and the new term, L_{JT} , describing the inductance of the transition from a linear to a cylindrical geometry.

GEOMETRY CONVERSION

The capacitor bank, C_1 , should not present any great design difficulties if the same approach of multiple parallel capacitors (as done with the C_2 bank) is used. The major difficulty arises in the conversion of the linear geometry of the laser to the cylindrical geometry of the thyatron. The electrical element connecting the primary and the discharge loop is capacitor bank C_1 . One side of this bank must connect to the linear geometry of the discharge loop (Figure 6.1.3) and the other side to the cylindrical geometry of the thyatron(s). To do this, with minimum inductance, a layout similar to the cross section illustrated in Figure 6.1.7 is necessary.

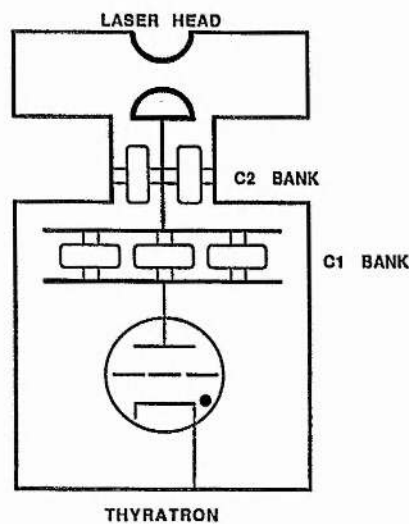


Figure 6.1.7 General layout of the laser head and modulator.

ENGINEERING NOTE: Assuming a 1% total efficiency of converting electrical energy into light, the thyratron(s) must be able switch an average power of about 12 to 13 kW. Thyratrons capable of handling this power are usually about 12 cm in diameter and about 30 cm long [McDuff, 1983] [McDuff and Rust, 1984 and 1985].

CAPACITOR BANK C1

There is a mismatch between the C_1 (60 nF) and C_2 (40 nF) banks so the voltage on C_2 will "ring up" to a larger value than initially stored on C_1 . This gives the circuit greater flexibility for the laser development effort. Again consulting the capacitor catalogs we find Manufacturer G makes a 1 nF capacitor that when arranged in a 4 X 15 matrix makes an ideal bank with a value of 60 nF. Arranged in this fashion, the bank will be 12.7 cm wide, to mate with thyratron(s) of approximate 12 cm diameter and 49.9 cm long, to mate with the 50 cm long C_2 capacitor bank.

The C_1 capacitor bank bus plate is chosen to have dimensions 15 cm X 55 cm. The C_1 bank is broken into 15 separate increments for analysis. This is justified because there should be no lateral current flow (down the 55 cm length of the capacitor bank bus plate). An equivalent circuit and layout of an increment of the C_1 bank appears in Figure 6.1.8. Values for the capacitance, inductance, and ESR, for the G1 capacitors are found in Chapter 4, Tables 4.1.2, 4.2.1, and 4.3.1 respectively. The inductance added to the C_1 bank by the bus plates, shown in the equivalent

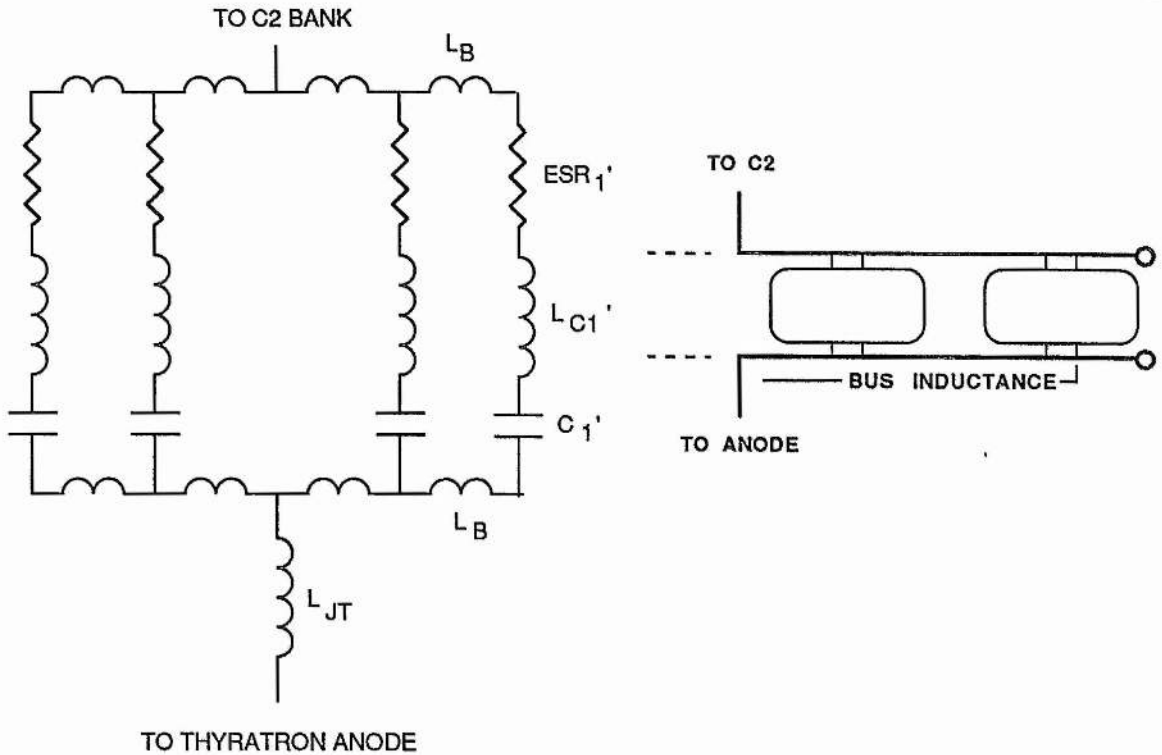


Figure 6.1.8 Layout and equivalent circuit of one fifteenth of the C_1 capacitor bank.

circuit as L_B , is calculated in the same manner as the discharge loop inductance (Equation 6.1.8). Values for the bus inductive elements, L_B , are found to be approximately 5 nH. The final values for the electrical parameters of the C_1 bank are calculated from 15 parallel circuits of the one shown in Figure 6.1.8. That is, C_1 equals sixty times C_1' , or 60 nF; L_{C1} equals L_{C1}' divided by sixty, or 417 pH; and ESR_1 equals one sixtieth of ESR_1' , or 25 microhms.

ENGINEERING NOTE: To reduce the inductance further and facilitate cooling, the capacitors are mounted to a perforated plate rather than a solid one. If a solid plate is used, because of the skin effect, current flows on the surface on around the edges of the plate back to the center where the connection to the C_2 is made. If the plate is

perforated, the current flow on the surface is toward the opposite side of the plate through the nearest hole. The perforated plate connecting to the C_2 bank will be sufficiently flexible to respond to the electrostrictive movement of the ceramic capacitors.

THYRATRON SELECTION AND MODULATOR MECHANICAL DESIGN

Before the inductance L_{JT} can be calculated, we must select a thyatron(s) capable of switching 13 kW in a short pulsewidth circuit. From previous investigations [McDuff, 1983][McDuff and Rust, 1984 and 1985] a 4.5" diameter ceramic envelope thyatron specially designed [Menown and Neale, 1978] for laser circuits is chosen as the switch. The thyatrons incorporate a "hollow anode" which enables the tube to conduct in the reverse direction without damage to electrodes or cathode coatings. Having a switch with reverse conduction capability relaxes the need to match the energy storage impedance to the vastly changing impedance of the laser gas. So as not to exceed the switching capability of the thyatron and compromise the reliability of the modulator, two tubes are operated in parallel. Having defined the basic layout of the laser head (Figure 6.1.4), the major components, and the total circuit configuration (Figure 6.1.7) a prototype mechanical assembly was designed. With the assistance of a mechanical engineer, a prototype laser head and modulator is designed. Shown in cross section in Figure 6.1.9, the design includes the spark preionizer and flow nozzle seen at the top of the diagram. Most of the electro-mechanical design considerations of the

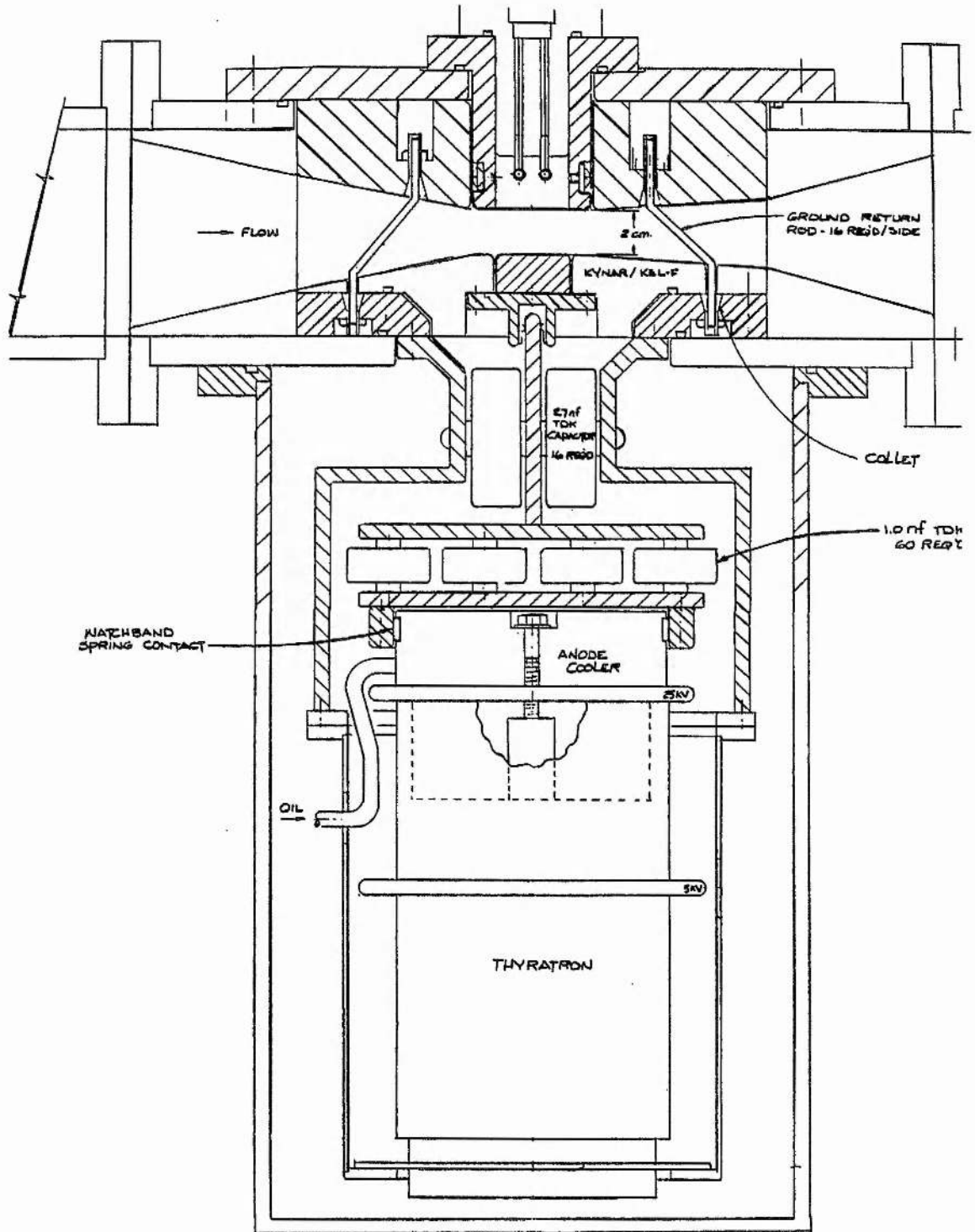
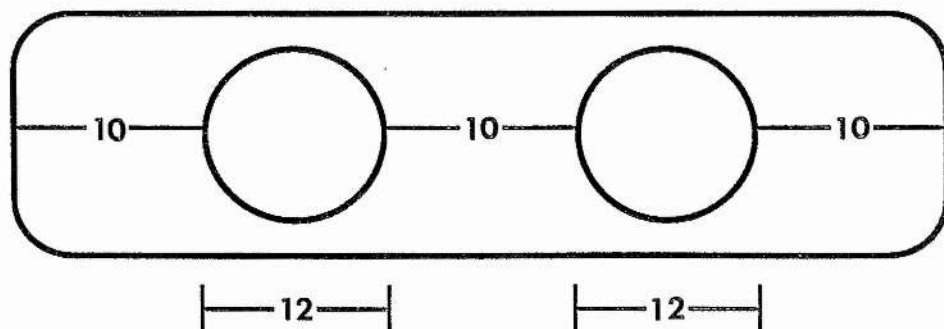


Figure 6.1.9 High repetition rate laser prototype modulator cross sectional diagram.

modulator have already been discussed or are intuitively obvious. One component of the modulator, the anode cooler, deserves some discussion. Referring to Figure 6.1.9, it is noted that the C_1 bank is connected to the thyratrons via the anode cooler. The anode cooler serves a dual purpose. First, it provides a means by which the anode is forced cooled, thus its name. Secondly, it acts as a flux excluder between the thyratrons and the capacitor bank. The anode connection on the thyatron is a post about 3 cm in diameter with a hole tapped for a bolt on top, as can be seen in the cut-out in Figure 6.1.9. Accounting for the skin effect, if the electrical connection is made at the post, the current must flow from the inside surface of the anode "cup" up the outside, around the corona ring back down the inside of the cup, radially inward, and up the post. To shorten this tortuous path, a cylinder of aluminium is machined to fit inside closely the anode cup and is secured by a bolt in the anode post. The cooler is pressed into a ring socket to make the connection to C_1 .

GEOMETRY TRANSITION INDUCTANCE

The transition from one geometry to another results in the addition of the inductance, L_{JT} . Viewing the C_1 bus plate from the thyatron side, we can draw a representative diagram shown in Figure 6.1.10. The circles in the diagram represent the anode cooler sockets for the two ceramic thyratrons. Since current flows on the outside of the conductors, the inductance opposing current flow is measured from outside diameter of the cooler to the edge of the bus



DIMENSIONS IN CM

Figure 6.1.10 Capacitor bank C_1 bus plate showing thyatron connections.

plate. The inductive component due to the anode cooler, L_{COOL} , is approximated by

$$L_{\text{COOL}} = \frac{\mu_0 \mu_r R}{2\pi} \quad (6.1.14)$$

where we have R = the mean path from the cooler to the edge of the bus plate.

Substituting into Equation 6.1.14 we get

$$L_{\text{COOL}} = \frac{4\pi * 10^{-7} (.11)}{2\pi} \frac{\text{Henry}}{\text{meter}} \text{ meter} = 22 \text{ nH}. \quad (6.1.15)$$

Since there are two tubes in parallel the transition inductance, L_{JT} , is half L_{COOL} , or about 11 nH.

THYRATRON INDUCTANCE AND RESISTANCE

The next two components of the primary loop equivalent circuit to be determined are the thyatron inductance and resistance. Examining the drawing in Figure 6.1.9, we can

approximate the inductance of the thyatron by the formula for coaxial cylinders,

$$\frac{L}{l} = \frac{\mu_0 \mu_r}{2\pi} \ln \frac{r_h}{r_t} \quad \frac{\text{Henry}}{\text{meter}} \quad (6.1.16)$$

where we have r_h = radius of the thyatron housing, and
 r_t = mean radius of the current path inside
the thyatron.

Substituting into Equation 6.1.16 we get,

$$\frac{L}{l} = \frac{4\pi * 10^{-7}}{2\pi} \ln \frac{0.16}{0.09} = 115 \text{ nH/m} . \quad (6.1.17)$$

The overall thyatron and housing length is approximately 22 cm giving the assembly a total inductance of about 25 nH. This gives a total inductance $L_{T\&H}$ for two tubes in parallel of 12.5 nH. Thyatron dissipation for short pulse circuits (Chapter 5) can be as little as 5% when the tube is triggered properly. Typical values for thyatron resistance in a laser circuit are between 0.1 and 0.5 ohms depending on the di/dt and current reversal. This calculation is verified from a computer modeling by C. Pirrie [1986]. We will choose the upper bound of this range for current calculation purposes later in this section.

CURRENT VIEWING RESISTOR

The last two elements in Figure 6.1.8 to be determined are the CVR value and the insertion inductance of this probe, designated L_p in the schematic. The CVR resistance is chosen to be 0.001 ohms to give an output of 1000

amps/volt. Since we will be dealing in the tens of kiloampere range, this value will give a large amplitude signal, thus increasing the signal in the signal-to-noise ratio. Mainly, 1000 amperes/volt is desirable because it is a convenient number for calculations.

CALCULATION OF DISCHARGE AND PRIMARY LOOP CURRENTS

We have now calculated or measured all the major electrical components that make up the equivalent circuit of the excimer laser modulator. Redrawing and labeling the values of the circuit components in Figures 6.1.5 and 6.1.8, we produce the equivalent circuits for the discharge and primary loops seen in Figure 6.1.11.

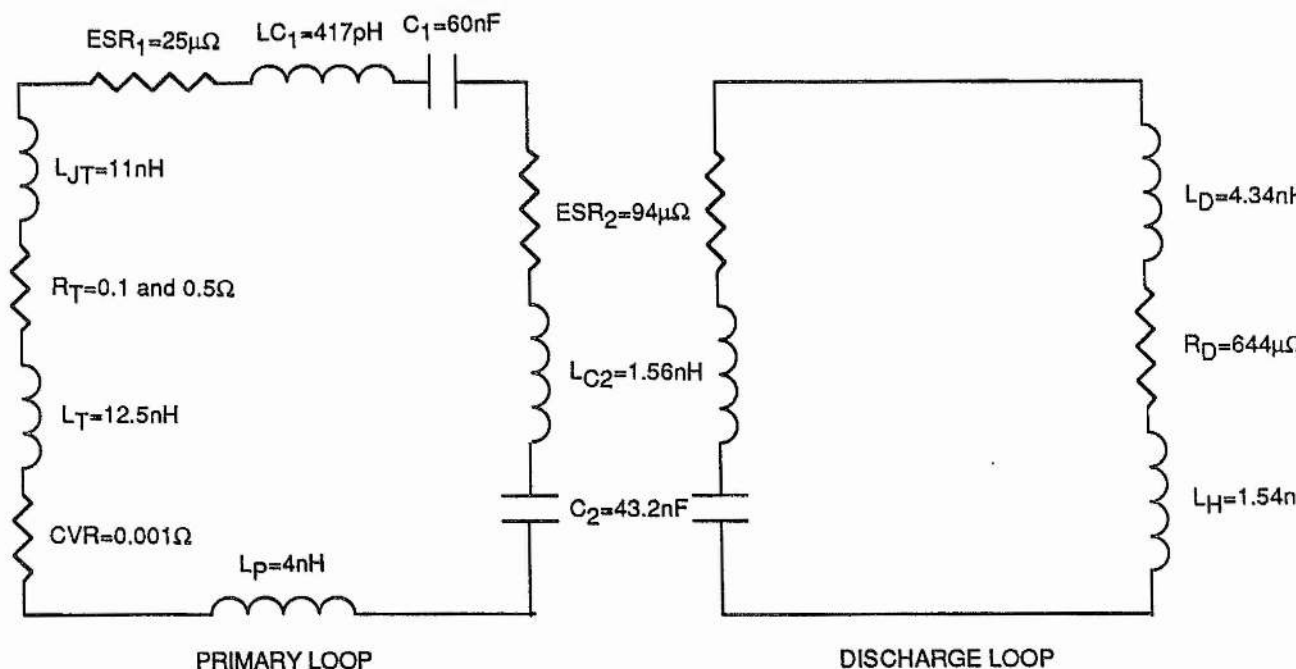


Figure 6.1.11 The primary and discharge loop equivalent circuits for the repetitive laser modulator.

From the above circuits, we can calculate the approximate time-dependent currents for the the discharge and primary loops with Equation 6.1.18 below. The primary loop current can be found by substituting the equivalent circuit values and the charge voltage on C_1 (for V_o) into

$$i(t) = \frac{V_o}{\omega L} e^{-\frac{R}{2L} t} \sin \omega t, \quad (6.1.18)$$

where ω (the natural frequency) is given by

$$\omega = \sqrt{\frac{C_1 + C_2}{LC_1C_2} - \left(\frac{R}{2L}\right)^2}. \quad (6.1.19)$$

Evaluating Equation 6.1.18, we find the thyratrons will switch a peak current of 15.5 kA collectively with a base pulsewidth of 89 nS. A single tube peak current of 7750 amperes and a pulsewidth of 89 nS translates into a di/dt of approximately $2 \cdot 10^{11}$ amperes/second which is an acceptable range for a thyatron designed for operation in a laser circuit [McDuff, 1983] [McDuff and Rust, 1984 and 1985] [Pirrie, 1986].

For the discharge loop, ω , in Equation 6.1.18 reduces to

$$\omega = \sqrt{\frac{1}{LC} - \left(\frac{R}{2L}\right)^2}. \quad (6.1.20)$$

In the discharge loop, V_o equals the voltage on C_2 when the laser gap conducts. Because of the mismatch between C_1 and C_2 , the peak charge voltage on C_2 can reach a maximum value

of 29.5 kV. Assuming the laser gap breaks down at maximum C_2 voltage, the laser current will have a peak value of approximately 52 kA and a base pulsewidth of 60 ns. The maximum energy stored in C_2 is 18.8 joules giving, a pump power (Equation 6.1.5) of 0.762 GW/1-atm. This is greater than the minimum value of 0.4 GW/1-atm specified for process requirements. Assuming a 2% electrical to laser light conversion efficiency in the gas, we should get approximately 375 mj/pulse laser output. Previous investigations [Butcher, et.al, 1982] demonstrated greater than 3% light extraction efficiency which would results in an average power output of over 200 watts for this design.

MODULATOR TEST

The modulator was constructed much as it appears in Figure 6.1.9. Thyatron and discharge loop current viewing resistors were added and do not appear in the cross sectional diagram. A maximum charge voltage on C_1 of only 15 kV could be achieved before arcing occurred inside the laser cavity. The extraneous arcing limited the operating voltage of the modulator and plagued the laser experimenters for many months. Ultimately, the modulator design was upgraded with a magnetic switch (discussed next) before the arcing problem was resolved and full voltage test could be performed. However, a full series of tests was performed on the modulator at 15 kV charge voltage with both neon and laser gas mix.

A digitized waveform of the thyatron current is shown in Figure 6.1.12. Superimposed on this waveform, in the

dotted line, is the calculated tube current (Equation 6.1.18) at 15 kV. The calculated current being based on the equivalent circuit does not include the effect of the voltage dependent breakdown of the laser gap. Laser breakdown is reflected in the characteristic "second peak" in the tube current waveform. This second peak is the result of energy remaining in C_1 being discharged through the gap when the laser conducts. However, from a thyatron point of view, this second peak and longer pulse width is not as critical as the magnitude of the current and the current rate of rise.

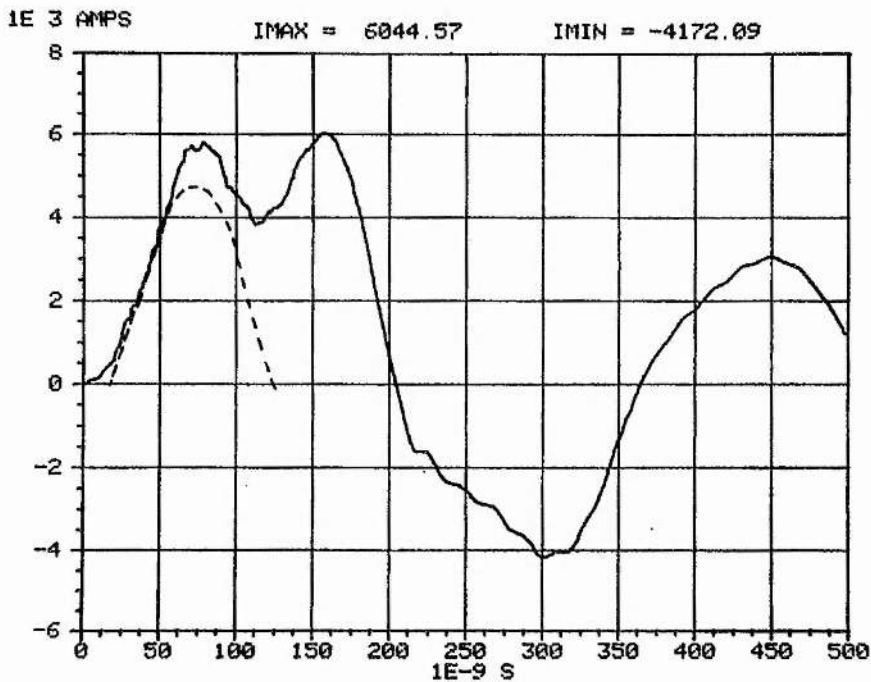


Figure 6.1.12 Primary loop current waveform.

Charting the measured and calculated peak current and di/dt for the primary loop in Table 6.1.2 we find an excellent agreement.

	CALCULATED	MEASURED	%DIFFERENCE
i_{peak} (kA)	4.8	6	20%
di/dt (A/s)	1.2×10^{11}	1.25×10^{11}	4%

Table 6.1.2 Comparison of calculated and measured primary loop current parameters.

A laser gap (C_2) voltage waveform is seen in Figure 6.1.13. The discharge gap breakdown voltage is only 8 kV, making the energy transfer efficiency from C_1 very poor.

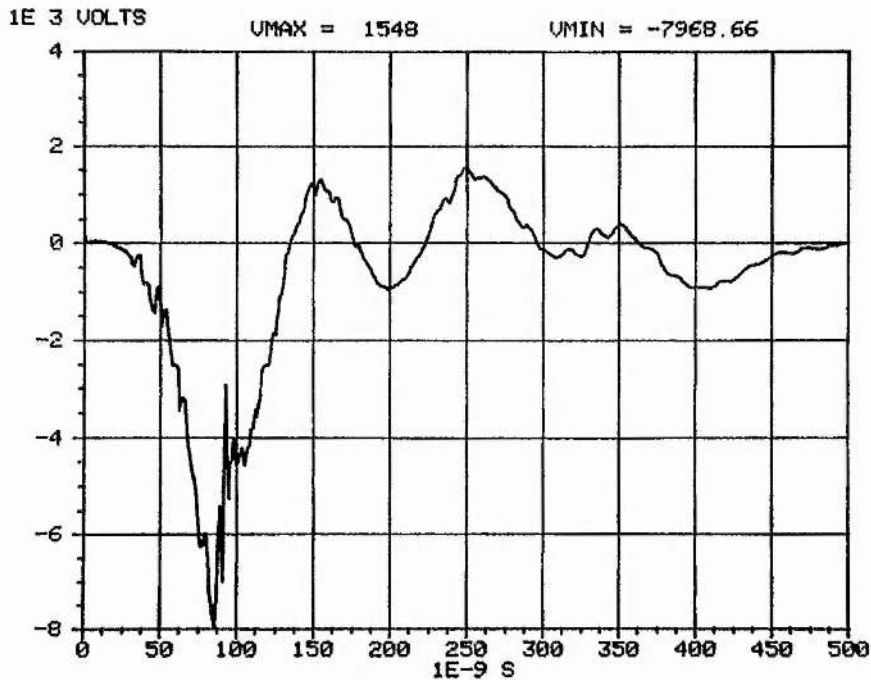


Figure 6.1.13 Laser gap voltage waveform.

The laser breakdown is a complex function of gas mix, preionization, electrode profile, etc. and is not pertinent to our discussion. Recalculating the laser current from Equation 6.1.18, substituting 8 kV (from Figure 6.1.13) for V_0 a comparison of the measured and calculated current parameters is made as before. The results are seen in

Figure 6.1.14. Referring to Figure 6.1.14, the laser current is measured with a CVR in one leg of the ground return making the waveform one half the actual amplitude.

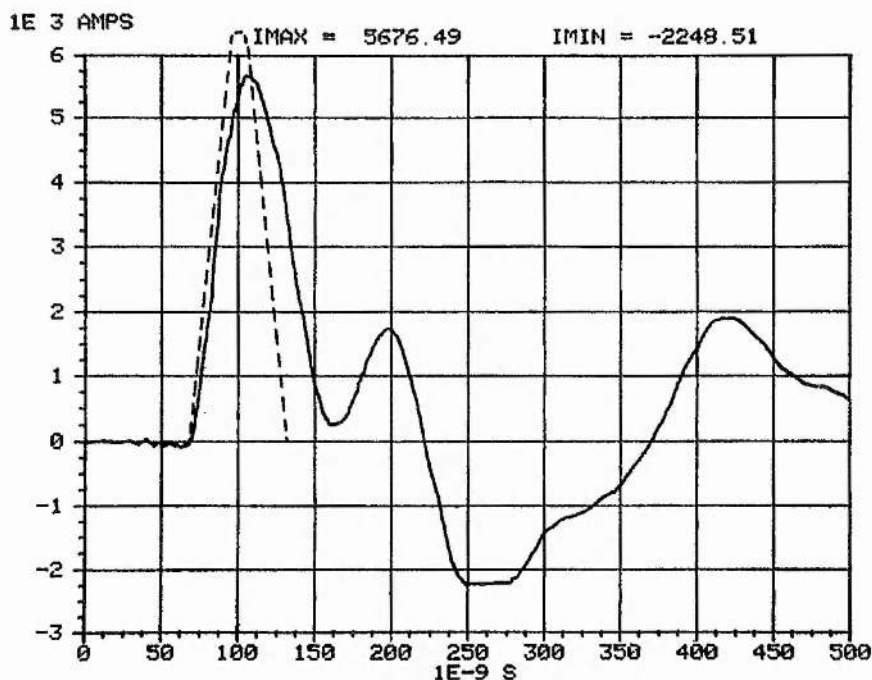


Figure 6.1.14 Discharge loop current waveform.

There is a 19% discrepancy between the calculated and the measured value of discharge loop current amplitude and a 40% difference in pulsewidth. Since the actual current is lower and the pulse is longer, the discrepancy is probably due to errors in the inductance calculations. Another factor contributing to the discrepancies in the measured and calculated currents is the gas impedance. Throughout the analysis the gas impedance is assumed to be zero. Gas impedance is a complex function of gas mix, preionization, ionization rates and cross sections, and is not well understood. Several research groups have attempted to develop computer codes to model rare gas halide laser

breakdown. Highly accurate results can be obtained for a particular case but no general model has been developed. For this reason, the approach described neglects the gas impedance entirely. The final circuit was somewhat more complex than the prototype shown in Figure 6.1.8 due to the inclusion of the discharge loop CVR, thus adding to the inaccuracy of the original circuit component calculations.

CONCLUSIONS

Even though the laser experienced arcing problems, enough data over a wide range of voltages was collected to verify the design approach described in the previous sections. The principle point of this design procedure is that no sophisticated computers are required. Using just a calculator (or even an antiquated slide rule) and paper, the engineer can design (as opposed to guess), with sufficient accuracy, a complete laser modulator. Values of the equivalent series resistance of the capacitors were included in the design even though their values had essentially no effect on the electrical results. The importance of the ESR appears in the cooling requirements of the modulator. At 500 pps, the C_2 capacitor bank with an ESR of 94×10^{-6} ohms will dissipate nearly 10 watts assuming the laser breaks down at maximum C_2 voltage. The entire laser modulator is enclosed in an oil tank as can be seen in Figure 6.1.9. Oil capacity of this tank is only 14 gallons with the modulator submerged. The entire heat load in the oil, including thyratron, drivers, heater transformer, etc. is approximately 1250 watts, of which nearly 9% is due to

capacitor and skin effect losses. Efficient design of the oil cooling system including heat exchanger, pump size, and cooling water requirement depends on accounting for even the smallest sources of heat dissipation. From Chapter 4, Section 4, the acoustic output from the capacitors and thyatron can be calculated. This parameter is important in the design of the oil containment tank to provide adequate acoustic insulation to meet safety standards. Cooling, insulation, and other design parameters are calculated in the same basic fashion as the electrical quantities. By accounting for all the factors, the most complex electrical design problems can be reduced to an elementary level. If a thorough understanding of the basic characteristics of components and physical phenomena are considered, the most sophisticated designs can be accomplished without the aid of "high technology" computational devices. One such design, a magnetic pulse compressor, is examined in the next section.

6.2 MAGNETIC PULSE COMPRESSOR

After several months of laser development experiments it was concluded that the addition of one stage of magnetic pulse compression was needed to sharpen the electrical pulse to the laser. Since all of the laser problems are associated with the discharge gap, the new design incorporates an easily removable pulsed or hot electrode. (The other electrode is grounded and contains the preionizer.) During the period of laser experiments, much progress had been made in the development of metal envelope dispenser cathode thyatrons for pulsed laser circuits

[McDuff, Rust, Menown, Neale, 1984][McDuff and Rust, 1984]. A single metal envelope thyatron was developed to replace both of the 4.5" ceramic tubes in the old laser modulator. The new thyatron boasted longer life, higher power handling capability, lower jitter, and a much higher thermal conductivity, making the cooling much more efficient.

There are two basic considerations in adding the magnetic pulse compressor stage: mechanical and electrical. Since a magnetic switch is point design (that is, it operates under one specific set of electrical parameters), the circuit must be correct the first time because there is little that can be done to change the operating point without massive mechanical rework. Mechanically, the upgraded modulator (with the new electrode design and magnetic compressor) must fit in the existing modulator oil containment vessel thus strict size constraints are imposed. This restriction required the electrical and mechanical design to be performed simultaneously. For ease of explanation, a review of the mechanical design will be cited first, followed by the electrical design procedure.

NEW LASER MODULATOR MECHANICAL LAYOUT

A cross sectional diagram of the upgraded laser modulator is seen in Figure 6.2.1. Referring to this figure the major components of the assembly can be described. To reduce the complexity of this figure, the topics of interest are labeled with letters. The letter A, denotes current viewing resistors. Working up from the bottom of the figure, the first "A" is a thyatron CVR designed to fit

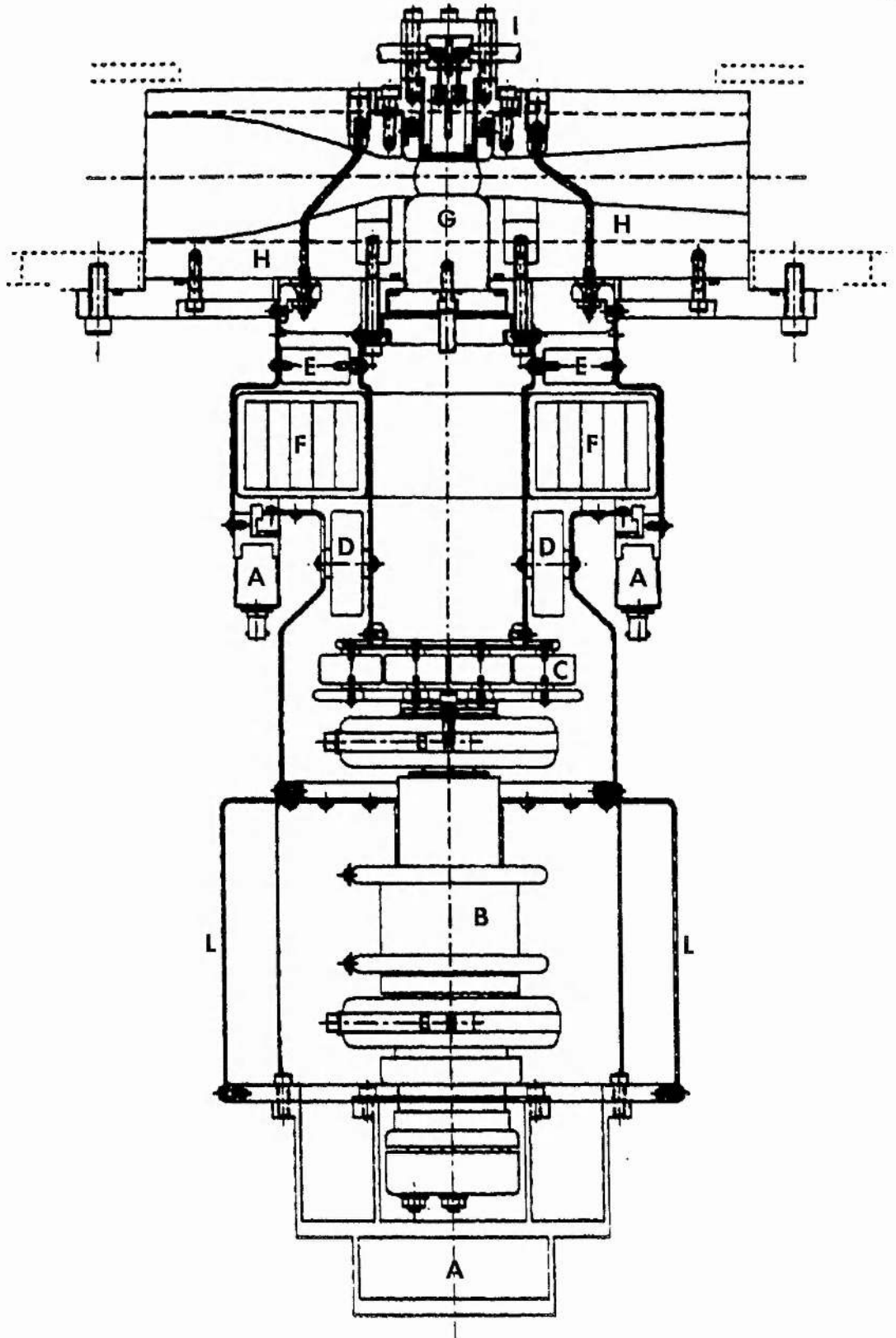


Figure 6.2.1 Cross sectional diagram of upgraded laser modulator.

the newly developed metal envelope thyratrons. As with all current viewing resistors in this investigation, it had a value of one milliohm. Further up the diagram one can see the two stripline CVRs, also labeled "A", that measure the discharge loop current. Mounted on the thyatron CVR is the new metal envelope thyatron, B. Letter "C" is the same 60 nF C_1 capacitor bank described in Section 6.1 as is the C_2 43.2 nF bank labeled "D". Part of the magnetic compressor, the magnetic peaking capacitor, is labeled "E" and its function is described later. The new bank is designated C_3 . Another new component to the upgrade modulator is the magnetic core, "F". The large space below the removable electrode "G" was added to facilitate rapid access and replacement. Component "H" is the Kynar high voltage electrode insulator machined as part of the flow nozzle. The grounded electrode and spark preionizer, seen at the top of the figure, is labeled by the letter "I".

A new feature was added to the upgraded design to allow the adjustment of the inductance of the primary discharge loop. This was accomplished by replacing the solid current return shroud around the thyatron with eight equally spaced 5 cm wide copper conductors, "L", in Figure 6.2.1. By changing the dimensions, or simply removing these plates, the area enclosed could be altered to "tune" the charge time of C_2 and thus the time at which voltage appears on the magnetic switch. Having a small range of control over the time at which voltage appears on the magnetic switch allows for fine tuning of its time jitter characteristics. Magnetic switch jitter is discussed in detail shortly.

The remainder of the modulator layout is somewhat self explanatory. Low inductance techniques were used throughout by keeping the area enclosed by the conduction path to minimum and large surface area conductors were used wherever possible. Using the same manner of analysis as with the original layout, inductance of the hardware can be estimated with standard calculation techniques. With the layout of the modulator in mind, the electrical design of the magnetic switch and associated circuitry can now be explained.

CORE MATERIAL SELECTION

For the core material, a lithium zinc ferrite was chosen rather than magnesium ferrite, iron, or metallic glass tapes for several reasons. Losses in most ferrites suitable for switch applications are much lower than metallic materials in short pulse (high frequency) operation. Loss in a metal tape used in short pulse circuits is dominated by the eddy current losses [Birx, 1980]. Because the lithium zinc ferrite has a resistivity on the order 10^7 ohms/cm, there are essentially no circulating currents in the core. There are several other contributors to the total loss in magnetic material, such as spin relaxation losses, which do not occur in "insulating" materials such as ferrites [Birx, 1980][Nunnally, 1982]. Most of these losses are highly frequency dependent but are not present in ferrite material. Thus, the design of ferrite pulse sharpeners is simplified from the aspect of frequency dependent loss calculations. However, ferrites

have one significant disadvantage: material properties limit their physical size. With metallic tapes, a core is simply "wound" to essentially any size; but high frequency ferrites cannot be manufactured in blocks much larger than 1 x 5 x 15 cm. This requires that many blocks or "tiles" be united to form a single uniform piece of ferrite. Even with this substantial engineering task, the advantages of ferrites still surpass the losses in metal tapes. Magnetic switch design using metallic tapes is a very thoroughly investigated topic by many researchers and is discussed in greater detail in numerous books and articles.

ELECTRICAL DESIGN OF MAGNETIC PULSE COMPRESSOR

Seven major issues must be addressed in the design of a ferrite pulse compressor. Each topic is addressed in the order listed below:

- A. Inductance
- B. Reluctance and Air Gaps
- C. Power and Core Heating
- D. Saturation Time
- E. Switching Jitter
- F. Core Reset
- G. Leakage Current and Peaking Capacitors.

A simplified schematic of the new modulator is shown in Figure 6.2.2. It is basically the same circuit as described in Section 6.1 (Figure 6.1.1) with the addition of the magnetic pulse compressor. Four components were added to the original circuit. The first is the variable inductance

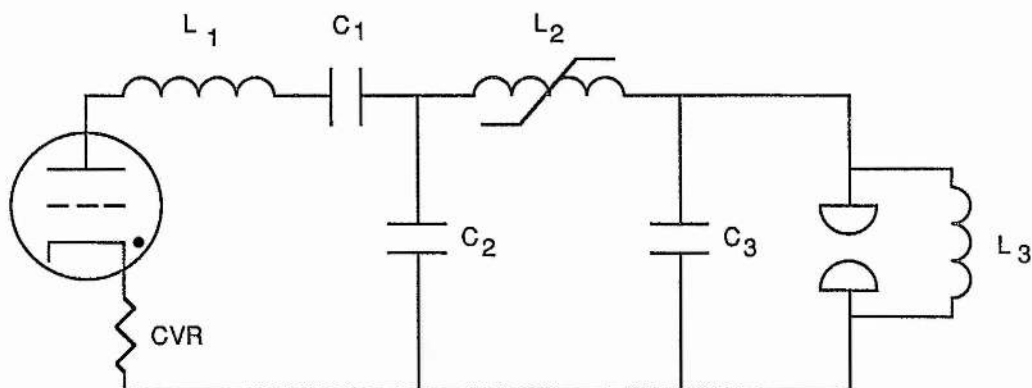


Figure 6.2.2 Modulator schematic with magnetic pulse compressor circuitry.

of the primary loop, L_1 , for adjustment of the C_2 charge time. The magnetic switch, L_2 , denoted by the symbol for a saturable inductance and the magnetic peaking capacitors, C_3 , are added into the discharge loop. The last component added is, L_3 , or charge around inductor as it is sometimes called. Actually, a circuit of this type has to have a charge path around the laser gap or C_1 cannot be charged. The first circuit had a charge around inductor, but it was not shown in Figure 6.1.1 because the value was not critical. Inclusion of the magnetic switch places restrictions on the value which the charge around inductor can have as will be seen later.

A. INDUCTANCE

The first topic, and probably the most important, is the unsaturated inductance, L_{UNSAT} , of the magnetic switch. If L_{UNSAT} is too small, the switch will not appear "open", C_2 will not be charged efficiently, and a large voltage will

appear on C_3 , causing the laser to break down prematurely. To fit the modulator into the modulator oil tank, (Figure 6.2.1) the maximum cross section of the switch is limited to 0.07×0.07 meters. In order that the pulsed electrode be removable, it must pass through the inside of the switch; this requirement sets the inside dimensions and the magnetic path length of the core. Having a fixed set of mechanical dimensions does not allow for optimization of the core volume so this is not considered. Parameters of the magnetic switch core needed to calculate the inductance are: the cross sectional area, A , is 0.0049 m^2 , and the mean magnetic path length, l , of 1.6 m . From

$$L = \frac{\int B \cdot ds}{\int H \cdot dl} = \frac{N \Phi}{i} = \frac{N \Delta B A}{H l / N} = \frac{N^2 \Delta B A}{H l} \quad (6.2.1)$$

where N is the number of turns on the core, and $\Delta B / \Delta H$, is the relative permeability of the magnetic material, we can modify Equation 6.2.1 to

$$L = \frac{N^2 \mu_0 \mu_r}{l} \text{ Henry.} \quad (6.2.2)$$

A BH curve (measured at 15 MHz) for the lithium zinc ferrite chosen for the core is seen in Figure 6.2.3. From the slope of this curve we can find the relative permeability to be approximately 2200 H/m. Substituting into Equation 6.2.2 the calculated unsaturated inductance of the one turn inductor, L_2 , is

$$L_{\text{UNSAT}} = 8.47 \text{ uH.} \quad (6.2.3)$$

The inductance of the unsaturated switch is almost 200 times the value of the primary loop inductance, making the impedance great enough that the "magnetic switch" to appear open to the primary circuit.

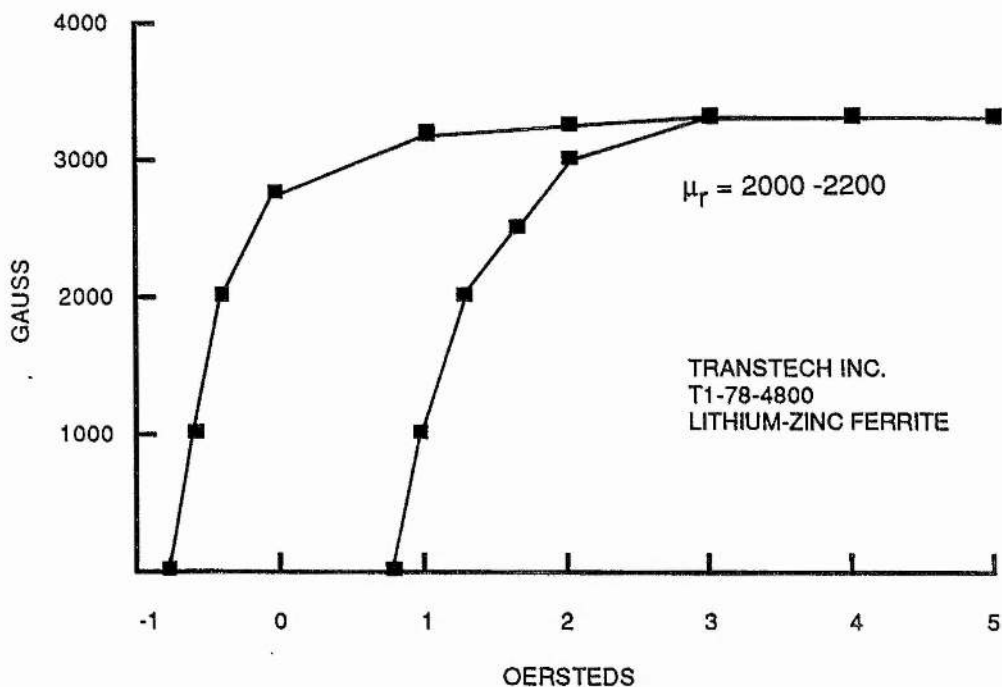


Figure 6.2.3 BH curve for the lithium zinc material used in the magnetic core.

B. RELUCTANCE AND AIR GAPS

Since the ferrite is manufactured in 15 cm long tiles, some 60 tiles must be assembled to make a core of the required size. This will result in 80 joints in the core, each being a possible site of an air gap. The effect of the air gaps increases the reluctance of the core. Reluctance is, by definition, the inverse of inductance, thus an increase in reluctance will reduce the unsaturated inductance of the core. To reduce this effect, the tiles

are machined to an exacting tolerance. The reluctance of a perfectly bonded core with no air gaps is 118 km/H. The reluctance of the air gap, R_g , is found by inverting Equation 6.2.2 or

$$R_g = \frac{l_{\text{gap}}}{\mu_0 A} \quad \text{m/H} \quad (6.2.4)$$

where we have l_{gap} = the length of the air gap and
 A = the area of the air gap.

Assuming the gap to be uniform over the cross sectional area of a joint, an inductance reduction of 11.37 nH per micrometer of air gap is calculated. With 80 possible gaps, the effect of air gaps could substantially reduce the unsaturated value of L_2 from its nominal 8.47 uH. Since it is impossible to determine the exact amount of gap that will be present in the finished core, the best practical action is to make every joint as well as possible.

C. POWER AND CORE HEATING

Power dissipation in ferrite material is dominated by anisotropic losses [Birx, 1980]. Since these losses are independent of frequency up to several hundred Mhz, they can be calculated the same as D.C. losses by

$$P_C = \int B \cdot ds \int H \cdot dl \quad \text{pr} \quad \text{watts}, \quad (6.2.5)$$

which reduces to

$$P_C = \Delta B A H_I l \quad \text{pr} \quad ,$$

where we have P_C = power dissipated in the core,
 prr = pulse repetition frequency,
 ΔB = flux change in Tesla,
 H_I = coercive force axis intercept in
 ampere-turns/meter,
 l = mean magnetic path length, and
 A = cross sectional area of the core.

Referring to the BH curve, we find the coercive force intercept is approximately 0.85 Oersteds or 68 ampere-turns/meter and the flux swing is 6400 Gauss or 0.64 Tesla. Substituting into Equation 6.2.5 we find the power dissipated in the core is

$$P_C = (0.64)(0.0049)(68)(1.6)(500) = 170 \text{ watts. (6.2.6)}$$

Thermal calculations show the temperature rise in the core with 170 watts of input power will be approximately 11°C based on the lithium-zinc ferrite thermal conductivity of 0.008 cal/cm-s-°C and a flowing oil temperature of 25°C. A temperature rise of 11°C will result in a saturation flux density reduction of 88 gauss or 9 milliTesla due to the temperature dependence of this parameter.

D. SATURATION TIME

The fourth topic on the list of design considerations is saturation time, t_{SAT} . Often, this parameter is defined in terms of a volt-second product. The time to saturation is found from Gauss's Law

$$e(t) = -N \frac{d\Phi}{dt} = \frac{N \Delta BA}{t_{SAT}}, \quad (6.2.7)$$

where we have $e(t)$ = time at voltage,

ΔB = flux density swing, and

t_{SAT} = the time which it takes the core to saturate under the influence of $e(t)$.

The term $e(t)$ in our case is the voltage across C_2 which is given by

$$e(t) = \frac{V_{C2}(\max)}{2} (1 - \cos \omega t) \quad (6.2.8)$$

Integrating $e(t)$ from zero to t_{SAT} , and solving Equation 6.2.7 for t_{SAT} , we get

$$t_{SAT} = \frac{2A \Delta B}{V_{C2}(\max)} = \frac{2(0.0049)(0.64)}{29,500} \frac{(m^2)(\text{Tesla})}{(v)} = 185 \text{ nS.} \quad (6.2.9)$$

The time to saturation determines the resonant frequency of the primary loop which brings us to the next issue of switching jitter.

E. SWITCHING JITTER

Pulse-to-pulse variation of the time at which the core saturates is defined as jitter. Jitter in a magnetic switch is the sum of the two functions $f\{e(t)\}$ and $f\{\Delta B_s\}$. The first term is dependent only on the fluctuations in the applied voltage. To achieve maximum transfer of energy, it is obvious that one would have the magnetic switch saturate at exactly $V_{C2} \max$ in our circuit. However, to achieve a charging voltage with no fluctuation requires a highly regulated power supply. An alternative method is to tune

the charging circuit, in our case the frequency of the primary loop, such that the maximum voltage on C_2 occurs just after the time the core saturates. Referring to Equation 6.2.9, the core should saturate at about 185 nS with a charge voltage on C_1 of 25000 volts.

Recalling the mismatch between C_1 and C_2 will result in a $V_{C_2\text{max}}$ of approximately 29.5 kV. To eliminate the $e(t)$ dependence we will vary the inductance of L_1 to give C_2 a charge time of about 190 nS. This is the reason for adding the variable inductance on the primary loop discussed above. From Equation 6.1.6 we obtain a value of 145 nH for L_1 for a 190 nS C_2 charge time.

The second function in the jitter equation is not as simple to deal with. The term ΔB_g is a function of the initial magnetization of the core and of temperature. Temperature can be controlled by forced cooling to maintain a constant temperature. With a temperature rise of only 11°C , fluctuation in the saturation time due to thermal variation will be seen as a long term drift not in pulse-to-pulse jitter. Initial magnetization, also referred to as the residual magnetization, can also be controlled by resetting the core to the same point on the BH curve after each pulse, thus assuring that the flux density swing is always the same and thus reducing the effect of the last term in the jitter equation. This brings us to the next design consideration, core reset.

F. CORE RESET

As explained above it is essential for low jitter and reproducible current pulses, that the core be reset to the same initial magnetization after each pulse. To do this, a reset pulse is supplied to the core to saturate the core in the reverse direction from flux swing during switching. The amount of current required, i_{RESET} , is found from

$$i_{\text{RESET}} = \int H_{\text{SAT}} \cdot dl = H_{\text{SAT}} l , \quad (6.2.10)$$

where we have H_{SAT} = coercive force at saturation, and

l = mean magnetic path length.

From the BH curve, we find the core will be well saturated at 3 Oersted, or 240 ampere-turns/meter, which gives a reset current of 384 amperes. The reset current must flow in the opposite direction of the discharge current which conveniently is the direction of the primary capacitor charging current. Referring to Figure 6.2.2, if the charging current through C_1 is greater than 384 amperes, this will reset the core. To achieve this peak current, the capacitor C_1 must be charged in approximately 4 μs . To charge C_1 this rapidly requires a command charge circuit. Also, to charge a 60 nF capacitor, the inductance of the the entire charging loop, including the charge around inductor, L_3 , must not exceed 27 μH . Therefore, the charge around inductor must be chosen so as: 1} not to slow the charging time below 4 ms ; 2} not load the discharge circuit by having too small a value; 3} not to develop enough of a voltage drop due to leakage current through the magnetic switch to cause the laser gap to break down. Calculation of the

leakage current through the magnetic switch and determining the value of the peaking capacitor C_3 are the last design considerations of the pulse compressor.

G. LEAKAGE CURRENT AND PEAKING CAPACITORS

Because a magnetic switch will not operate into an open circuit, it is necessary to provide a load that will draw enough current to allow the core to saturate. Turning our attention to the BH curve once more, it is seen that a coercive force of at least 3 Oersteds is required before the ferrite can saturate. From Equation 6.2.10, we calculate about 384 amperes are required to saturate the core. Therefore, the capacitor C_3 is added to the circuit to provide a presaturation load for the magnetic switch. By using a capacitor instead of sizing the charge around to act as the load, we will return all of the leakage energy to the laser at the time of conduction. Current flow in the charge around inductor is in the direction opposing the discharge current when the current from the capacitor C_3 is in the same direction. This point is clearly seen in Figure 6.2.2. Capacitor C_3 must be large enough to allow the 384 amperes to "leak" through the magnetic switch but not charge to a voltage high enough to break down the laser gap. Knowing the current in C_3 , is required to be

$$i_{C_3}(t) = 384 \sin \omega_2 t \quad (6.2.11)$$

where ω_2 is given by

$$\omega_2 = \sqrt{\frac{C_2 + C_3}{L_{UNSAT} C_2 C_3}} = \text{the natural frequency, } (6.2.12)$$

we can solve for C_3 . Solving Equation 6.2.11, we find a capacitor of about 2 nF is required to pass 384 amperes. Checking the voltage developed across a 2 nF C_3 , $V_{C_3}(t)$, by integrating the current from zero to t_{SAT} and dividing by C_3 we calculate a maximum voltage of 12 kV. This is too great a voltage to impress across the laser head for 190 ns (t_{SAT}) so we must reduce the value of C_3 . Using a 4 nF capacitor for C_3 , a current 440 amperes will leak through the switch and only 7000 volts will be developed across the laser head which is acceptable for the laser design. If L_3 is made at least ten times the value of the discharge loop inductance it will not load the discharge loop down and the voltage developed across this inductor will be several times less than V_{C_3} . This voltage is calculated in the same manner that the voltage on C_3 was determined.

PULSE COMPRESSOR CIRCUIT AND TESTING

Modifying the modulator to accommodate the core and C_3 increased the size of the discharge loop considerably. Splitting the discharge loop into two separate circuits was necessary to allow for a removal of the pulsed electrode. When the core saturates, the saturated inductance of L_2 is calculated by the mechanical dimensions of the loop comprised of C_2 and the laser gap. Using Equation 6.1.8, as done in Section 6.1, the inductance of one half the discharge loop is found to be about 32 nH. This method of determining the inductance accounts for leakage inductance. The largest contributor to this inductance is the large area

occupied by the core of saturated $\mu_r = 1$. However, under the restriction set forth by laser requirements, the total inductance of the loop is acceptable at 16 nH, just greater than the limit of 15.5 nH set by Equation 6.1.6. It was necessary to add a considerable inductance to the primary loop to increase the discharge time to 190 nS for reduction of magnetic switch jitter. Redrawing the simplified schematic of the laser and simplifying we get the lumped equivalent circuit in Figure 6.2.4.

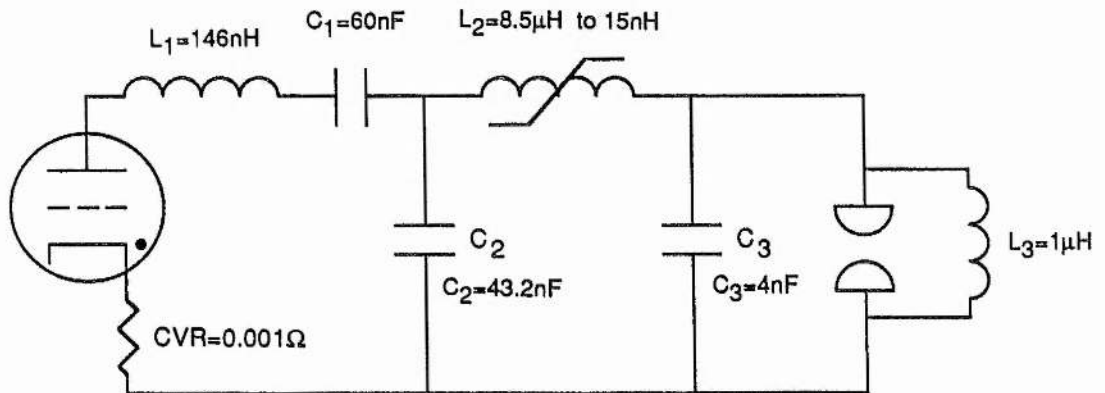


Figure 6.2.4 Final lumped equivalent circuit of upgraded laser modulator.

Calculating the primary loop current from Equation 6.1.18, we get a peak current of 10.4 kA with a base pulsewidth of 190 nS for a charge voltage of 25 kV on C_1 . The magnitude of the laser current, assuming C_2 is charged to the maximum of 29.5 kV, is approximated by substituting Equation 6.1.19 into Equation 1.1.18. Solving, we get a discharge current with a peak value of 48.5 kA and a base pulsewidth of 82 nS. The last electrical parameter of

importance is the voltage developed across C_3 which was previously calculated at 7 kV.

The completed modulator was tested with a laser gas mix with considerably better results than with the first design. Waveforms in the next four figures are data taken at 500 pps repetition rate at a C_1 charge voltage of 25 kV, the design point. All waveforms are in time synchronization with a time scale of 50 ns/division. The following waveforms were acquired during testing with a XeCl gas mix. For these tests, a spark type preionization was employed and the laser discharge collapsed into an arc after approximately 20 ns thus limiting the average output power to about 130 watts. Using x-ray preionization stabilized the discharge, improved the beam uniformity and increased the average power output to over 200 watts at 500 pps.

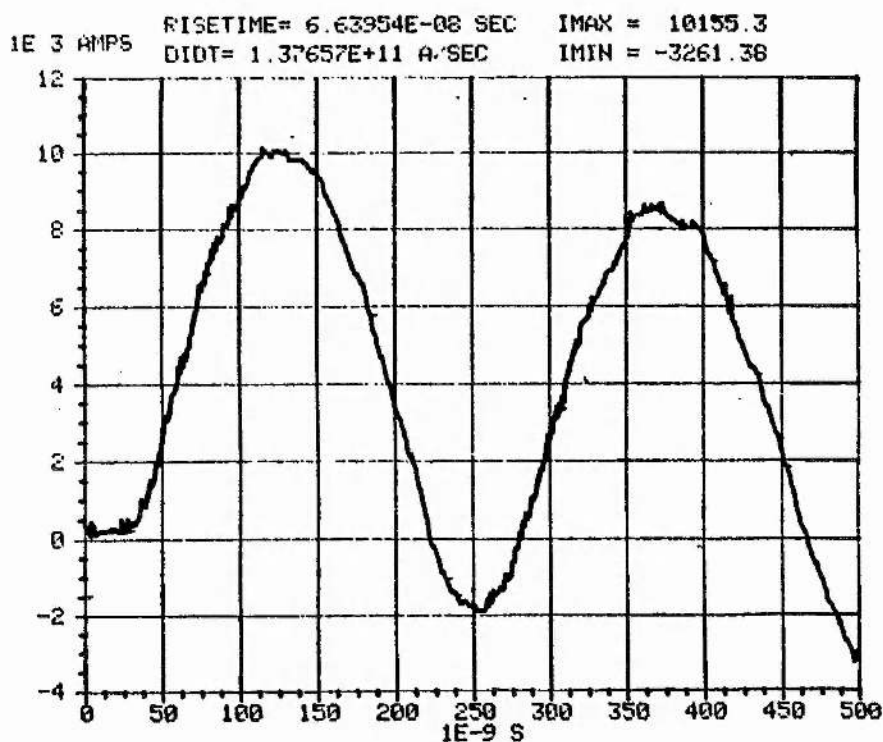


Figure 6.2.5 Primary loop current waveform.

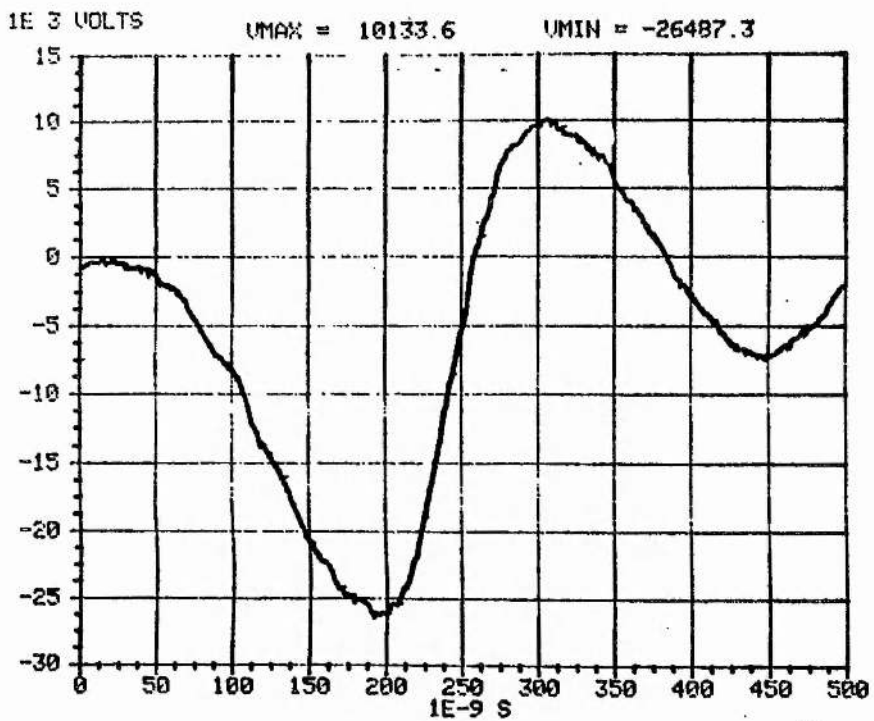


Figure 6.2.6 Voltage waveform across C_2 , primary side of the magnetic switch.

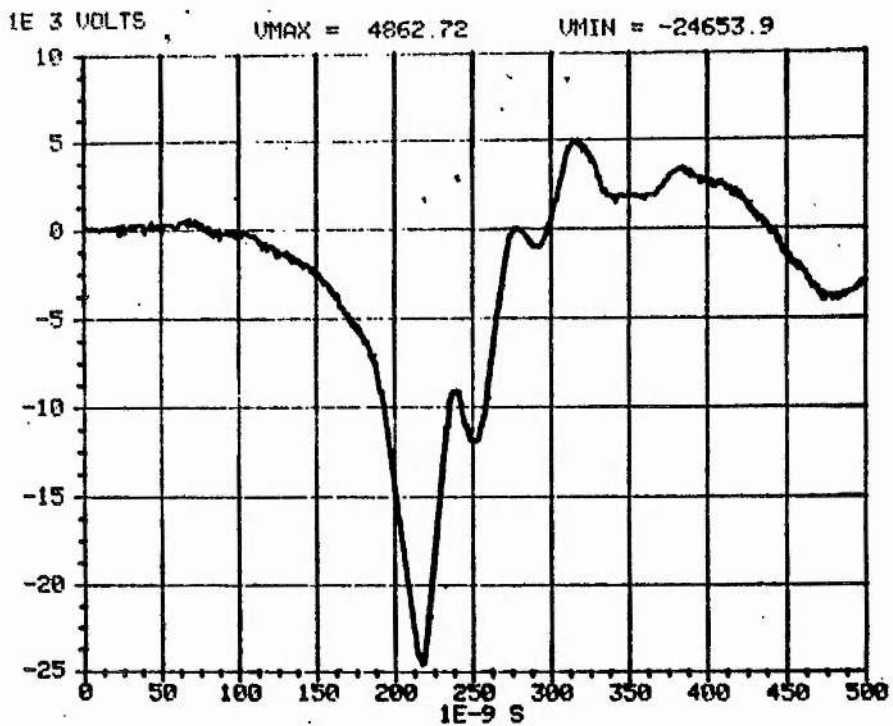


Figure 6.2.7 Voltage waveform across C_3 , or laser gap.

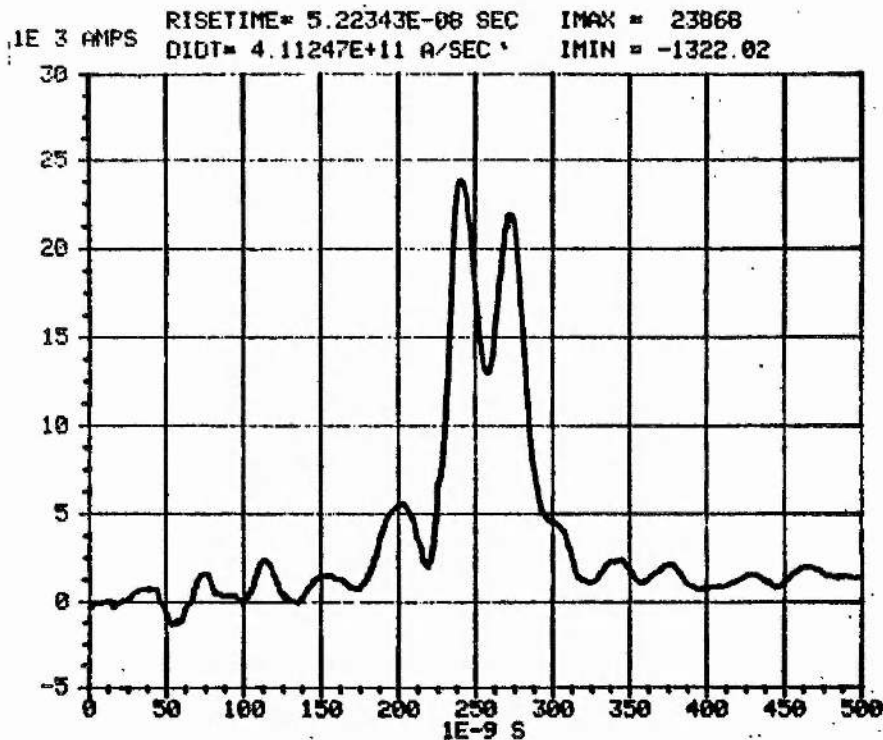


Figure 6.2.8 Discharge loop current waveform. (One half amplitude)

Referring to the laser current, Figure 6.2.8, a strange double hump is seen in the waveform. Lasing occurred during the first current peak, then the uniform discharge would collapse into an arc on one end of the laser electrode. When the arc formed, initially it was of high impedance and the laser current decreased, as the arc developed the current would increase due to the decreasing impedance, resulting in the "double hump" in the waveform. From the laser electrode voltage waveform it is difficult to determine the exact magnitude of the voltage developed on C_3 due to leakage current. However, it is not greater than the calculated 7 kV so the approach to this calculation is

correct. The voltage on C_2 reveals that the majority of the energy from C_1 is being transferred to C_2 in the time of 190 nS. The charge time of C_2 , was tuned to the exact value by varying the inductance of the thyatron housing. A comparison of the measured and calculated electrical parameters is found in Table 6.2.1.

PARAMETER	CALCULATED	MEASURED	% DIFFERENCE
Primary Loop			
$i_{(peak)}$	10.4 kA	10.1 kA	3%
di/dt	1.3×10^{11} A/s	1.38×10^{11} A/s	6%
$V_{C_2}^{max}$	29.5 kV	26.5 kV	10%
Discharge Loop			
$i_{(peak)}$	48.5 kA	47.7 kA	1.6%
Pulsewidth	82 nS	95 nS	14%
di/dt	1.3×10^{12} A/s	1.9×10^{12} A/s	31%

Table 6.2.1 Key electrical parameter comparison for the upgraded laser modulator.

CONCLUSIONS

One point that should be mentioned is the fact that we were extremely fortunate that the magnetic core could be built with essentially no air gaps in any of the 80 joints. The self inductance of the core with one turn was 8.1 uH measured with an inductance meter. This calculates to a total air gap of only 32 micrometers for all 80 joints.

The upgraded laser modulator resulted in somewhat better laser performance than the original design but the laser was still plagued with arcing on the ends of the electrodes when the spark or corona type preionization was used. With the addition of the replaceable electrode many different electrode profiles were tested with as many results. The average laser output power and beam stability was greatly affected by the particulars of the gas mix and the preionization. By far the best overall performance of the laser was achieved with x-ray preionization. Modulator performance was essentially independent of the type of gas load or method of laser preionization. Only variations in the gap breakdown voltage and the gap current were reflected in the electrical measurements as the load was varied. Regardless, the design procedure for the entire modulator and magnetic switch was verified. Again, no sophisticated computers were needed to do the complete modulator design. It has been demonstrated in this chapter that the design of a high power laser modulator is basically simple. This is not surprising, inasmuch as there are only two loops and six electrical components in the circuit.

REFERENCES FOR CHAPTER 6

- Birx, D.L., "Basic Principles Governing Design of Magnetic Switches," Lawrence Livermore National Laboratory, UCID-18831, 1980.
- Butcher, R.R., Tennant, R.A., Erickson, G.F., Swisher, S.L., Willis, W.L., "A High Average Power Excimer Laser," Proceedings of CLEO, 1981.
- McDuff, G., "Test and Evaluation of the CX-1574C Thyatron for Use in Excimer Lasers," EEV Technical Reprint EEV Co. Ltd. Chelmsford, Essex, England, CMI 2QU, 1983.
- McDuff, G. and Rust, K., "Evaluation of Bidirectionally Conducting Thyratrons for Pulsed Excimer Lasers," IEEE Sixteenth Power Modulator Symposium, June 1984.
- McDuff, G. and Rust, K., "A Short Note on Hollow Anode Metal Envelope Thyratrons for High-Power High Repetition-Rate Lasers," EEV Technical Reprint, EEV Co. Ltd. Chelmsford, Essex, England, CMI 2QU, 1985.
- Menown, H. and Neale, C., "Thyratrons for Short Pulse Laser Circuits," IEEE Thirteenth Pulse Power Modulator Symposium, June, 1978.
- National Bureau of Standards, U.S. Dept. of Commerce, Circular C74, 1937.
- Nunnally, W.C., "Magnetic Switches and Circuits," Los Alamos National Laboratory, LA-8862-MS, 1982.
- Pirrie, C.A., Menown, H., Nicholls, N., "Advanced Thyratrons as Switches for the Nineties," IEEE Seventeenth Power Modulator Symposium, June, 1986.

APPENDIX 1

Tektronix P6015 High Voltage Probe Modifications

The Tektronix P6015 High Voltage probe is used for all D.C. and general pulse voltage measurements. Manufacturer ratings of this probe are 20 kV D.C. and 40 kV peak for a 50% duty factor. By modifying the P6015 and operating in oil, these ratings can be doubled. Frequency compensation of the modified probe remains as stated in the instructions as does the 1000X attenuation factor. The steps for modification are:

1. Remove the 100 M high voltage resistor in the high voltage section of the probe.
2. Remove the red plastic freon float from inside the high voltage section and discard it.
3. Replace the high voltage resistor with a high voltage carbon deposited film epoxy coated resistor (such as a Dale, Inc., F43TU) of the same value.
4. Refill the high voltage section until the freon covers 2mm of the gold plated high voltage resistor end connector visible through the end of the probe.
5. Build a stress relief ring "corona ring" of 7mm copper tubing with two 2 cm wide thin copper strips attached such that these strips will slide between the probe body and the plastic case. This "corona ring" reduces the field enhancement on the edge of the high voltage section of the probe body. Addition of the ring increases the input capacitance of the probe because of the increased surface area of the probe body (which is grounded) and the closer

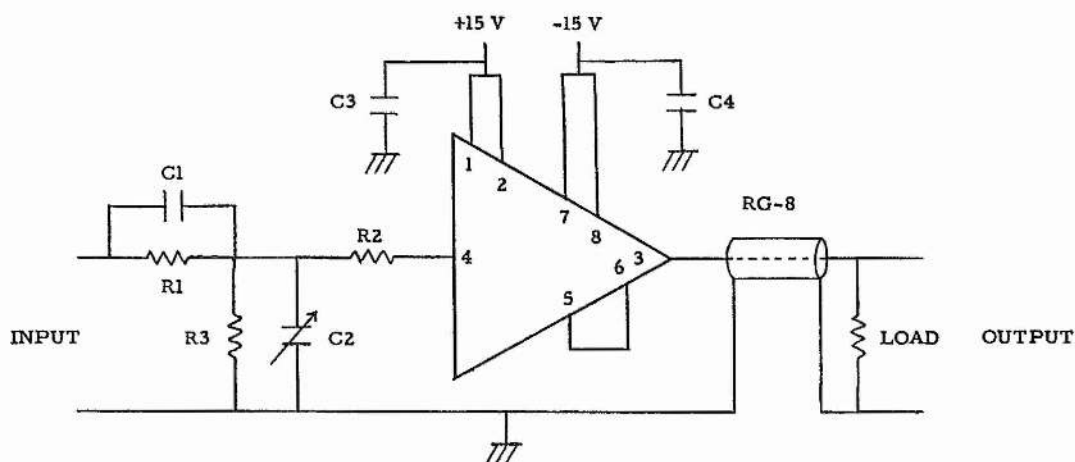
spacing between the probe tip and the probe body. This will increase the risetime of the probe to about 5 or 6 nS instead of the specified 4 nS. As always be sure to compensate and operate the probe in the vertical (tip down) position for optimum frequency response.

6015 Line Driver Buffer Amplifier

The 6015 Line Driver is specifically designed to be used in conjunction with the Tektronix P6015 High Voltage Probe. Due to the short length of the high resistance nichrome coaxial cable connecting the high voltage section of the probe and the compensation box, it is necessary to locate recording instruments physically close to the experiment. Using the 6015 Line Driver allows for remote location of the recording instruments while retaining both the D.C. and high frequency response of the probe. Typical risetime of the 6015 Line Driver when terminated into a 50 ohm load is approximately 4 nS. When driving a longer length of cable, say 100 meters, a typical risetime of 9 nS can be expected.

The heart of the line driver is the National Semiconductor LH0063C unity gain operational amplifier. This device is a specially selected laser-trimmed FET to ensure fast response times. Circuit layout and construction is extremely critical with the LH0063C to prevent the device from self oscillating. A special double-sided printed circuit board is required to minimize stray capacitance and component lead length. One side of the printed circuit board acts as a ground plane. It is necessary to connect

the other side of the printed circuit board to the output of the amplifier to prevent unwanted self oscillations. The added capacitance directly on the output lead of the LH0063C resulting from connecting one side of the circuit board, "the output plane", damps the self oscillations. The circuit board fits inside a Model 2411 Pomona Box and is soldered directly to the type N connectors mounted on the box. Type N connectors give a 2 to 3 nS faster risetime than the BNC type connectors and are far less prone to driving the op-amp into self oscillation. An electrical schematic and parts list of the line driver is seen in Figure 1.



C1	3pfd 50V monolythic ceramic
C2	4-15 pfd E.F. Johnson 279-0115-005 trimmer
C3,4	4.7 ufd 35V tantalum
R1	909 k 1/8 watt carbon composition
R2	51 1/8 watt carbon composition
R3	97 k 1/8 watt carbon composition
IC	National LH0063K op amp

Figure 1 The 6015 Line Driver schematic and parts list.

All components are standard except C2, which must be an E.F. Johnson, Ryton Micro-J-279-0115-005 trimmer capacitor to prevent the LH0063C from oscillating. Other ceramic trimmer capacitors will not produce the desired electrical response in this circuit. A photo of the amplifier, both sides of the circuit board, and the operation amplifier mounted on a board are seen in Figure 2.

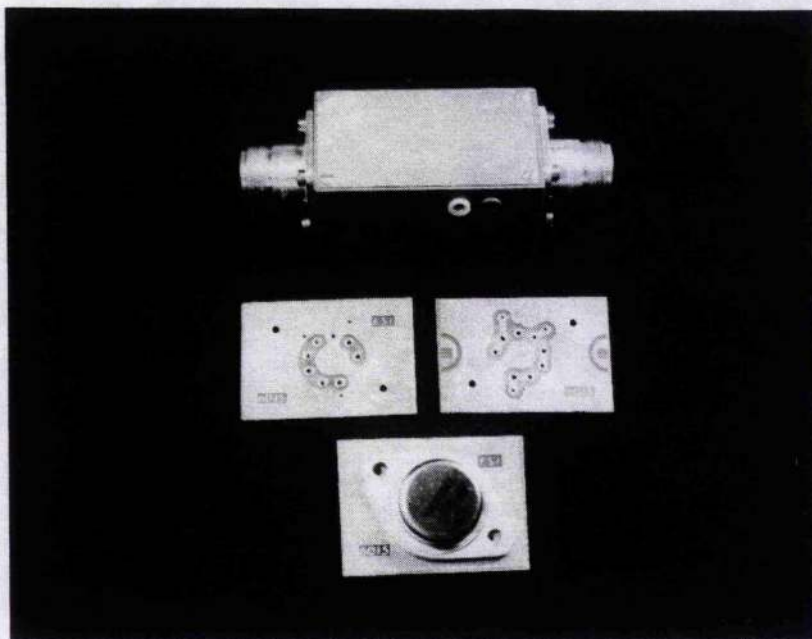


Figure 2 Photo of the 6015 Line Driver Hardware.

Compensation of the Tektronix P6015/6015 Line Driver remains the same as written in the probe manual. The trimmer capacitor, C2, adjusts only the droop of the pulse. Maximum output of the 6015 Line Driver is 10 volts. The overall attenuation of the probe/driver combination is in the range of 10000 to 12000 depending on the particular LH0063C and must be determined after frequency compensation.

Low Resistance Fast Response Voltage Probe

The diagram in Figure 3 shows the cross section of the high voltage section of the 1 nS risetime probe. The high

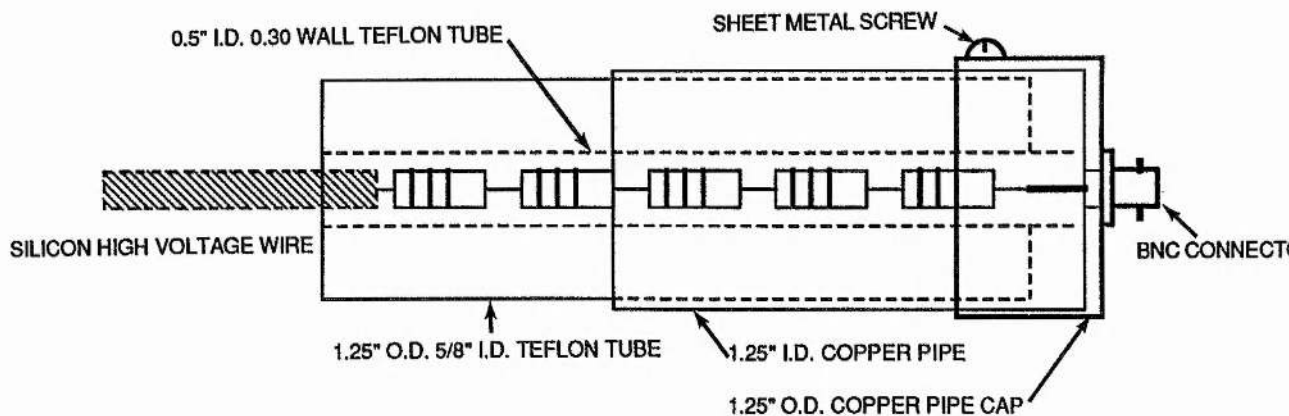
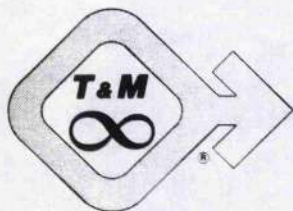


Figure 3 Cross section of the fast response low resistance probe.

voltage section consists of five 1000 ohm, 2 watt, Allen Bradley hot molded carbon composition resistors potted inside a 1/2" diameter Teflon tube. This sub-assembly is slid into the larger Teflon tube which has an I.D. of 1/2". The larger tube is then inserted into the copper pipe and the resistors lead soldered to the BNC connector on the copper end cap. Input capacitance of the high voltage section is 35.8 pfd and the input inductance is 16.8 nH minimum.

The low voltage section consists of five or six Allen Bradley resistors connected in parallel to give an attenuation of 1000X. These resistors are mounted in a small electronic box with one male and one female BNC connector for ease of mating with the high voltage section and signal cables.

The output of the low voltage section is typically 5 ohms and can be coupled into a 50 ohm cable with minimum attenuation. The cable must be terminated into a 50 ohm load to prevent reflected signal. Total power dissipation of the probe is 20 watts and the maximum input energy per pulse is 10 joules, both limited by the Allen Bradley resistors. A maximum input voltage, before flashover of the large Teflon tube to the copper pipe, is 120 kV.



T&M RESEARCH PRODUCTS, INC.

PHONE (505) 268-0316

• 129 RHODE ISLAND NE

• ALBUQUERQUE, NEW MEXICO 87108

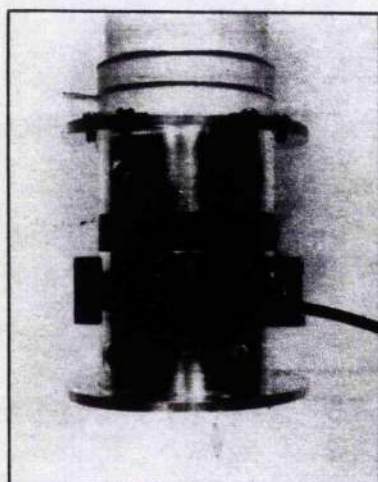
SERIES D — CURRENT VIEWING RESISTORS

Description

This series is a specially designed CVR for use in measuring cathode currents of ceramic-metal hydrogen thyatrons. These units allow simplified measurements that have been complicated or impossible to make up to now. Design importance is placed on system interface, cooling, and measurement capability. Insertion inductance is matchable to system requirements. An additional advantage is the dual measurement with the Current Viewing Probe supplied.

Features

- Simplified mounting of both the CVR and Tube
- Current Viewing Probe (Rogowski coil) included
- CVR power ratings exceed those of the tube
- Broad bandpass
- Fast risetime
- Tube shielding available
- Operation in air or oil
- Custom-designed CVR's available for any tube
- Cooling provided for CVR and tube flange



Specifications

Model*	Resistance ohms	Bandpass MHz	Risetime nsec	E _{max} joules	Tube**
D50-2-CP	.01	400	1nsec	50	HY-3
D125-2-CP	.0025	400	1nsec	125	HY-5
DLI-3-CP	.010	800	450psec	150	HY-3013
DLI-5-CP	.0025	800	450psec	250	HY-5313
DLI-275-CP	.001	800	450psec	275	HY-7

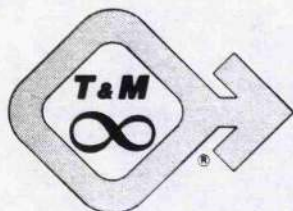
*For additional information about Rogowski coils see CURRENT VIEWING PROBES page.

**EG&G tube type. CVR's for other tubes or special mounting are available.

Standard resistance tolerance $\pm 4\%$. Closer tolerance available. Each unit labeled with exact resistance value accurate to $\pm 0.2\%$.

Ordering Information

When ordering please specify model number, tube type, cooling needed, and special requirements.



T&M RESEARCH PRODUCTS, INC.

PHONE (505) 268-0316

• 129 RHODE ISLAND NE

• ALBUQUERQUE, NEW MEXICO 87108

SERIES W — CURRENT VIEWING RESISTORS (Bar Strap Type — Flat Cable Input)

Description

Terminating type CVR in flat configuration. Designed for systems utilizing very wide flat transmission lines where conventional current measurements are not possible. Insertion of two or more in a row makes it possible to measure current distribution within a transmission line. Dual current measurement is possible with the use of an optional Current Viewing Probe installed within the CVR unit.

Features

- Ease of Installation
- Current Viewing Probe available
- Broad Bandpass
- Fast risetime
- Low Inductance
- Special lengths available
- BNC output signal connector
- Flange input available
- Side mounting clamps available
- Custom designed units available
- Lengths up to 60" available



Specifications

Model	Resistance ohms	Bandpass MHz	Risetime nsec	E _{max} joules	Length inches	Wattage
W-2-005-2FC	.005	400	2	125	2	5
W-2-0025-4FC	.0025	400	2	275	4	10
W-2-001-6FC	.001	400	2	275	6	15
W-2-0005-12FC	.0005	400	2	550	12	30
W-2-0005-18FC	.0005	400	2	1250	18	45
W-2-0025-24FC	.00025	400	2	1050	24	60

Standard resistance tolerance $\pm 4\%$. Closer tolerance available. Each unit labeled with exact resistance value accurate to $\pm 0.2\%$.

Ordering Information

When ordering please specify model number. If di/dt probe is desired with CVR unit add "-P" to model number.
Example: W-2-005-2FC-P. For custom-designed unit please specify your requirements: Length of unit, resistance, joules, and mounting requirements. For information about di/dt probe see CURRENT VIEWING PROBE page.

APPENDIX 2

FORCE ON A CAPACITOR

Consider the parallel plate capacitor similar to the one illustrated in Figure 1.

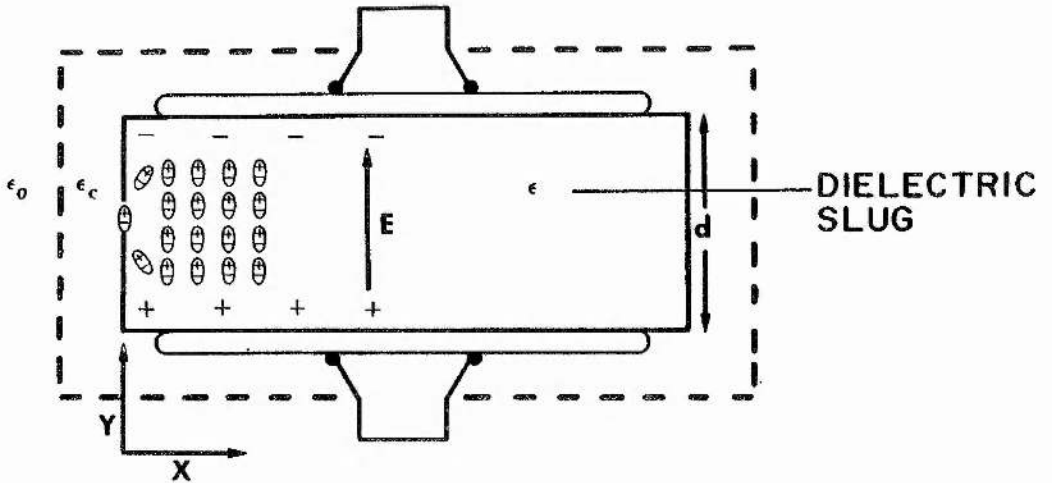


Figure 1 Diagram for force analysis in a capacitor.

The charge on the capacitor is given by

$$q = C(y)v \quad , \quad (1)$$

where we have q = charge in coulombs,

$C(y)$ = position dependent capacitance, and

v = voltage across the plates.

Differentiating the charge, q , with respect to time we get the current given by

$$i = \frac{dq}{dt} = \frac{d[C(y)v]}{dt} \quad . \quad (2)$$

Expanding the time derivative of the capacitance and applying the the chain rule of differentiation we get

$$i = C(y) \frac{dv}{dt} + v \frac{dC(y)}{dy} \frac{dy}{dt} \quad . \quad (3)$$

The last term of Equation (3) accounts for the electro-mechanical movement of the plates. If dy/dt is zero, i.e. the the capacitor is perfectly rigid, then Equation (3) reduces to the normal circuit theory formula. For electrical considerations the second term is neglected. From an acoustic generation standpoint we must next consider the second term and the power delivered to the capacitor. The power, p , delivered to a capacitor is given by

$$p = vi = v \frac{d[C(y)v]}{dt} \quad (4)$$

Again expanding the time derivative of the capacitance and applying the the chain rule of differentiation we get

$$p = \frac{d[0.5C(y)v^2]}{dt} + 0.5v^2 \frac{d[C(y)]}{dy} \frac{dy}{dt} \quad (5)$$

Equation (5) can be put into the form

$$p = \frac{dW}{dt} + f(y) \frac{dy}{dt} \quad (6)$$

where the power delivered to a capacitor goes into increasing the energy storage, W , and the mechanical power $f(y) \cdot dy/dt$ given below as

$$W = 0.5 C(y)v^2 \quad \text{and} \quad f(y) = 0.5v^2 \frac{dC(y)}{dy} \quad (7)$$

The capacitance of the system is given by

$$C(y) = \epsilon A/y \quad (8)$$

where we have A = the area of the plates,

ϵ = permittivity of the dielectric, and

y = the distance of plate separation.

For a constant voltage, V , using Equation (7) we find the force is

$$f(y) = 0.5 V^2 \frac{dC(y)}{dy} = -0.5 \frac{\epsilon AV^2}{y^2} \quad (9)$$

The negative sign indicates that the force acts in the direction to decrease y , or simply, the plates are attracted due to opposing charges.

In this derivation we have neglected the fringe fields at the edge of the conductors. If the dielectric is linearly polarized, i.e. not permanently polarized, the polarization will have components in both the x and y direction as depicted in Figure 1. The polarization force density, F , can be written as

$$F = (P \cdot \nabla) E \quad (10)$$

where we have P = the polarization vector and

E = the electric field.

Forces arise from the fringe fields at the edge of the capacitor plates. Applying Equation (10) to the diagram in Figure 1 we can see that there is a net force trying to pull the dielectric material into the capacitor. The force acting on a unit volume (force density) is given by

$$F_x = P_x \frac{\partial E_x}{\partial x} + P_y \frac{\partial E_x}{\partial y} \quad (11)$$

Since $P = \epsilon E$ we can write

$$F_x = \epsilon \left(E_x \frac{\partial E_x}{\partial x} + E_y \frac{\partial E_x}{\partial y} \right) \quad (12)$$

Because the electric field is curl free, $\nabla \times E = 0$, the force density can be simplified to

$$F_x = \frac{\epsilon}{2} \frac{\partial (E_x^2 + E_y^2)}{\partial x} \quad (13)$$

The total force, f_x , is obtained by integrating the force density (Equation 13) over the volume ($d*w*x$) of the dielectric. The result can be written as

$$f_x = \frac{\epsilon V^2 w}{2 d} \quad (14)$$

where we have d = the plate separation,

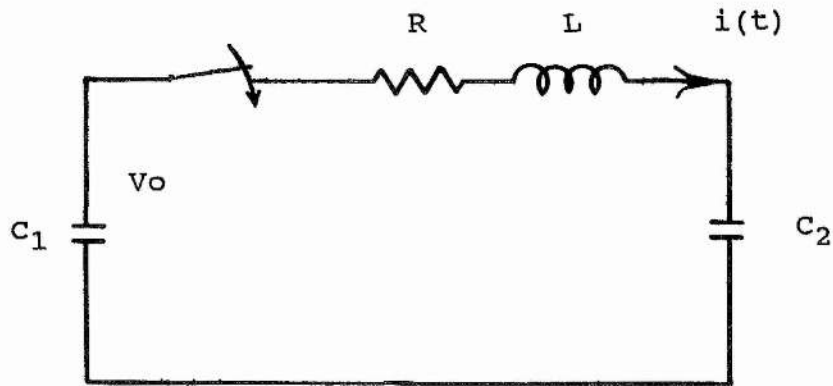
w = the plate width into the paper, and

x = the x dimension of the dielectric.

Equation (14) tells us that the force is independent of voltage polarity and acts to pull larger permittivity material into the capacitor.

APPENDIX 3

CHARGE SYSTEM ANALYSIS



C_1 = Power supply filter capacitor

L = Resonant charge series inductor

R = Resonant charge series inductor resistance

C_2 = Capacitor to be charged

V_0 = Initial voltage on C_1

$V_{C1}(t)$ = Time dependent voltage on C_1

$V_{C2}(t)$ = Time dependent voltage on C_2

$i(t)$ = Time dependent current in the loop

From Kirchoffs Law, we can write

$$0 = \frac{1}{C_1} i(t) + V_{C1}(0-) + R \frac{di}{dt} + L \frac{d^2i}{dt^2} + i_L(0-) + \frac{1}{C_2} i(t) + V_{C2}(0-) \quad .$$

Taking the Laplace transform, we get

$$0 = \frac{1}{C_1} I(s) + V_0 + R s I(s) + L s^2 I(s) + \frac{1}{C_2} I(s) \quad .$$

Solving for $I(s)$ and simplifying gives us

$$I(s) = \frac{-V_o}{s^2 L + sR + C_1 + C_2 / C_1 C_2} .$$

Completing the square of the denominator and taking the inverse Laplace transform we get the following equation for $i(t)$,

$$i(t) = \frac{V_o}{\omega L} e^{-\frac{R}{2L} t} \sin \omega t ,$$

where (the natural frequency) is given by

$$\omega = \sqrt{\frac{C_1 + C_2}{LC_1 C_2} - \left(\frac{R}{2L}\right)^2} .$$

We then obtain

$$V_{C1}(t) = V_o - \frac{V_o C_2 e^{-\frac{R}{2L} t}}{(C_1 + C_2)} \left[(1 - \cos \omega t) + \frac{R}{2L} \sin \omega t \right]$$

and

$$V_{C2}(t) = \frac{V_o C_2 e^{-\frac{R}{2L} t}}{C_1 + C_2} \left[(1 - \cos \omega t) + \frac{R}{2L} \sin \omega t \right] .$$

Usually the resistance of the charging inductor is small

$$\frac{R}{2L} \ll \left[\frac{1}{L \left(\frac{C_1 C_2}{C_1 + C_2} \right)} \right]^2 ,$$

so we can write

$$i(t) = V_0 \sqrt{\frac{C_1 C_2}{(C_1 + C_2)L}} e^{-\frac{R}{2L} t} \sin \omega t ,$$

where

$$\omega = \sqrt{\frac{C_1 + C_2}{LC_1 C_2} - \left(\frac{R}{2L} \right)^2} \quad \text{where } \left(\frac{R}{2L} \right)^2 \rightarrow 0$$

thus, we obtain

$$V_{C_1}(t) = V_0 \left[1 - \frac{C_2}{C_1 + C_2} (1 - \cos \omega t) \right] e^{-\frac{R}{2L} t}$$

and

$$V_{C_2}(t) = \frac{V_0 C_2}{C_1 + C_2} (1 - \cos \omega t) e^{-\frac{R}{2L} t} .$$

The efficiency of the charging is given by V_{C2}/V_{C1} or

$$\text{EFF} = \frac{C_1}{C_1 + C_2} \left[1 + e^{-\left(\frac{\pi R}{2 \sqrt{\frac{LC_1 C_2}{C_1 + C_2}}} \right)} \right].$$